SCENARIO EARTHQUAKES FOR SAINT LOUIS, MO, AND MEMPHIS, TN, AND SEISMIC HAZARD MAPS FOR THE CENTRAL UNITED STATES REGION INCLUDING THE EFFECT OF SITE CONDITIONS

Final Technical Report

Prepared under USGS External Grant Number 1434-HQ-97-GR-02981
(Scenario Earthquakes and Seismic Hazard Mapping for the New Madrid Region)

Recipient:
Risk Engineering, Inc.
4155 Darley Avenue, Suite A
Boulder, CO 80305 USA

Principal Investigators:
Dr. Gabriel R. Toro and Dr. Walter J. Silva

January 10, 2001

Research supported by the U.S. Geological Survey (USGS), Department of the Interior, under USGS award number 1434-HQ-97-GR-02981. The views and conclusions contained in this document are those of the authors and should not be interpreted as necessarily representing the official policies, either expressed or implied, of the U.S. Government

External Grant Number 1434-HQ-97-GR-02981

SCENARIO EARTHQUAKES FOR SAINT LOUIS, MO, AND MEMPHIS, TN, AND SEISMIC HAZARD MAP S FOR THE CENTRAL UNITED STATES REGION INCLUDING THE EFFECT OF SITE CONDITIONS

Gabriel R. Toro
Risk Engineering, Inc., 4155 Darley Avenue suite A, Boulder, CO 80303
Telephone: (978)266-2639 FAX: (978)266-2639 toro@riskeng.com

Walter J. Silva
Pacific Engineering and Analysis, 311 Pomona Avenue, El Cerrito, CA 94530
Telephone: (510)528-2821 FAX: (510)528-2821 pacific_engineering@juno.com

TECHNICAL ABSTRACT

This study utilizes the current state of knowledge--and associated uncertainties--on the rates and characteristics of earthquakes in the New Madrid and Wabash Valley seismic zones, ground motions in the central and eastern United States, and the dynamic response of soil deposits in the region, to construct probabilistic scenarios for Saint Louis and Memphis and seismic hazard maps for the entire region.

The scenarios provide engineers, disaster planners, and financial-loss analysts with a detailed and realistic representation of the characteristics (including time histories) of earthquakes that are representative of the design conditions (e.g., 2% probability in 50 years).

The hazard maps include the effect of soil-column thickness, regional surficial geology, and nonlinear soil response. These maps provide a level of detail superior to that of national maps.

NON-TECHNICAL ABSTRACT

This study utilizes the current state of knowledge characteristics of earthquakes in the New Madrid and Wabash Valley seismic zones, and the shaking that these earthquakes produce, to construct probabilistic scenarios for Saint Louis and Memphis and seismic hazard maps for the entire region.

The scenarios provide engineers, disaster planners, and financial-loss analysts with a detailed and realistic representation of the characteristics (including time histories) of earthquakes that are representative of the design conditions typically used in building codes.

The hazard maps include the effect of soil thickness and surficial geology, as well as differences in the behavior of soils under weak and strong motions. These maps provide more detail than national hazard maps.

Scenario Earthquakes and Seismic Hazard Mapping for the New Madrid Region

External Grant Number 1434-HQ-97-GR-02981

Gabriel R. Toro Risk Engineering, Inc., 4155 Darley Avenue suite A, Boulder, CO 80303

Telephone: (978)266-2639 FAX: (978)266-2639 toro@riskeng.com

NEHRP Element(s): II, I **Keywords:** Earthquake scenarios, Earthquake Probabilities, Strong ground motion, amplification, seismic zonation

This study utilizes the current state of knowledge about earthquakes in the New Madrid and Wabash Valley seismic zones, and about ground motions and site response in the region, to construct probabilistic scenarios for Saint Louis and Memphis and seismic hazard maps for the entire region. The scenarios provide engineers and disaster planners with a detailed and realistic representation of the characteristics (including time histories) of earthquakes that are representative of the design conditions (e.g., 2% probability in 50 years). The maps include the effect of depth and provide a level of detail superior to that of national maps.

ACKNOWLEDGMENTS

This research was supported by the U.S. Geological Survey (USGS), Department of the Interior, under USGS award number 1434-HQ-97-GR-02981, to Risk Engineering, Inc. Walt Silva of Pacific Engineering and Analysis, Steve McCaskie of Sverdrup Civil, and Bob Herrmann of Saint Louis University served as subcontractors/consultants.

Glenn Rix and Salomé Romero of Georgia Tech contributed substantially to this work by sharing their data and insights on the shear-wave velocities in Memphis and surrounding areas. A number of other researchers and engineers provided data or insights that were used in this study, most notably Arch Johnston, John Schneider, Paul Mayne, Rob Williams, Steven Horton, Howard Hwang, and Richard Dart.

Table of Contents

Section 1
INTRODUCTION

This study utilizes models that represent the current state of knowledge--and associated uncertainties--on the rates and severity of earthquakes in the New Madrid and Wabash Valley seismic zones, and on ground motions and site response characteristics in the central and eastern United States, to construct probabilistic scenarios for Saint Louis and Memphis and seismic hazard maps for the entire region.

Sections 2, 3, and 4 document the inputs used for these calculations, namely, the seismic-source characterization, the attenuation equations for rock, and the amplification factors. Section 5 presents the development of scenario events and the associated ground motions. Section 6 presents the probabilistic seismic-hazard maps for both rock and soil conditions.

Section 2
SEISMIC SOURCE CHARACTERIZATION

2.1 INTRODUCTION

This Section documents the seismic sources used in this study to characterize seismicity in the New Madrid and Wabash regions, as well as other potential seismic sources in the region. The New Madrid and Wabash regions have been the focus of many seismological and geological studies over the past eight years, resulting in a better understanding of earthquakes in these regions. Still, many uncertainties remain and the existing data are open to alternative interpretations. As a result, the characterization of seismic sources for this study has the dual objective of representing the current state of knowledge about earthquakes in study region and representing the limitations in that state of knowledge. This objective is accomplished by specifying alternative seismic-source geometries and seismicity parameters, and assigning weights to them according to their credibility.

The work of Van Arsdale and Johnston (1999) contains a detailed summary of geological and seismological studies on the New Madrid and Wabash regions and develops interpretations based on these studies. This information is used to define the most of the seismic sources presented here, to quantify the rates of occurrence for large earthquakes, to specify maximum magnitudes for these sources, and to develop weights for alternative sources and parameters.

Another important source of information on maximum magnitudes in the New Madrid region is the work of Hough et al. (1999), who re-interpreted the New Madrid intensity data and obtained magnitude estimates in the range of 7.1 to 7.5 for the three main 1811-1812 New Madrid events. The New Madrid maximum magnitudes used in this study are obtained by giving roughly equal weight to the Van Arsdale and Johnston (1999) and Hough et al. (1999) interpretations.

The rates of occurrence for small and moderate earthquakes are calculated using a statistical analysis of the historical earthquake catalog. Appendix B of Risk Engineering (1999) documents the selection, modification, and analysis of the earthquake catalog.

Traditionally, seismic-hazard studies for sites in the central and eastern United States have used Nuttli's m_{Lg} magnitude to characterize earthquake size because this is the magnitude used in all regional catalogs and in most attenuation equations for the region. Most of the recent information, coming from paleoliquefaction and other geological studies, is provided in the form of moment magnitude **M** (Hanks and Kanamori, 1979), because this magnitude has a physical basis. Recent attenuation equations for the region are provided in terms of **M** (e.g., Atkinson and Boore, 1997) or in terms of both **M** and m_{Lg} (Toro et al., 1997). Because this study makes extensive use of paleoliquefaction and geological data to characterize the New Madrid and Wabash zones, it utilizes **M** to characterize earthquake size.

2.2 SEISMIC SOURCES IN THE NEW MADRID SEISMIC ZONE (NMSZ)

Extensive geological, geophysical, and seismological work has been conducted within the NMSZ. As a result of these efforts, specific seismogenic faults in the NMSZ have been identified and studied in detail, particularly the Reelfoot Fault near the town of New Madrid. Johnston and Schweig (1996) have associated each of the three 1811-1812 earthquakes with a specific fault by using historical accounts and geological evidence (Figure 2-1; see also Figures A-18 and A-21 in Van Arsdale and Johnston, 1999). Their interpretation is consistent with the spatial distribution and source characteristics of contemporary NMSZ seismicity (Figure 2-2). This study uses those faults, augmented to the north in order to represent more diffuse patterns of seismicity, to characterize the main pattern of seismicity in the NMSZ.

The December 11, 1811 event is associated with a strike-slip rupture on the Blytheville arch - Cottonwood Grove fault or with the Blytheville arch - Bootheel lineament. Both interpretations yield identical results, except for sites in the immediate vicinity of the northern ends of these faults. This uses the former interpretation, with a fault length of 125 km (Figure 2-1).

The January 23, 1812 event is associated with a strike-slip rupture on the East Prairie fault (EPE) on the northern portion of the NMSZ. This interpretation is supported by fault-mechanics arguments and by limited historical data and is more poorly constrained than those for the other New Madrid events. The northern portion of the NMSZ is also the one with the most diffuse pattern of seismicity (see Figure 2-2). This diffuse seismicity is represented by the "East Prairie extension" (EPE) seismic source, which is shown in Figures 2-3 and 2-4. The remote possibility that faults in the East Prairie extension connect with the Fluorspar-district faults is reflected by the long version of the East Prairie extension.

The February 7, 1812 event is associated with a thrust rupture on the Reelfoot fault. This study uses a length of 72 km for the Reelfoot fault.

Datable paleoliquefaction features and displaced geologic units provide a chronology of large pre-historic earthquakes, which complement the historical seismicity catalog. One crucial assumption in this study's interpretation of the paleoearthquake chronology is that a large seismic-moment release in the region involves events on all three NMSZ faults, which occur within a time interval of the order of months or a few years (more precisely, within a time interval shorter than the temporal resolution of the paleoearthquake chronology). This assumption is supported by the 1811-1812 events, by the observation that the history of displacement on the Reelfoot fault is consistent with the paleoliquefaction history (even though the paleoliquefaction features at the northern and southern extremes of the NMSZ could not have been caused by events on the Reelfoot fault), and by the observation that the Reelfoot and Ridgely faults have similar displacement histories. Van Arsdale and Johnston (1999) contains a detailed discussion of these issues.

As a consequence of this assumption, each of the three main NMSZ events is considered to have occurred in each one of the three NMSZ faults. Another consequence of this assumption is that the occurrences of large earthquakes in the NMSZ are not independent in time. As a result, the standard PSHA assumption of temporal independence between events must be modified (see Appendix E).

Based on the paleo-earthquake chronology discussed above, each of the three faults is assigned mean recurrence intervals of 500 to 1,000 years (see Table A-1 of Van Arsdale and Johnston, 1999). Based on strain-rate considerations, the 1000-year recurrence interval is given more weight and the 500-year interval is given a lower maximum magnitudes. The resulting logic trees for the rates of large earthquakes and maximum magnitudes on the three NMSZ faults are shown in Figures 2-5 through 2-8. The logic tree for East Prairie and East Prairie extension is somewhat more complicated, in order to avoid double-counting of seismicity.

The combined magnitude-recurrence model of the three NMSZ faults and the East Prairie extension is characteristic, with the exponential portion controlled by historical seismicity and the characteristic portion controlled by paleoseismic and geological information. For the purposes of seismicity calculations, the Reelfoot rift was sub-divided into areas associated with each of the NMSZ faults, as shown in figure 2-10. Each event was assigned to the fault corresponding to the area where it falls. This approach is necessitated by the location errors of earlier historical earthquakes. Maximum-likelihood calculations were performed for each fault separately and for the rift as a whole. The b value obtained for the rift as a whole was assigned to each individual fault, rather than the b value obtained for that fault, because the former is more stable. Half the historical seismicity in the East-Prairie Extension area was assigned to the East Prairie fault; the other half was assigned to the East-Prairie extension. Table 2-1 lists the rates and b values for the NMSZ faults and for all seismic sources considered in this study.

Events in the characteristic portion of the magnitude-recurrence models for the three NMSZ segments are treated as occurring in temporal clusters, so that if one event occurs in one of these segments, events will occur in the other NMSZ segments, with a time delay much shorter than the mean time between clusters (EPF and EPE are considered as one segment for this discussion). Events in the exponential portion of the magnitude-recurrence models are treated as independent (in the usual way). Appendix E presents the mathematical formulation of the clustering model.

2.3 THE WABASH VALLEY SEISMIC ZONE

The treatment of the Wabash Valley seismic zone in this study is based on Van Arsdale and Johnston (1999) and is more detailed than the treatment in Risk Engineering (1999) because of the dominant contribution of Wabash seismicity to Seismic Hazard in Saint Louis.

We treat the Wabash seismicity as two separate seismic sources with overlapping geometries. The first source, which we denote as the Wabash Proper seismic source, is associated with the two largest Wabash paleoearthquakes (**M** ~7.2 and ~7.6 according to Pond and Martin, 1997), which occurred roughly within the mapped extent of the Wabash Valley Fault System. The second source, which we denote as the Wabash Large seismic source is associated with smaller paleoearthquakes and with instrumental seismicity, which occurred in a wider area of Southern Illinois, Indiana, and Southeastern Missouri.

The logic trees in Figures 2-11 and 2-12 describe our treatment of the uncertainty in the geometries, rates, and maximum magnitudes of the Wabash sources. The uncertainty in geometry is characterized by means of three alternative source geometries, which are shown in Figure 2-13. The uncertainty in the activity rate for the New Madrid Proper source is high because only two events have been observed and is assumed to be negatively correlated with maximum magnitude. The activity rates in the Wabash Large seismic zone were computed using the seismicity catalog.

2.4 OTHER FAULTS

The SE Flank fault (see Van Arsdale and Johnston, 199)--also referred to as the Crittenden County fault zone--and the Commerce/Benton Hills fault, are located at or near the SE and NW margins of the Reelfoot rift. These faults show no evidence of large earthquakes during the Quaternary, but they show evidence of two events during the Holocene (one on each fault; Van Arsdale and Johnston, 1999). In spite of its low activity rate, the SE Flank fault may contribute significantly to seismic hazard in Memphis because of its proximity. The Commerce/Benton Hills fault contributes little to seismic hazard at Memphis and Saint Louis, but is included here mainly for the sake seismic-hazard maps in Section 4.

For SE Flank fault, we use a rate of 4.7E-3 events for the exponential portion of the magnitude-recurrence model (based on 13 M>2.5 events in 20 years, as observed by Chiu et al., 1997). The rate of characteristic events and the associated maximum magnitudes are based on Van Arsdale and Johnston (1999) and are given in Figure 2-14. The same parameters are arbitrarily assigned to the Commerce/Benton Hills fault.

2.5 OTHER SEISMIC SOURCES

Other important geophysical features of the New Madrid region include the Reelfoot rift and the less active Rough Creek graben. The boundary between these two structures is not well defined. This study considers two alternative locations (Figure 2-15).

This study considers a source zone to represent earthquakes that occur in the Reelfoot rift, but are not associated with the NMSZ faults and the EPE. Because all historical seismicity on the rift was assigned to the NMSZ faults and the EPE, one could assume zero seismicity for the Reelfoot rift source zone and still be consistent with historical seismicity. Instead, this study assigns to this seismic source a rate equal to 10% of the total historical seismicity observed on the rift. As a result, this study accounts for 110% of the historical seismicity on the Reelfoot rift. This is within the error bars of the historical data and allows us to account for the possibility of moderate earthquakes occurring off the main NMSZ faults.

The magnitude-recurrence model for the Rough Creek graben are determined from the historical seismicity on the graben. The maximum magnitudes for the Reelfoot rift and Rough Creek graben are specified on the basis of Table A-1 of Van Arsdale and Johnston (1999).

We also define background zones covering portions of the study region not already covered by the sources described above (see Figure 2-16. The definition of these sources is taken from Risk Engineering (1994) and is modified slightly to match the geometries of the Wabash, Reelfoot rift, and Rough Creek graben sources. Two geometries are used for the Ozarks source, which correspond to the Intermedia and Broad geometries of the Wabash source (see Figure 2-12). The maximum magnitude for these source are given in Table 2-2. The rates of small and moderate earthquakes, and associated b values, were computed using the seismicity catalog and are listed in Table 2-1.

2.6 REFERENCES

Atkinson, G.M. and D.M. Boore. (1997). "Some Comparisons Between Recent Ground-Motion Relations." *Seismological Research Letters,* v.68, no. 1, pp. 24-30.

Chiu, Shu-Chioung C., Chiu, Jer-Ming, and Johnston, Arch C. (1997). "Seismicity of the Southeastern Margin on Reelfoot Rift, Central United States." *Seismological Research Letters,* v.68, pp. 785-796.

Hanks, T., and H. Kanamori (1979). "A Moment Magnitude Scale." J. Geoph. Res., 89, B5, May.

Hough, S., J.G. Armbruster, L. Seeber, and J.F. Hough (1999). *On the Modified Mercalli Intensities and Magnitudes of the 1811/1812 New Madrid, Central United States, Earthquakes.* USGS Open-File Report 99-565.

Johnston, A.C., and Schweig, E.S., 1996. The enigma of the New Madrid earthquakes of 1811- 1812. An. Rev. Earth Planet. Sci., 24: 339-384.

Mueller, C., M. Hopper, and A. Frankel (1996). *Preparation of Earthquake Catalogs for the Interim National Seismic Hazard Maps: Documentation*, January 19.

Pond, E.C., and Martin, J.R., 1997. Estimated magnitudes and accelerations associated with prehistoric earthquakes in the Wabash Valley region of the central United States. Seism. Res. Lett., 68, n. 4, 611-623.

Risk Engineering, Inc. (1994). *Ground Motion Eastimates for Building Codes in the Central United States.* Final Technical Report to USGS, Grant 1434-92-G-2226.

Risk Engineering, Inc. (1999). *Rev. 3 to Updated Probabilistic Seismic Hazard Analysis for the Paducah Gaseous Diffusion Plant, Paducah, Kentucky--Final Report.* Prepared for Lockheed-Martin Utility Services, Available through NRC Public Documents Library, Accession Number 9905140175, docket no. 07007001.

Toro, G.R., N.A. Abrahamson and J.F. Schneider (1997). A Model of Strong Ground Motions from Earthquakes in Central and Eastern North America: Best Estimates and Uncertainties. *Seismological Research Letters,* v.68, no. 1, pp. 41-57.

Van Arsdale, R. and A. Johnston (1999). *Geological and Seismological Setting of the New Madrid Seismic Zone and the Wabash Valley Seismic Zone.* Appendix A of Risk Engineering, Inc. (1999), Rev. 3 to Updated Probabilistic Seismic Hazard Analysis for the Paducah Gaseous Diffusion Plant, Paducah, Kentucky--Final Report. Prepared for Lockheed-Martin Utility Services, Available through NRC Public Documents Library, Accession Number 9905140175, docket no. 07007001.

Table 2-1
Seismicity Parameters (Exponential Portion)

Seismic Source (i)	ν_i	$\sigma\{\ln[\nu_i]\}$	**b**	$\sigma(b)$	$\boldsymbol{\rho}$
E. Prairie Extension	4.5E-03	0.30	0.86	0.05	0.83
E. Prairie fault	4.5E-03	0.30	0.86	0.05	0.83
Reelfoot fault	9.3E-03	0.28	0.86	0.05	0.90
Blytheville arch-CGF	7.9E-03	0.29	0.86	0.05	0.89
SE Flank fault	4.7E-3	-	0.86	-	-
Commerce/Benton Hills fault	4.7E-3	-	0.86	-	-
Wabash Large (intermediate geometry)	1.9E-02	0.16	0.92	0.05	0.61
Wabash Large (extended geometry)	2.7E-02	0.21	0.92	0.05	0.48
Ozarks (goes with Wabash intermediate)	1.0E-02	0.42	0.88	0.08	0.97
Ozarks (goes with Wabash extended)	5.6E-03	0.57	0.89	0.11	0.97
Arkansas	4.1E-03	0.87	0.65	0.17	0.95
Ouachita	5.4E-04	1.25	1.19	0.25	0.98
Midcontinent	2.9E-04	1.76	1.16	0.35	0.98
Southeastern U.S.	1.9E-03	0.93	0.92	0.18	0.97

Notes:
1. ν_i is the annual rate of earthquakes with M>5 in source *i*
2. ρ is the correlation coefficient between $\ln[\nu_i]$ and b.

Table 2-2
Maximum Magnitudes for
Background Sources

Source(s)	**M**	**Weight**
Ozarks, Arkansas[1]	6.2	0.5
	7.2	0.5
Midcontinent,Ouachita[2]	5.5	0.2
	5.8	0.6
	6.8	0.2
Southeastern U.S.[2]	5.5	0.2
	5.9	0.6
	7.2	0.2

[1] Source: Van Arsdale and Johnston (1999).

[2] Source: Risk Engineering (1994; magnitudes converted from m_{Lg} to **M**)

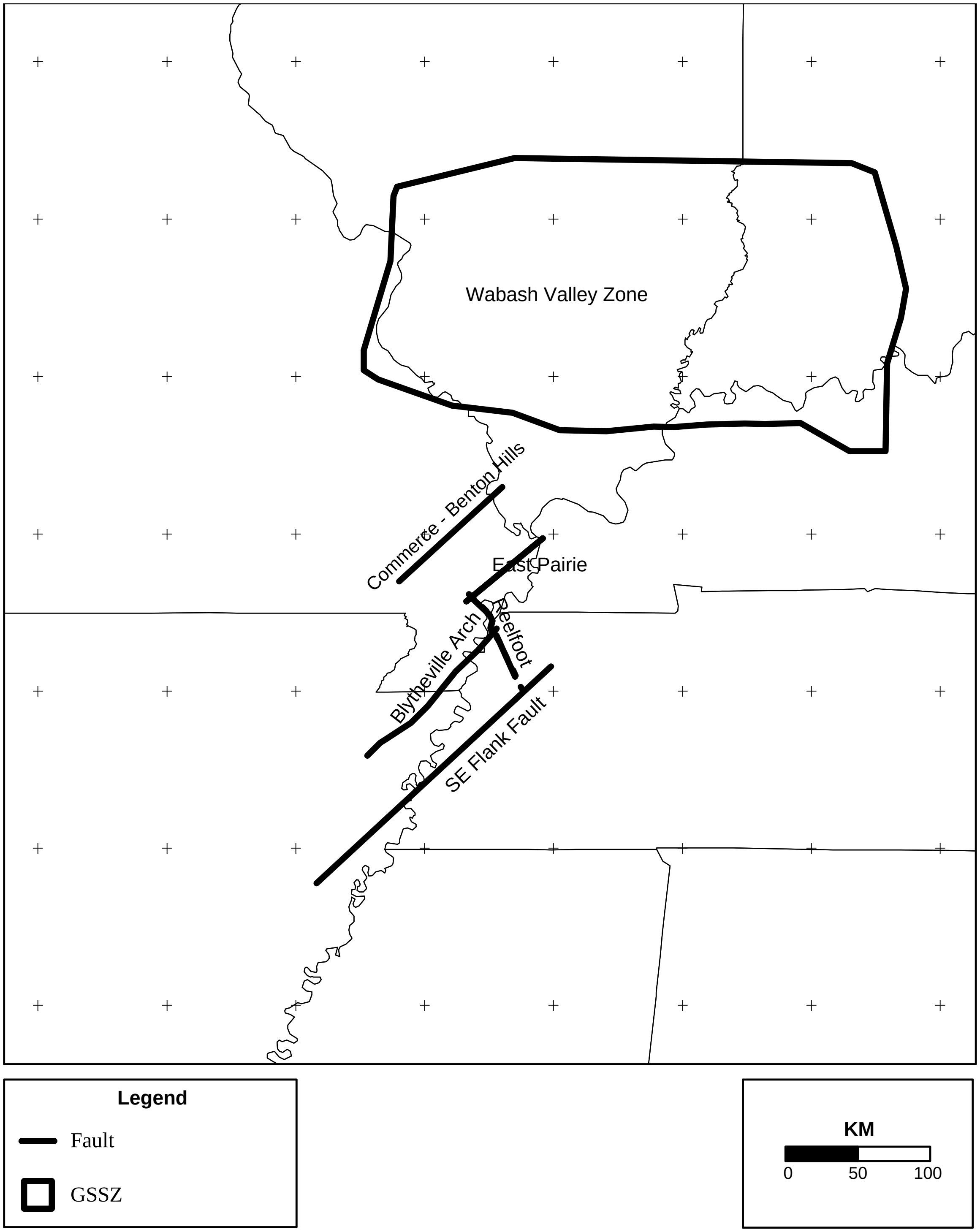

Figure 2-1. Map showing NMSZ and other seismic sources considered in this study.

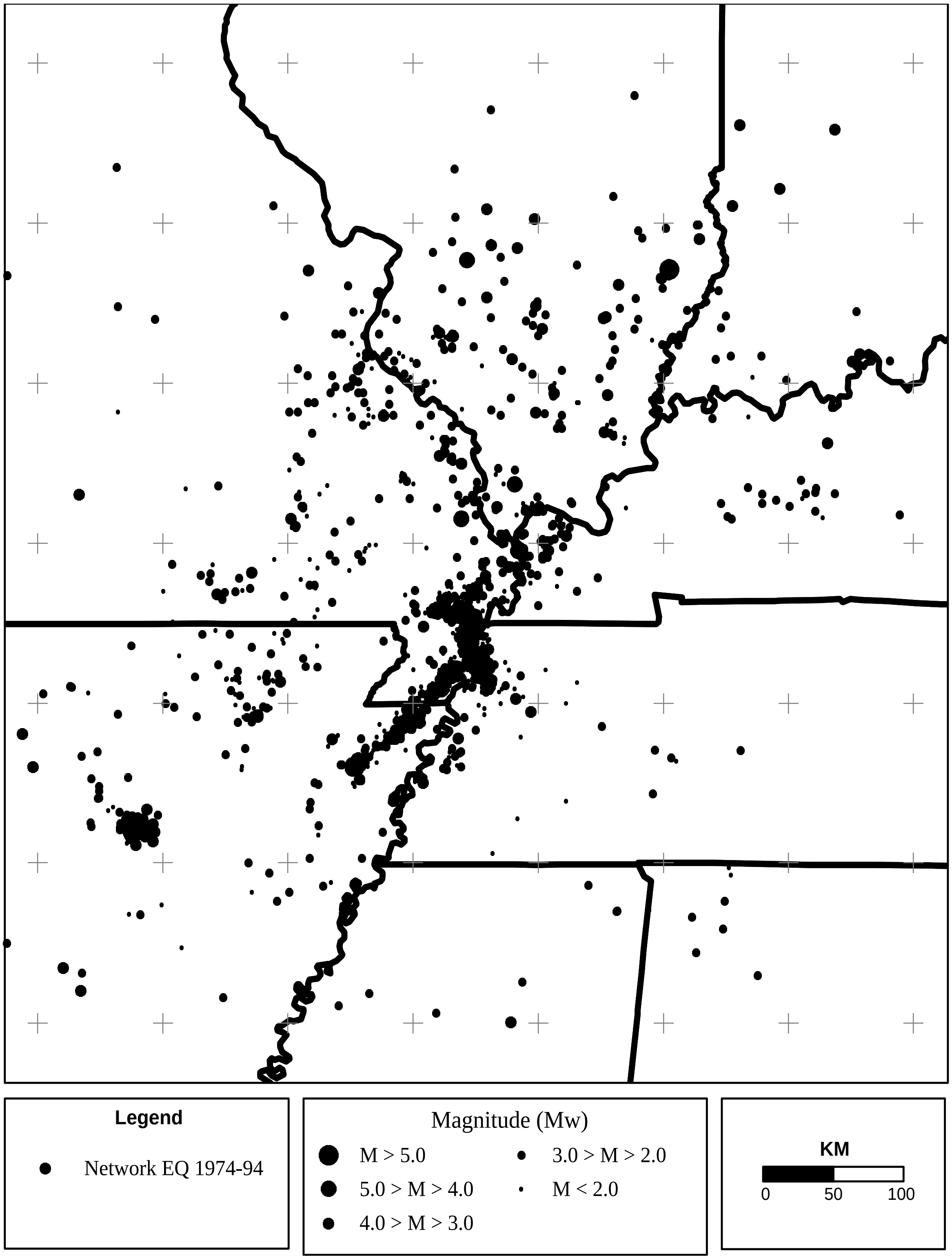

Figure 2-2. Map showing events in the New Madrid earthquake catalog (1974-1997).

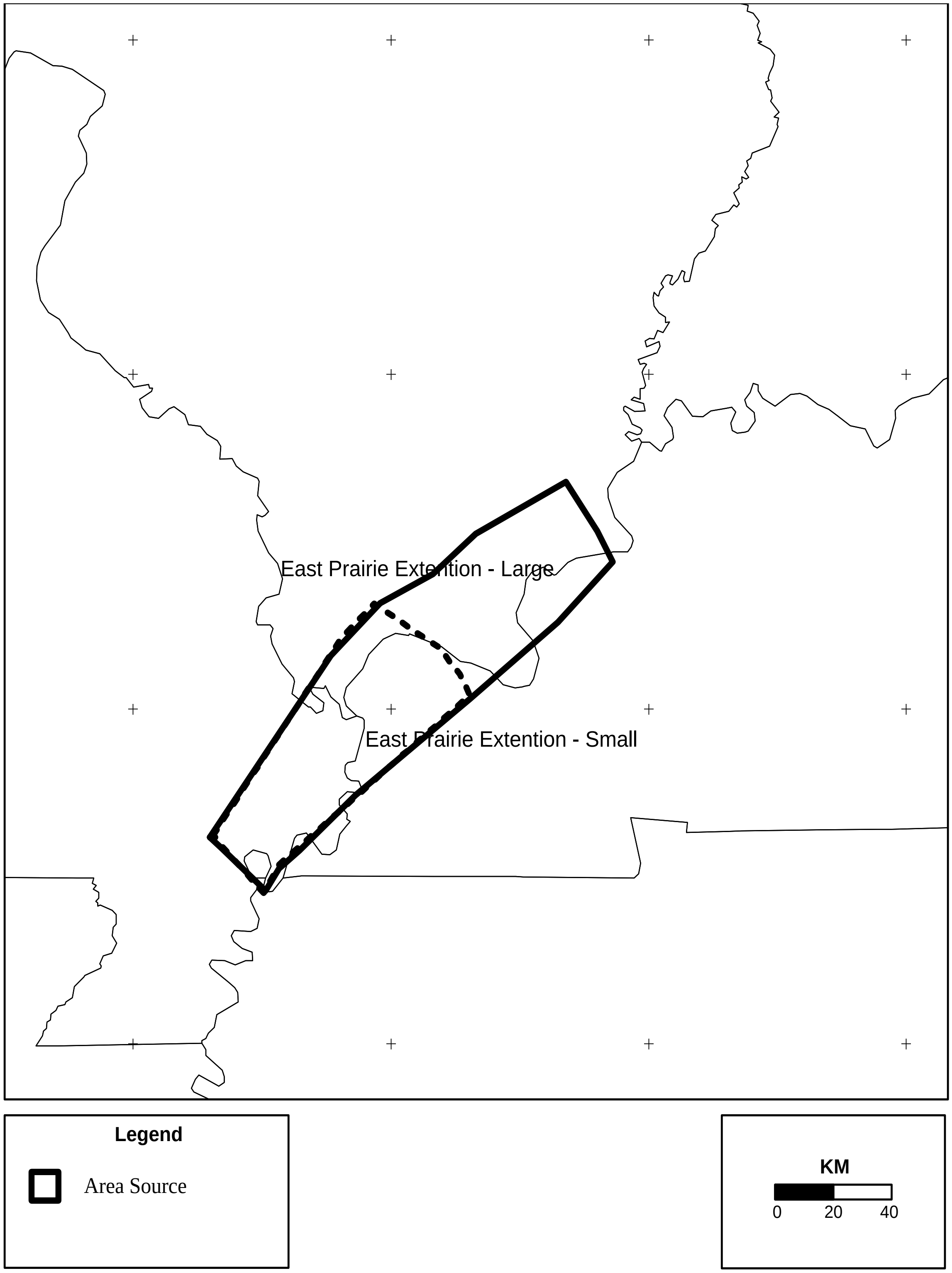

Figure 2-3. Map showing the two alternative geometries of the East Prairie fault extension (EPE).

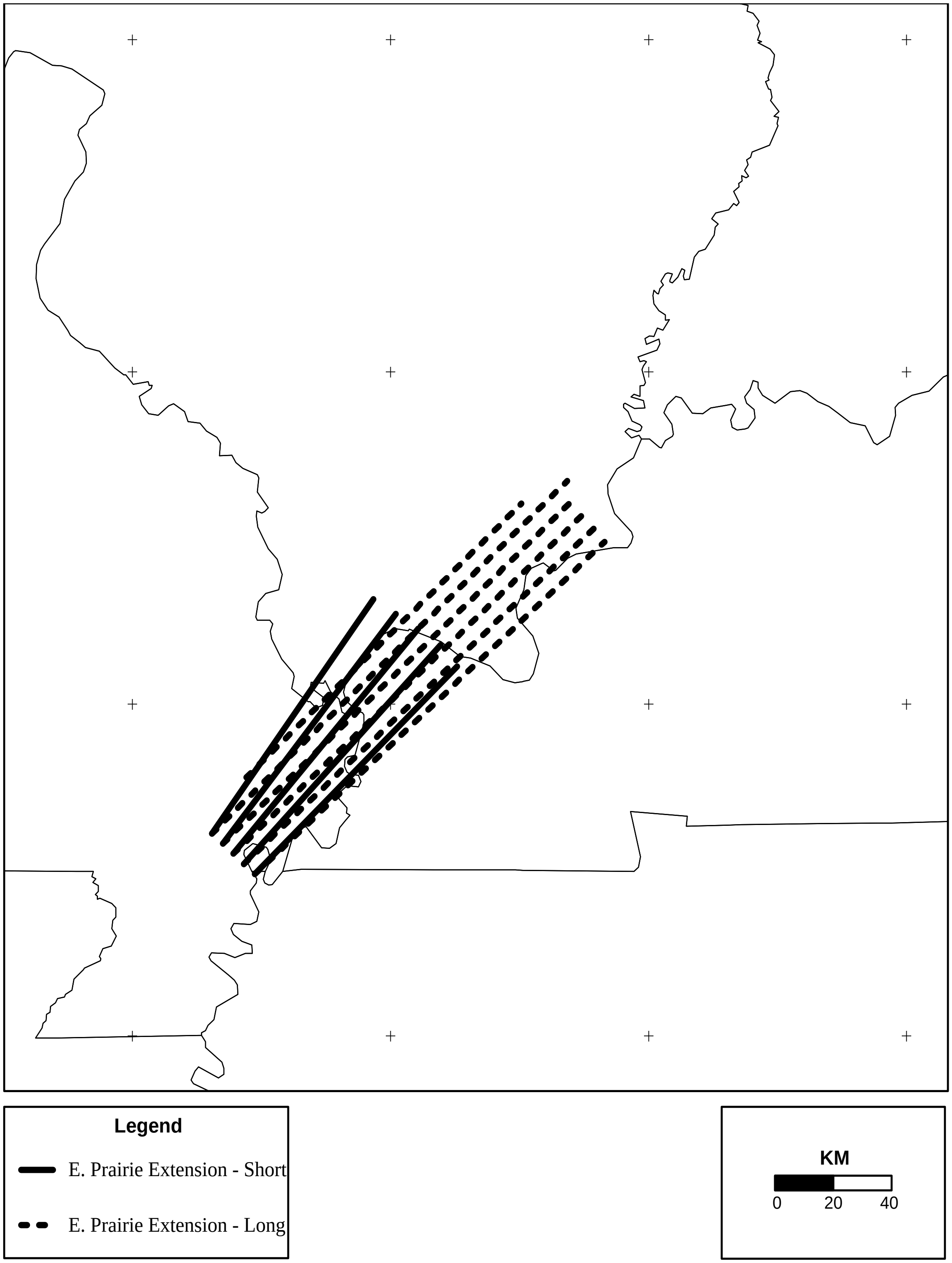

Figure 2-4. Map showing the faults used to represent the East Prairie fault extension (EPE) in the seismic hazard calculations.

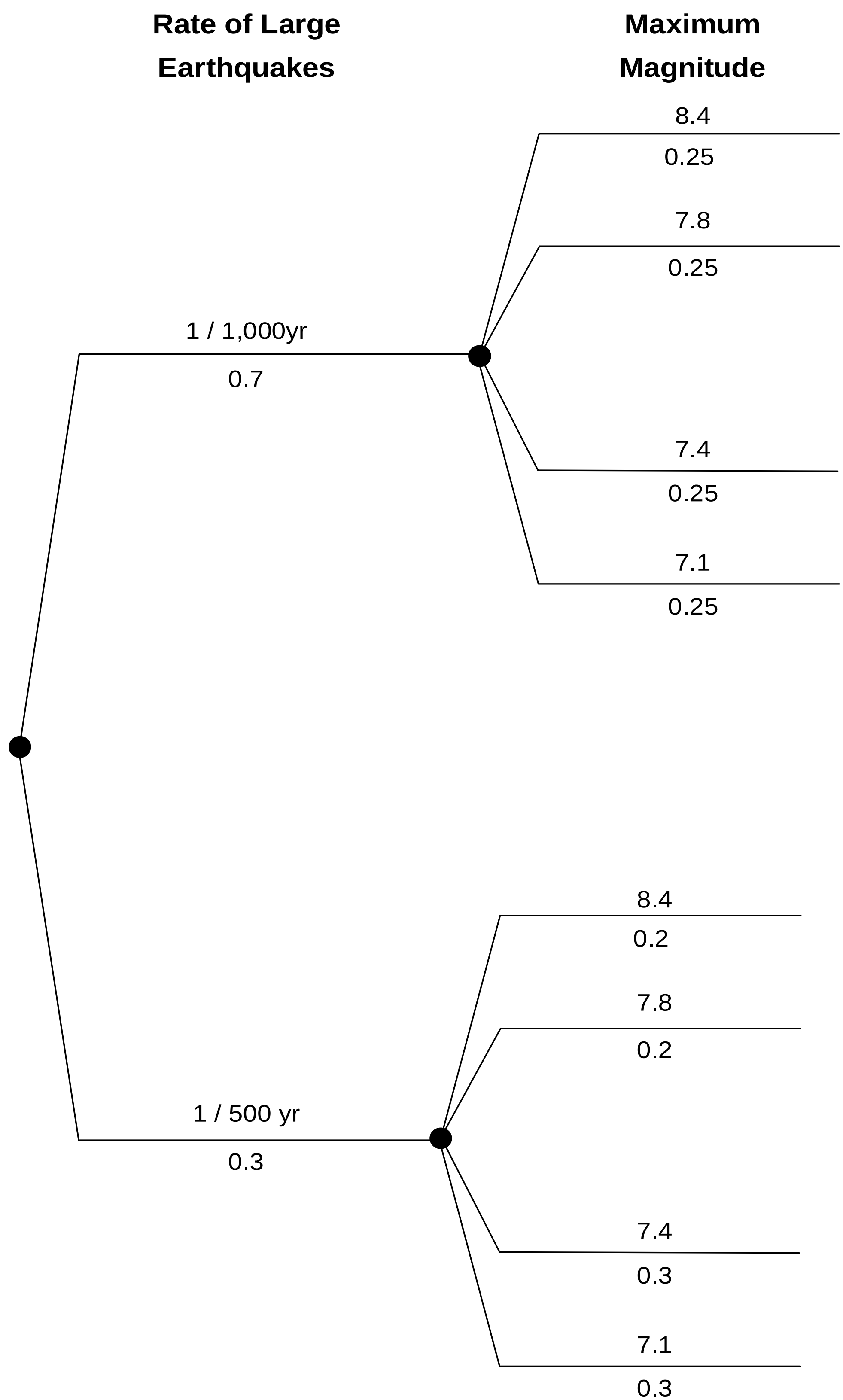

Figure 2-5. Logic tree for the rate of large events and maximum magnitude on the Blytheville Arch-CGF fault. The logic tree for the Reelfoot fault is identical.

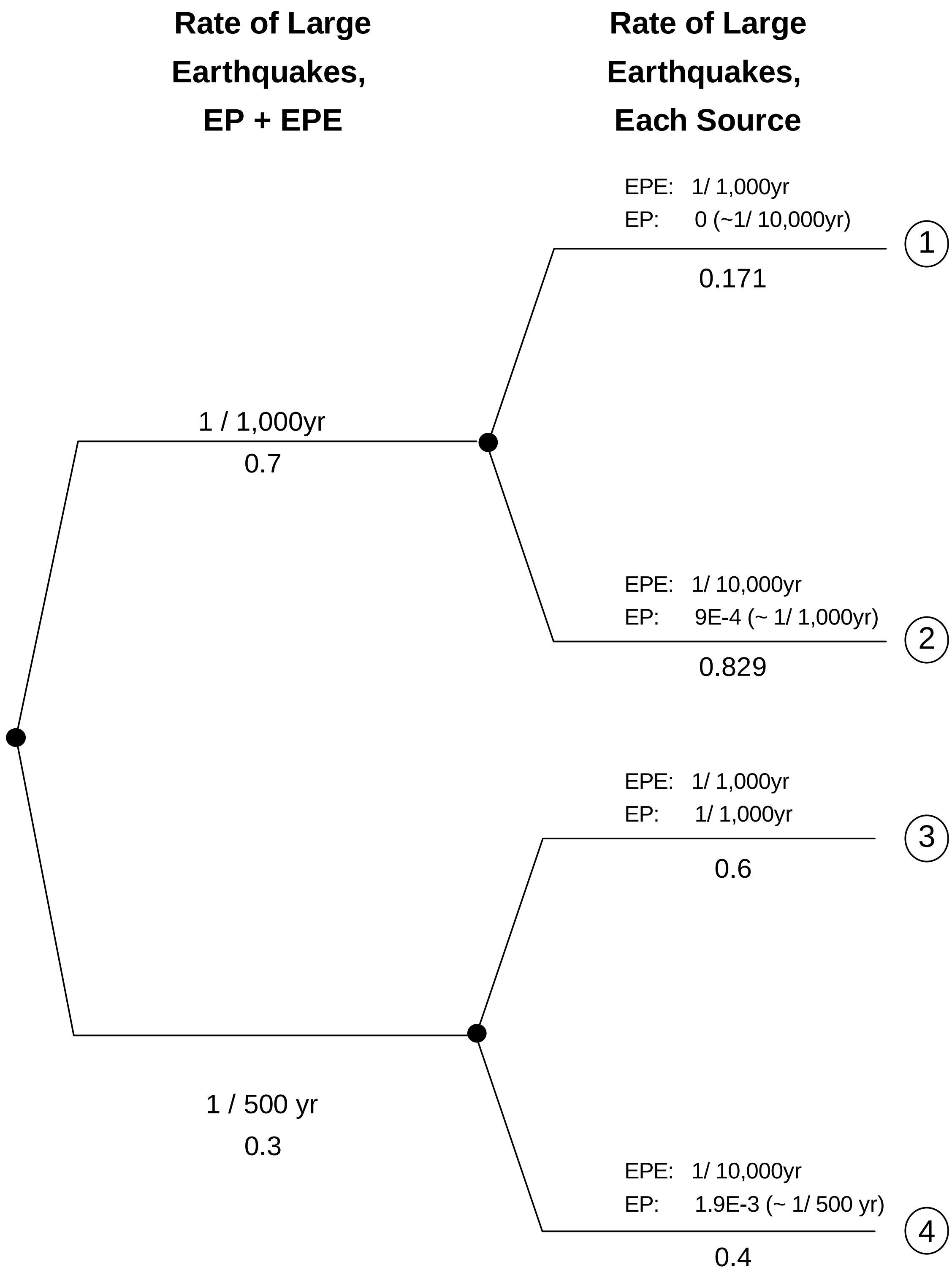

Figure 2-6. Logic tree for the rates of large events on the East Prairie fault and East Prairie extension. The trees for the corresponding maximum magnitudes and source geometries are shown in Figures 2-7 and 2-8.

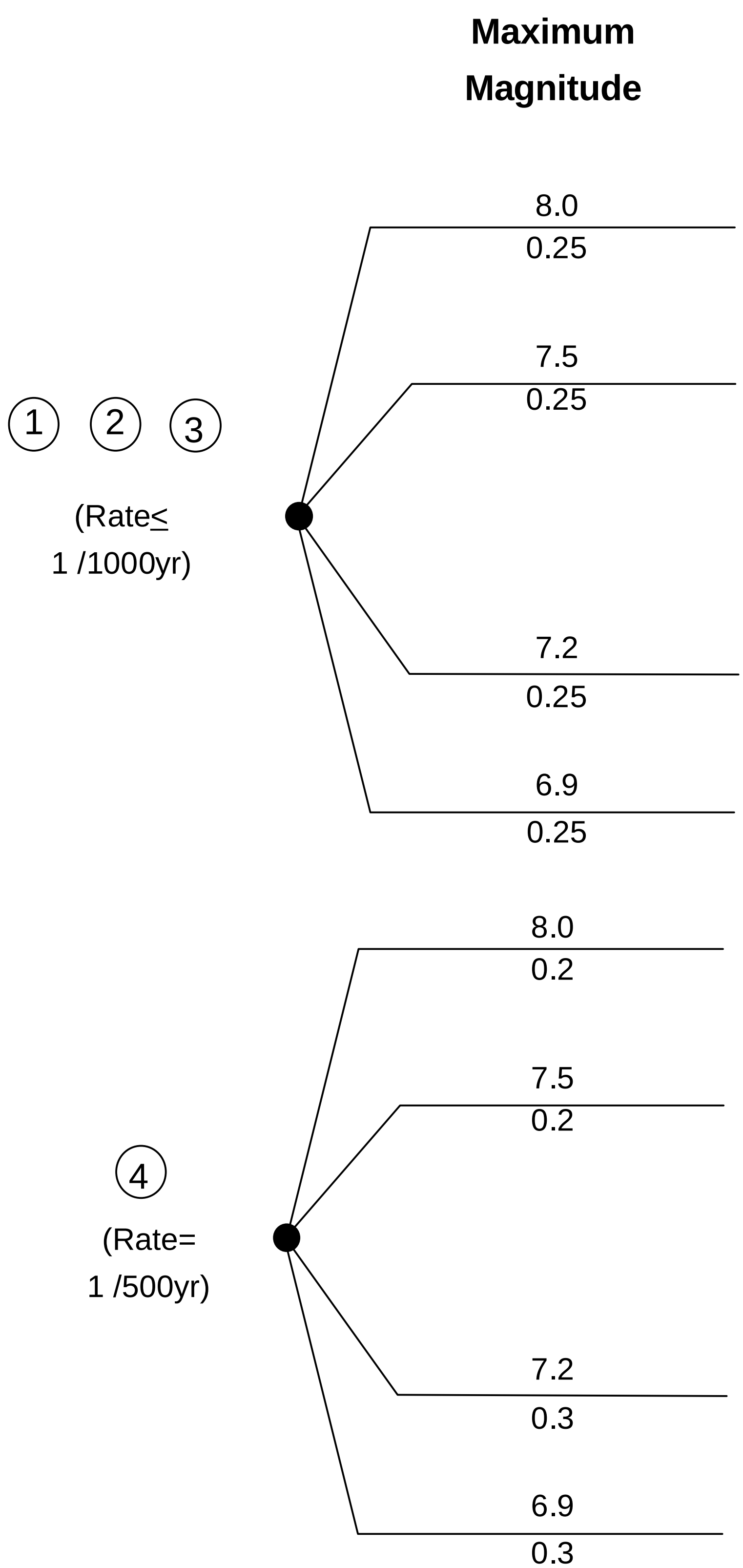

Figure 2-7. Logic trees for the maximum magnitude of the East Prairie fault.

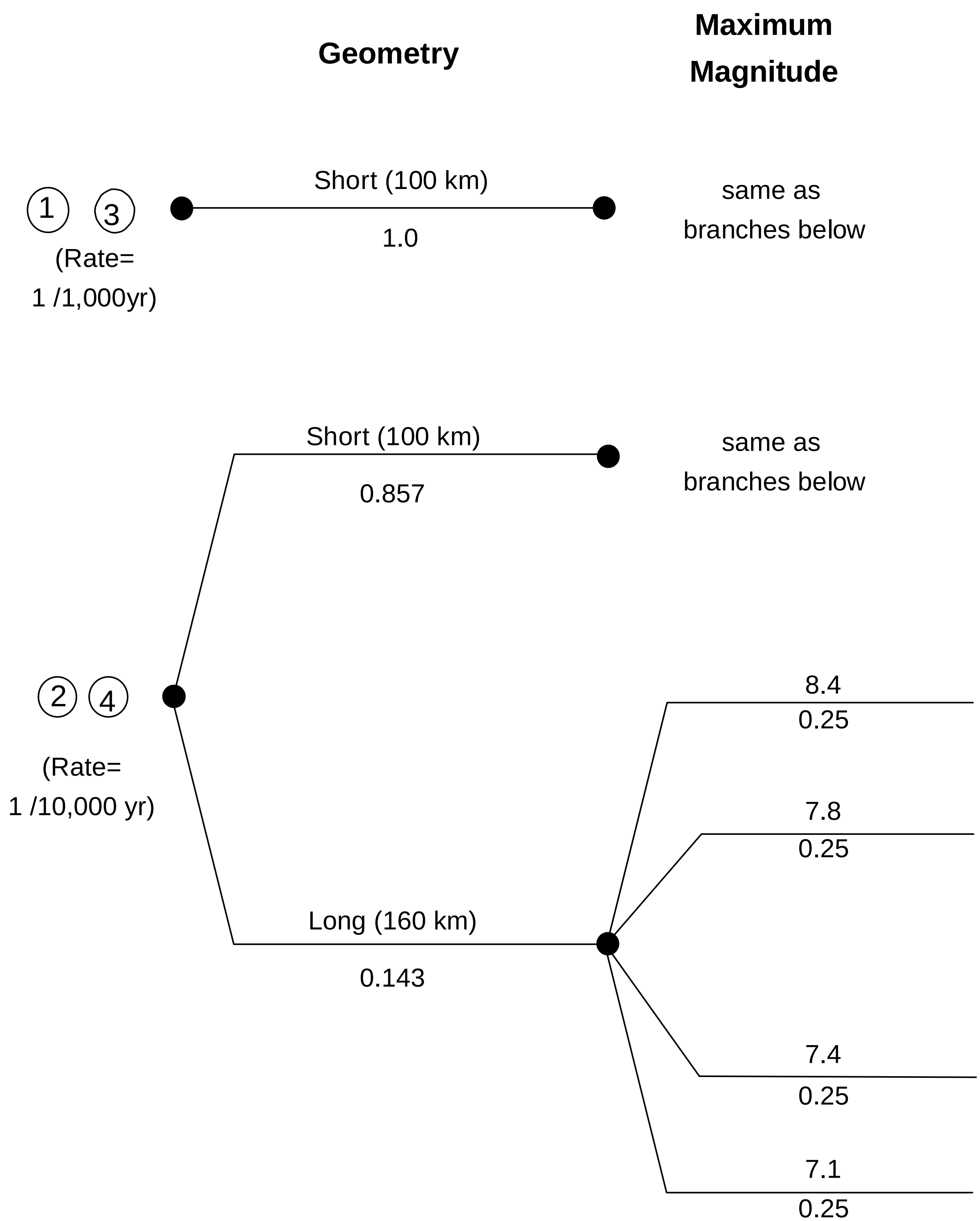

Figure 2-8. Logic tree for the maximum magnitude and geometry of the East Prairie extension (EPE).

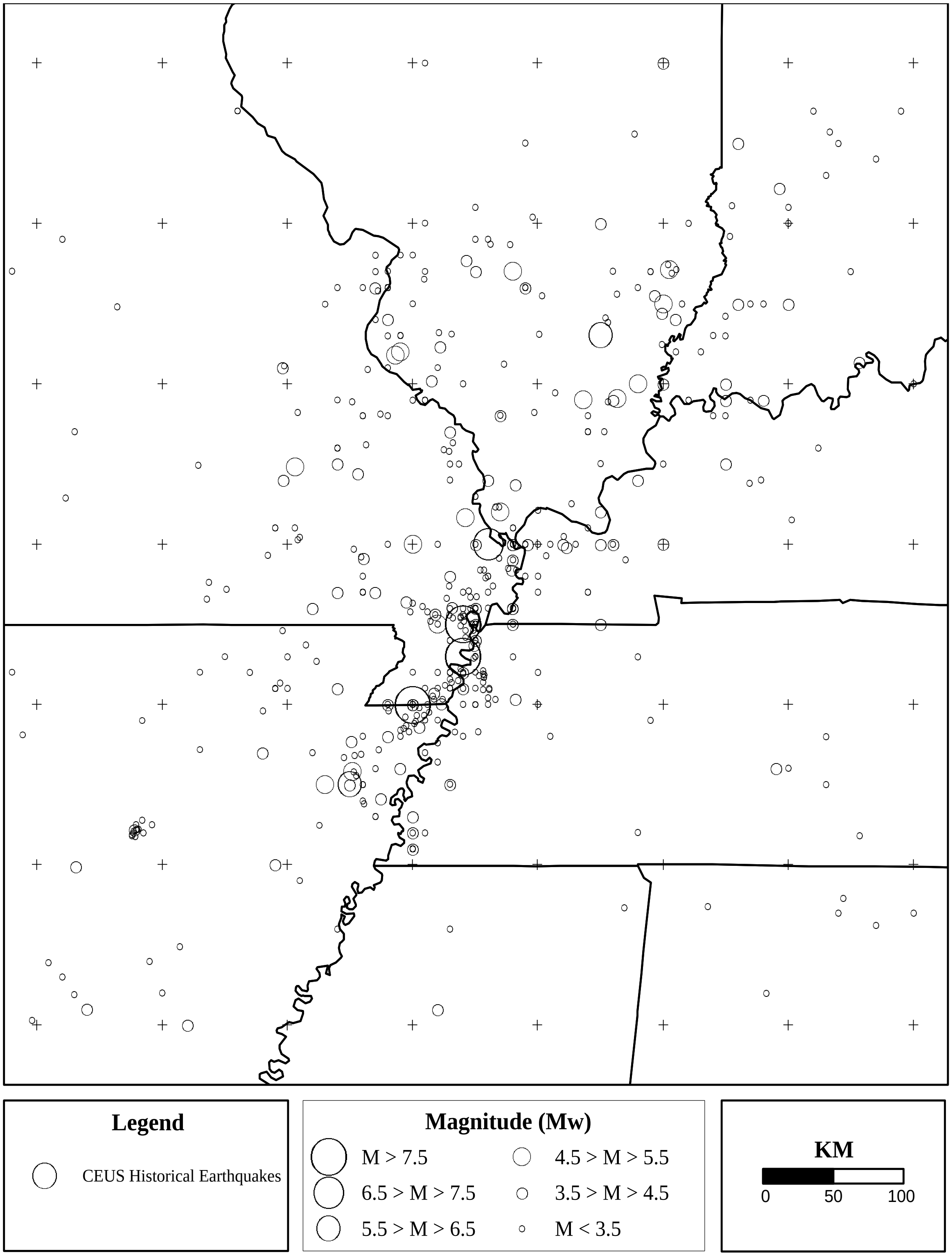

Figure 2-9. Map showing events in the historical earthquake catalog.

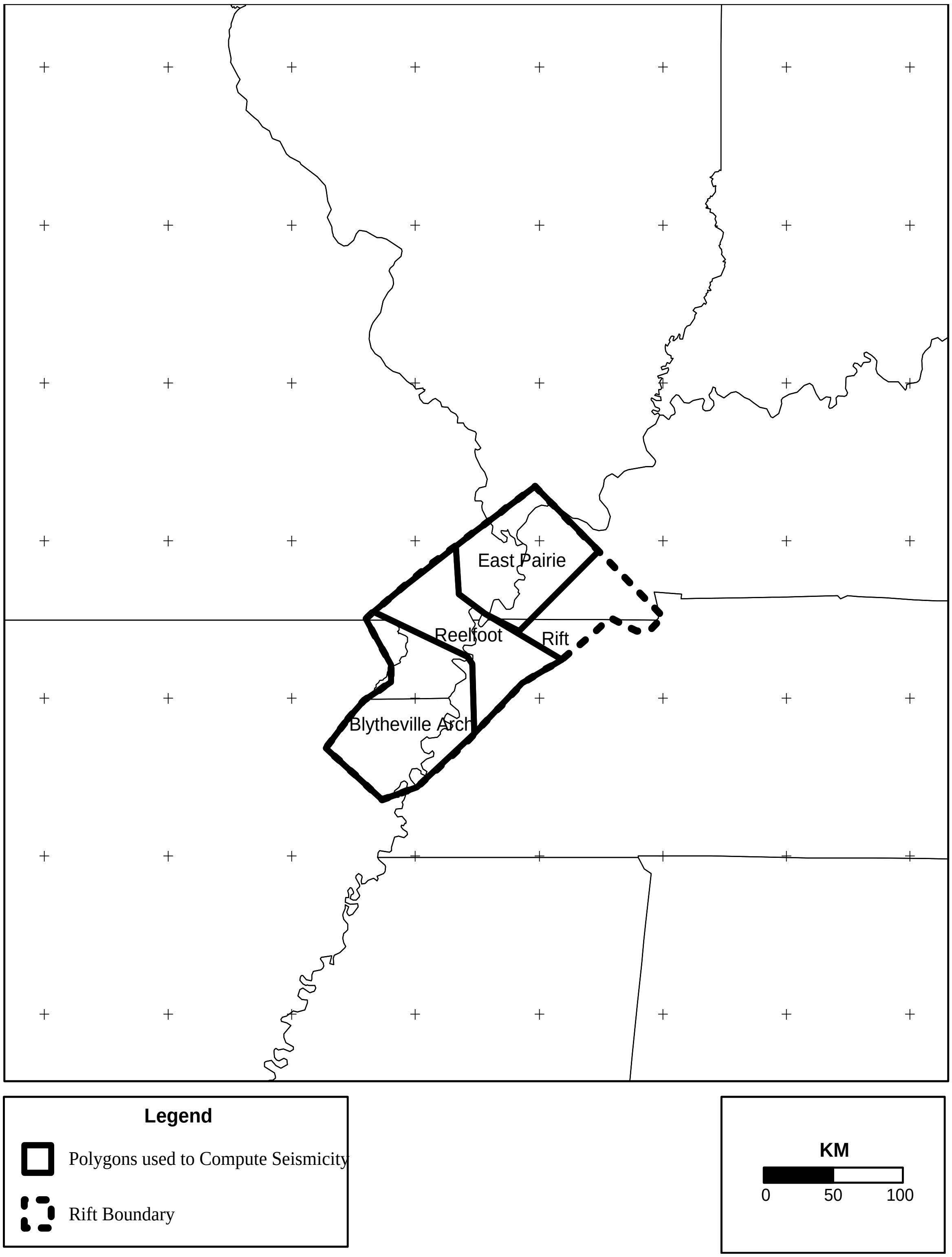

Figure 2-10. Map showing the areas used to assign historical seismicity to the NMSZ faults.

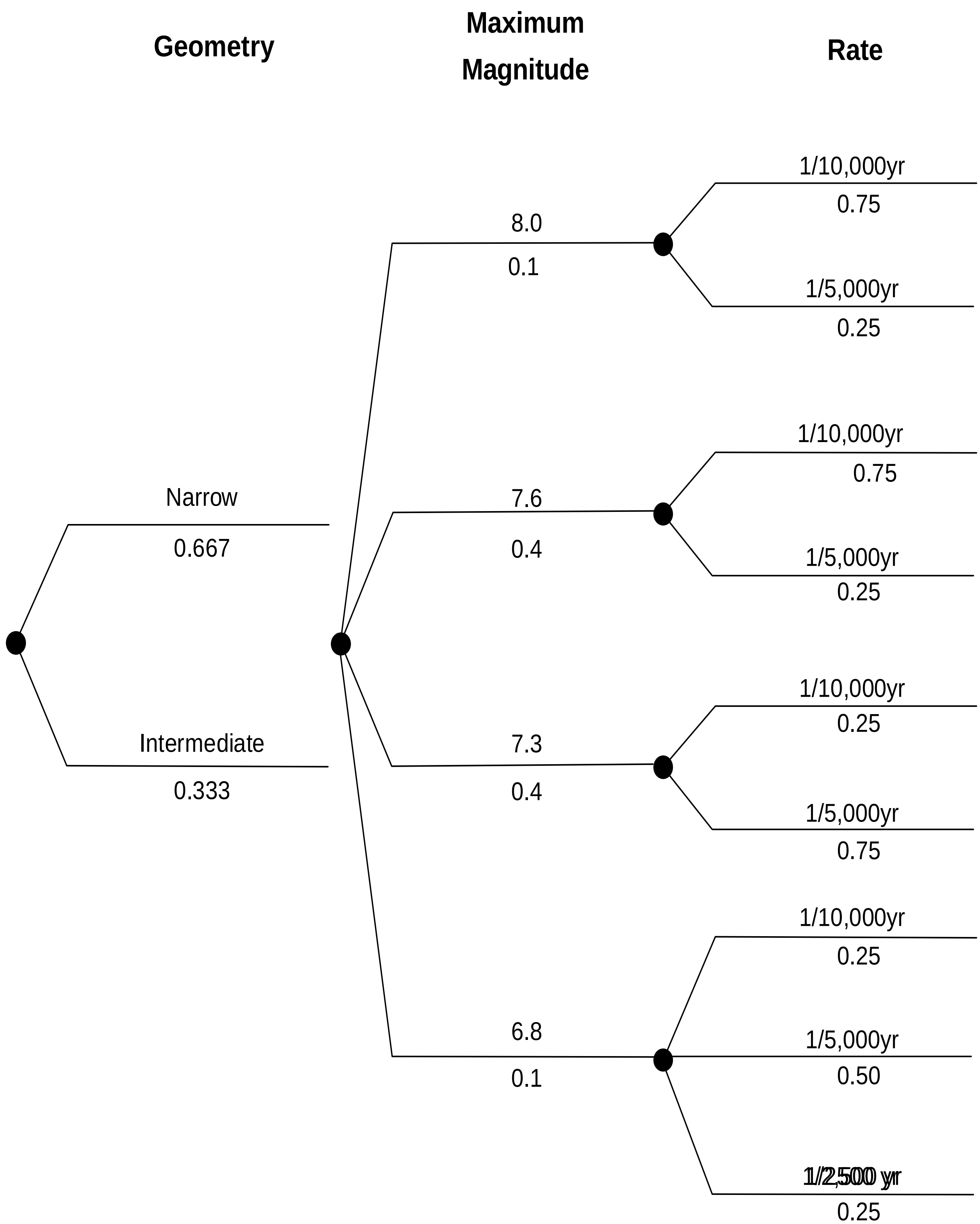

Figure 2-11. Logic tree for the geometry, maximum magnitude, and recurrence rate of the Wabash Proper seismic source.

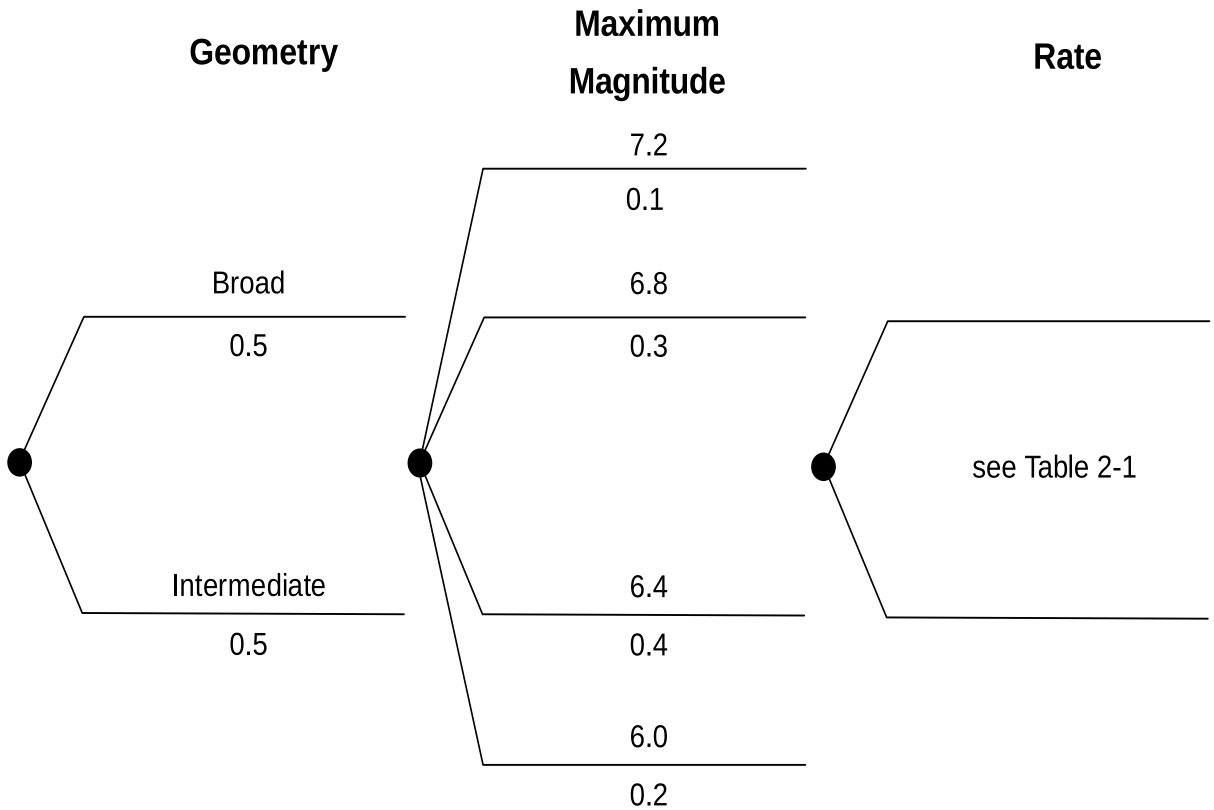

Figure 2-12. Logic tree for the geometry, maximum magnitude, and recurrence rate of the Wabash Large seismic source.

Wabash Geometries

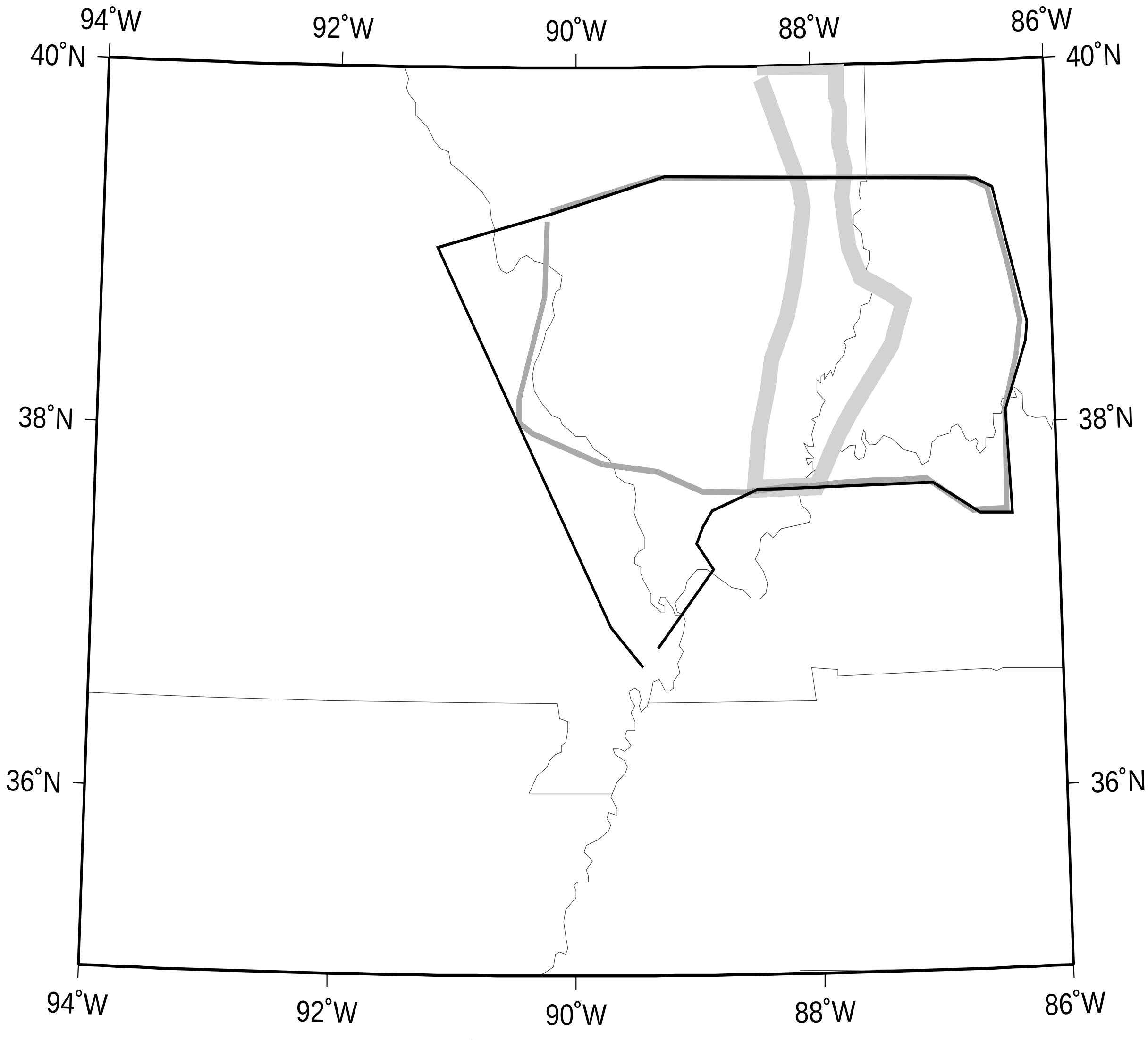

Figure 2-13. Alternative geometries of the Wabash seismic sources (narrow, intermediate, and broad geometries).

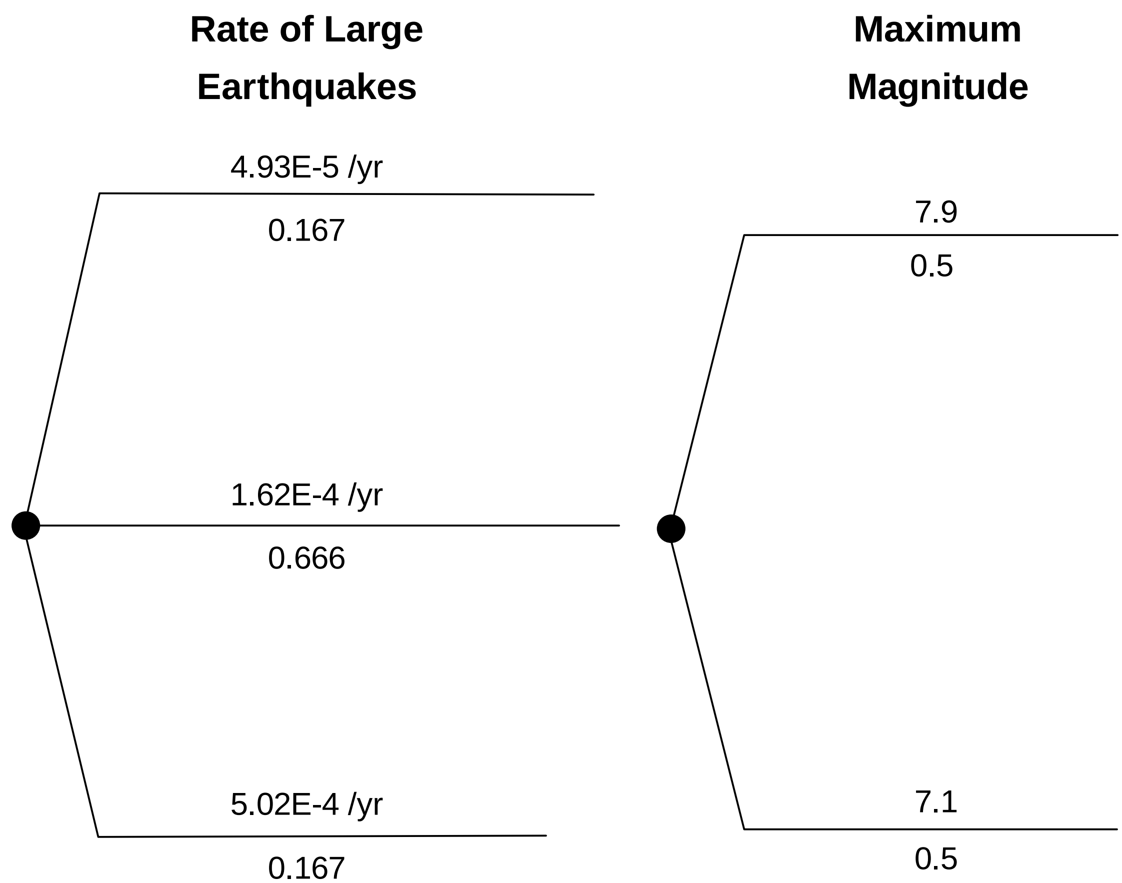

Figure 2-14. Logic tree for the rate of large earthquakes and the maximum magnitude in the SE Flank fault (also known as Crittenden County fault.

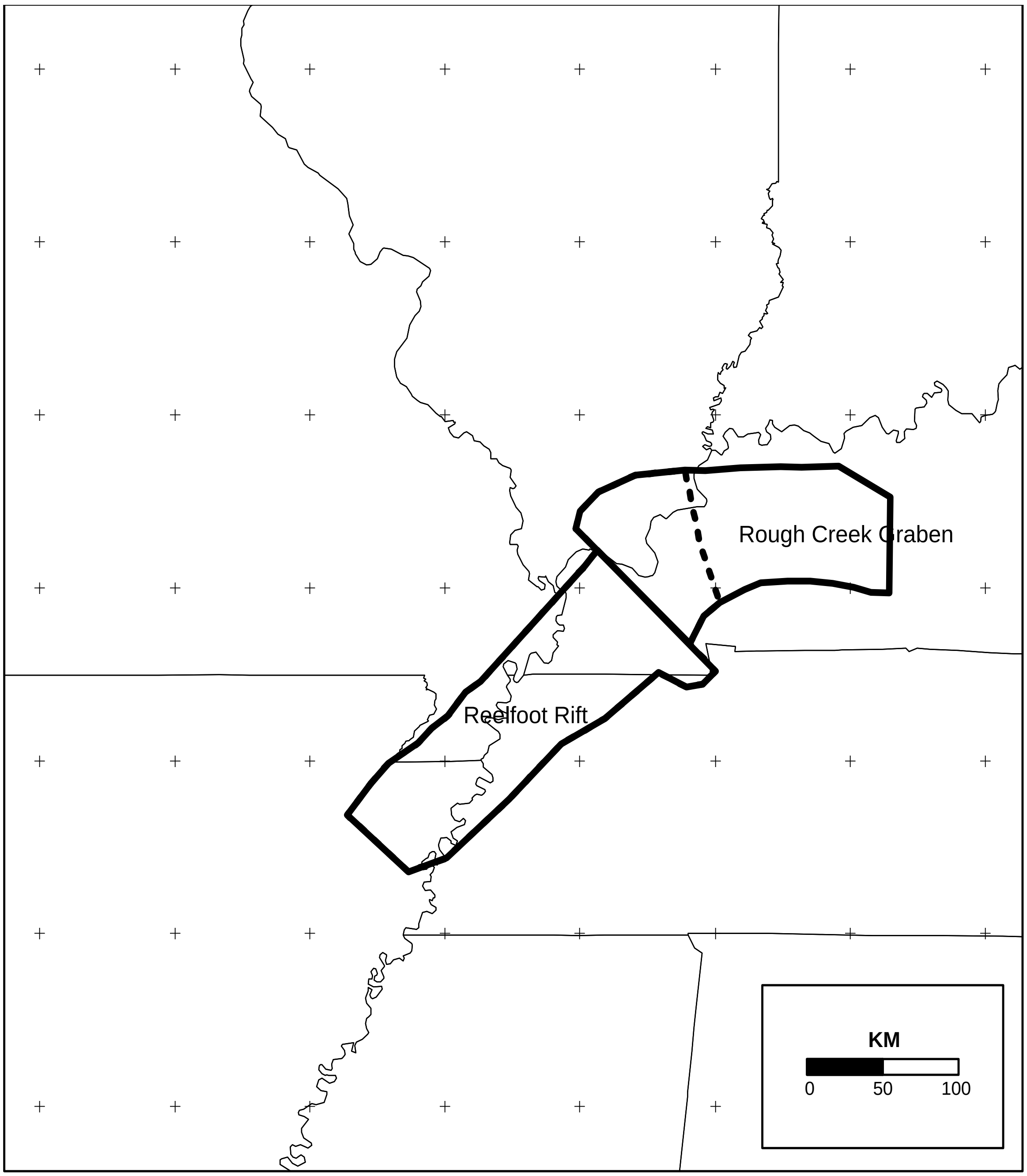

Figure 2-15. Map showing the two alternative locations of the boundary between the Reelfoot rift and the Rough Creek graben. Solid, boundary based on seismicity (60% weight); dashed, boundary based on geology (40% weight).

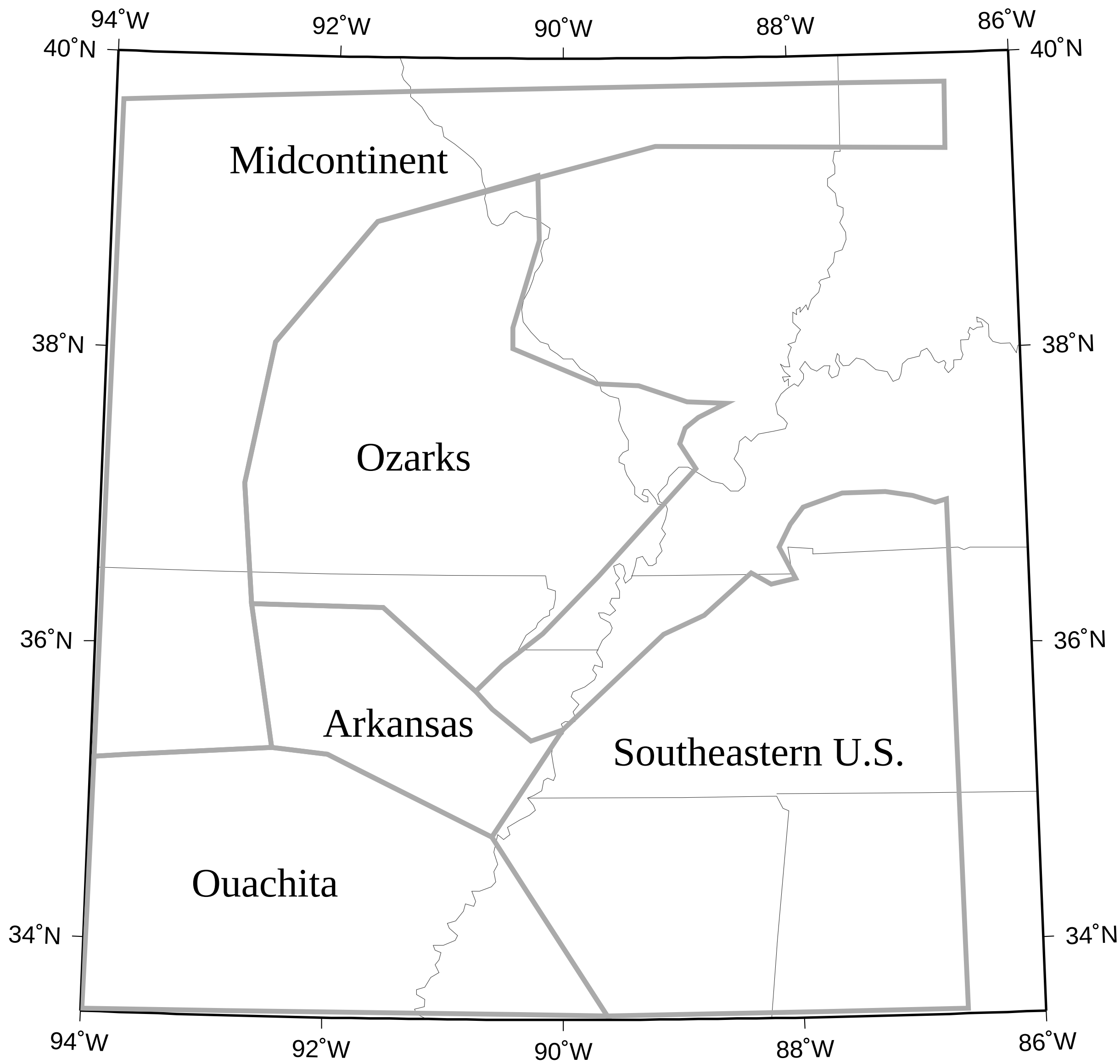

Figure 2-16. Background seismic sources.

Section 3

DEVELOPMENT OF SINGLE AND DOUBLE CORNER SOURCE MODEL CEUS ATTENUATION RELATIONS FOR GENERIC HARD ROCK SITE CONDITIONS

The process of developing site and region specific attenuation relations involves exercising the stochastic point source model (Schneider et al., 1993; Toro et al., 1997; McGuire et al., 2000) for a suite of magnitudes and distances and then regressing on the predicted ground motions. Regional- and site-specific elements are introduced through the selection of appropriate model parameters and their uncertainties. Parametric uncertainty about the median ground motion regression (which includes regression uncertainty) is estimated through multiple ground motion estimates at each magnitude and distance based on random model parameters. This process results in a regression equation for median ground motions (5% damped response spectra) as a function of magnitude and distance as well as estimates of the uncertainty, both of which are required for probabilistic seismic hazard analyses. This process has been applied to a number of Department of Energy sites as well as many other commercial projects and forms the basis for a number of current CEUS attenuation relations. As a result, the process is both mature and stable, undergoing the scrutiny of widespread applications to engineered structures.

3.1 POINT SOURCE MODEL PARAMETERS

Dependent parameters for the point-source model include source depth (H), stress drop ($\Delta\sigma$), Q (f) model (deep crustal damping), kappa (shallow crustal damping), a crustal model, and a shallow profile along with nonlinear dynamic material properties parameterized through G/Gmax and hysteretic damping curves. Independent parameters are magnitude and distance, which were selected to cover the appropriate range in **M** and *R* in the hazard analyses. Three magnitudes were run (**M** 5.5, 6.5, and 7.5) over the distance range of 1 to 400 km (Table 3-1).

For the dependent parameters, base case (mean or median) values and their uncertainties are listed in Table 3-1. The source depth distribution is based on CEUS seismicity (EPRI, 1993) while the

Q(f) [$Q(f) = Q_\sigma f^\eta$] model is based on inversions of the 1988 **M** 5.8 Saguenay earthquake using the point-source model (Silva et al., 1997). WUS stress drops based on inversions of the Abrahamson and Silva (1997) empirical attenuation relation show a magnitude dependency (EPRI, 1993; Atkinson and Silva, 1997). CEUS stress drops (Table 3-1) were assumed to follow the same magnitude scaling as WUS. The **M** 5.5 stress drop was set to 160 bars to correspond to Atkinson's (1993) value (adjusted to the midcontinent crustal model (Table 3-1), which is based on high frequency spectral levels from CEUS earthquakes. In her database of CEUS earthquakes the mean magnitude is about 5.5. Interestingly, these stress drop values result in an average (over magnitude) difference of about a factor of two between CEUS (122 bars, Table 3-1) and WUS (65 bars, Silva et al., 1997), in agreement with Hanks and Johnston's (1992) analysis of intensity data.

The kappa value for the CEUS rock site is 0.006 sec (Table 3-1), and is based on analyses of recordings at hard rock CEUS sites (EPRI, 1993). The variability in kappa σ_{ln} = 0.30, is assumed to be the same in WUS and CEUS and is the observed variability in kappa values at rock sites in northern California that recorded the **M** 6.9 1989 Loma Prieta earthquake (EPRI, 1993). While this uncertainty of 0.3 for kappa may seem low to characterize both epistemic (uncertainty in the median value) and aleatory (uncertainty about the median value) variability in a site specific kappa value, the point-source modeling uncertainty (Silva et al., 1997) already accommodates the effects of kappa variability. This arises because a fixed kappa value of 0.03 sec was used to characterize the linear rock damping at all rock sites in the validation exercises. As a result, site specific departures of kappa from the assumed constant value of 0.03 sec increases model deviations from recorded motions, and this results in larger estimates of model uncertainty. While it is possible that the total variability in the attenuation relations is overestimated due to this probable double counting, validations are sparse for the CEUS (and are nonexistent for deep soil sites), and are sparse for **M** larger than about 7.0 in the WUS. As a result, assessment and partition of appropriate variability is not an unambiguous issue, particularly in the CEUS, and the approach taken here was to follow prudent design practice and not underestimate uncertainty.

The crustal model used is appropriate for hard rock conditions in the central and eastern U.S. (EPRI, 1993). This model is shown in Figure 3-1, contrasted with a generic soft rock (WUS) profile (Silva et al., 1997). The CEUS profile is significantly stiffer than the WUS profile for depths less than about 4.5 km.

To include the effects of profile variability on the computed motions, the shallow portion of the profile is randomized. To illustrate the profile variability, Figure 3-2 shows median and $\pm 1\sigma$ shear-wave velocity profiles based on 30 random profiles for the WUS and CEUS rock sites (Figure 3-1). The profile randomization scheme was developed by Toro and is based on a probabilistic model of velocity profiles, which was developed on the basis of more than 500 measured profiles (EPRI, 1993; Silva et al., 1997). Separate model parameters have been obtained for WUS rock (both hard and soft) as well as soil conditions. For WUS rock the soft rock model was used. For the CEUS profile, the WUS hard rock model was used, since there are few, if any, shallow CEUS rock geotechnical profiles with which to develop statistics on variability.

The profile variability models for rock are based on a probabilistic analysis of all rock profiles in the database and therefore are appropriate for generic applications. Site-specific applications would likely result in a lower variability that reflects random (aleatory) variations over the dimensions of a foundation (or to a foundation dimension extending outside the footprint) as well as uncertainty in the mean or base case profile (epistemic). To develop these non-generic or small area models, multiple closely spaced holes are necessary. Such an analysis was undertaken at a deep soil site in the CEUS, and a footprint correlation model was developed (Silva et al., 1997). However, similar data are not currently available for rock sites. The use of a generic statistical model for both WUS and CEUS rock sites therefore may also contribute to an overestimate of the variability in the rock outcrop attenuation relations.

3.2 ATTENUATION RELATIONS

The functional form used in the regression analyses accommodates both magnitude saturation, due to both a magnitude-dependent stress drop and potential nonlinear response, and a magnitude- dependent, far-field attenuation (Table 3-1):

$$\ln(y) = C_1 + C_2 M + (C_6 + C_7 M) \cdot \ln (R + e^{C_4}) + C_{10} (M - 6)^2 \qquad (3\text{-}1)$$

where R is taken as the closest distance to the surface projection of the rupture (Boore et al., 1997). In arriving at this functional form, about 15 variations were used in regression analyses. This particular form resulted in an optimum combination of low sigma, accommodation of significant trends with **M** and R, stability over oscillator frequency (smoothness in spectral shape), and simplicity. The fictitious depth term, C_4 in Equation 3-1, appears to be related to nonlinear site response, being nearly constant for CEUS rock (with a value near 3) and increasing strongly with frequency for soft rock and for soil profiles (Silva et al., 1999). For the CEUS both single and double corner source models (Atkinson and Boore, 1995) were run to accommodate epistemic uncertainties in CEUS source processes.

To illustrate the nature of the fits to the simulations as well as the distribution about the regression lines, Figures 3-3 shows peak accelerations **M** 7.5 for the CEUS single corner source model rock conditions. In general, the model captures the trends in the simulations for the hard rock site conditions. The increase in variability about the regression line at large distance is a result of the variability in Q(f) while the large variability at close distance is due to the range in source depth.

3.2.1 Attenuation Relations for CEUS Single and Double Corner Source Rock Site Conditions.

Attenuation curves of peak acceleration for M 5.5, 6.5, and 7.5 for CEUS Single and Double Corner source models and rock site conditions predicted by the regression equations are shown in Figures 3-4a and 3-4b respectively. For the single corner source model, magnitude saturation at close distances is apparent in the decreasing jumps in peak acceleration as M increases (Figure 3-4a). This is due principally to the magnitude dependent stress drops (Tables 3-1). For the double corner CEUS relation, the implied stress drop associated with high frequency ($f \geq 1$ Hz) ground motion is independent of magnitude with a value of about 150 bars (for the CEUS crustal model; Figure 3-1, Table 3-2). This results in significantly higher large magnitude high frequency motions (Boore and Atkinson, 1992; McGuire et al., 2000) as well as constant magnitude scaling

(Figure 3-4b). The CEUS single corner relation shows lower peak accelerations, particularly at large magnitude, than the Toro et al., 1997 and EPRI, 1993 relations. The difference results from the assumption of decreasing stress drop with increasing magnitude (Table 3-1). Toro et al. (1997) used a constant stress drop of 120 bars, perhaps resulting in motions that may be too high at large magnitudes and somewhat low at small magnitudes. Tables 3-3 and 3-4 list the regression coefficients along with the uncertainty due to parametric variability and repression fit. For the CEUS double corner source model, since variabilities were not available for the low and high frequency stress drops (corner frequencies), the single corner parametric variability was assumed to be appropriate.

To illustrate the resulting spectra for typical conditions, Figure3-5a shows spectral accelerations (5% damping) at a distance of 10 km for magnitudes 5.5, 6.5, and 7.5 for the CEUS single corner source model and rock site conditions. Since the regression coefficients were not smoothed (Equation 3-1), some of the crustal resonances are present in the spectra. For M 6.5, Figure 3-5b shows median and ± 1 σ estimates of the CEUS single corner rock site spectra. Interestingly, the logarithmic standard deviation displayed in Figure 3-5b decreases at low frequency, which is opposite the trend in most empirical WUS regressions (Abrahamson and Shedlock, 1997). This is due to the variability in stress drop being the major contributor to variability in the ground motions (Silva, 1992). The modeling uncertainty, however, increases with decreasing frequency (Silva et al., 1997) and, when combined with the parametric uncertainty, reverses the trend exhibited in Figure 3-5b. Apparently neither the model nor regressions on recorded motions capture deterministic elements in the WUS strong ground motions at low frequency. Interesting, the empirical relation of Campbell (1997), when including depth to basement material (V_S = 3 km/sec) results in a largely frequency-independent sigma. Since the sigma is computed over all site conditions, the depth dependency suggests that the effects of deep sedimentary basins may not be fully captured in the other empirical relations, which neglect such a term.

For the CEUS double corner source model and rock site conditions, Figures 3-6a and 3-6b show corresponding plots (Table 3-4). The differences in motions between the two source models depends on magnitude as well as frequency. The single corner source model generally shows larger low frequency motions and smaller high frrequency motions than the double corner source model (McGuire et al., 2000), with the difference being greatest at large magnitude ($M \geq 6.5$). The large difference in ground motion variabilities between the single and double corner source models (Figures 3-5b and 3-6b) reflects the large contribution of stress drop variability. This variability is not included in the double corner estimates of variability.

Logarithmic (natural log units) uncertainties for both WUS and CEUS rock site conditions are shown in Figure 3-7. The parametric sigma reflects variation about the median regression over the magnitude and distances listed in Table 3-1. It includes only the variability in motions due to parametric variability as well as goodness-of-fit using the functional form shown in Equation 3-1. The total variability includes the modeling uncertainty which was estimated by modeling (using the single corner frequency source model) recorded motions from 18 earthquakes (WUS and CEUS) at about 500 sites in the rupture distance range of about 1 to 400 km (Silva et al., 1997). The total uncertainty is used in the hazard calculations and is assumed to be the same for the single and double corner source models.

3.3 USE OF ATTENUATION EQUATIONS IN HAZARD CALCULATIONS

The probabilistic hazard calculations performed in Section 5 for the development of scenario spectra for Saint Louis and Memphis utilize both the single-corner and double-corner models documented here, with weights of 2/3 and 1/3, respectively. The difference between these two models provides a representation of the epistemic uncertainty in ground-motion prediction at rock-sites in the Central and Easter United States. The probabilistic hazard calculations performed in Section 6 for the development of regional seismic hazard maps utilize the single-corner model alone.

The calculations in both Sections 5 and 6 utilize the total sigma (parametric+modeling) shown in Figure 3-7, rather than the parametric sigma given in Tables 3-3 and 3-4. As discussed earlier, these sigma values may over-estimate the aleatory uncertainty. The net effect on the combined (epistemic+aleatory) uncertainty is not believed to be large.

3.4 REFERENCES

Abrahamson, N.A and K.M. Shedlock (1997). “Overview.” *Seis. Research Lett.*, 68(1), 9-23.

Abrahamson, N.A. and W.J. Silva (1997). “Empirical response spectral attenuation relations for shallow crustal earthquakes.” *Seism. Soc. Am.*, 68(1), 94-127.

Atkinson, G.M and W.J. Silva (1997). "An empirical study of earthquake source spectra for California earthquakes." *Bull. Seism. Soc. Am.* 87(1), 97-113.

Atkinson, G.M. and Boore, D.M. (1995). "Ground motion relations for eastern North America." *Bull. Seism. Soc. Am.*, 85(1), 17-30.

Atkinson, G.M. (1993). "Source spectra for earthquakes in eastern North America." *Bull. Seism. Soc. Am.*, 83(6), 1778-1798.

Boore, D.M, and W.B. Joyner (1997). “Site amplifications for generic rock sites.” *Bull. Seism. Soc. Am.*, 87(2), 327-341.

Boore, D.M., W.B. Joyner and T.E. Fumal (1997). "Equations for estimating horizontal response spectra and peak acceleration from Western North American earthquakes: A summary of recent work." *Seism. Res. Lett.* 68(1), 128-153.

Boore, D.M., Atkinson, G.M. (1992). "Source spectra for the 1988 Saguenay, Quebec, earthquakes." *Bull. Seism. Soc. Am.*, 82(2), 683-719.

Campbell, K W. (1997). "Empirical near-source attenuation relationships for horizontal and vertical components of peak ground acceleration, peak ground velocity, and pseudo-absolute acceleration response spectra." *Seism. Soc. Am.*, 68(1), 154-176.

Electric Power Research Institute (1993). "Guidelines for determining design basis ground motions." Palo Alto, Calif: Electric Power Research Institute, vol. 1-5, EPRI TR-102293.
vol. 1: Methodology and guidelines for estimating earthquake ground motion in eastern NA.
vol. 2: Appendices for ground motion estimation.
vol. 3: Appendices for field investigations.
vol. 4: Appendices for laboratory investigations.
vol. 5: Quantification of seismic source effects.

Hanks, T.C. and A.C. Johnston (1992). “Common features of the excitation and propagation of strong ground motion for north American earthquakes.” *Bull. Seism. Soc. Am.*, 82(1), 1-23.

McGuire, R.K., W. J. Silva, and C. Costantino (2000). “Technical Basis for Revision of Regulatory Guidance on Design Ground Motions.” Report to US Nuclear Regulatory Commission, in press.

Schneider, J.F., W.J. Silva, and C.L. Stark (1993). Ground motion model for the 1989 M 6.9 Loma Prieta earthquake including effects of source, path and site. *Earthquake Spectra*, 9(2), 251-287.

SHAKE (1992). "*A computer program for conducting equivalent linear seismic response analyses of horizontally layered soil deposits*." Sponsored by Structures Building and Fire Research Lab., Nat'l Institute of Standards and Technology, Gaithersburg, Maryland. Modifications by I. Idriss and J. Sun.

Silva, W.J. and R. Darragh (1995). "Engineering characterization of earthquake strong ground motion recorded at rock sites." Palo Alto, Calif: Electric Power Research Institute, TR-102261.

Silva, W.J. (1997). "Characteristics of vertical strong ground motions for applications to engineering design." *Proc. Of the FHWA/NCEER Workshop on the Nat'l Rep. Of Seismic Ground Motion for New and Existing Highway Facilities, Technical Report NCEER-97-0010.*

Silva, W.J., N. Abrahamson, G. Toro, C. Costantino (1997). "Description and validation of the stochastic ground motion model." Submitted to Brookhaven National Laboratory, Associated Universities, Inc. Upton, New York.

Silva, W.J. (1992). "Factors controlling strong ground motions and their associated uncertainties." Dynamic Analysis and Design Considerations for High Level Nuclear Waste Repositories, *ASCE* 132-161.

Toro, G.R., N.A. Abrahamson, and J.F. Schneider (1997). "Model of strong ground motions from earthquakes in Central and Eastern North America: Best estimates and uncertainties." *Seismological Research Let.*, 68(1), 41-57.

Vucetic, M. and R. Dobry (1991). "Effects of Soil Plasticity on Cyclic Response," *Journal of Geotechnical Engineering, ASCE,* 117(1), 89-107.

Wald, D.J. and T.H. Heaton (1994). "A dislocation model of the 1994 Northridge, California, earthquake determined from strong ground motions." *U.S. Geological Survey,* Open-File Rpt. 94-278.

Table 3-1
PARAMETERS FOR CEUS ROCK OUTCROP SIMULATIONS

M	5.5, 6.5, 7.5
D(km)	1, 5, 10, 20, 50, 75, 100, 200, 400

30 simulations for each M, *R* pair = 810 runs

Randomly vary source depth, $\Delta\sigma$, kappa, Q_o, η, profile

Depth, $\sigma_{\ln H} = 0.6$, $\bar{H}$ (M > 5) = 10 km; Intraplate Seismicity (EPRI, 1993)

M	Lower Bound (km)	$\bar{H}$ (km)	Upper Bound (km)
5.5	3	8	30
6.5	4	10	30
7.5	5	12	30

$\Delta\sigma$, $\sigma_{\ln\Delta\sigma} = 0.7$ (EPRI, 1993)

M	$\Delta\sigma$ (bars)
5.5	160
6.5	120
7.5	95

AVG. $\Delta\sigma$ (bars) = 122; Assumes M 5.5 = 160 bars (Atkinson, 1993) with magnitude scaling taken from WUS (Silva et al., 1997)

Q(s), $\overline{Q_o} = 351$, *Saguenay earthquake inversions*; $\sigma_{lnQ_o} = 0.4$, (Silva et al., 1997)

$\eta = 0.84$, *Saguenay earthquake inversions*; $\sigma_\eta = 0$, (Silva et al., 1997)

Varying Q_o only is sufficient, since ± 1 σ covers range of CEUS inversions from 1 to 20 Hz

Kappa, $\bar{\kappa} = 0.006$ sec $\sigma_{\ln\kappa} = 0.3$, (EPRI, 1993)

Profile, Midcontinent Crust (EPRI, 1993), randomize to 300m

Geometrical attenuation $R^{-(a + b M)}$, a = 1.0296, b = -0.0422
$R^{-(a + b M)/2}$, R > 100 km

Based on inversions of the Abrahamson and Silva (1997) relation

Table 3-2 CEUS CRUSTAL MODEL (EPRI, 1993 MIDCONTINENT)		
Thickness (km)	V_S (km/sec)	Density (cgs)
1.0	2.830	2.52
11.0	3.520	2.71
28.0	3.750	2.78
	4.620	3.35

TABLE 3-3 ENA SINGLE CORNER FREQUENCY ROCK ATTENUATION COEFFICIENTS

FREQ.(Hz)	C1	C2	C4	C5	C6	C7	C8	C10	SIGMA
0.20	-16.20991	2.49652	2.70000	.00000	-1.58692	.05635	.00000	-.59273	.4167
0.40	-10.16041	1.83310	2.80000	.00000	-1.87976	.08425	.00000	-.57716	.5078
0.50	-7.71149	1.54904	2.90000	.00000	-2.03483	.09820	.00000	-.51778	.5194
0.60	-6.08736	1.33854	2.90000	.00000	-2.11588	.10738	.00000	-.46899	.5220
1.00	-1.84398	.81332	3.00000	.00000	-2.44002	.14132	.00000	-.35788	.5276
1.30	.00430	.57674	3.00000	.00000	-2.57387	.15757	.00000	-.29458	.5581
2.00	2.43166	.27522	3.00000	.00000	-2.75419	.17904	.00000	-.19872	.5634
2.50	3.39155	.16089	3.00000	.00000	-2.83133	.18792	.00000	-.18914	.5783
3.00	4.07443	.07375	3.00000	.00000	-2.89207	.19480	.00000	-.13571	.5751
4.00	5.29015	-.02768	3.10000	.00000	-3.05076	.20786	.00000	-.13790	.5827
5.00	5.81926	-.07821	3.10000	.00000	-3.09271	.21166	.00000	-.13063	.5888
6.00	6.14411	-.10668	3.10000	.00000	-3.12637	.21465	.00000	-.11957	.5922
7.00	6.45032	-.13433	3.10000	.00000	-3.15042	.21655	.00000	-.11286	.5961
8.00	6.64633	-.14804	3.10000	.00000	-3.17080	.21812	.00000	-.10990	.6050
10.00	7.63608	-.22487	3.20000	.00000	-3.30190	.22694	.00000	-.09675	.6225
12.00	7.85878	-.23912	3.20000	.00000	-3.32890	.22891	.00000	-.09573	.6381
14.00	8.02846	-.25176	3.20000	.00000	-3.35244	.23069	.00000	-.09286	.6482
16.00	8.18918	-.26865	3.20000	.00000	-3.37280	.23226	.00000	-.08486	.6519
18.00	8.34875	-.28887	3.20000	.00000	-3.39042	.23362	.00000	-.07596	.6540
20.00	8.49056	-.30814	3.20000	.00000	-3.40586	.23484	.00000	-.06867	.6573
25.00	8.79761	-.35210	3.20000	.00000	-3.43792	.23746	.00000	-.05063	.6725
31.00	9.67978	-.42541	3.30000	.00000	-3.58327	.24787	.00000	-.04007	.6929
40.00	10.04410	-.46691	3.30000	.00000	-3.62090	.25119	.00000	-.05504	.7326
50.00	10.15048	-.49206	3.30000	.00000	-3.63049	.25133	.00000	-.01202	.7451
100.00	8.32910	-.39607	3.20000	.00000	-3.49089	.24863	.00000	-.05120	.6534
PGA	8.01521	-.36903	3.20000	.00000	-3.47207	.24770	.00000	-.06451	.6387
PGV	5.60957	.38668	2.90000	.00000	-3.12813	.24391	.00000	-.23165	.5251

TABLE 3-4. ENA DOUBLE CORNER FREQUENCY ROCK ATTENUATION COEFFICIENTS

FREQ.(Hz)	C1	C2	C4	C5	C6	C7	C8	C10	SIGMA
0.20	-13.34719	1.91021	2.70000	.00000	-1.54032	.04731	.00000	-.38333	.4167
0.40	-8.16519	1.39932	2.90000	.00000	-1.90878	.08018	.00000	-.23634	.5078
0.50	-6.80414	1.26025	2.90000	.00000	-2.02956	.09463	.00000	-.19126	.5194
0.60	-5.79540	1.15773	2.90000	.00000	-2.13792	.10789	.00000	-.16775	.5220
1.00	-3.11160	.92878	3.00000	.00000	-2.52258	.15109	.00000	-.18150	.5276
1.30	-1.84321	.81242	3.00000	.00000	-2.64729	.16641	.00000	-.18533	.5581
2.00	.27394	.60149	3.00000	.00000	-2.80138	.18464	.00000	-.16462	.5634
2.50	1.30196	.49268	3.00000	.00000	-2.86111	.19122	.00000	-.17390	.5783
3.00	2.09397	.39888	3.00000	.00000	-2.90936	.19644	.00000	-.12758	.5751
4.00	3.53297	.27523	3.10000	.00000	-3.05421	.20762	.00000	-.13367	.5827
5.00	4.22534	.20596	3.10000	.00000	-3.08968	.21056	.00000	-.12575	.5888
6.00	4.66605	.16347	3.10000	.00000	-3.12045	.21318	.00000	-.11309	.5922
7.00	5.05561	.12547	3.10000	.00000	-3.14287	.21486	.00000	-.10489	.5961
8.00	5.31133	.10435	3.10000	.00000	-3.16283	.21639	.00000	-.10100	.6050
10.00	6.37944	.01780	3.20000	.00000	-3.29300	.22504	.00000	-.08614	.6225
12.00	6.65330	-.00290	3.20000	.00000	-3.32066	.22708	.00000	-.08411	.6381
14.00	6.85694	-.01977	3.20000	.00000	-3.34480	.22891	.00000	-.08055	.6482
16.00	7.04234	-.03969	3.20000	.00000	-3.36590	.23053	.00000	-.07201	.6519
18.00	7.21940	-.06199	3.20000	.00000	-3.38405	.23190	.00000	-.06274	.6540
20.00	7.37512	-.08287	3.20000	.00000	-3.40016	.23315	.00000	-.05512	.6573
25.00	8.34631	-.17182	3.30000	.00000	-3.54380	.24297	.00000	-.03648	.6725
31.00	8.60903	-.20481	3.30000	.00000	-3.57998	.24612	.00000	-.02542	.6929
40.00	8.99110	-.24821	3.30000	.00000	-3.61832	.24933	.00000	-.03957	.7326
50.00	9.12345	-.27688	3.30000	.00000	-3.63110	.24966	.00000	.00639	.7451
100.00	7.30879	-.18410	3.20000	.00000	-3.49724	.24682	.00000	-.02587	.6534
PGA	6.98479	-.15610	3.20000	.00000	-3.47944	.24601	.00000	-.03936	.6387
PGV	6.51003	.23997	3.00000	.00000	-3.18672	.23808	.00000	-.12459	.5251

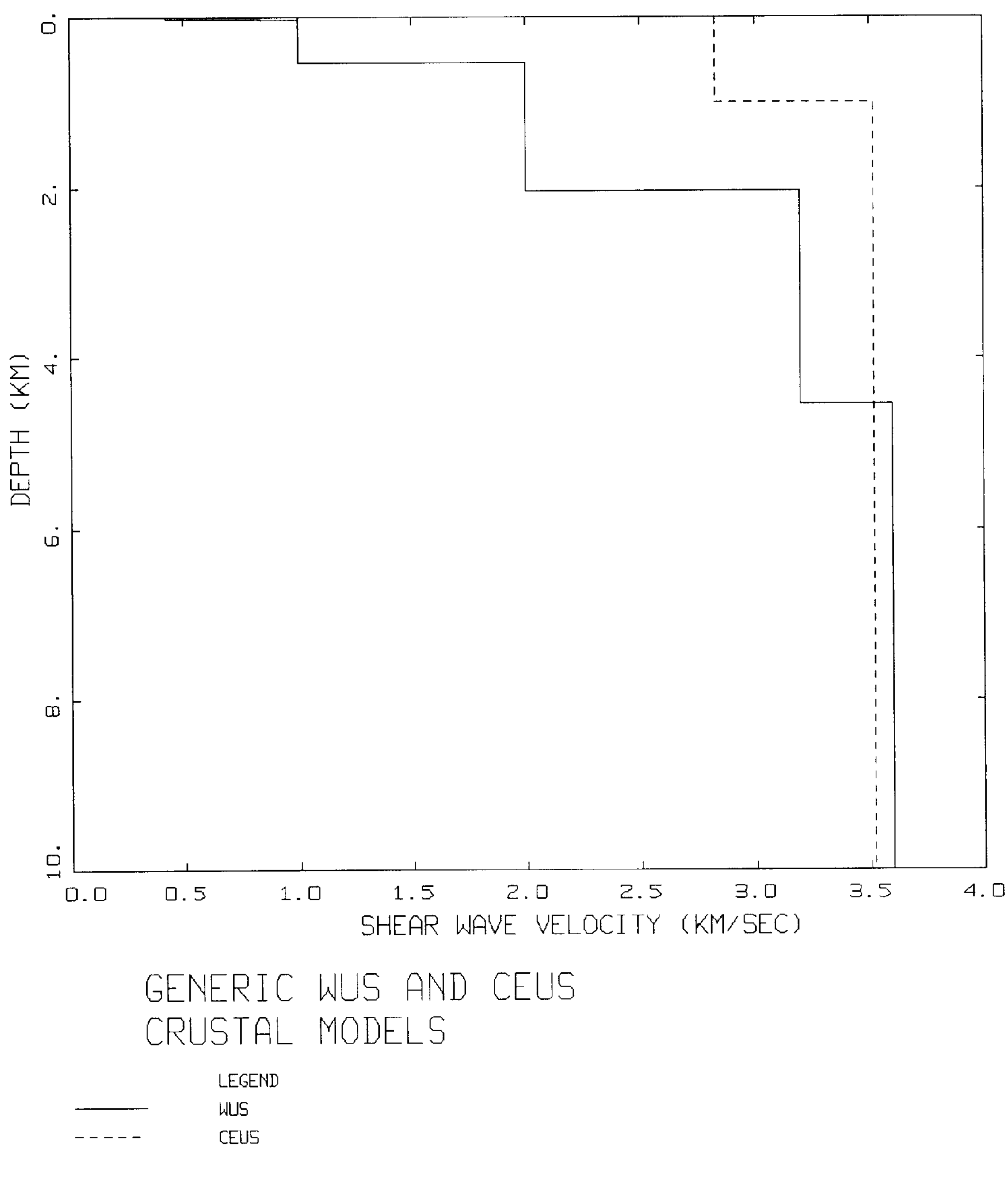

Figure 3-1. Comparison of generic shear-wave velocity profiles for WUS (Los Angeles) and CEUS crustal conditions.

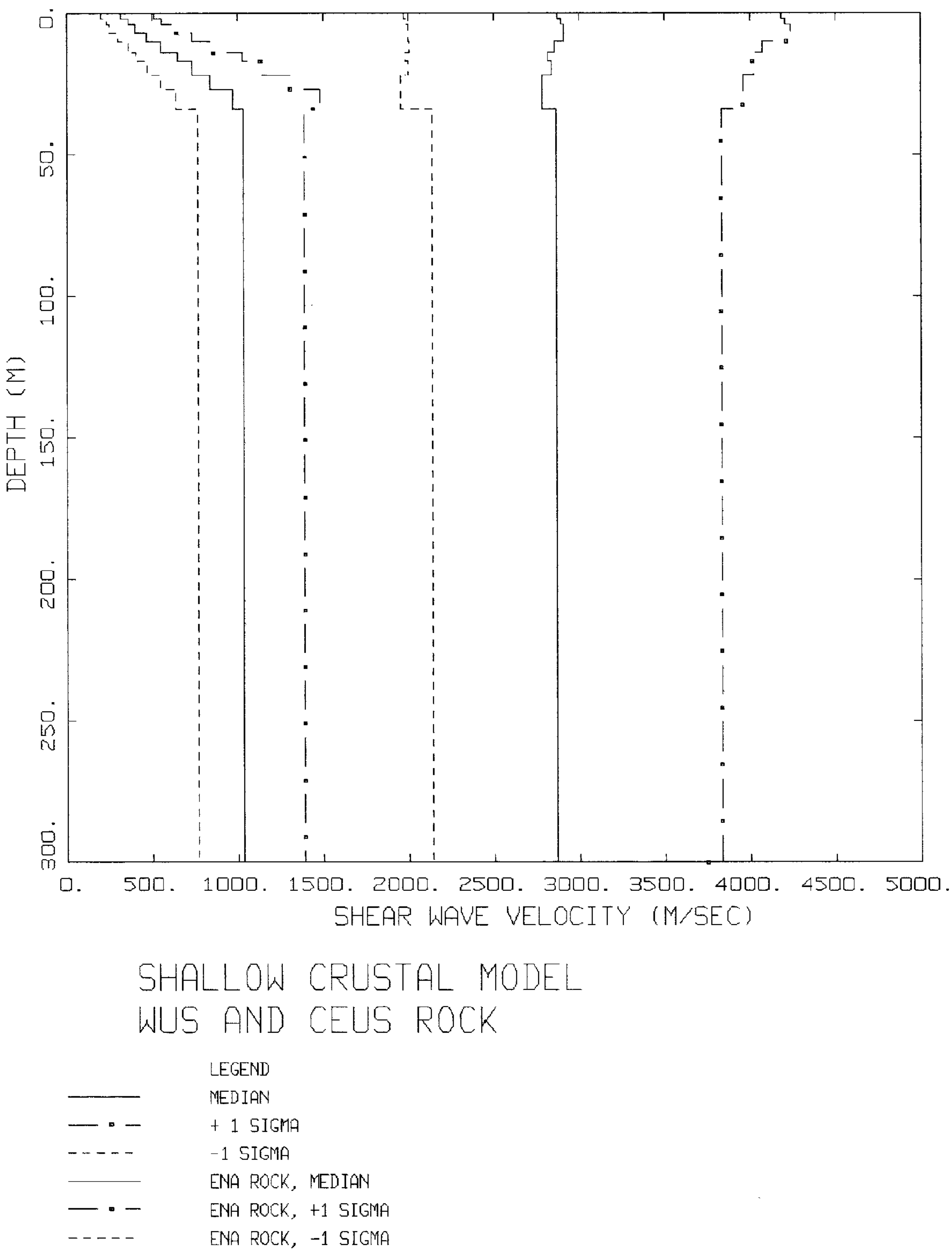

Figure 3-2. Variations in base case shallow crustal velocities. Solid lines are median estimates from a suite of randomly generated profiles (30) using base-case profiles (Figure 3-1) as input. Ranges reflect ± 1 σ estimates.

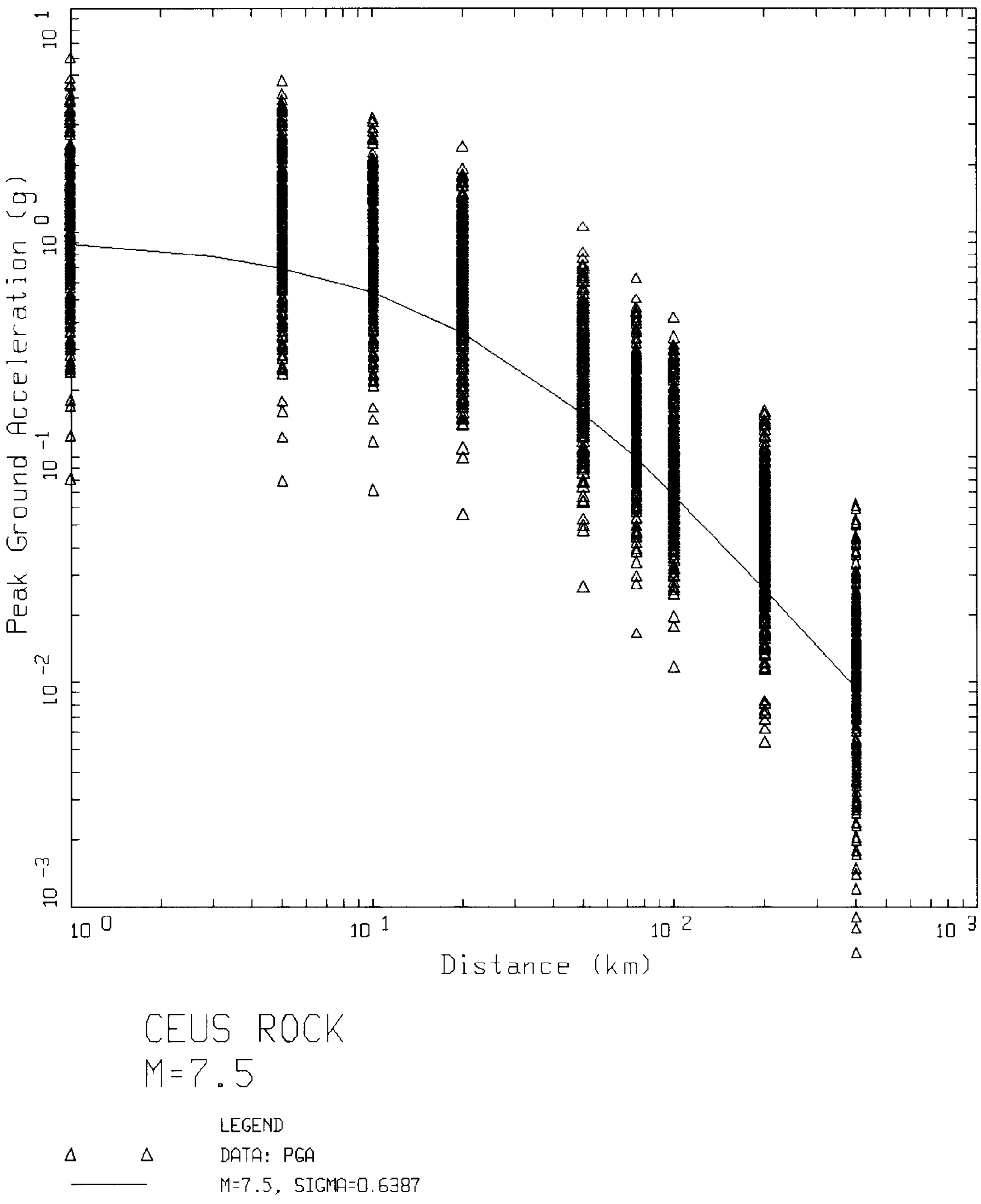

Figure 3-3. Peak acceleration estimates and regression fit at **M** 7.5 for CEUS rock site conditions (single corner source model).

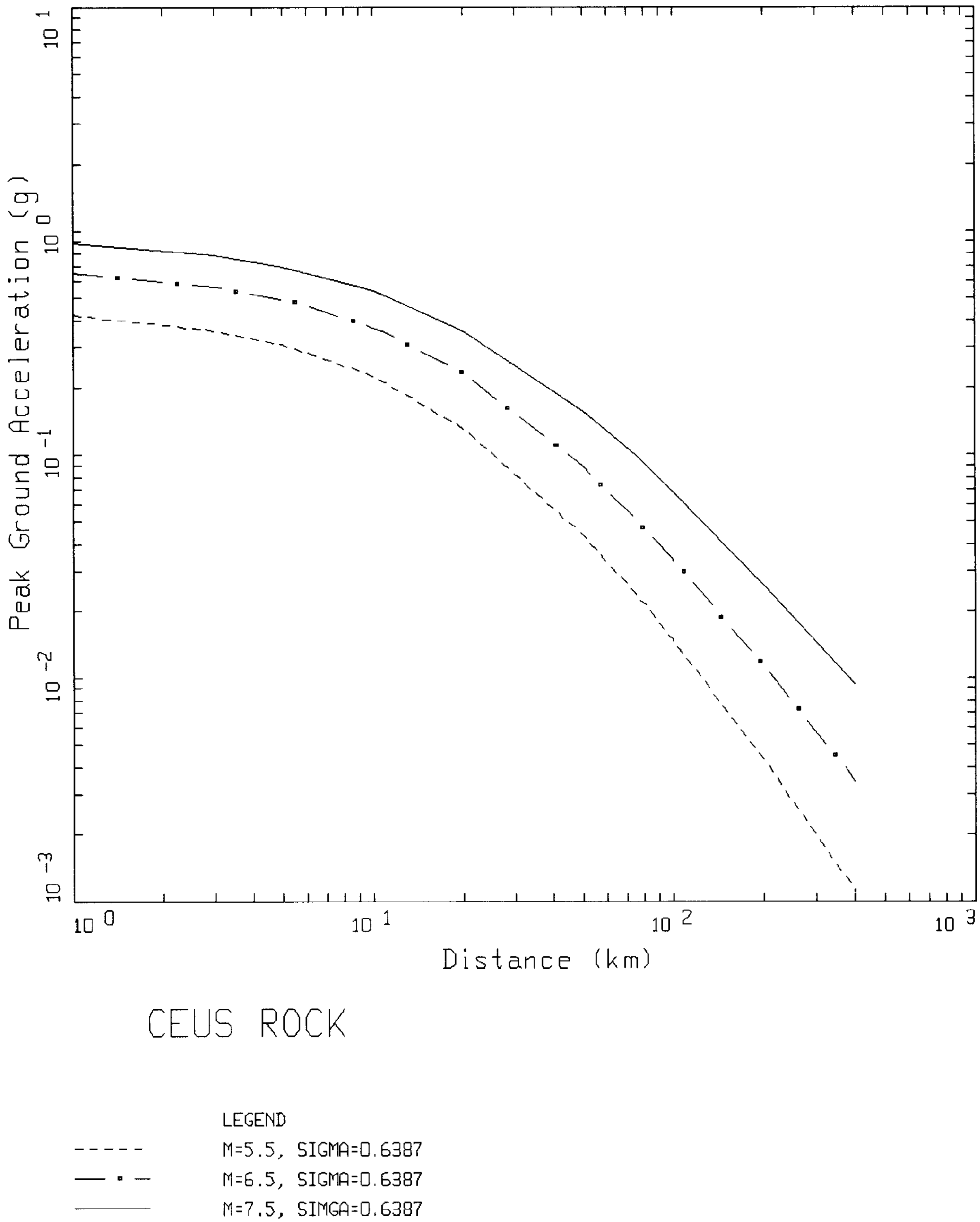

Figure 3-4a. Attenuation of median peak horizontal acceleration at **M** 5.5, 6.5, and 7.5 for CEUS rock site conditions (single corner source model).

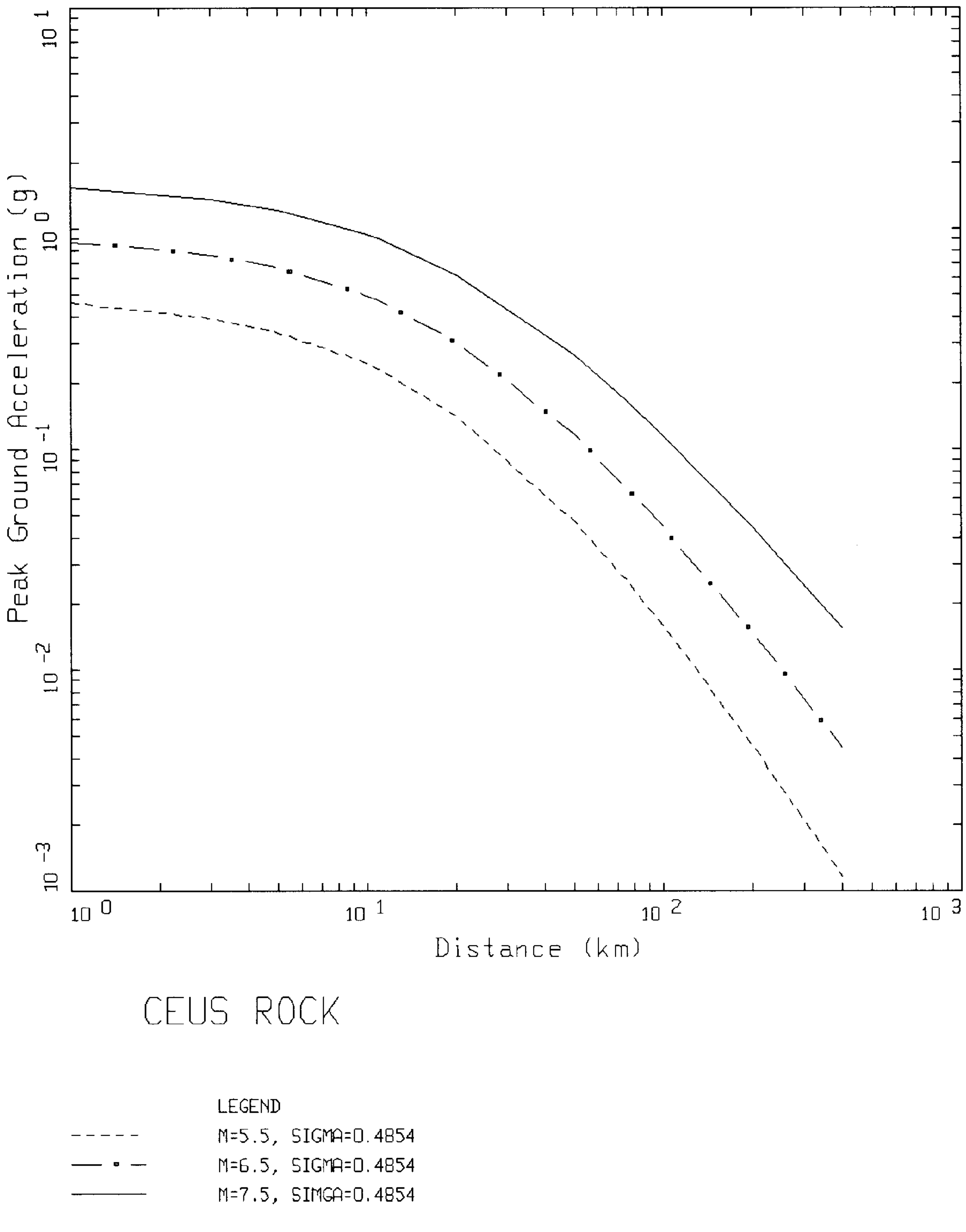

Figure 3-4b. Attenuation of median peak horizontal acceleration at **M** 5.5, 6.5, and 7.5 for CEUS rock site conditions (double corner source model).

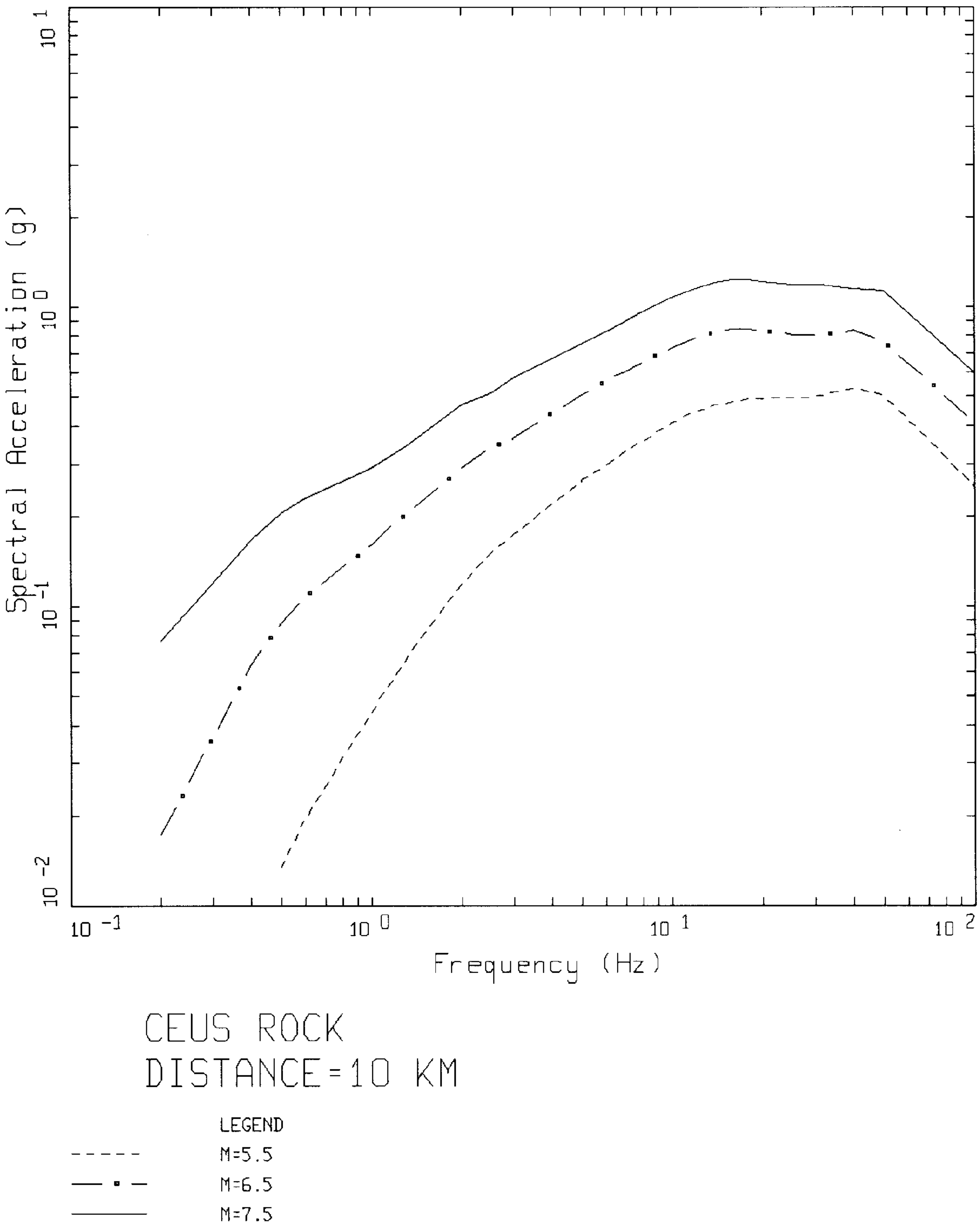

Figure 3-5a. Median response spectra (5% damping) at a distance of 10 km for magnitudes **M** 5.5, 6.5, and 7.5: CEUS rock site (single corner source model).

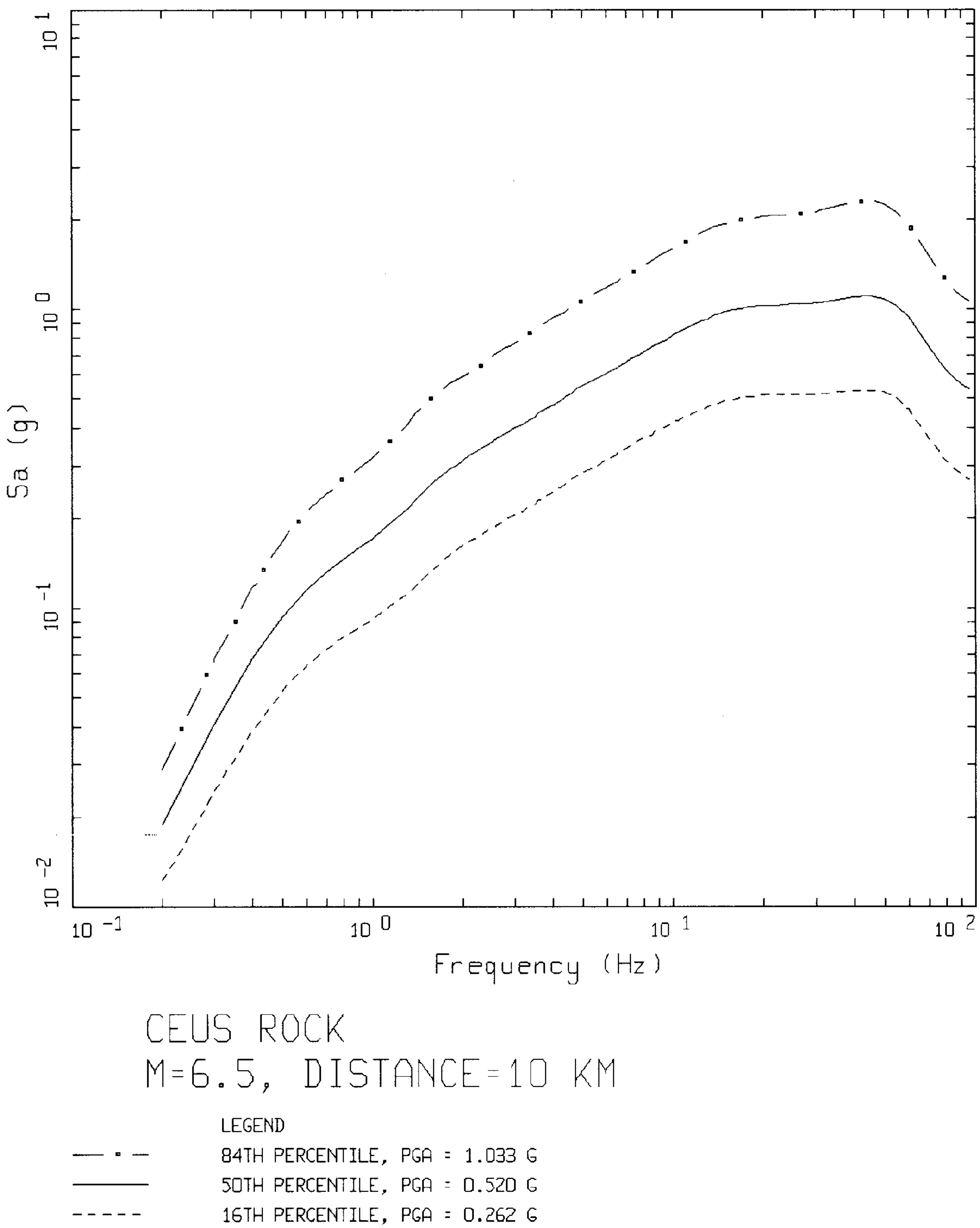

Figure 3-5b. Response spectra (5% damping) at a distance of 10 km for **M** 6.5 showing median and ± 1 σ estimates (parametric and regression uncertainty): CEUS rock site (single corner source model).

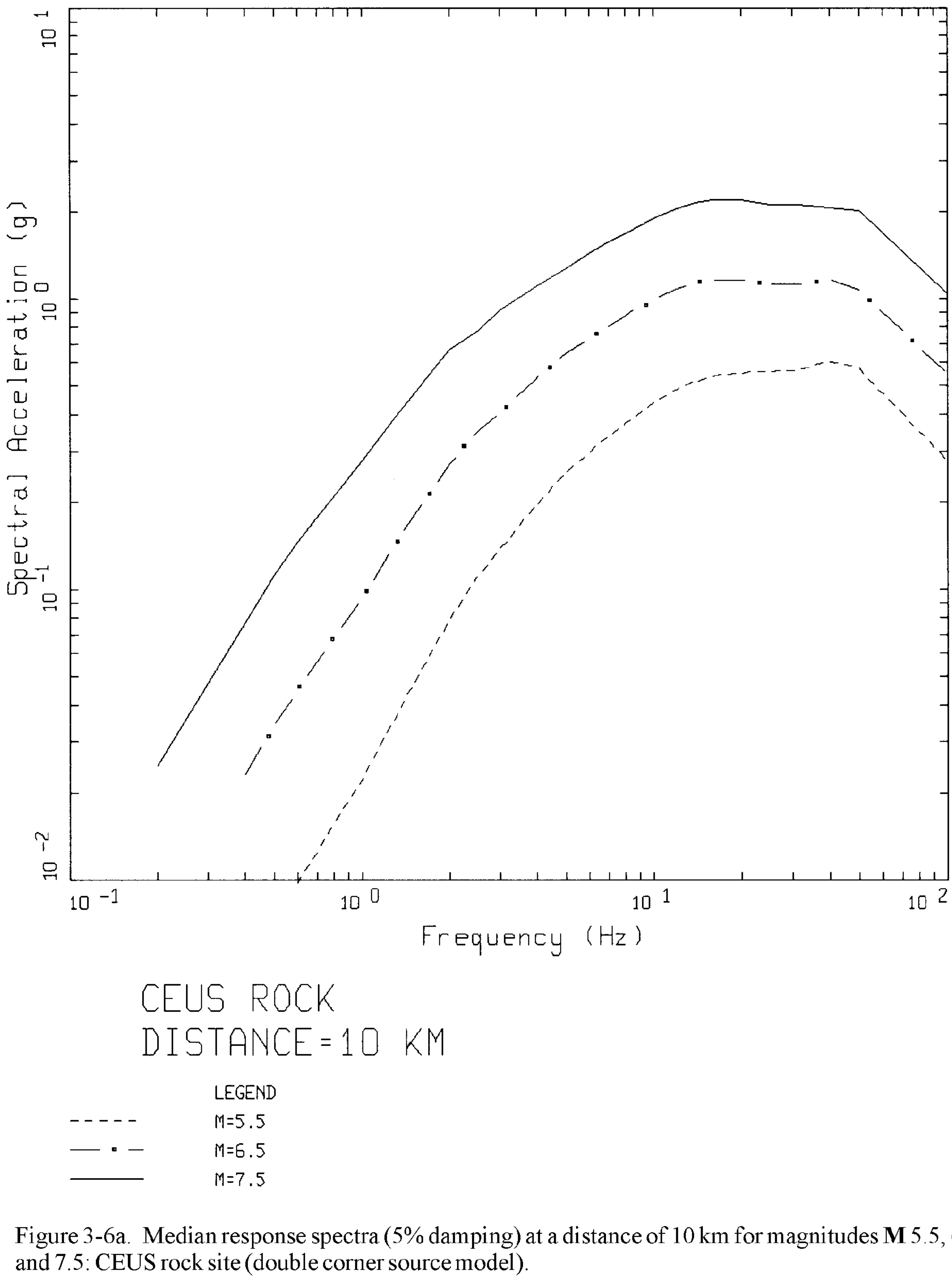

Figure 3-6a. Median response spectra (5% damping) at a distance of 10 km for magnitudes **M** 5.5, 6.5, and 7.5: CEUS rock site (double corner source model).

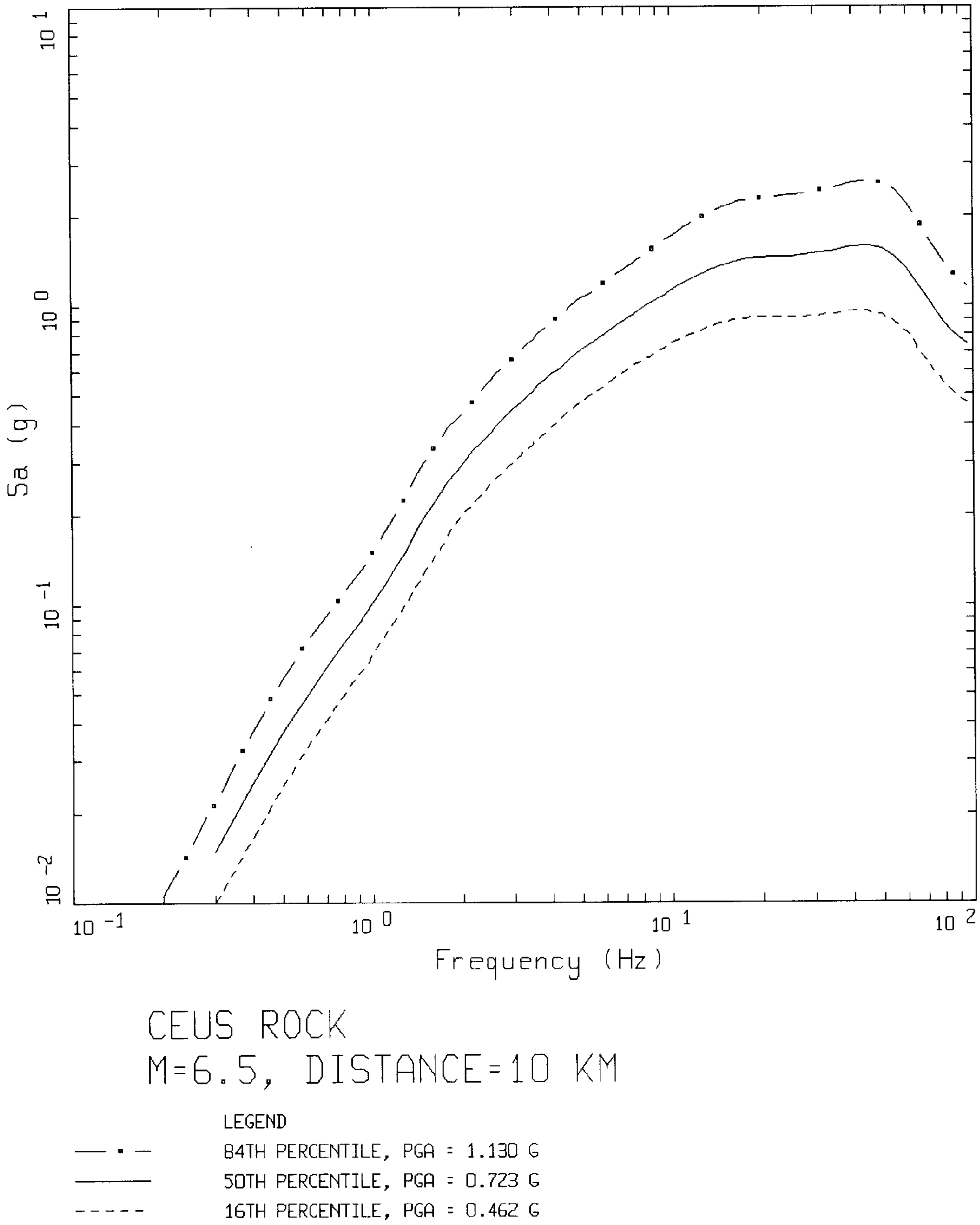

Figure 3-6b. Response spectra (5% damping) at a distance of 10 km for **M** 6.5 showing median and $\pm$ 1 σ estimates (parametric and regression uncertainty): CEUS rock site (double corner source model) variability in stress drop not included.

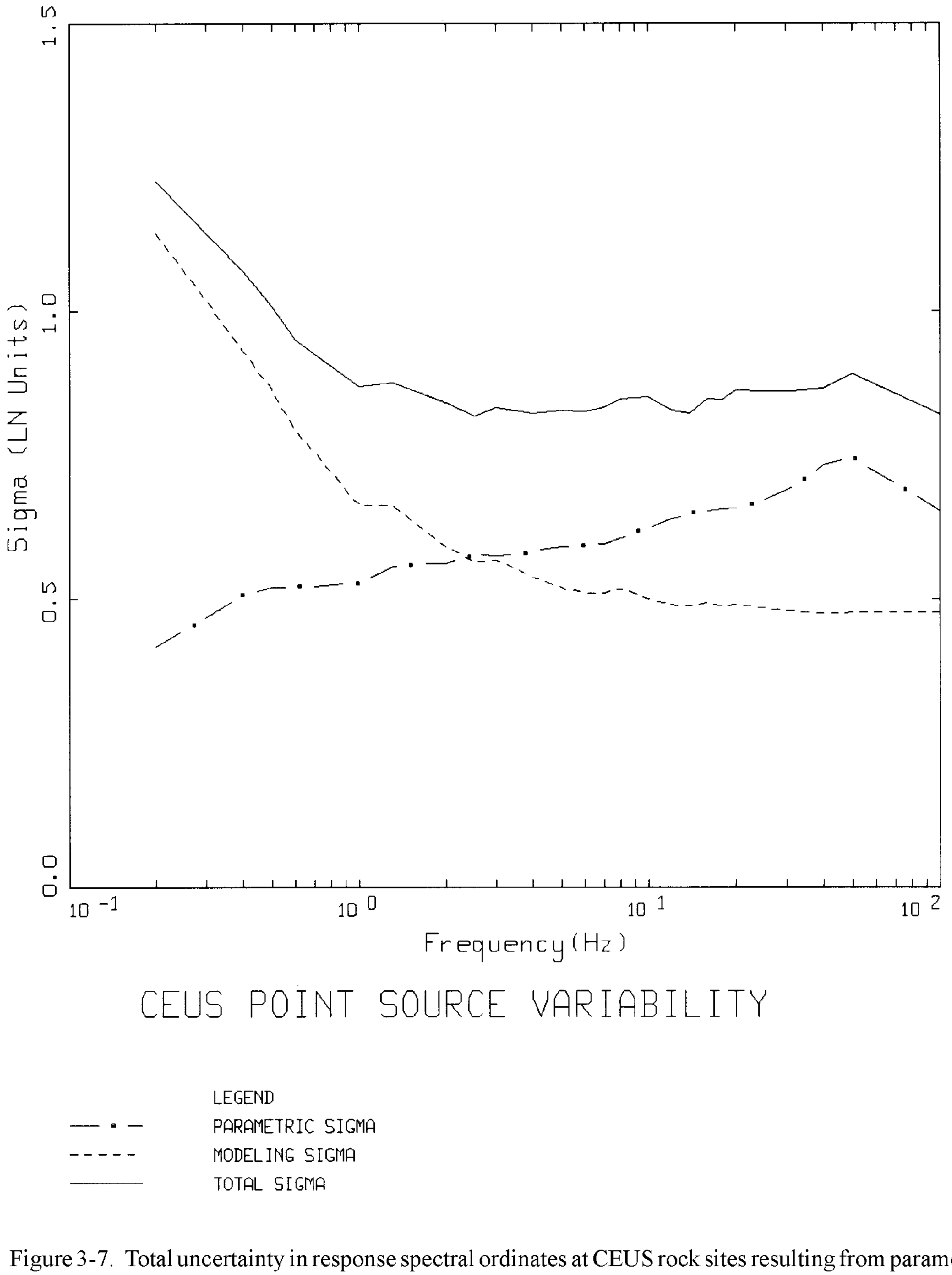

Figure 3-7. Total uncertainty in response spectral ordinates at CEUS rock sites resulting from parametric variability, regression fit, and modeling uncertainty over all magnitudes and distances (Table 3-3).

Section 4
AMPLIFICATION FACTORS BASED ON SURFACE GEOLOGY

Observations of the effects of the ground on shaking during earthquakes have a long history. Del Barrio, in the 1855 Proceedings of the University of Chile states* "...a movement.... must be modified while passing through media of different constitutions. Therefore, the earthquake effects will arrive to the surface with higher or lesser violence according to the state of aggregation of the terrain which conducted the movement. This seems to be, in fact, what we have observed in the Colchagua Province (of Chile) as well as in many other cases" (Del Barrio, 1855). In 1862, Mallet (1862) noted the effect of geology upon earthquake damage. Milne (1908) observed that in soft "damp" ground it was easy to produce vibrations of large amplitudes and long duration, while in rock it was difficult to produce vibrations of sufficient amplitude to be recorded.

Wood (1908) and Reid (1910), using apparent intensity of shaking and distribution of damage in the San Francisco Bay area during the 1906 earthquake, gave evidence that the severity of shaking can be substantially affected by the local geology and soil conditions. Gutenberg (1927, 1957) developed amplification factors representing different site geology by examining recordings of microseisms and earthquakes from instruments located on various types of ground. Figure 4-1 shows average spectral shapes (response spectral acceleration divided by peak acceleration) computed from recordings made on rock and soil sites at close distances to earthquakes in the magnitude range of about **M** 6 to 7. The differences in spectral shapes are significant and depend strongly upon the general site classifications. These variations in spectral content represent average site dependent ground motion characteristics and result from vertical variations in soil material properties (Mohraz, 1976; Seed et al., 1976; Hayashi et al., 1971). Due primarily to the limited number of records from earthquakes of different magnitudes, spectral content in terms of response spectral shapes was for some time interpreted not to depend upon magnitude nor distance, but primarily on the stiffness and depth of the local soil profile. However, with an increase in the strong motion database, it has become apparent that spectral shapes depend strongly upon magnitude as well as site conditions (Silva and Green, 1989; Idriss, 1985; Joyner

---

*Translated from the old Spanish by Professor Ricardo Dobry.

and Boore, 1982), and distance (Silva and Green, 1989), and that site effects extend to rock sites as well (Silva and Darragh, 1995; Campbell , 1988, 1985, 1981; Cranswick et al., 1985; Boatwright and Astrue, 1983).

Examples of differences in spectral content largely attributable to one-dimensional site effects at rock sites can be seen in comparisons of response spectral shapes computed from motions recorded in both active and stable tectonic regions (Silva and Darragh, 1995). Figure 4-2 shows average spectral shapes (Sa/amax) computed from recordings made on rock at close distances to large and small earthquakes. For both magnitudes (moment magnitude **M** 6.4 and 4.0), the motions recorded in Eastern North America (ENA), a stable tectonic region, show a dramatic shift in the maximum spectral amplification toward higher frequencies compared to the Western North American (WNA) motions. These differences in spectral content are significant and are interpreted as primarily resulting from differences in the shear-wave velocity and damping in the rocks directly beneath the site (Silva et al., 2000a; Silva and Darragh, 1995; Silva and Green, 1989; Boore and Atkinson, 1987; Toro and McGuire, 1987). Also evident in Figure 4-2 is the strong magnitude dependency of the response spectral shapes. The smaller earthquakes show a much narrower bandwidth. This is a consequence of higher corner frequencies for smaller magnitude earthquakes (Silva and Darragh, 1995; Silva and Green, 1989; Boore, 1983).

The difference in spectral content due to soil site effects, as shown in Figure 4-1, and due to rock site effects, as shown in Figure 4-2, are dramatic and illustrate the degree to which one-dimensional site conditions (vertical variations in dynamic material properties) control strong ground motions.

In order to capture these geologically controlled differences in ground motions, site amplification factors are developed in a manner that is appropriate for the Mississippi Embayment as well as Glacial Till covered regions north of the embayment. The amplification factors are developed for 5% damped response spectra (values at 100 Hz apply to peak acceleration) and are relative to a hard rock site. The factors accommodate nonlinear soil response and are produced as a function of expected hard rock peak acceleration values. Because of this, they may be applied to any size earthquake at any distance with knowledge only of the expected rock peak acceleration. The factors are considered appropriate for rock outcrop peak accelerations over 1g and over the frequency range of 0.1 to 100.0 Hz. At long periods, due to possible basin effects, care should be exercised in applying the factors to deep soil sites at frequencies less than about 0.5 Hz for distant (> 50 km) earthquakes.

4.1 SURFACE GEOLOGY BASED PROFILES

The study area includes the Mississippi embayment, depicted in the central portion of Figure 4-3, as well as the Ozarks of Mississippi, Arkansas, and Missouri to the west and northwest of the embayment. Also included in the study area are the loess covered uplands northeast of the embayment in Tennessee and Kentucky as well as the Glacial Till zone to the north of the embayment, which includes the city of Saint Louis and portions of Indiana.

The Mississippi embayment, the most significant site response unit in the study area, is a large wedge-shaped syncline structure that dips and fans out southward from near Cairo Illinois at the junction of the Mississippi and Ohio rivers to about the 32d parallel. The structure includes parts of Alabama, Arkansas, Illinois, Kentucky, Louisiana, Mississippi, Missouri, Tennessee, and Texas (Cushing, 1964; Grohskopf, 1955). The embayment region was periodically occupied by an arm of the sea in which as much as several thousand feet of sediment were deposited in the study area. Sediment depths in the study area range from zero to about 3,000 ft (Figure 4-4).

Within the Mississippi embayment, sediments ranging in age from Jurassic to Quaternary have been deposited. The maximum thickness of about 18,000 ft lies well south of the study area. In Louisiana and Mississippi Units ranging in age from Cretaceous to Quaternary crop out within the study area (Figure 4-3). These units of sands, clays, gravels, silts, lignite, marl, chalk, and limestone range in thickness from zero at the outcrop of Paleozoic rocks to over two thousand feet at the axis of the embayment structural trough (Cushing et al., 1964).

At New Madrid, a test well penetrated the sediments (embayment lowlands) to the Paleozoic basement rock (dolomite) at a depth of about 2,000 ft (Crone and Russ, 1979). The stratigraphic column from the well is shown in Table 4-1 and indicates the units and their approximate thicknesses. To complement the vertical section, a generalized cross-section of the embayment at the latitude of Memphis (about 30^o 15', Figure 4-3) is shown in Figure 4-5. The Figure shows the major structural units (layers) generally continuous across the embayment and thinning to the west and east with a maximum depth to paleozoic basement material of about 3,000 ft.

4.1.1 Large Scale Site Response Units

Based on the regional surface geology, past zonation work (Toro et al., 1992), examination of construction related borehole data for the city of St. Louis, Mo. By Steven McLaskie (Sverdrup Civil, Inc.; personal communication, 1999), and suggestions of Professor Glenn Rix and Dr. Salome Romero (personal communication 2000), the study area was divided into four distinct site response units (Figure 4-3). Finer scale variations are certainty present, such as in the Lowlands region (Figure 4-3) where there are small scale differences in shallow soil types ranging from meander belt deposits of the Mississippi River consisting of thick clean sands interbedded with clays near the surface to braided stream terraces of Glacial outwash. The stream terraces grade from clay to silt near the surface to clean sands and gravels at the base (30-50m) (Obermeier, 1988). Consideration of such small scale changes in surficial materials, without local measured shear-wave velocities or correlations to blow count is not warranted in view of the uncertainties in the computed response. Any differences in computed response due to small scale effects would have a large statistical uncertainty resulting from the uncertainty in inferred changes in material properties. Providing uncertainties in dynamic material properties are accommodated appropriately in estimating site effects (Roblee et al., 1996), small scale fractures, lacking site specific measurements, would reflect a large range in dynamic material properties, resulting in an averaging or smearing out of any distinct features in amplification. The four adapted large scale site response units are principally based on stastically distinct amplification (at least 20% difference over an octave or so in frequency), considering uncertainties in dynamic material properties.

4.1.1.1 Lowlands and Uplands. In the Mississippi embayment and adjacent areas recent reflection (shear-wave), downhole, crosshole, and seismic cone data have become available (Romero and Rix, 2000; Romero et al.,2000; Williams et al., 2000; Hwang et al., 1999; Schneider, 1999; Schneider and Main, 1998; Liu et al., 1997; Street et al., 1995; Dorman and Smalley, 1994; Harris et al., 1994; Dorman and Hwang, 1993) permitting, at least for the top 300 ft, estimates of median shear-wave velocity profile for the Lowlands and Uplands site response units.

For the Lowlands, Figure 4-6 shows the median and ± 1σ profiles along with a smooth model estimate (for extrapolation to greater depths). The smooth profile is taken from a WUS generic deep soil profile which is based on approximately 200 measured shear-wave velocity profiles, with a few extending to a depth of about 2000 ft. The empirical WUS deep soil profile was slightly stiffer and largely parallel to the median Lowlands profile. The smooth Lowlands profile is taken as the WUS deep soil minus a constant shear-wave velocity of 150 ft/sec. It provides an acceptably close fit to the median Lowlands profile and forms a reasonable basis to extend the profile to a depth of about 600 ft, where it merges with the Preliminary Memphis, Tennessee Reference Profile (Romero et al., 2000; personal communication). Use of the measured Lowlands profiles along with an adjusted empirical deep soil profile was adopted in the shallow portion to be more appropriate for an average Lowlands profile. The deeper portion of the Recommended Memphis Reference Profile has shear-wave velocities very similar to those inferred from the sonic log of the New Madrid Test Well (Crone and Russ, 1979) if one assumes a Poisson's ratio from the Haynes No. 1 well. Dorman and Smalley (1996), using dispersed surface waves from the **M** 4.6, 1991 Risco Missouri earthquake recorded at Memjphis and traveling in the sedimentary column (3 to 5 sec period waves), estimated shear-wave velocities to a depth of about 1 km. By combining the surface wave dispersion information with the densities and sonic velocities of the Haynes No. 1 well, they were able to estimate a general shear-wave velocity profile. The Haynes No. 1 well lies along and midpoint in the path (about 150 km long) from the source south to Memphis. The shear-wave velocities inferred from the 3 to 5 sec surface waves are likely not reliable in the upper 100 to 200m of the profile (due to the long wavelength, about 1 km) but the dispersion data do provide a good constraint on the overall deep shear-wave velocities, which are in general agreement with the Memphis Recommended profile as well.

For the Uplands site response unit, Figure 4-7 shows the median and ± 1σ shear-wave velocity profiles based upon available measurements. The smooth model is merged into the Memphis Recommended profile at a depth near 250 ft. Comparisons between the Lowlands and Uplands base case profiles are shown in Figure 4-8 to 500 ft and in Figure 4-9 to 1 km. In general the

Lowlands is significantly softer than the Uplands for depths extending to about 300 to 400 ft. In the shallower portion, top 100 to 200 ft, the Uplands consist of loess (fine glacially derived eolian silty clay) bluffs east of the Mississippi river (Figure 4-3) overlying the Jackson formation (Table 4-1). The Mississippi valley alluvium is largely absent in these areas with the increased shear-wave velocities over those of the Lowlands profile likely due to the presences of the stiffer loess.

4.1.1.2. Glacial Till. For the Glacial Till site response unit (Figure 4-3), a generic stiff profile based on measured shear-wave velocities at CEUS nuclear power plants was used (EPRI, 1993). This profile was developed to be consistent with both till and cohesionless soil sites in the CEUS. The gradient profile results in amplifications that are slightly larger than corresponding uniform velocity profiles (till like) using constant velocities averaged over the corresponding depths. The gradient shear-wave velocity profile is shown in Figure 4-10 and extends to a depth of 1,000 ft, the greatest depth of interest.

4.1.1.3. Ozark Rock. For the Ozark Rock (Figure 4-3), the implied crustal model is a generic CEUS hard rock crustal structure (Table 3-2) which forms the basis for the attenuation relations developed in Section 3. This model has a 1 km thick surficial layer with a shear-wave velocity of 2.83 km/sec. This attribute is typical of crustal models and results in a high frequency amplification of about 1.3. Because of this, it is considered a more appropriate surficial hard rock outcrop than the second layer of the embayment crustal model (Table 4-4).

4.1.2. Small Scale Site Response Units

4.1.2.1 Uplands High Shallow Velocity. Glenn Rix and Salome Romero (personal communication, 2000) have identified limited embayment Upland areas which have anomalous shallow high velocity layers, possibly due to the presence of gravels. To accommodate potential differences in response due to these shallow high velocity zones, separate profiles were developed by Dr. Romero which accommodate realistic ranges in range in impedance contrasts; their depths, sizes (amplitudes), and thicknesses. The three profiles shown in Figure 4-11 then reflect the epistemic uncertainty in the shallow high velocity Upland profiles.

4.1.2.2 Crowley's Ridge. Crowley's Ridge is distinguished stratigraphically from the Lowlands by the Lafayette formation replacing the Mississippi Valley alluvium and lying unconformally on the Jackson (Randall et al., 1988). The Lafayette formation may be typified as a generally very dense clayey sandy gravel with a blow count of about 50 and an average thickness of about 25 ft (WCC, 1991). Lacking region specific data to characterize its shallow dynamic material properties, Crowley's Ridge is assumed to be the same in response as the Uplands. The stiffer loess covering of the Uplands, compared to the Lowlands, (Figure 4-8), serving to emulate the dense sandy gravels the Lafayette formation.

4.1.3 NEHRP Categories

For comparison of the generic profiles with the NEHRP (UBC 1997) categories, Table 4-2 lists the average shear-wave velocities (based on travel time) to 30m along with the NEHRP site category (Table 4-3). Both the Lowlands and Uplands profiles classify as NEHRP category D but they do display significantly different response, particularly at high loading levels (Section 4.2.4). This is not new as both analytical and empirical amplification factors show resolvable and stable differences based on surface geology and within a single NEHRP category (Silva et al., 1999).

The Glacial Till profile as well as two of the high shallow velocity Uplands profiles are sufficiently stiff to be classified as NEHRP category C. With this interpretation, the majority of the study area would be classified as NEHRP D with the Glacial Till region as NEHRP C and the Ozark Rock area as NEHRP A (hard rock).

4.2 GEOLOGY BASED AMPLIFICATION FACTORS

Certainly the most satisfying approach to account for the effects of surficial materials on strong ground motion is empirical. Ideally, amplification factors could be developed based entirely upon observation of strong ground motion. Studies using data recorded on rock and on different classes of soil profiles, such as stiff soils and deep cohesionless soils, have demonstrated large differences in spectral amplification (Sa/amax) and in spectral velocity due to the presence of the soils (Abrahamson and Silva, 1997; Joyner and Fumal, 1984; Seed et al., 1976; Mohraz, 1976). Empirical studies of geologically based amplification factors for the San Francisco Bay area (Borcherdt and Glassmoyer, 1992; Borcherdt, 1970) and for the Los Angeles area (Silva et al., 1999; Borcherdt et al., 1997; Harmsen, 1997; Borcherdt, 1996) have shown large and stable differences in amplification. While these studies are extremely useful in a general sense, the limited number and size of earthquakes and different types of profiles as well as poorly known recording site conditions preclude relying directly upon empirical results. In particular, few data are available for very high levels of shaking and for a variety of site conditions. Also, few ground motion recording sites have detailed soil/rock profiles for which reliable soil/rock properties are available. For applications to the CEUS, an added complication is the suitability of empirical WUS site amplification to CEUS conditions (Silva et al., 1999). Because of these limitations, some form of computational analysis is desirable and direct observations of soil response can then be used as calibrations and to provide a basis for assessing the reasonableness of analytical results.

4.2.1 Methodology

The conventional computational approach in developing spectral amplification factors appropriate for specific profiles would involve selection of suitable time histories to serve as control or rock outcrop motions and a suitable nonlinear computational formulation to transmit the motion through the profile.

4.2.1.1 Equivalent-Linear Computational Scheme. The computational scheme which has been most widely employed to evaluate one-dimensional site response assumes vertically-propagating plane shear waves. Departures of soil response from a linear constitutive relation are treated in an approximate manner through the use of the equivalent-linear approach.

The equivalent-linear approach, in its present form, was introduced by Seed and Idriss (1970). This scheme is a particular application of the general equivalent linear theory introduced by Iwan (1967). Basically, the approach is to approximate a second order nonlinear equation, over a limited range of its variables, by a linear equation. Formally this is done in such a way that an average of the difference between the two systems is minimized. This was done in an ad-hoc manner for ground response modeling by defining an effective strain which is assumed to exist for the duration of the excitation. This value is usually taken as 65% of the peak time-domain strain calculated at the midpoint of each layer, using a linear analysis. Modulus and damping curves are then used to define new parameters for each layer based on the effective strain computations. The linear response calculation is repeated, new effective strains evaluated, and iterations performed until the changes in parameters are below some tolerance level. Generally a few iterations are sufficient to achieve a strain-compatible linear solution.

This stepwise analysis procedure was formalized into a one-dimensional, vertically propagating shear-wave code called SHAKE (Schnabel et al., 1972). Subsequently, this code has easily become the most widely used analysis package for one-dimensional site response calculations.

The advantages of the equivalent-linear approach are that parameterization of complex nonlinear soil models is avoided and the mathematical simplicity of linear analysis is preserved. A truly nonlinear approach requires the specification of the shapes of hysteresis curves and their cyclic dependencies. In the equivalent-linear methodology the soil data are utilized directly and, because at each iteration the problem is linear and the material properties are frequency independent, the damping is rate independent and hysteresis loops close.

While the assumptions of vertically propagating shear waves and equivalent-linear soil response certainly represent approximations to actual conditions, their combination has achieved demonstrated success in modeling observations of site effects (Schneider et al., 1993; EPRI, 1993; Silva et al., 1988; Schnabel et al., 1972).

4.2.1.2 RVT Based Computational Scheme. The computational scheme employed to compute the site response uses the stochastic model to generate the power spectral density and spectral acceleration of the rock or control motion. This motion or power spectrum is then propagated through the one-dimensional soil profile using the plane-wave propagators of Silva (1976). In this formulation only SH waves are considered. Arbitrary angles of incidence may be specified but normal incidence is used throughout the present analyses.

In order to treat possible material nonlinearities, an RVT (Random Vibration Theory) based equivalent-linear formulation is employed. Random process theory is used to predict peak time domain values of shear strain based upon the shear strain power spectrum. In this sense the procedure is analogous to the program SHAKE except that peak shear strains in SHAKE are measured in the time domain. The purely frequency domain approach obviates a time domain control motion and, perhaps just as significant, eliminates the need for a suite of analyses based on different input motions. This arises because each time domain analysis may be viewed as one realization of a random process. In this case, several realizations of the random process must be sampled to have a statistically stable estimate of site response. The realizations are usually performed by employing different control motions with approximately the same level of peak acceleration and response spectrum.

In the case of the frequency domain approach the estimates of peak shear strain as well as oscillator response are, as a result of the random process theory, fundamentally probabilistic in nature. Stable estimates of site response can then be computed by forming the ratio of spectral acceleration predicted at the surface of a soil profile to the spectral acceleration predicted for the control motion.

The procedure of generating the point-source stochastic power spectrum computing the equivalent-linear layered-soil response, and estimating peak time domain values has been incorporated into a single code termed RASCALS (Schneider et al., 1993).

4.2.2 G/Gmax and Hysteretic Damping Curves

Two sets of generic G/Gmax and hysteretic damping curves are used for the largely cohesionless (PI ≤ 30%) soils in the study area (Figure 4-3). The recent EPRI (1993) curves were developed for generic applications to cohesionless soils in the general range of gravelly sands to low plasticity silts or sandy clays (Figure 4-12). The EPRI (1993) curves have recently been validated at 48 San Francisco Bay area cohesionless soil sites through modeling strong ground motions from the Coyote Lake, Morgan Hill, and Loma Prieta earthquakes (Silva et al., 1997). This set of curves was also used to develop amplification factors for CEUS nuclear power plants using the Generic Till profile shown in Figure 4-10 (EPRI, 1993).

For the geologic units which are considered cohesionless soils in the Los angeles area (Qts, Qo, Qy, Saugus), recent strong ground motion analyses for about 80 sites which recorded the 1994 Northridge earthquake found the EPRI G/Gmax and hysteretic damping curves showed too much nonlinearity (Silva et al., 1997). As a result, a revised set of G/Gmax and hysteretic damping curves were developed for Peninsular Range cohesionless soils and are shown in Figure 4-13. Because there are currently insufficient laboratory dynamic test data for the soils in the regions of interest, it is difficult to preclude, a priori, the possibility of the study area soils having nonlinear properties similar to those in the Los Angeles area. The two sets of curves, EPRI (Figure 4-12) and Peninsular Range (Figure 4-13), are considered to reflect the range in base case G/Gmax and hysteretic damping curves throughout the study area or the epistemic uncertainty in dynamic material properties. Complete suites of amplification factors are developed for each set of curves for the Uplands and Lowlands profiles. The envelopes are then used as the final amplification factors. For the Glacial Till profile (Figure 4-3) only the EPRI curves are used. This profile is stiff enough to show little difference in response between EPRI and Peninsular Range nonlinear dynamic material properties, even at the highest loading level (0.75g).

4.2.3 Specification of Control Motions

The control or baserock outcrop motions are computed using the Catchings (1999) Mississippi embayment crustal model with the top (Vs = 2.0 km/sec) layer stripped off (Table 4-4). The shear-wave velocity of the basement outcropping layer is 3.5 km/sec (Table 4-4), consistent with paleozoic basement shear-wave velocities of the study area (Bob Herrmann, personal communication, 2000; Toro et al., 1992). The base case soil profiles are placed on top of the paleozoic basement of the Catchings (1999) crustal model to compute consistent rock and soil motions.

Since time histories are not required for the RVT based equivalent-linear site response analyses, the stochastic point-source model is used to compute the motions at the surface of the baserock or reference rock as well as the other profiles. Both qualitative assessments and quantative validations of the stochastic point-source model (Silva et al., 1997; Silva and Darragh, 1995; EPRI, 1993; Schneider et al., 1993; Silva et al., 1990; Boore and Atkinson, 1987; Silva and Lee, 1987; Toro and McGuire, 1987; Boore, 1986, 1983; McGuire et al., 1984; Hanks and McGuire, 1981) have demonstrated that it provides accurate ground motion estimates, making it an appropriate choice to produce ground motions representative of the geologic based profiles (Silva et al., 2000c).

To generate the motions, a **M** 6.5 earthquake is used with the distance (epicentral) varied to produce a suite of distinct peak acceleration values at the surface of the reference rock unit (Table 4-5). The same source and path parameters are then used for the soil unit profiles resulting in a suite of amplification factors (5% damped response spectra) as a function of reference rock outcrop peak acceleration values (Silva et al., 2000a, 1999; EPRI, 1993; Toro et al., 1992). For the point-source, a stress drop of 110 bars (Section 3) is used for all the profiles. For the paleozoic basement outcropping crustal model (Table 4-4) a kappa value of 0.006 sec is used (Section 3). The soil profiles have a total kappa value of 0.058 sec at their maximum depths, based on inversions of regional earthquakes located and recorded within the deeper portions of the embayment study area (Figure 4-3) (Bob Herrmann, personal communication, 2000) The total kappa value includes the small strain damping in the nonlinear zone. The soil sites are treated as potentially nonlinear to the top of the paleozoic basement (Table 4-4) provided this depth is $\leq$ 500 ft. The depth to this assumed basement material varies from 10 to 4,000 ft, depending upon category depth (Table 4-6). All soils are constrained to be linear in response below 500 ft (Silva et al., 1999; 1997).

The Q(f) model is 900 $f^{0.30}$ and is based on the same inversions of regional earthquakes used to estimate the soil kappa value (0.058 sec). The Q(f) and kappa values are then self consistent, an important and often overlooked consideration in selecting model parameters.

To generate motions which cover the range from linear response to the potentially largest horizontal motions to be expected, seven distances are run with expected reference rock outcrop peak accelerations ranging from 0.05g to 0.75g (Table 4-5). The magnitude and stress drop is fixed at **M** 6.5 and 110 bars respectively with the assumption that the amplification factors (ratios) are not highly sensitive to either magnitude or stress drop (EPRI, 1993). Since the hard rock profile is randomized in velocity and layer thickness, the median peak acceleration does not exactly correspond to the target peak acceleration (Table 4-5). In general, the median values are very close, within about 5% of the target which is considered acceptable since the amplifications vary little for a 5% to 10% change in input motions.

The profile randomization scheme, which varies both layer velocity and thickness, is based on a correlation model developed from an analysis of variance on about 500 measured shear-wave velocity profiles (EPRI, 1993; Silva et al., 1997). Figure 4-14 shows the paleozoic basement outcrop 5% damped pseudo acceleration spectra (median and ± 1 σ) for the lowest level of motion, 0.05g. The profile is varied over the top 70m, the maximum depth constraining the hard rock profile correlation model (Silva et al., 1997). The parametric variability, reflected in the sigma (σ_{ln} = 0.18 for PGA), includes profile velocity and layer thickness variation.

To accommodate variability in the modulus reduction and damping curves on a generic basis for the soil profiles, the curves were independently randomized about the base case values. A log normal distribution was assumed with a σ_{ln} of 0.1 for G/Gmax and 0.3 for hysteretic damping at a cyclic shear strain of 3 x 10^{-2}% with upper and lower bounds of 2σ. The truncation was necessary to prevent modulus reduction or damping models that are not physically possible. The uncertainties are based on an analysis of variance of laboratory test data from materials of the same type, cohesionless or cohesive, and similar depths. The uncertainties then represent within soil category (type and depth range) aleatory uncertainty (randomness). The random curves are generated by sampling the transformed normal distribution with an appropriate σ_{ln}, computing the change in normalized modulus reduction or percent damping at 3 x 10^{-2}% shear strain, and applying this factor at all strains. The random perturbation factor is reduced or tapered near the ends of the strain range to preserve the general shape of the median curves (Silva, 1992).

The remaining reference rock outcrop median spectra (5% damping) are shown in Figure 4-14. These median spectra then represent the denominator or reference geologic unit in the amplification factors.

4.2.4 Development of Site Amplification Factors

Site amplification factors are computed as the ratio of 5% damping response spectral acceleration (Sa) computed at the surface of each site for each randomized profile to the median 5% damping response spectral acceleration (Sa) computed for the reference rock outcrop motion (Figure 25). In addition, peak acceleration, peak particle velocity, and peak particle displacement were computed for the site and reference outcrop as well. Levels of reference rock outcrop peak acceleration values of 0.05, 0.1, 0.2, 0.3, 0.4, and 0.75g were used to accommodate the effects of material nonlinearity upon site response. For reference outcrop motions exceeding 0.75g, the amplification factors for 0.75g may be used as well as interpolation for intermediate values. Table 4-5 shows the magnitude (**M)**, distance (R), peak acceleration, peak particle velocity, peak particle displacement as well as V/A and AD/V^2 ratios computed for the outcrop motions.

To accommodate likely profile depth ranges appropriate for the study area, categories based upon depth to basement (taken here as top of the second layer of the Catchings, 1999, embayment crustal model, Table 4-4) were developed. The categories reflect a mean depth and a range over which the amplification factors are considered applicable. Table 4-6 lists the categories, depth ranges, and the corresponding geologic units which are considered to have underlying basement material. The range in depth to basement material over which the amplification factors for each depth category are considered applicable are based on the randomized (uniform distribution) depth range. While the depth randomization is intended to capture the profile depth range over which the amplification factors may be applied, the factors are strictly only applicable for a reduced range about the mean depth. That is, averaging amplifications computed for deep profiles with those computed for shallow profiles broadens the amplification but tends to lower the values at frequencies above and below the fundamental frequency of the mean profile depth. This effect becomes more pronounced as the depth range is increased. An enveloping scheme needs to be developed over amplification factors developed using overlapping depth ranges to produce factors strictly appropriate for applications to wide depth ranges. As a result, the mean category depths and ranges have been selected to be about ± 50% of the mean depth (mean times 1.5 and mean divided by 1.5).

4.2.5 Amplification Factors For The Study Area

Figure 4-15 shows an example of the median and ± 1σ amplification factors (5% damped response spectra) computed for the Uplands Category 7 (2,000 to 4,000 ft, Table 4-6) using the Peninsular Range G/Gmax an hysteretic damping curves. The profile and depth range is appropriate for Memphis. The variability reflects uncertainty in shear-wave velocity, layer thickness, profile depth (to paleozoic basement), and nonlinear properties on a generic basis. The fundamental resonance is near 5 sec, in general agreement with the empirical H/V resonance (about 0.22 Hz) observed by Bodin and Horton (1999) for the same location. Also seen in Figure 4-15 are the effects of nonlinearity with the high frequency ($f \geq 1$ to 2 Hz) amplitudes decreasing as the expected rock outcrop peak acceleration increases. The complete suite of amplification factors is shown in the Appendixes (A to D). The shifting of the resonances to lower frequencies as loading levels increase is apparent for the shallow depth categories (see Appendixes). This is another consequence of nonlinearity and cautions against using empirical amplification factors developed from low levels of motions for applications to design cases, which generally reflect high loading levels.

To compare results using the Peninsular Range and EPRI G/Gmax and hysteretic damping curves, Figures 4-16a and 4-16b show amplification factors (Category 7) for the Uplands and Lowlands profiles respectively. For the Uplands profile, little difference is seen in the factors between the EPRI and Peninsular Range curves, even at the 0.75g loading levels. However for the softer Lowlands profile, Figure 4-16b shows 20 to 30% differences at high frequency ($f \geq 5$ Hz) and for expected rock peak accelerations of 0.4g and above. The more linear Peninsular Range curves result in larger high frequency motions, as expected. While these results suggest that the more linear curves are conservative, this is not the case for the shallower depth categories (Silva et al., 2000a). In general the more linear curves result in higher motions for frequencies above the low-strain fundamental column resonance. However, motions computed using more nonlinear curves are often higher below the low-strain fundamental resonance due to the greater shift of the resonances to lower frequencies. To accommodate epistemic uncertainty in nonlinear dynamic material properties enveloping is the only safe course of action. This is also consistent with applications to probabilistically derived control motions. In this case, soil motions at the same hazard level as the control motions are desired (hazard consistent), as if the UHS had been computed using category or site specific soil attenuation relations. The approach which is more hazard insistent is to envelop the amplification factors (Silva et al., 2000b).

Comparison of the Uplands and Lowlands envelop (final) and the Glacial Till amplification factors are shown in Figures 4-17a to 4-17g for depth categories 1 to 7 (Glacial Till does not have categories 6 and 7, Table 4-6). For depth categories 1 and 2 (mean depths of 30 and 75 ft) little difference is seen in the envelop factors for Uplands and Lowlands, except at high frequency (f ≥ 5 Hz) and around 0.4g and above. For the deeper categories the softer Lowlands is distinct from the stiffer Uplands at low and high frequency with a crossover near 1 Hz: Lowlands generally controls low frequency while Uplands controls the high frequency. Interestingly, the Glacial Till controls the high frequencies (f ≥ 5 Hz) for the shallow depth categories (1, 2, and 3) but also controls at some low frequencies for the deeper categories and some loading levels (e.g. depth category 5, Figure 4-17e, near 1 Hz). Features such as these may serve as guidance in developing site amplification factors for wide applicability, such as NEHRP. Base-case profiles that span category stiffness ranges reflecting epistemic uncertainty (uncertainty in mean or base case profile) should each be randomized to accommodate aleatory uncertainty and then median (or more conservative fractile levels) amplification factors enveloped to form a factor truly appropriate for the category: the wider the category (average stiffness, depth, etc) the broader (not necessarily higher) the amplification factors.

To illustrate depth category dependency, Figures 4-18a to 4-18c show Uplands and Lowlands envelope (EPRI and Peninsular Range curves) median as well as the Glacial Till median amplification factors. The shifting of the fundamental resonances, with depth category is easily seen. The randomization smooths the resonances and the factor of two in mean depth preserves a distinct set of factors without large gaps in amplification between them. Clearly profile depth is important and depth independent factors would again require enveloping the suites of factors over depth categories.

Finally Figure 4-19 compares the median factors computed for the Uplands high shallow velocity profiles (Figure 4-11) with the base-case Uplands factors (envelop of Peninsular Range and EPRI curves). Throughout most of the frequency ranges and control motion levels, the high velocity profile number 3 with Peninsular Range curves shows the largest amplification. This profile has the shallowest and thickest high velocity layer (Figure 4-11). For the larger control motions (0.20g and above) and for frequencies above about 1 Hz, the base-case Uplands amplification is about midway between the shallow high velocity suites computed using the Peninsular Range and EPRI sets of nonlinear dynamic material properties. The difference between the base-case envelop Uplands factors and the high velocity Peninsular Range suite is small, less than about

20%. For site specific applications where footprint rather than generic profile randomization may be used (smaller velocity COV with depth) larger more significant differences would likely occur (Silva et al., 1997).

As with all studies of this type which are regional in nature, largely because of the unavailability of site specific measured values of dynamic material properties, departures in response from those predicted in this study could be large. The results presented here then should be viewed in the broad context of defining initial estimate of expected levels of motion and how they may vary within the embayment and surrounding areas. The amplification factors developed in this project may be used to approximately accommodate the effects of near surface geology for seismic hazard evaluations.

4.3 REFERENCES

Abrahamson and Silva (1997). "Empirical response spectral attenuation relations." to appear in Seismological Research Letters.

Boatwright, J., and Astrue, M. (1983). "Analysis of the aftershocks of the New Brunswick earthquake." *Workshop on Site-Specific Effects of Soil and Rock on Ground Motion and the Implications for Earthquake-Resistant Design.* USGS Open-File Rept. 83-245.

Bodin, P. and S. Horton (1999). “Broadband microtremor observation of basin resonance in the Mississippi embayment, Central US.” *Geophysical Research Lett.*, 26(7), 903-906.

Boore, D.M., and Atkinson, G.M. (1987). "Stochastic prediction of ground motion and spectral response parameters at hard-rock sites in eastern North America." *Bull. Seism. Soc. Am.*, 77(2), 440-46

Boore, D.M. (1986). "Short-period P- and S-wave radiation from large earthquakes: implications for spectral scaling relations." *Bull. Seism. Soc. Am.*, 76(1) 43-64.

Boore, D.M. (1983). "Stochastic simulation of high-frequency ground motions based on seismological models of the radiated spectra." *Bull. Seism. Soc. Am.*, 73, 1865-1894.

Borcherdt, R. D. (1997). “Estimates of site-dependent response spectra for new and existing highway facilities (methodology and justification).” *Proc. Of the NCEER Workshop on the Nat’l Representation of Seismic Ground Motion for New and Existing Highway Facilities,* edited by M.S. Power and R.L. Mayes.

Borcherdt, R. D. (1996). "Preliminary amplification estimates inferred from strong ground-motion recordings of the Northridge earthquake of January 17, 1994.” *Proceedings of the Internatonal Workshop on Site Response Subjected to Strong Earthquake Motions.* Yokosuka Japan, 1-26.

Borcherdt, R. D. and Glassmoyer, G. (1992). "On the Characteristics of Local Geology and Their Influence on Ground Motions Generated by the Loma Prieta Earthquake in the San Francisco Bay region, California." *Bull. Seism. Soc. Am.*, 82(2), 603-641.

Borcherdt, R.D. (1970). "Effects of local geology on ground motion near San Francisco Bay." *Bull. Seism. Soc. Am.*, 60:29-61.

Campbell, K.W. (1988). "Predicting strong ground motion in Utah." *Evaluation of Regional and Urban Earthquake Hazards and Risk in Utah,* edited by W.W. Hays and P.L. Gori, USGS Prof. Paper.

Campbell, K.W. (1985). "Near-source estimation of strong ground motion for the Eastern United States: second quarter progress report - FY 1985." Submitted to *Nuclear Regulatory Commission*, 14 pages.

Campbell, K.W. (1981). "Near-source attenuation of peak horizontal acceleration." *Bull. Seism.*

Soc. Am., 71(6), 2039-2070.

Catchings, R. D. (1999). “Regional Vp, Vs, Vp/Vs, and Poisson’s ratios across earthquake source zones from Memphis, Tennessee, to St. Louis, Missouri.” *Bull. Seism. Soc. Am.*, 89(6), 1591-1605.

Cranswick, E., Wetmiller, R., and Boatwright, J. (1985). "High-frequency observations and source parameters of microearthquakes recorded at hard-rock sites." *Bull. Seism. Soc. Am.*, 75(6), 1535-1567.

Crone, A.J., Russ, D. (1979). "Preliminary report on an exploratory drill hole--New Madrid test well-1-X in southeast Missouri." *USGS* Open-File Report 79-1216.

Cushing, E.M., Boswell, E.H., and Hosman, R.L. (1964). "General Geology of the Mississippi embayment." *USGS* Professional Paper 448-B.

Dorman, J. and R. Smalley (1994). “Low-frequency seismic surface waves in the upper Mississippi embayment.” *Seis. Research Lett.*, 65(2), 137-167.

Dorman, J. and H. Hwang (1993). "Characteristics and possible structural effects of strong ground motion in Memphis." *USGS*, Award No. 1434-93-G-23640.

Electric Power Research Institute (1993). "Guidelines for determining design basis ground motions." Palo Alto, Calif: Electric Power Research Institute, vol. 1-5, EPRI TR-102293.
vol. 1: Methodology and guidelines for estimating earthquake ground motion in eastern North America.
vol. 2: Appendices for ground motion estimation.
vol. 3: Appendices for field investigations.
vol. 4: Appendices for laboratory investigations.
vol. 5: Quantification of seismic source effects.

Grohskopf, J.G. (1955). "Subsurface geology of the Mississippi embayment of southeast Missouri." State of Missouri Dept. of Business and Admin., Division of Geolog. Survey and Water Resources, T.R. Beveridge, State Geologist, Rolla, Missouri.

Gutenberg, B. (1927). *Grundlagen der Erdlebenkunde*. Berlin.

Gutenberg, B. (1957). "Effects of ground on earthquake motion." *Bull. Seism. Soc. Am.*, 47(1), 221-250.

Hanks, T.C., and McGuire, R.K. (1981). "The character of high-frequency strong ground motion." *Bull. Seism. Soc. Am.*, 71, 2071-2095.

Harmsen, S.C. (1997). “Determination of site amplification in the Los Angeles urban area from inversion of strong-motion records.” *Bull. Seism. Soc. Am.,* 87(4), 866-887.

Harris, J.B. R.L. Street, J.D. Kiefer, D.L. Allen, and Z.M. Wang (1994). "Modeling site response in the Paducah, Kentucky area." *Earth. Spectra*, 10(3), 519-538.

Hayashi, S., H. Tsuchida, and E. Kurata (1971). "Average response spectra for various subsoil conditions." *Third Joint Meeting, US-Japan Panel on Wind and Seismic Effects,* UJNR, Tokyo.

Hwang, H., M-C. Chien, Y.H. Pan, J-M. Chiu, and S. Pezeshk (1999). “Stratigraphy and Shear Wave Velocity Profile for Mississippi embayment at Mud Island, Memphis.” Personal Communication.

Idriss, I.M. (1985). "Evaluating seismic risk in engineering practice." *Proc. Eleventh Internat. Conf. on Soil Mech. and Foundation Eng.*, San Francisco, edited by A.A. Balkema, Rotterdam, 1, 255-320.

Iwan, W.D. (1967). "On a class of models for the yielding behavior of continuous and composite systems." *J. Appl. Mech.,* 34, 612-617.

Joyner, W.B., and Fumal, T.E. (1984). "Use of measured shear-wave velocity for predicting geologic site effects on strong ground motion." *Proc. Eighth World Conf. on Earthq. Engin.*, San Francisco, 2, 777-783.

Joyner, H.B. and D.M. Boore (1982) "Prediction of earthquake response spectra." *USGS,* Open-File Rept. 82-977.

Liu, H-P., Y. Hu, J. Dorman, T-S. Chang, and J-M. Chiu (1997). "Upper Mississippi embayment shallow seismic velocities measured in situ." *Engineering Geology,* 46:313-330.

Mallet, R. (1862). "*Great Neopolitan earthquake of 1857, London.*" 2 vols.

McGuire, R.K., A.M. Becker, and N.C. Donovan (1984). "Spectral estimates of seismic shear waves." *Bull. Seism. Soc. Am.*, 74(4), 1427-1440.

Milne, J. (1908). "*Seismology, London.*" 2nd edition.

Mohraz, B. (1976). "A study of earthquake response spectra for different geological conditions." *Bull. Seism. Soc. Am.,* 66(3) 915-935.

Obermeier, S.F. (1988). "Liquefaction potential in the central Mississippi Valley." *USGS Bulletin,* Denver, CO, Tech. Rept. 1832, 1-6.

Reid, H.F. (1910). "The California earthquake of April 18, 1907." *The Mechanics of the Earthquake,* Carnegie Inst. of Washington, Publ. 87, 21.

Roblee, C.J., W.J. Silva, G.R. Toro, and N. Abrahamson (1996). "Variability in Site-Specific Seismic Ground-Motion Predictions." Uncertainty in the Geologic Environment: From Theory to Practice, Proceedings of "Uncertainty '96" *ASCE* Specialty Conference, Edited by C.D. Shackelford, P.P. Nelson, and M.J.S. Roth, Madison, WI, Aug. 1-3, pp. 1113-1133.

Romero, S. and G. J. Rix (2000). “Regional variations in near surface shear wave velocity in the greater Memphis area.” School of Civil and Environmental Engineering Georgia Institute of Technology, Personal Communication.

Romero, S. G. Hebeler, and G. J. Rix (2000). “Preliminary reference profile for Memphis, Tennessee.” School of Civil and Environmental Engineering Georgia Institute of Technology, Personal Communication.

Seed, H.B. and I.M. Idriss (1970). "*Soil moduli and damping factors for dynamic response analyses.*" Earthq. Eng. Res. Center, Univ. of Calif. at Berkeley, Report No. UCB/EERC-70/10.

Schnabel, P.B., Lysmer, J., and Seed, H.B. (1972). *SHAKE: a Computer Program for Earthquake Response Analysis of Horizontally Layered Sites.* Earthq. Engin. Res. Center, Univ. of Calif. at Berkeley, EERC 72-12.

Schneider, J.A. (1999)“*Liquefaction response of soils in Mid-America evaluated by seismic cone tests.*” A Thesis Presented to the Academic Faculty, Georgia Institute of Technology.

Schneider, J.A. and P.W. Mayne (1998). “Results of seismic piezocone and flat plate dilatometer tests performed in Blytheville, AR, Steele, MO, and Shelby County, TN.” Georgia Institute of Technology, Interim Report *MAEC* Project No. GT-3, GTRC Project No. E20-677.

Schneider, J.F., W.J. Silva, and C.L. Stark (1993). Ground motion model for the 1989 **M** 6.9 Loma Prieta earthquake including effects of source, path and site. *Earthquake Spectra,* 9(2), 251-287.

Seed, H.B., C. Ugas and J. Lysmer. (1976). "Site-dependent spectra for earthquake resistant design." *Bull. Seism. Soc. Am.*, 66(1), 221-243.

Silva, W.J., Darragh, R. Gregor, N., Martin, G., Kircher, C. Abrahamson, N. (2000a). “Reassessment of site coefficients and near-fault Factors for building code provisions.” *USGS Grant award* #98-HQ-GR-1010.

Silva, W. J. R. McGuire, and C. Costantino. (2000b). “Comparison of Site Specific Soil UHS to Soil Motions Computed with Rock UHS.”*Proc. of the OECE-NEA Workshop on Engineering Characterization of Seismic Input, Nov., 15-17, 1999, NEA/CSNI/R(2000)2.*

Silva, W. J., R.R. Youngs, and I.M. Idriss (2000c). "Development of Design Response Spectral Shapes for Central and Eastern U.S. (CEUS) and Western U.S. (WUS) Rock Site Conditions."*Proc. of the OECE-NEA Workshop on Engineering Characterization of Seismic Input, Nov., 15-17, 1999 NEA/CSNI/R(2000)2.*

Silva, W. J.,S. Li, B. Darragh, and N. Gregor (1999). "Surface Geology Based Strong Motion Amplification Factors for the San Francisco Bay and Los Angeles Areas."A PEARL report to PG&E/CEC/Caltrans, Award No. SA2120-59652.

Silva, W.J., N. Abrahamson, G. Toro and C. Costantino. (1997). "Description and validation of the stochastic ground motion model." Report Submitted to Brookhaven National Laboratory, Associated Universities, Inc. Upton, New York 11973, Contract No. 770573

Silva, W.J. and R. Darragh (1995). "Engineering characterization of earthquake strong ground motion recorded at rock sites." Palo Alto, Calif:Electric Power Research Institute, TR-102261.

Silva, W.J. (1992). "Factors controlling strong ground motions and their associated uncertainties." *Dynamic Analysis and Design Considerations for High Level Nuclear Waste Repositories, ASCE* 132-161.

Silva, W.J., Darragh, R.B., and Wong, I.G. (1990). "Engineering characterization of earthquake strong ground motions with applications to the Pacific Northwest." in Hays, W.W., ed., *Proceedings of the Third NEHRP Workshop on earthquake Hazards in the Puget sound/Portland region*, U.S. geological Survey Open-File report (in press).

Silva, W.J., and Green, R.K. (1989). "Magnitude and distance scaling of response spectral shapes for rock sites with applications to North American tectonic environment." *Earthquake Spectra,* 5(3), 591-624.

Silva, W. J.; Turcotte, T.; Moriwaki, Y. (1988). "Soil Response to Earthquake Ground Motion," Electric Power Research Institute, Walnut Creek, California, Report No. NP-5747.

Silva, W.J., and Lee, K. (1987). "*WES RASCAL code for synthesizing earthquake ground motions.*" State-of-the-Art for Assessing Earthquake Hazards in the United States, Report 24, U.S. Army Engineers Waterways Experiment Station, Misc. Paper S-73-1.

Silva, W.J. (1976). "Body Waves in a Layered Anelastic soilid." *Bull. Seis. Soc. Am.*, vol. 66(5), 1539-1554.

Street, R., Woolery, E. and Wang, Z. (1995). "A short note on shear-wave velocities and other site conditions at selected strong-motion stations in the New Madrid seismic zone." *Seis. Resea. Letters*, 66(1), 56-63.

Toro, G.R., W.J. Silva, R.K. McGuire and R.B. Herrmann (1992). "Probabilistic seismic hazard mapping of the Mississippi embayment." *Seism. Res. Letters*, 63(3), 449-475.

Toro, G.R., and McGuire, R.K. (1987). "An investigation into earthquake ground motion characteristics in eastern North America." *Bull. Seism. Soc. Am.*, 77, 468-489.

Uniform Building Code (1997) *Uniform Building Code."* Published by International Conference of Building Officials, Whittier, California.

Williams, R., W.J. Stephenson, A.D. Frankel, E. Cranswick, M.E. Meremonte, and J.K. Odum

(2000). “Correlation of 1- to 10-Hz earthquake resonances with surface measurements of S-wave reflections and refractions in the upper 50m.” Submitted to *BSSA*.

Wood, H.O. (1908). "Distribution of apparent intensity in San Francisco, in the California earthquake of April 18, 1906." Report of the State Earthquake Investigation Commission, Wash., D.C.: Carnegie Institute, 1, 220-245.

Table 4-1
PRELIMINARY STRATICGRAPHIC SECTION FOR
NEW MADRID-1-X TEST WELL
(FROM CRONE AND RUSS, 1979)
(Subject to future revisions and reinterpretation)

Age	Total depth (ft)	Unit Thickness (ft)	Unit or Formation		General Lithologic Description
Quaternary	0 - 135 ±	135 ±	Misssissippi Valley alluvium		20 ft of clay and silty clay overlying sand and gravel. Gravel occurs in lower 15 ft (?).
Eocene	135 - 270 (?)	135 (?)	Jackson Formation		Sand with interbedded gray silt and clay.
	270 (?) - 1048	778 (?)	Claiborne Group	Cockfield (?) Formation	Gray to gray-green silty clay and silty sandy clay; some lignite.
				Cook Mountain (?) Formation	Gray to gray-green silty clay and silty sandy clay; some lignite.
				Memphis Sand	Sand, lignite, minor interbeds of clay.
--?--	1048 - 1377	329 (?)	Wilcox Group	Flour Island Formation	Clay and silty clay with interbeds of sand and silt.
				Fort Pillow Sand	Sand, medium to coarse; glauconite.
				Old Breastworks Formation	Clay, sandy and silty; noncalcareous.
Paleocene	1377(?)-1703(?)	326 (?)	Midway Group	Porters Creek Clay	Clay, generally calcareous; silty and glauconitic at base.
				Clayton Formation	Limestone, glauconitic, fossiliferous; some clay.
Cretaceous	1703 (?)-1706 (?)	3 (?)	Owl Creek Formation		Clay.
	1706 (?)-2023	317 (?)	McNairy Sand		Sand, quartzose, fine to coarse grained; interbedded with clay, dk. Gray to black.
Paleocene	2023-2316 +	293 +	Paleozoic dolomite		Dolomite, dk. Gray to white, fine to coarse crystalline, contains pyrite.

Table 4-2

SITE RESPONSE UNITS AND NEHRP CATEGORIES

Profile	$\overline{V_S}$ (30m)	NEHRP (UBC 97) Category
Lowlands	774 ft/sec (236m/sec)	D
Uplands	994 ft/sec (303m/sec)	D
Upland (1)	1050 ft/sec (320m/sec)	D
Upland (2)	1266 ft/sec (386m/sec)	C
Upland (3)	138 ft/sec (422m/sec)	C
Glacial Till	1522 ft/sec (464m/sec)	C

Table 4-3

SITE CLASSIFICATIONS

Average shear-wave velocity to a depth of 30m is:

USGS Site Classification (Boore et al., 1994)	NEHRP 1994	UBC 1997
A = > 750 m/s	A = > 1,500 m/s	> 5,000 ft/sec
B = 360 - 750	B = 760 - 1,500	2,500 - 5,000
C = 180 - 360	C = 360 - 760	1,200 - 2,500
D = < 180 m/s	D = 180 - 360	600 - 1,200
	E = < 180	< 600 ft/sec

GEOMATRIX Site Classification

Geotechnical subsurface characteristics (Robert Youngs, personal communications)

A = Rock. Instrument on rock (V_S > 600 mps or < 5m of soil over rock.

B = Shallow (stiff) soil. Instrument on/in soil profile up to 20m thick overlying rock.

C = Deep narrow soil. Instrument on/in soil profile at least 20m thick overlying rock, in a narrow canyon or valley no more than several km wide.

D = Deep broad soil. Instrument on/in a soil profile at least 20m thick overlying rock, in a broad valley.

E = Soft deep soil. Instrument on/in deep soil profile with average V_S < 150 mps.

Relations To Building Code Classifications

UBC	USGS	NEHRP	GEOMATRIX
S1	A + B	B + C	A + B
S2	B + C	C + D	C + D
S3	D	E	E
S4	E		

Table 4-4 EMBAYMENT CRUSTAL MODEL (Catchings, 1999)		
Thickness (km)	V_S (km/sec)	Density (cgs)
3.0	2.0	2.55
7.0*	3.5	2.77
14.0	3.6	2.82
19.0	4.2	3.15
16.0	4.5	3.34
	4.7	3.45

Table 4-5 CEUS HARD ROCK REFERENCE SITE GROUND MOTION PARAMETERS									
Target Outcrop PGA(g)	Median Outcrop PGA(g)	Median Outcrop PGV (cm/sec)	Median Outcrop PGD (cm)	Median Outcrop V/A (cm/sec/g)	Median Outcrop AD/V^2 ($gcm/cm/sec^2$)	Dist. (km)	Depth (km)	**M**	$\Delta\sigma$ (bars)
0.05	0.052	37.9	1.44	73.38	5.09	86.00	8.00	6.5	110
0.10	0.104	6.45	2.31	62.34	5.12	48.00	8.00	6.5	110
0.20	0.211	11.92	4.17	57.58	6.06	26.00	8.00	6.5	110
0.030	0.305	16.65	5.77	54.52	6.23	18.00	8.00	6.5	110
0.040	0.405	21.64	7.47	53.38	7.47	13.00	8.00	6.5	110
0.501	0.515	27.06	9.31	52.58	6.42	9.30	8.00	6.5	110
0.75	0.758	39.08	13.38	51.59	6.51	3.00	8.00	6.5	110

$Q(F) = 900\ f^{0.30}$

kappa = 0.006 sec

---

*Assume hard rock outcrop layer

Table 4-6

DEPTH CATEGORIES AND DEPTH RANGES

Category	Mid-Depth (ft)	Range* (ft)
1	30	10 - 50
2	75	51 - 100
3	150	101 - 200
4	350	201 - 500
5	750	501 - 1000
6	1500	1001 - 2000
7	3000	2001 - 4000

Geologic Units and Depth Categories

Geologic Unit	Depth Categories
Lowlands	1, 2, 3, 4, 5, 6, 7
Uplands	1, 2, 3, 4, 5, 6, 7
Uplands (shallow high velocity 1)	7
Uplands (shallow high velocity 2)	7
Uplands (shallow high velocity 3)	7
Glacial Till	1, 2, 3, 4, 5

*Range of profile depth over which category applies as well as range of depth randomization for each category. Profile depth is defined as depth to basement material.

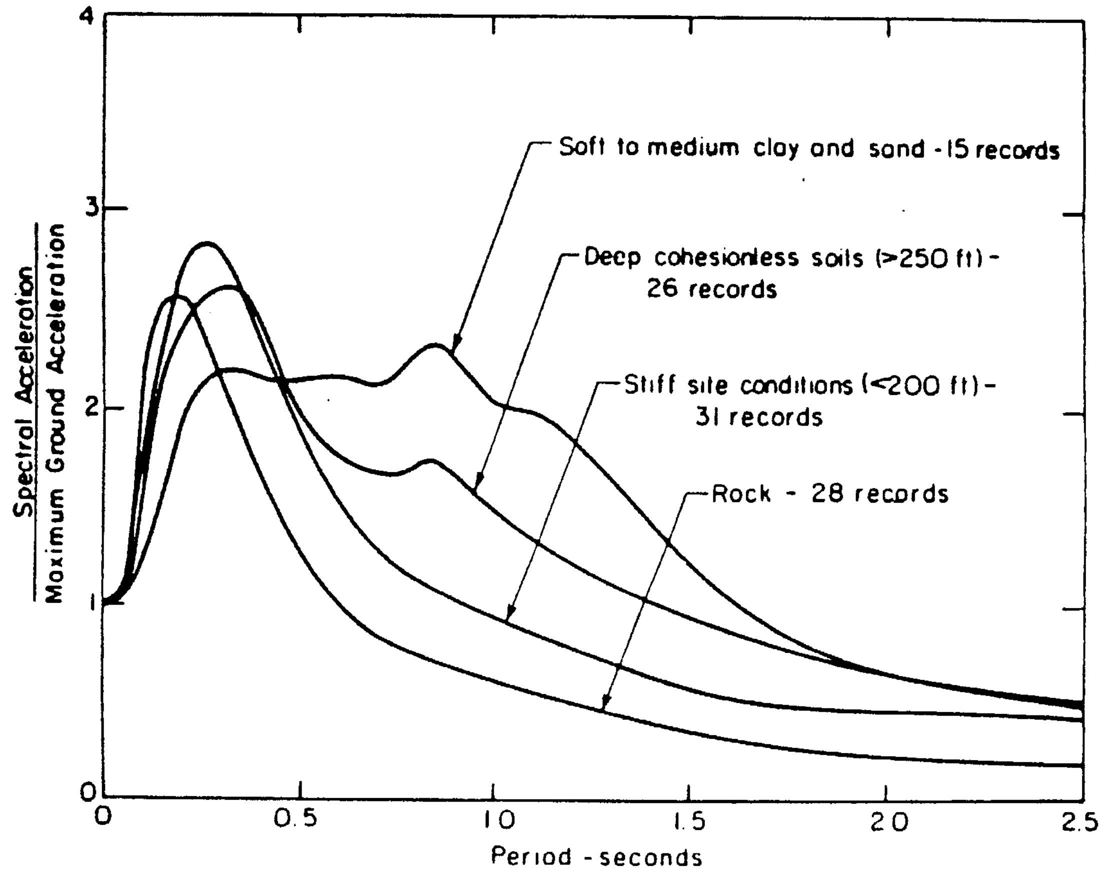

Figure 4-1. Effects of near surface soil conditions on 5% damped response spectral shapes (Source: Seed, Ugas, and Lysmer, 1976).

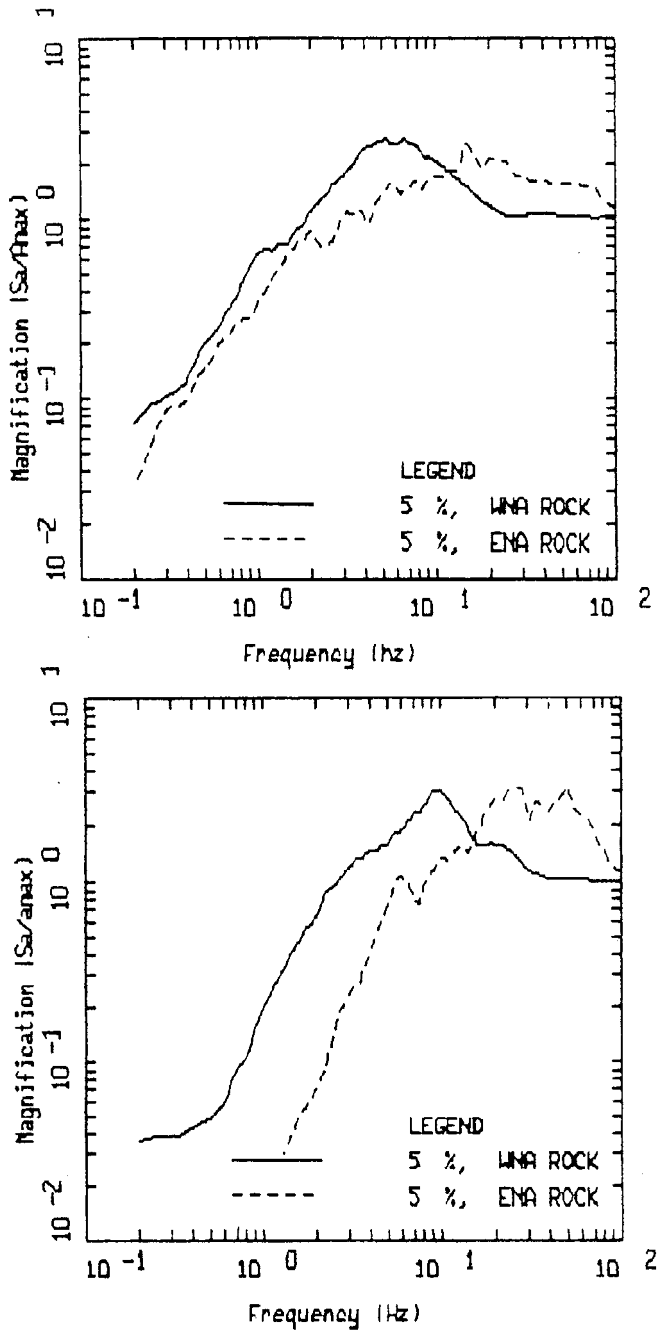

Figure 4-2. Effects of hard (ENA) and soft (WNA) rock site conditions on 5% damped response spectral shapes for **M** ~ 6.5 (Upper) and **M** ~ 4.5 (lower) earthquakes (Source: Silva and Darragh, 1995).

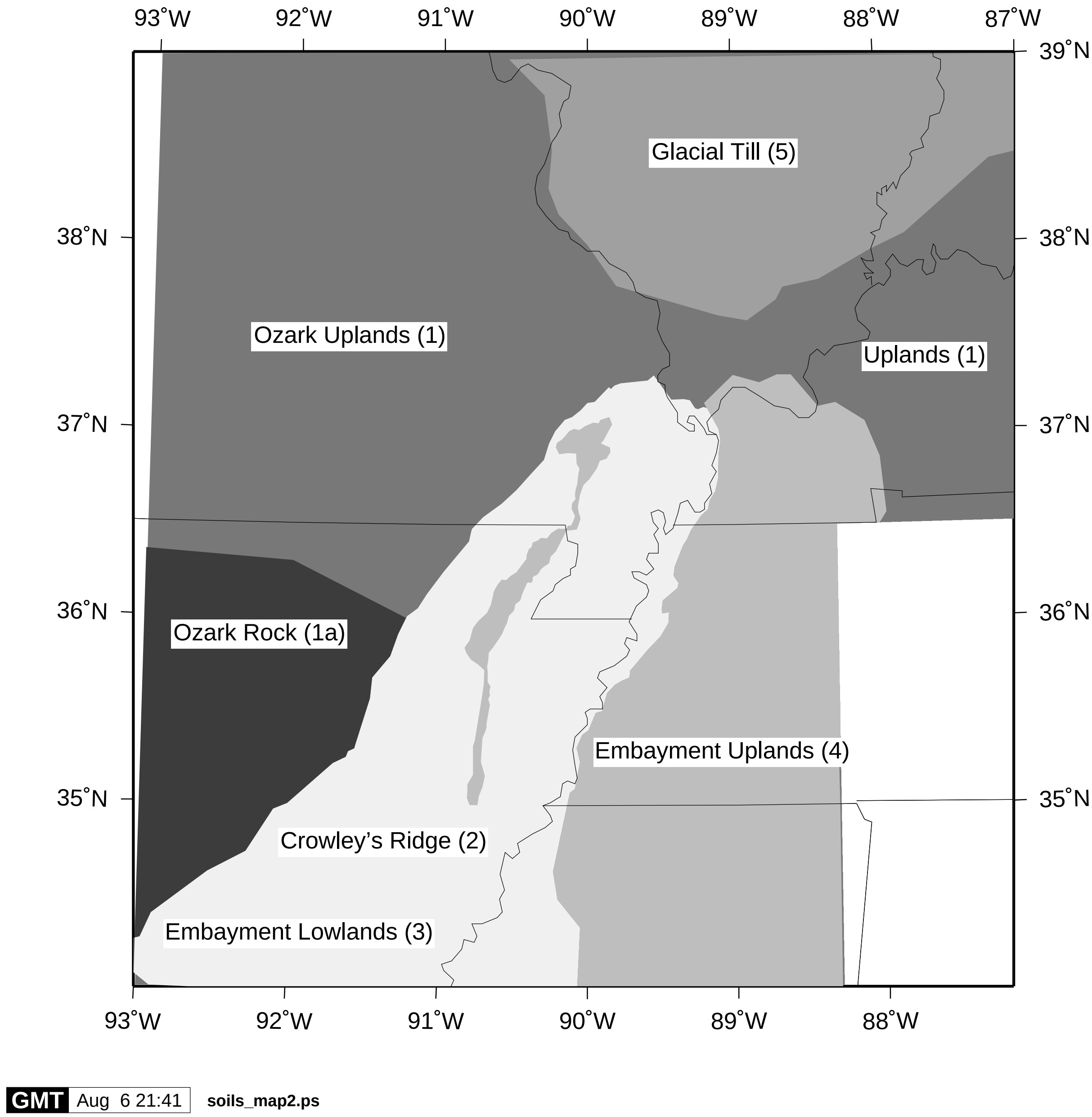

Figure 4-3. Map of the study area showing site response units.

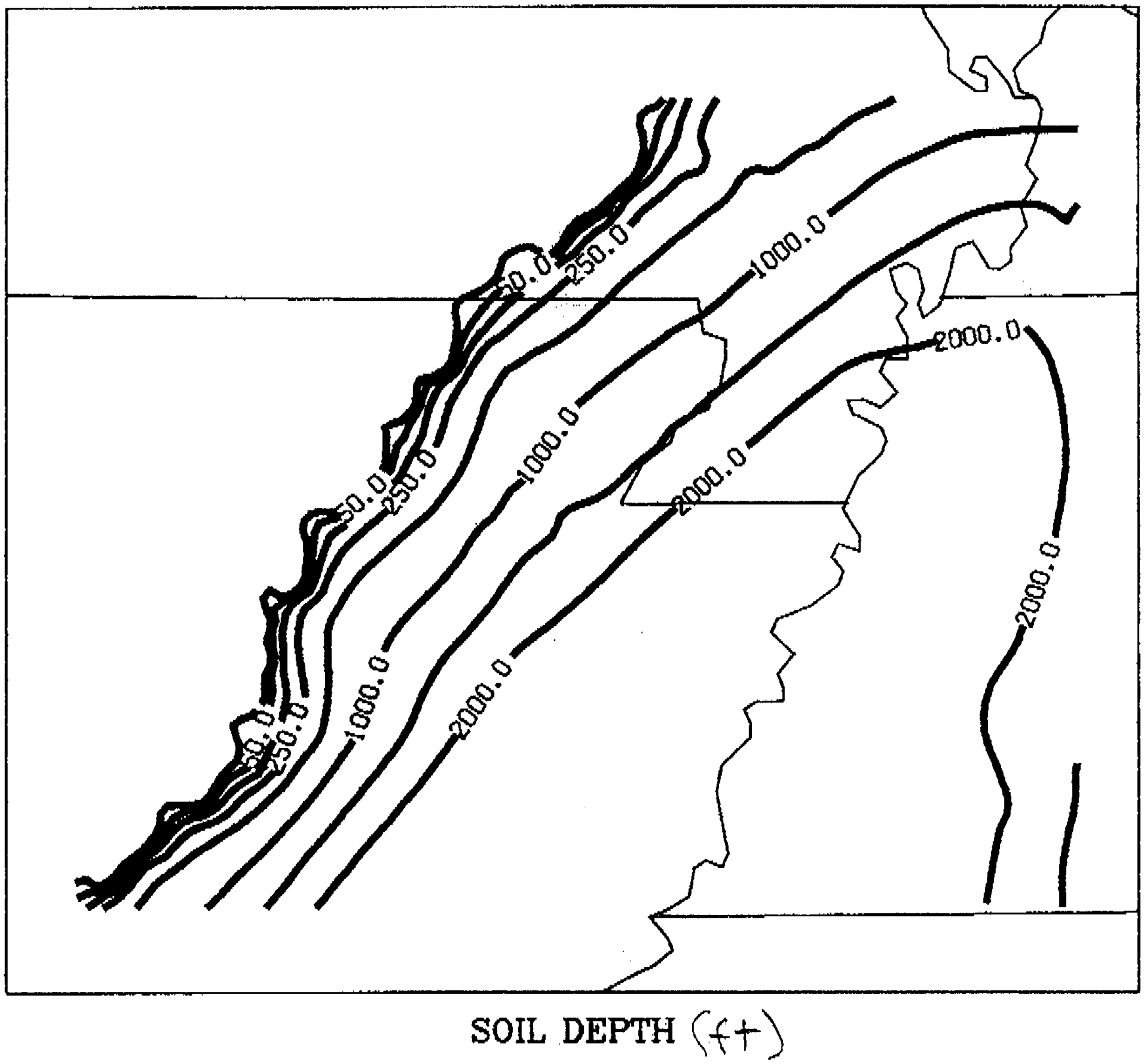

Figure 4-4. Paleozoic basement depth for the Mississippi embayment portion of the study area.

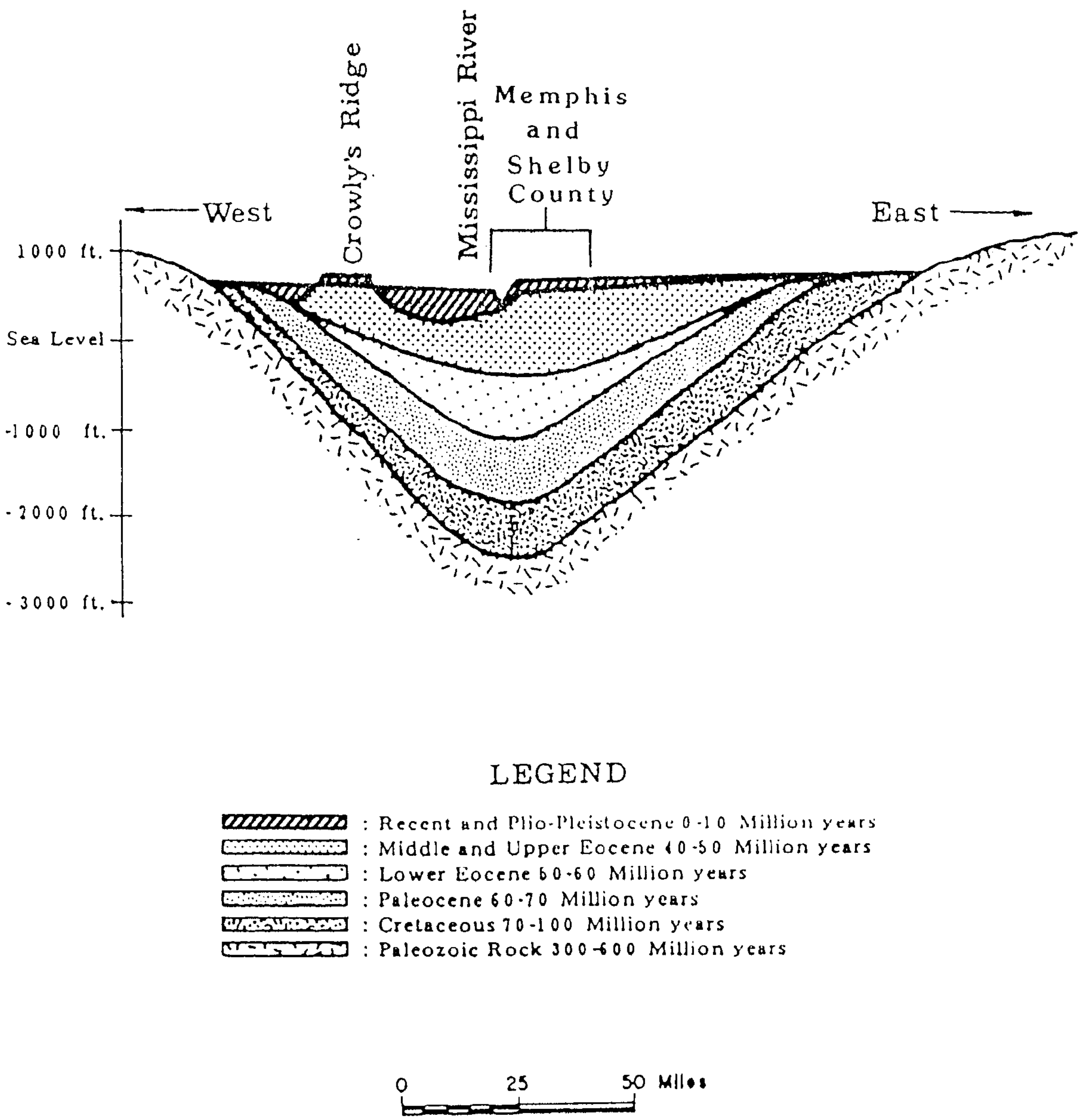

Figure 4-5. Cross section of the Mississippi Embayment at the latitude near Memphis Tennessee (source Ng Et eal., 1989).

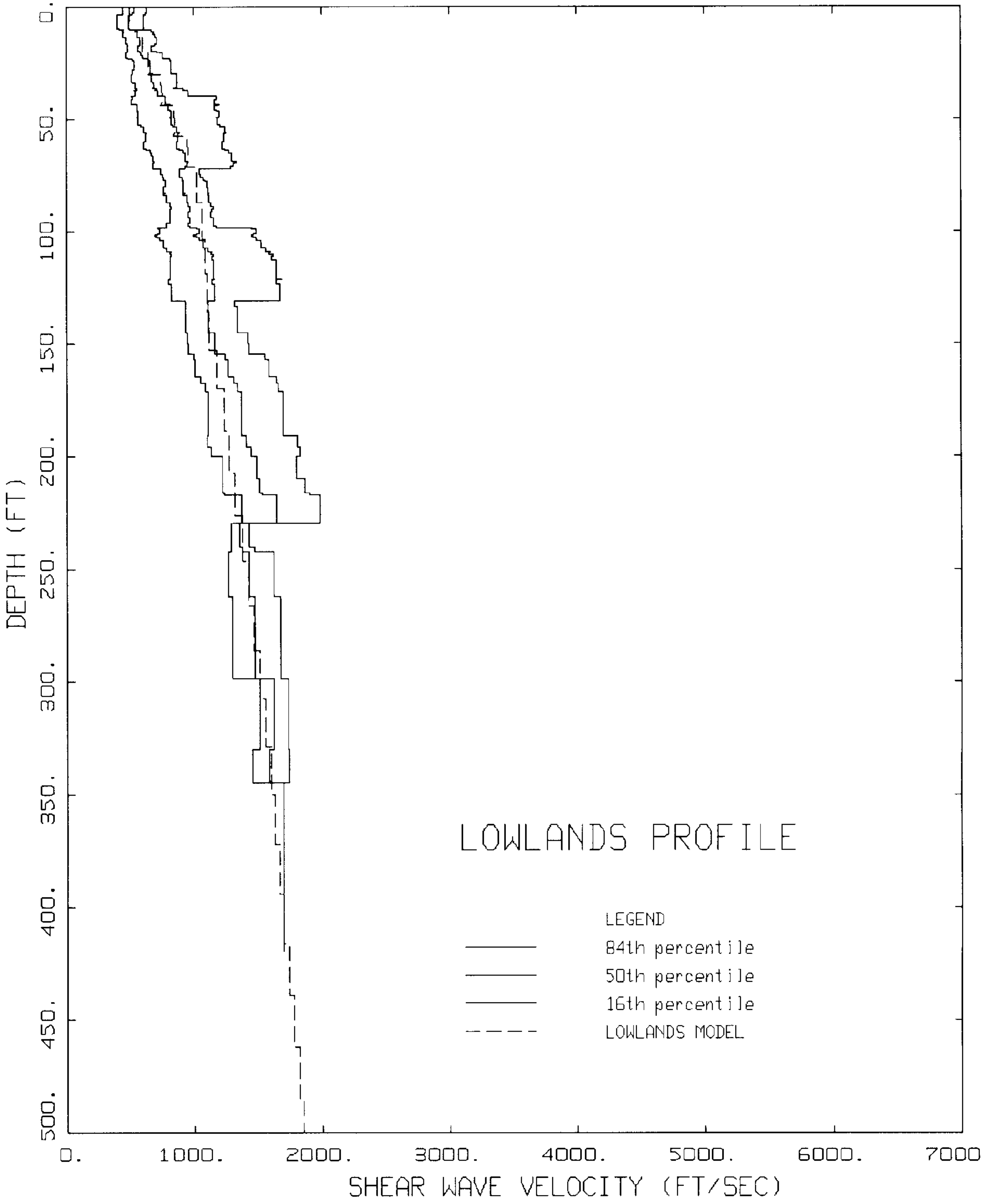

Figure 4-6. Median and ± 1σ shear-wave velocity profiles based on available measurements along with smooth model, Lowlands (Figure 4-3).

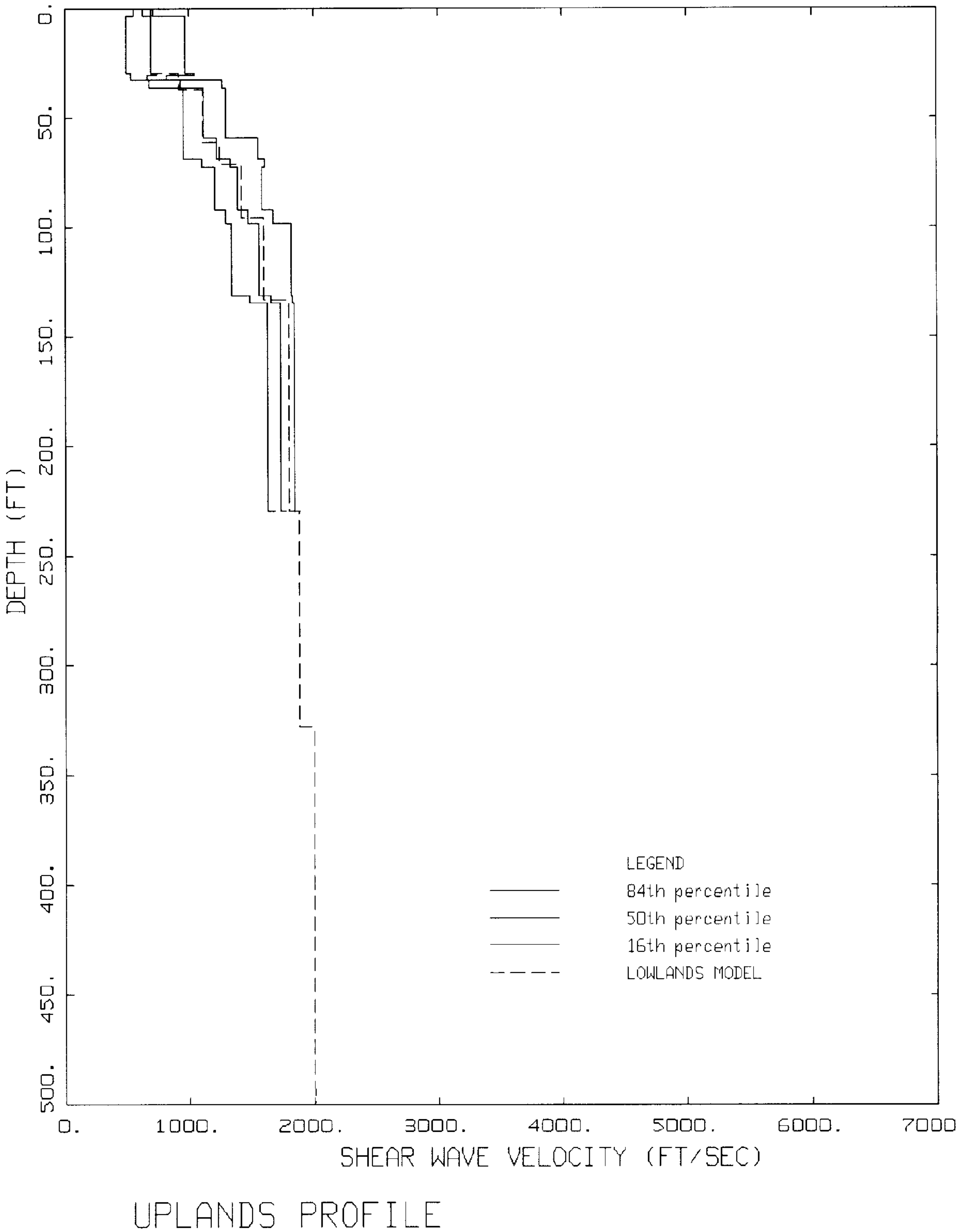

Figure 4-7. Median and ± 1σ shear-wave velocity profiles based on available measurements along with smooth model, Uplands (Figure 4-3).

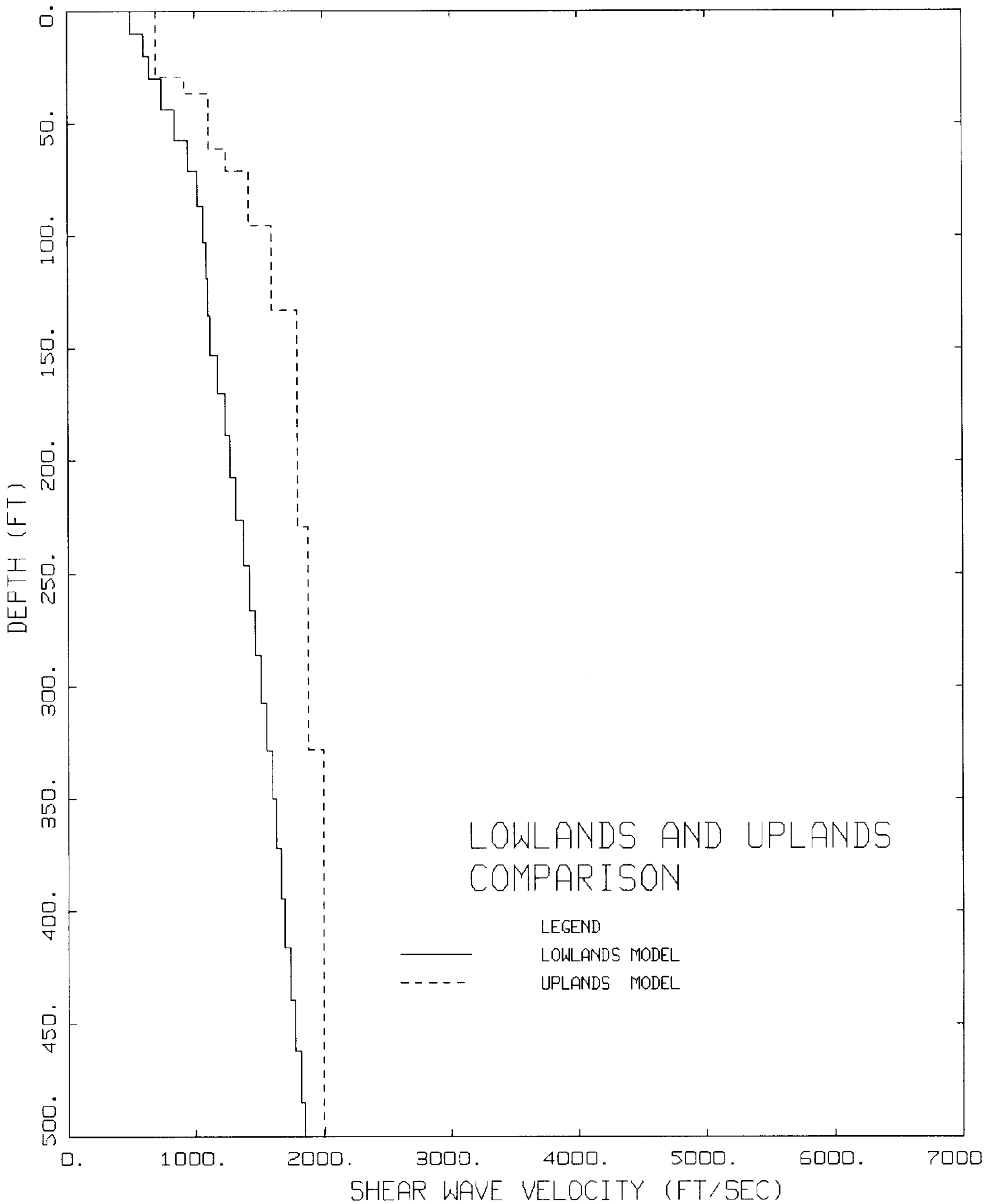

Figure 4-8. Comparison of Lowlands and Uplands base-case shear-wave velocity models to a depth of 500 ft.

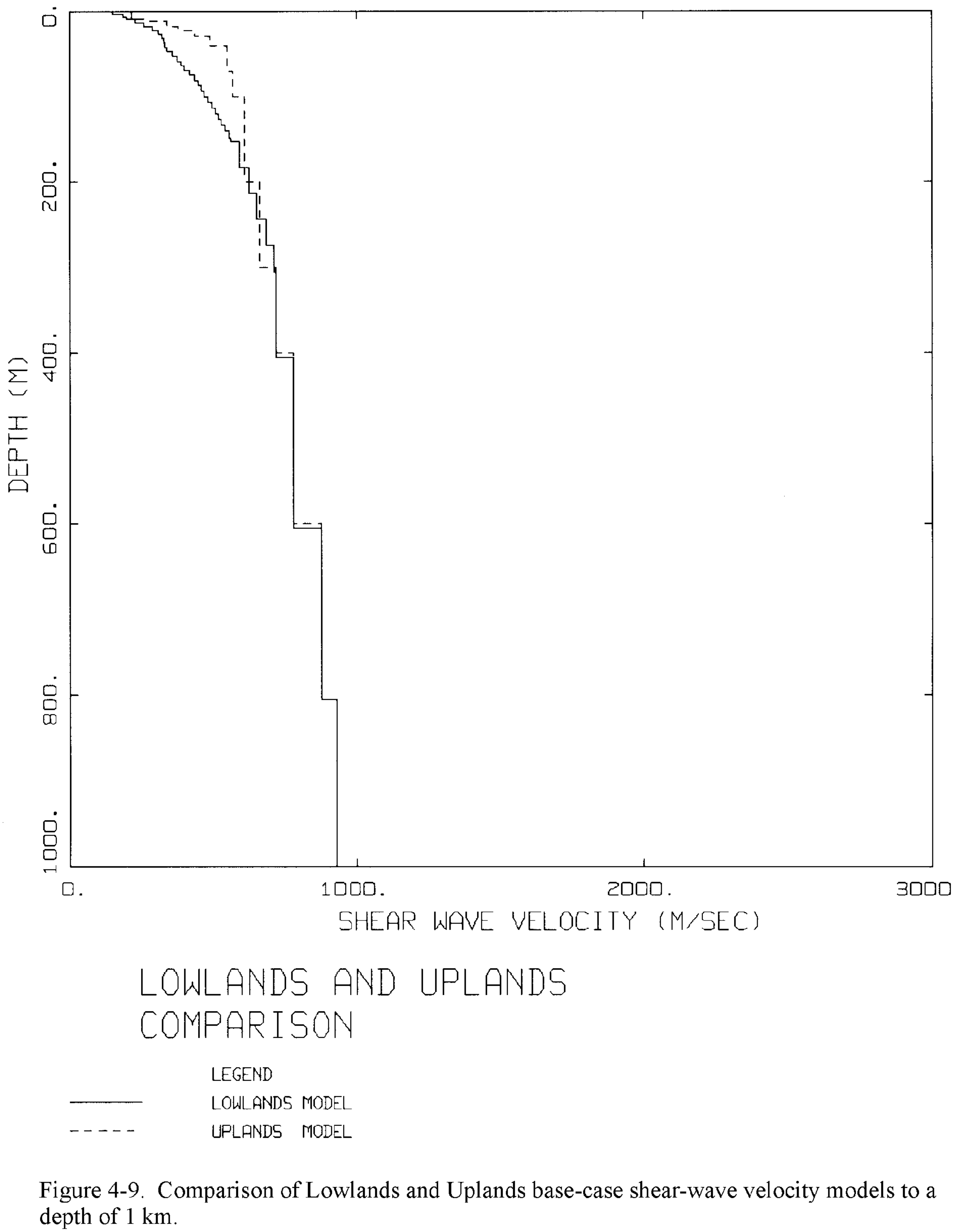

Figure 4-9. Comparison of Lowlands and Uplands base-case shear-wave velocity models to a depth of 1 km.

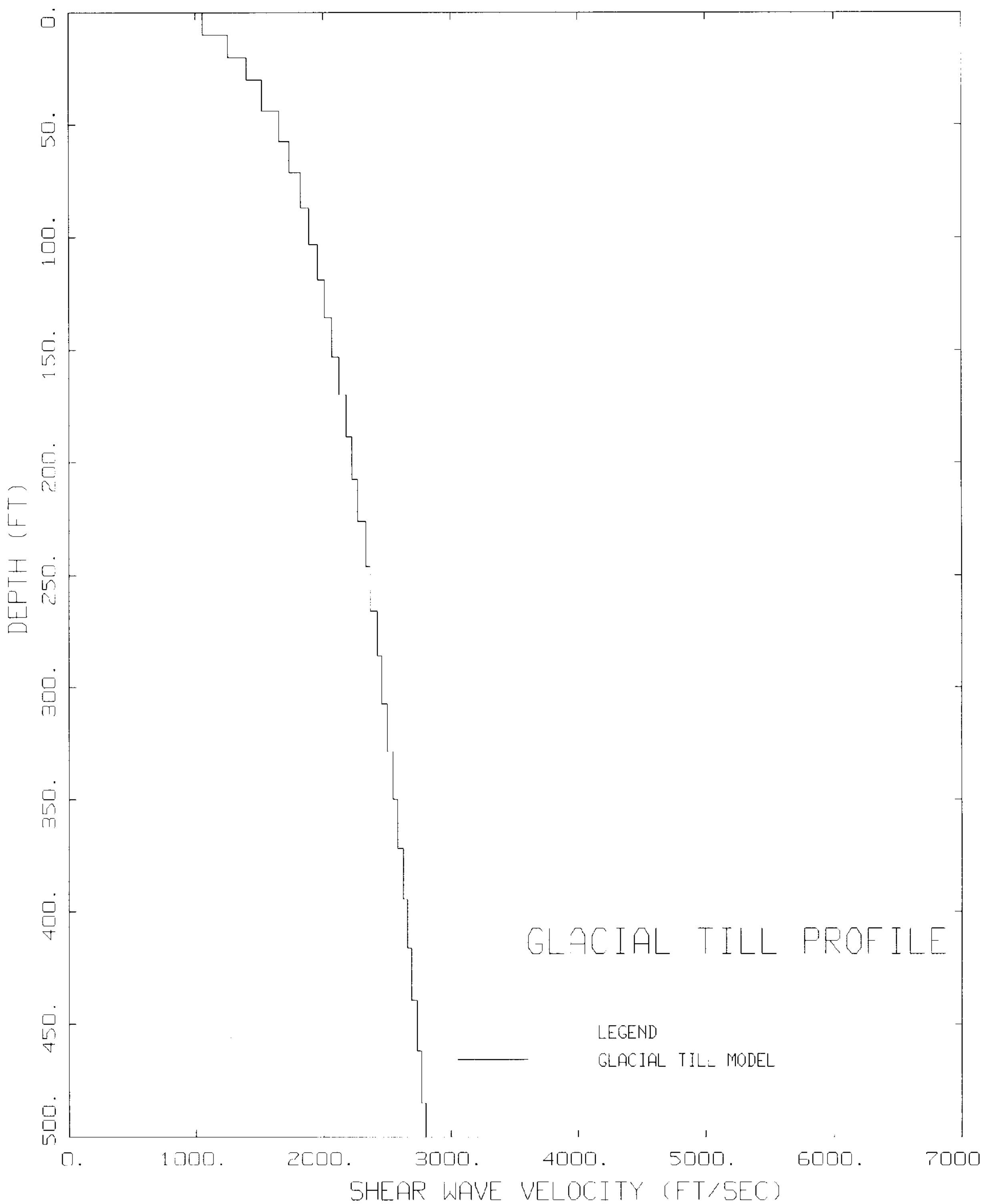

Figure 4-10. Shear-wave velocity profile adopted for Glacial Till (EPRI, 1993).

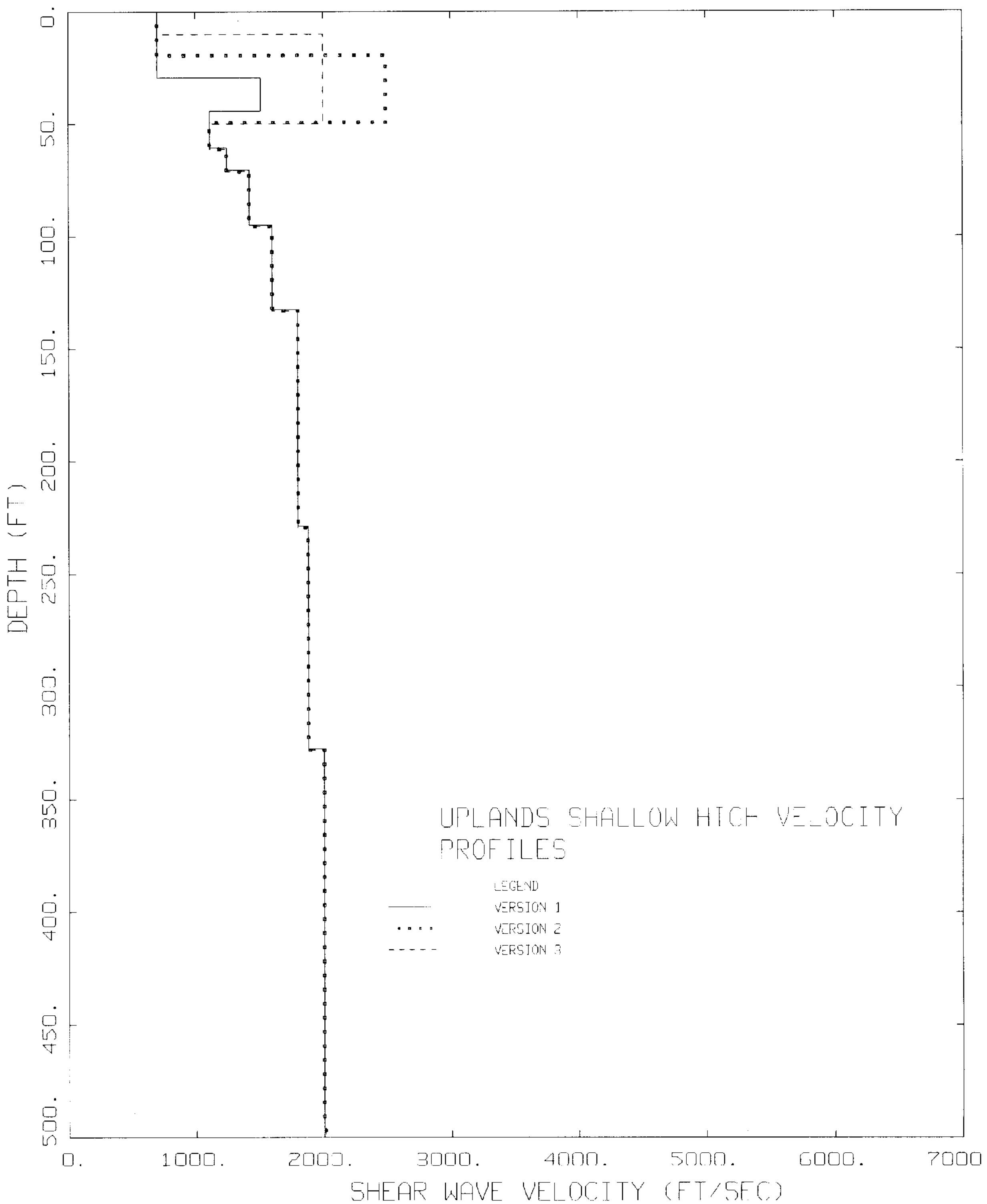

Figure 4-11. Comparison of Uplands shallow high velocity base-case profiles.

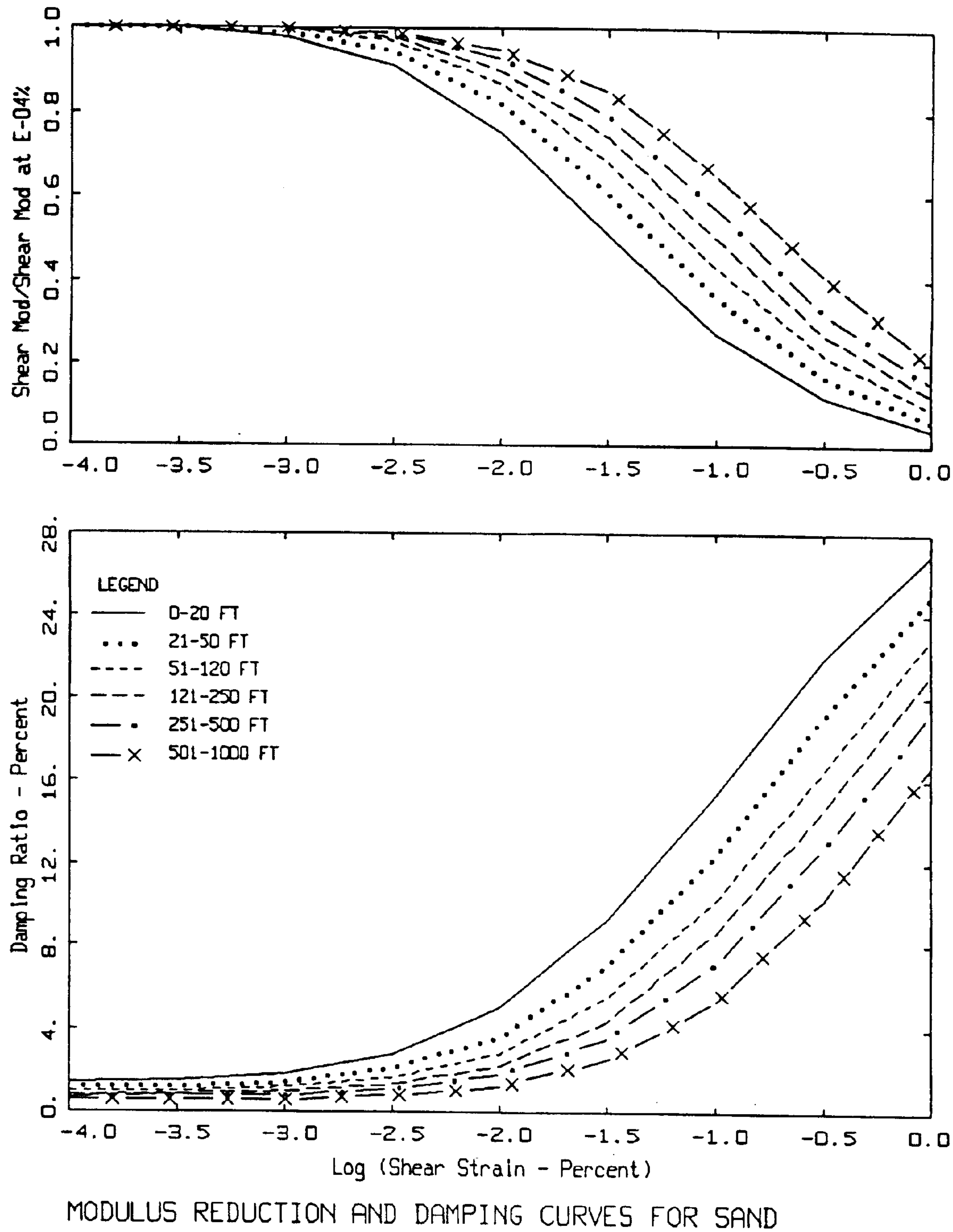

Figure 4-12. EPRI (1993) generic G/Gmax and hysteretic damping curves.

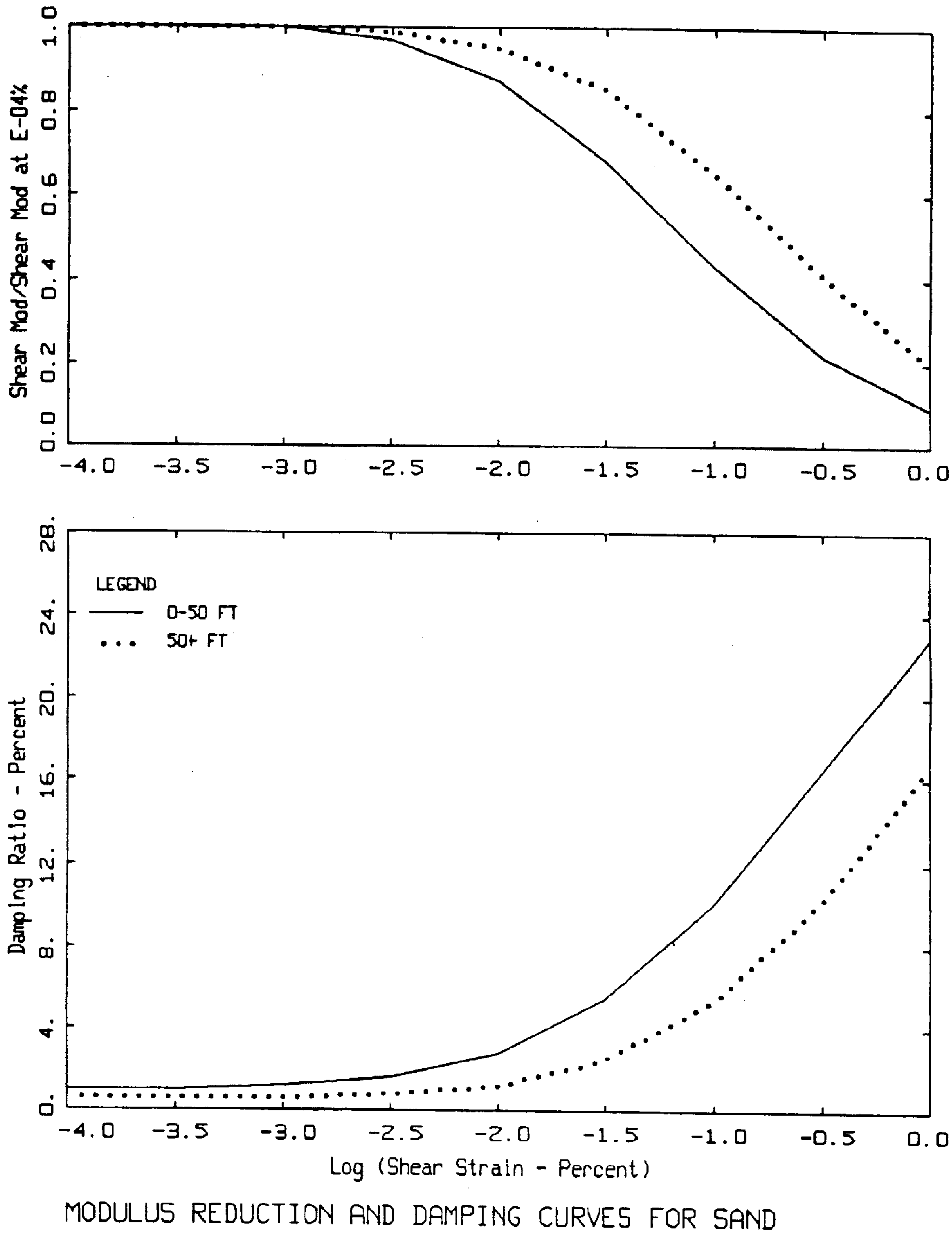

Figure 4-13. Generic G/Gmax and hysteretic damping curves for Peninsular Range southern (California) cohesionless soil site conditions (Silva et al., 1997).

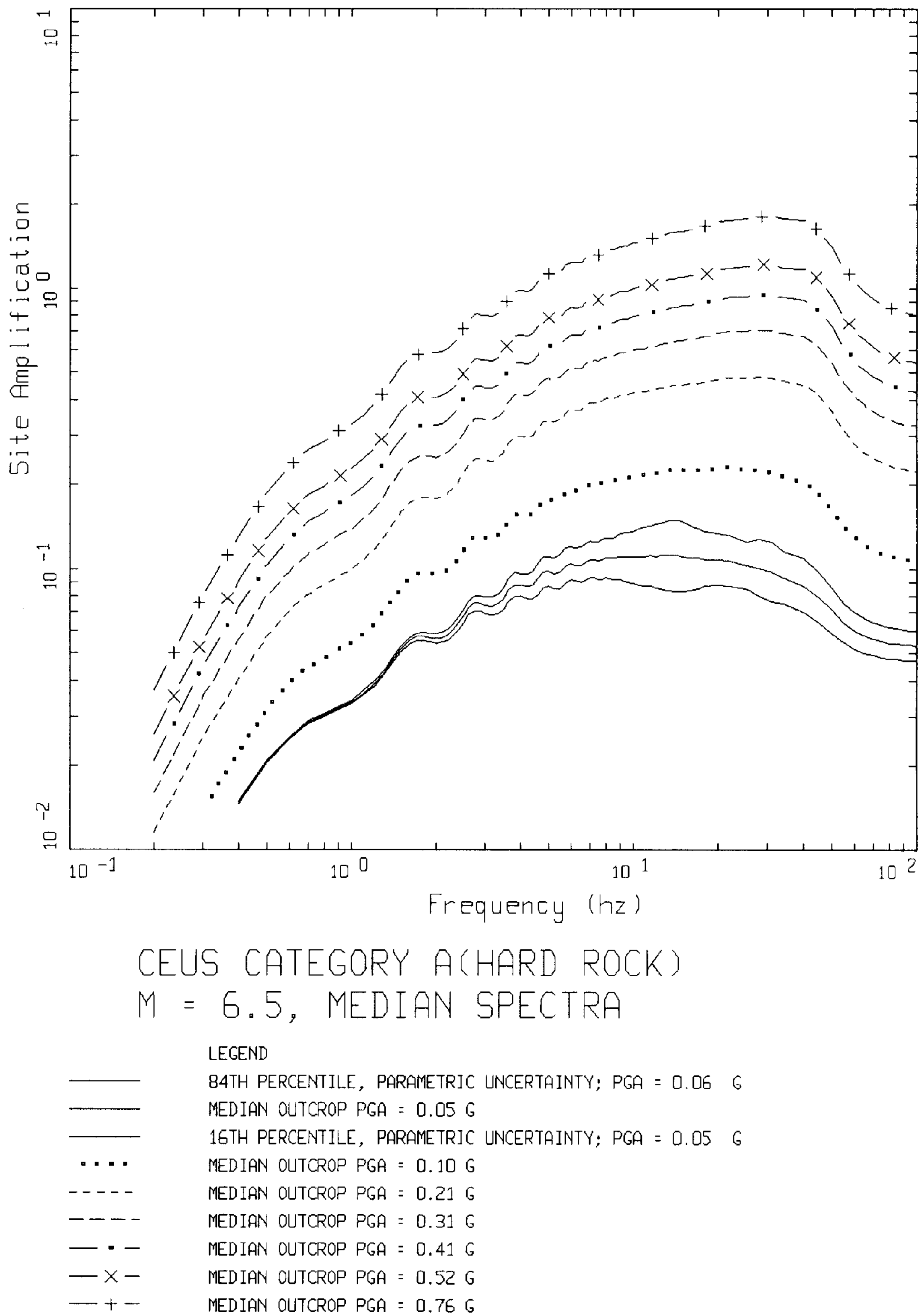

Figure 4-14. Hard rock outcrop median response spectra (5% damped).

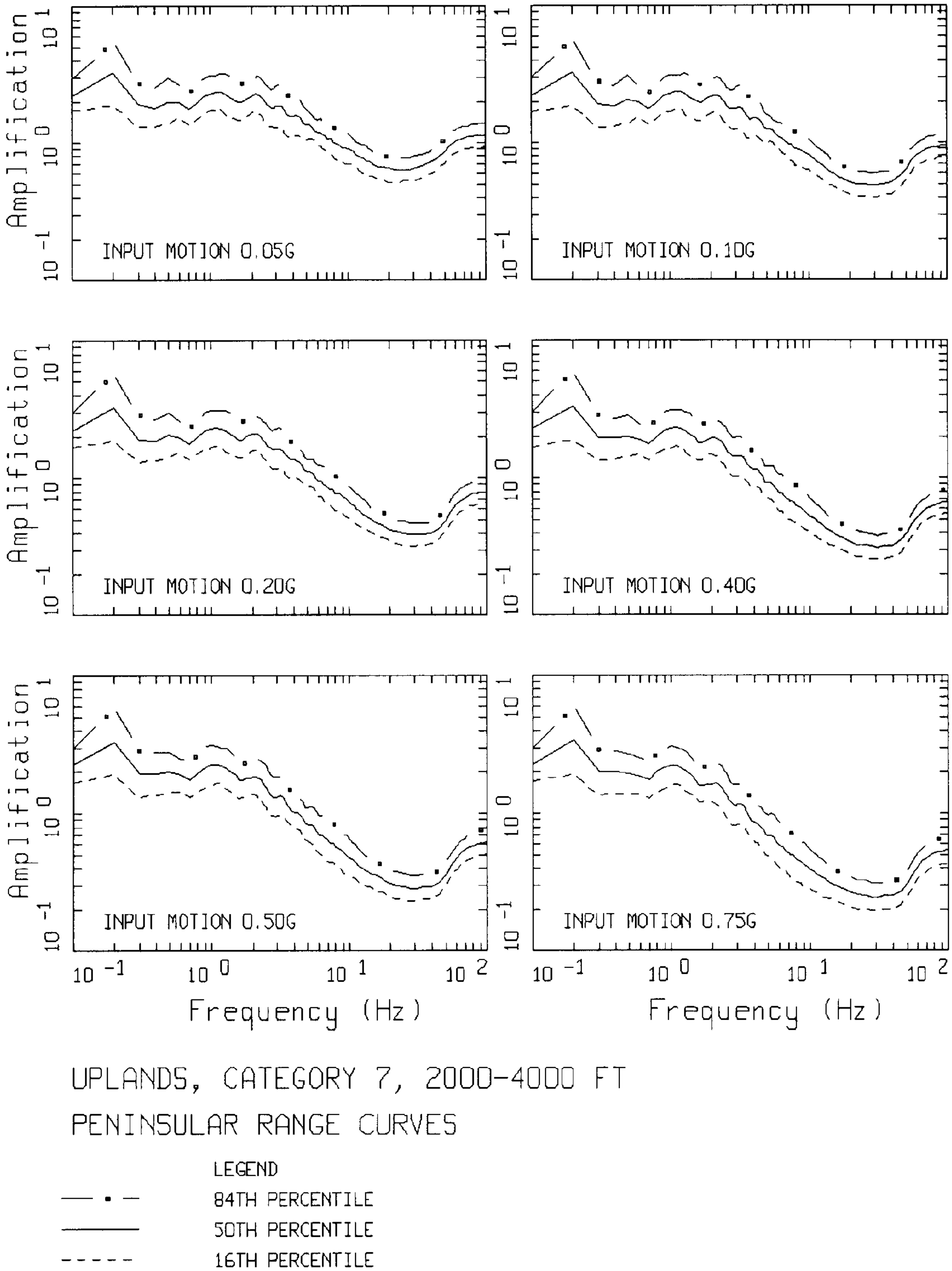

Figure 4-15. Median and ± 1σ amplification factors (5% damped response spectra) computed for the Uplands profile, depth category 7 (2,000 to 4,000 ft), and using Peninsular Range G/Gmax and hysteretic damping curves.

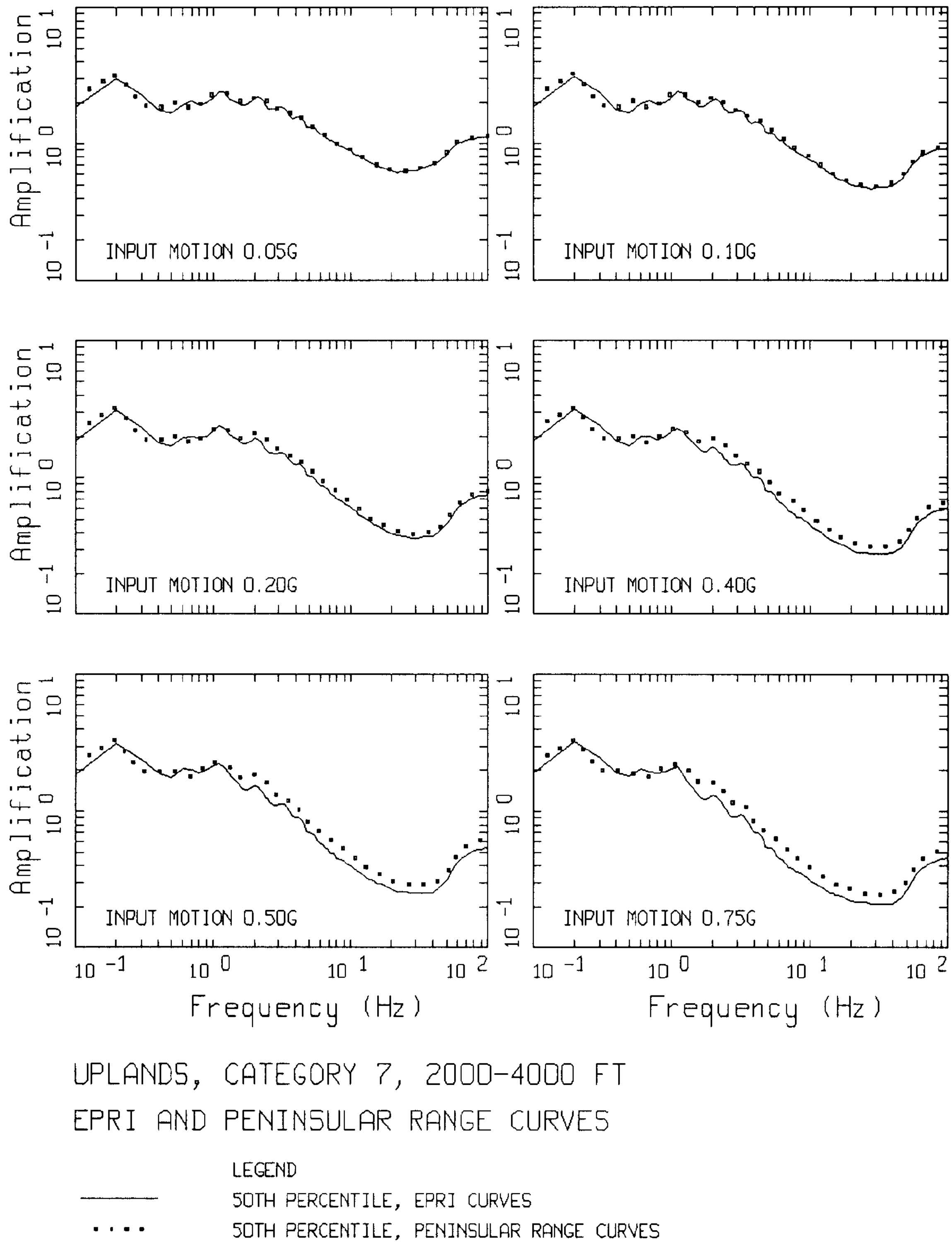

Figure 4-16a. Comparison of median amplification factors computed for depth category 7 (2,000 to 4,000 ft) using EPRI and Peninsular Range nonlinear dynamic material properties: Uplands profile.

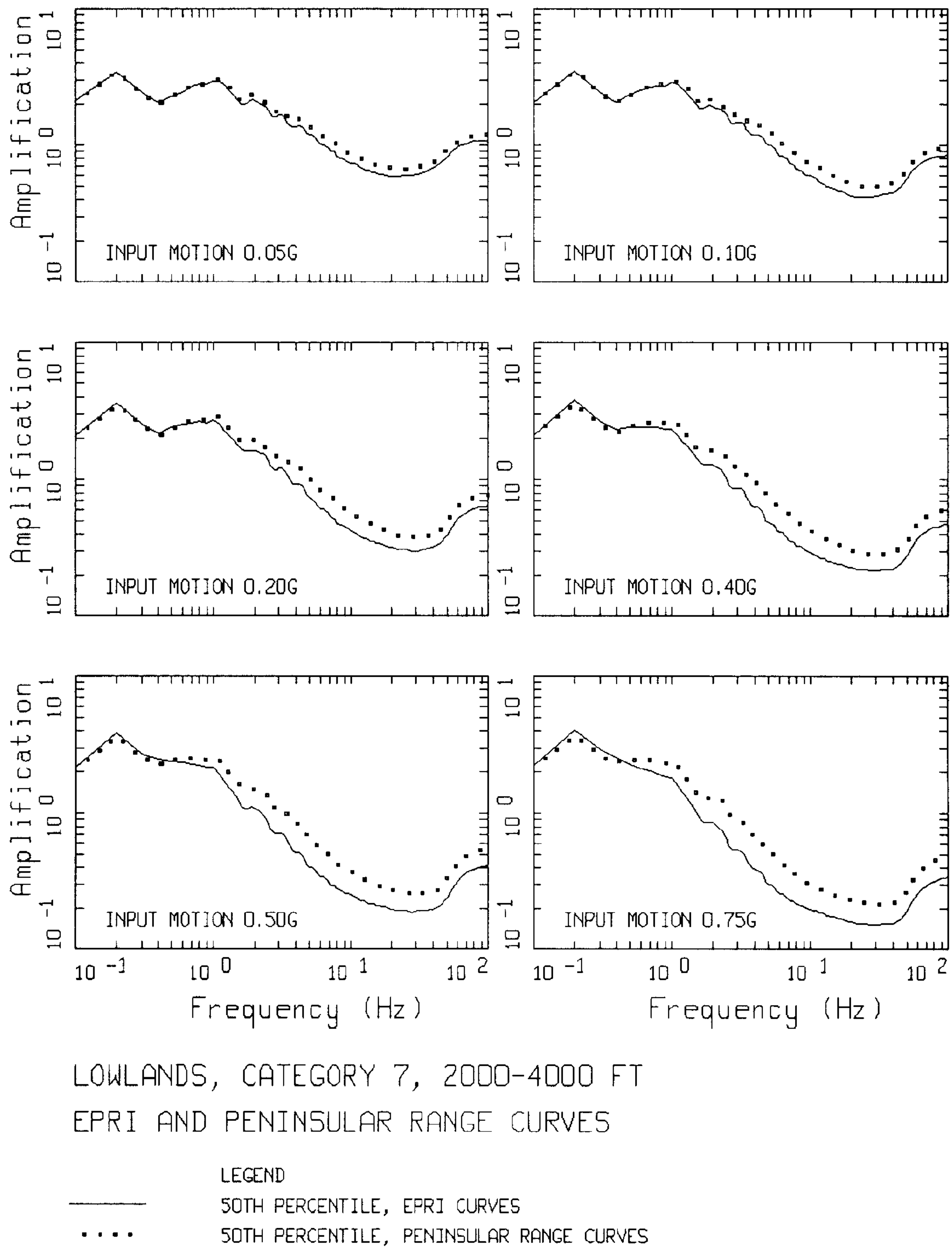

Figure 4-16b. Comparison of median amplification factors computed for depth category 7 (2,000 to 4,000 ft) using EPRI and Peninsular Range nonlinear dynamic material properties: Lowlands profile.

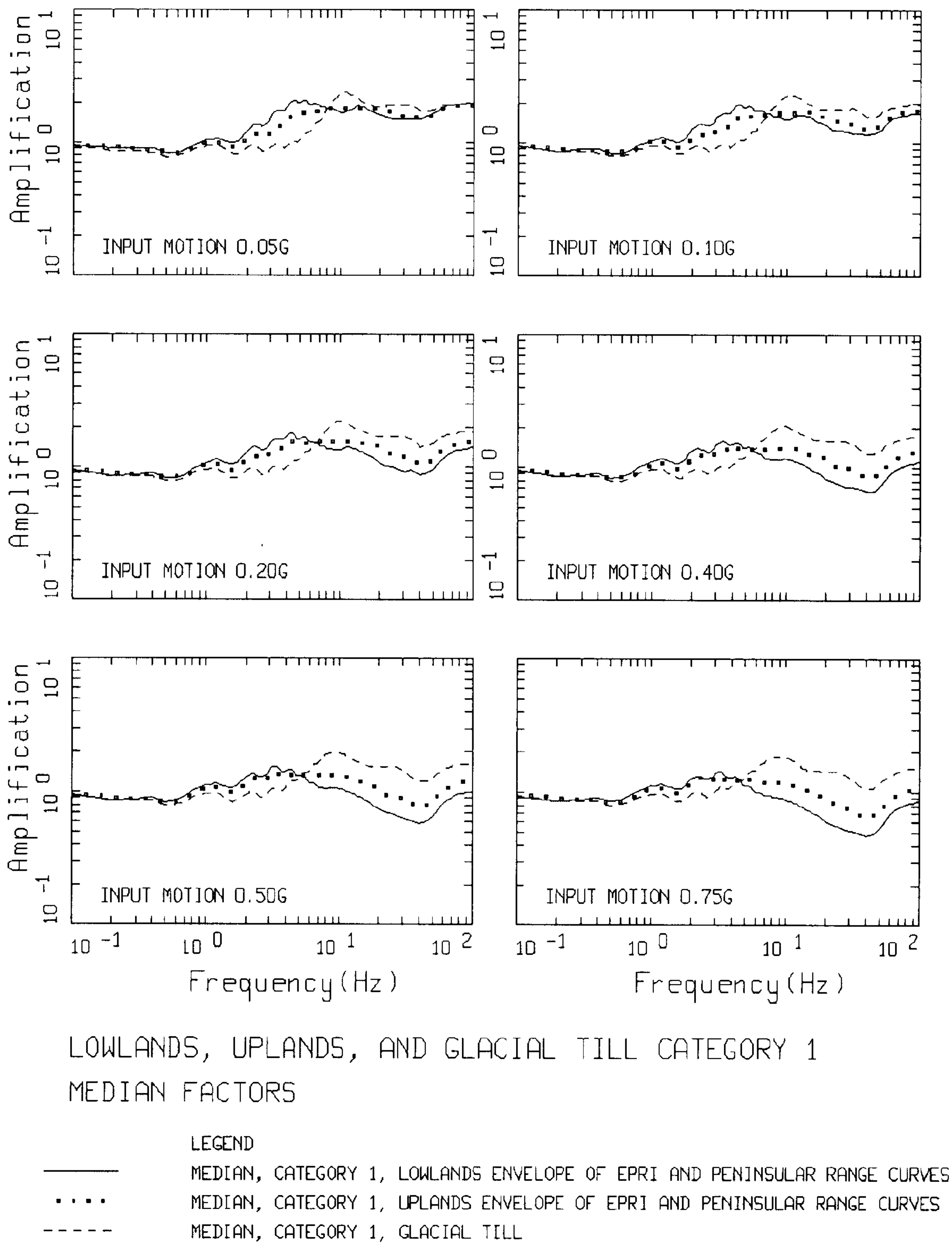

Figure 4-17a. Comparison of median amplification factors computed for the Lowlands, Uplands, and Glacial Till profiles. Lowlands and Uplands reflect envelopes using EPRI and Peninsular Range nonlinear dynamic material properties. Depth category 1 (10 to 50 ft).

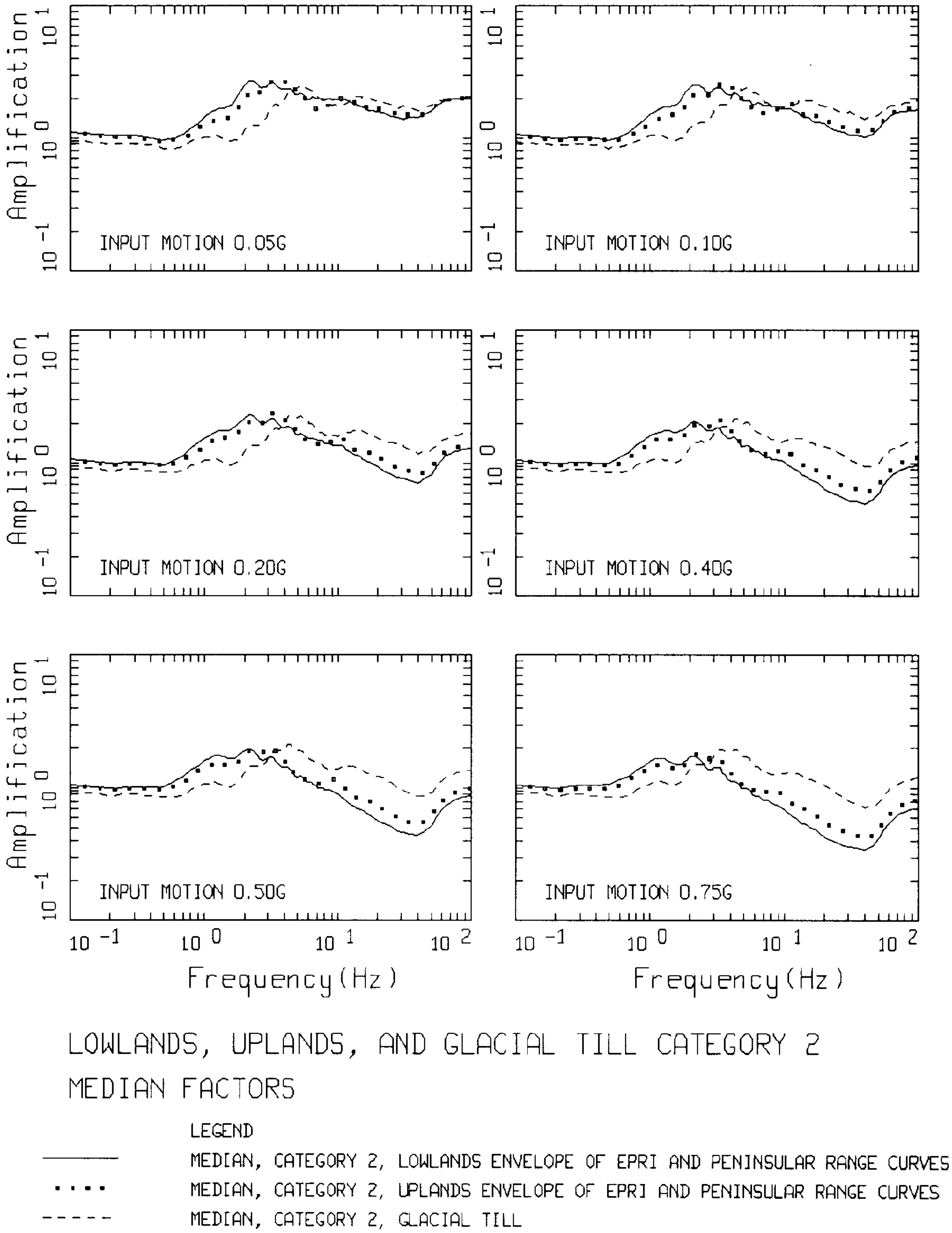

Figure 4-17b. Comparison of median amplification factors computed for the Lowlands, Uplands, and Glacial Till profiles. Lowlands and Uplands reflect envelopes using EPRI and Peninsular Range nonlinear dynamic material properties. Depth category 2 (51 to 100 ft).

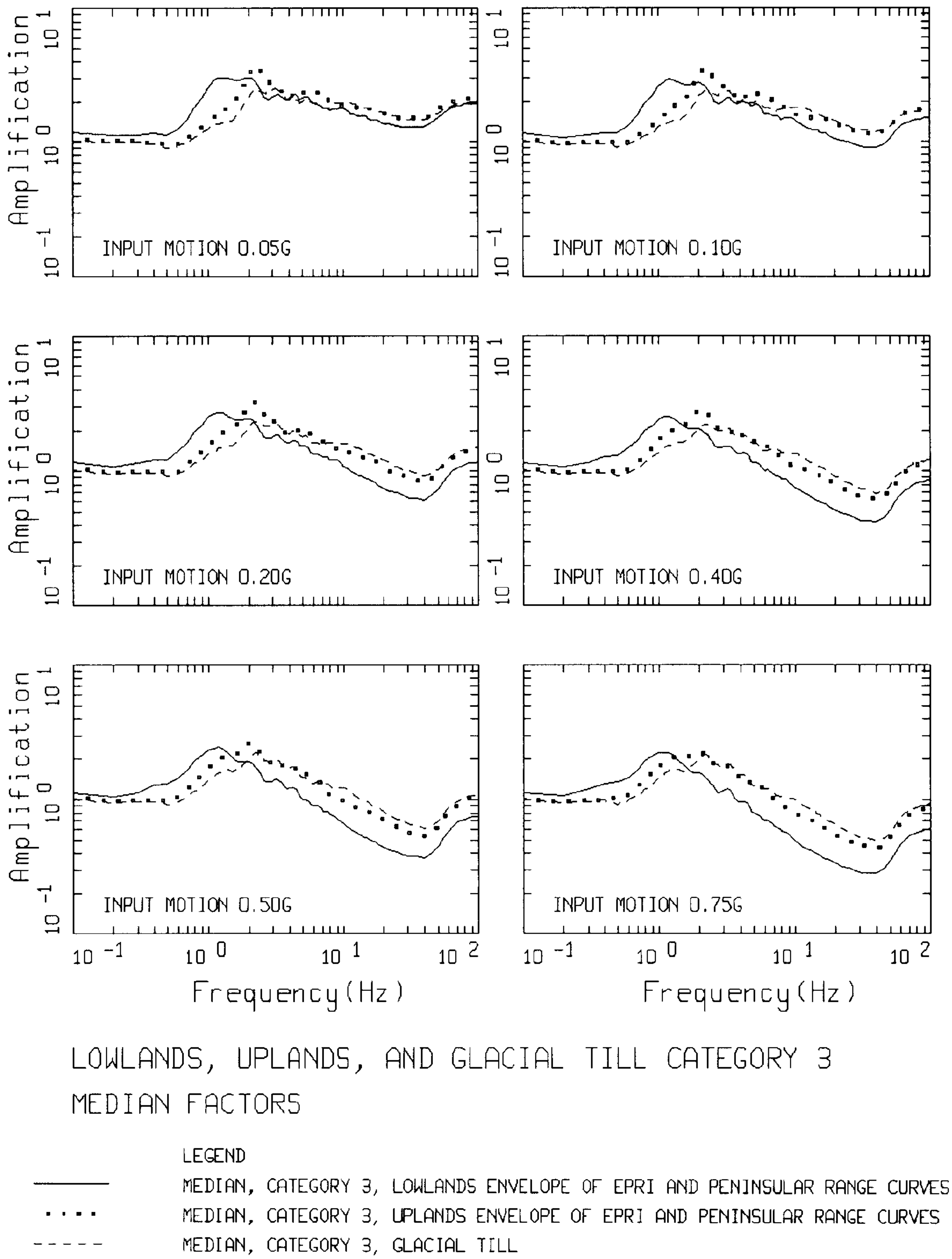

Figure 4-17c. Comparison of median amplification factors computed for the Lowlands, Uplands, and Glacial Till profiles. Lowlands and Uplands reflect envelopes using EPRI and Peninsular Range nonlinear dynamic material properties. Depth category 3 (101 to 200 ft).

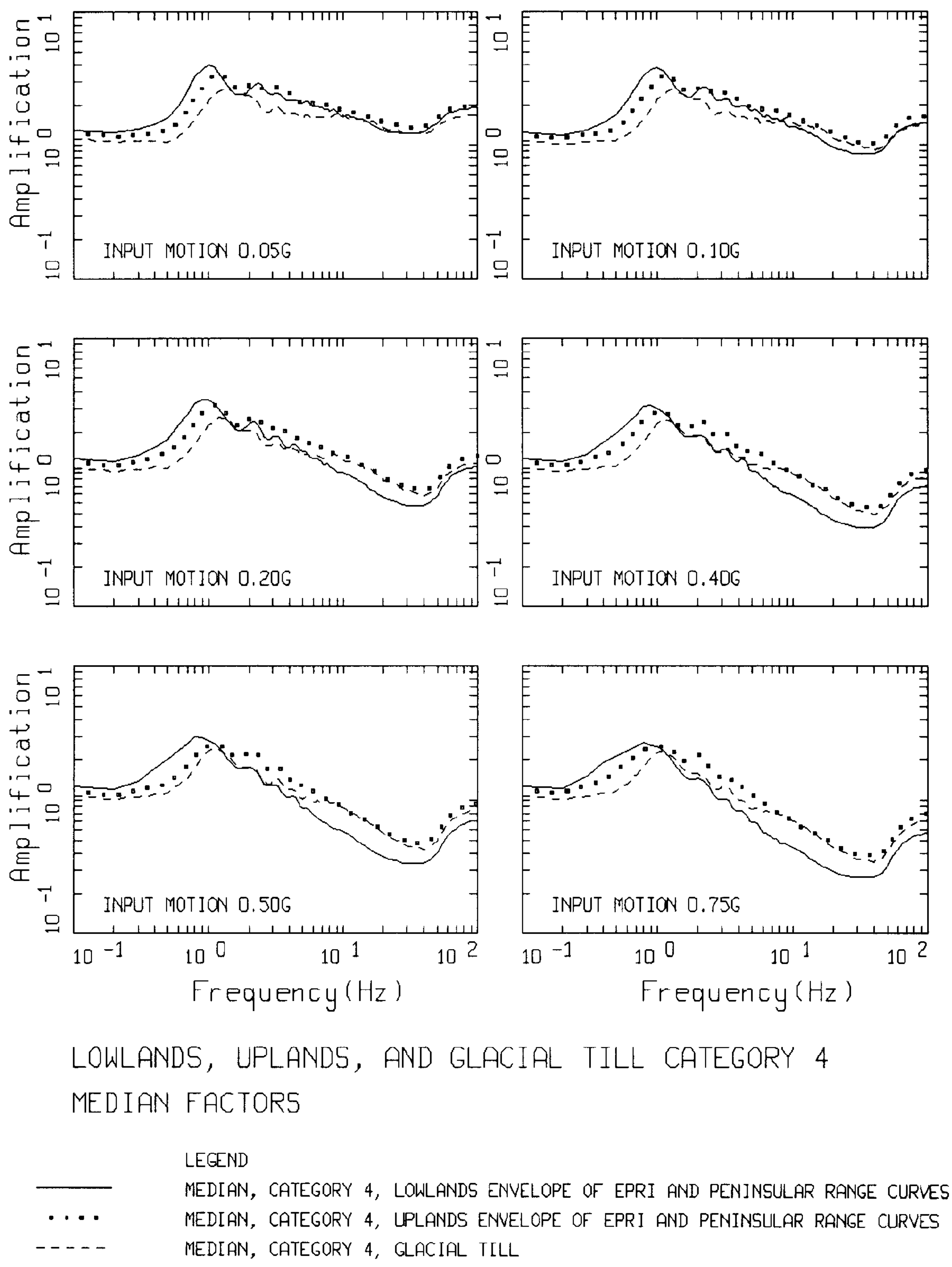

Figure 4-17d. Comparison of median amplification factors computed for the Lowlands, Uplands, and Glacial Till profiles. Lowlands and Uplands reflect envelopes using EPRI and Peninsular Range nonlinear dynamic material properties. Depth category 4 (201 to 500 ft).

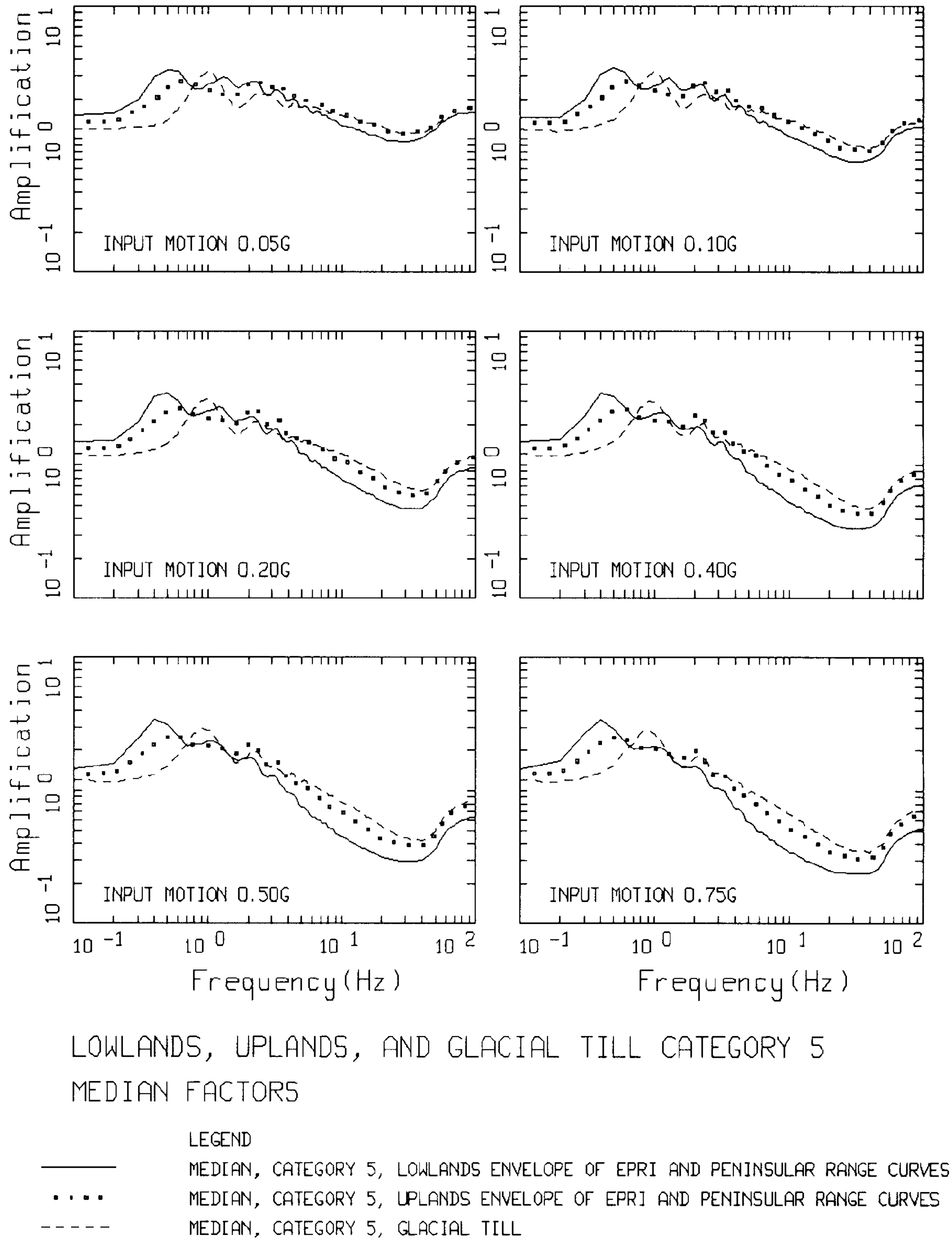

Figure 4-17e. Comparison of median amplification factors computed for the Lowlands, Uplands, and Glacial Till profiles. Lowlands and Uplands reflect envelopes using EPRI and Peninsular Range nonlinear dynamic material properties. Depth category 5 (501 to 1,000 ft).

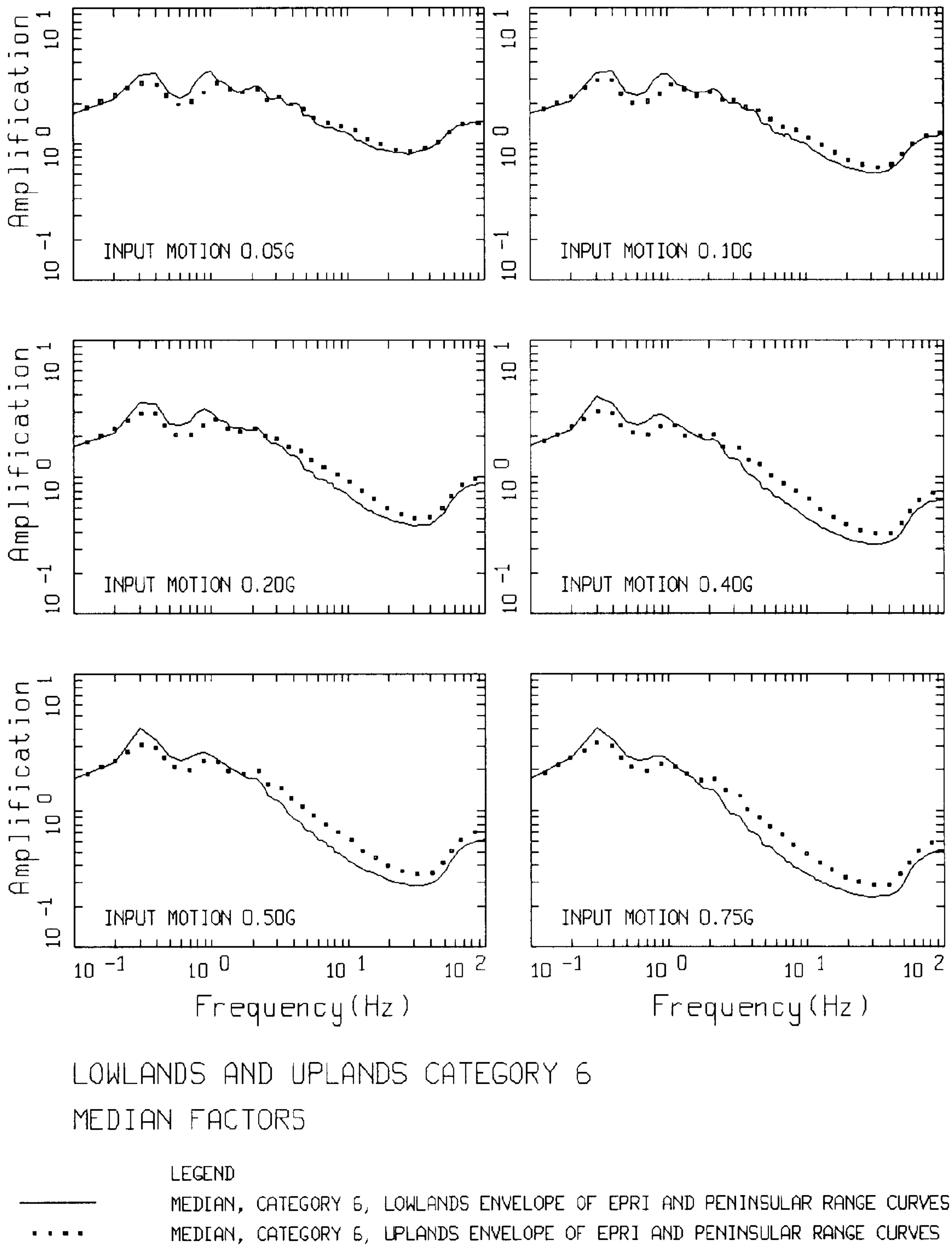

Figure 4-17f. Comparison of median amplification factors computed for the Lowlands and Uplands profiles. Lowlands and Uplands reflect envelopes using EPRI and Peninsular Range nonlinear dynamic material properties. Depth category 6 (1,001 to 2,000 ft).

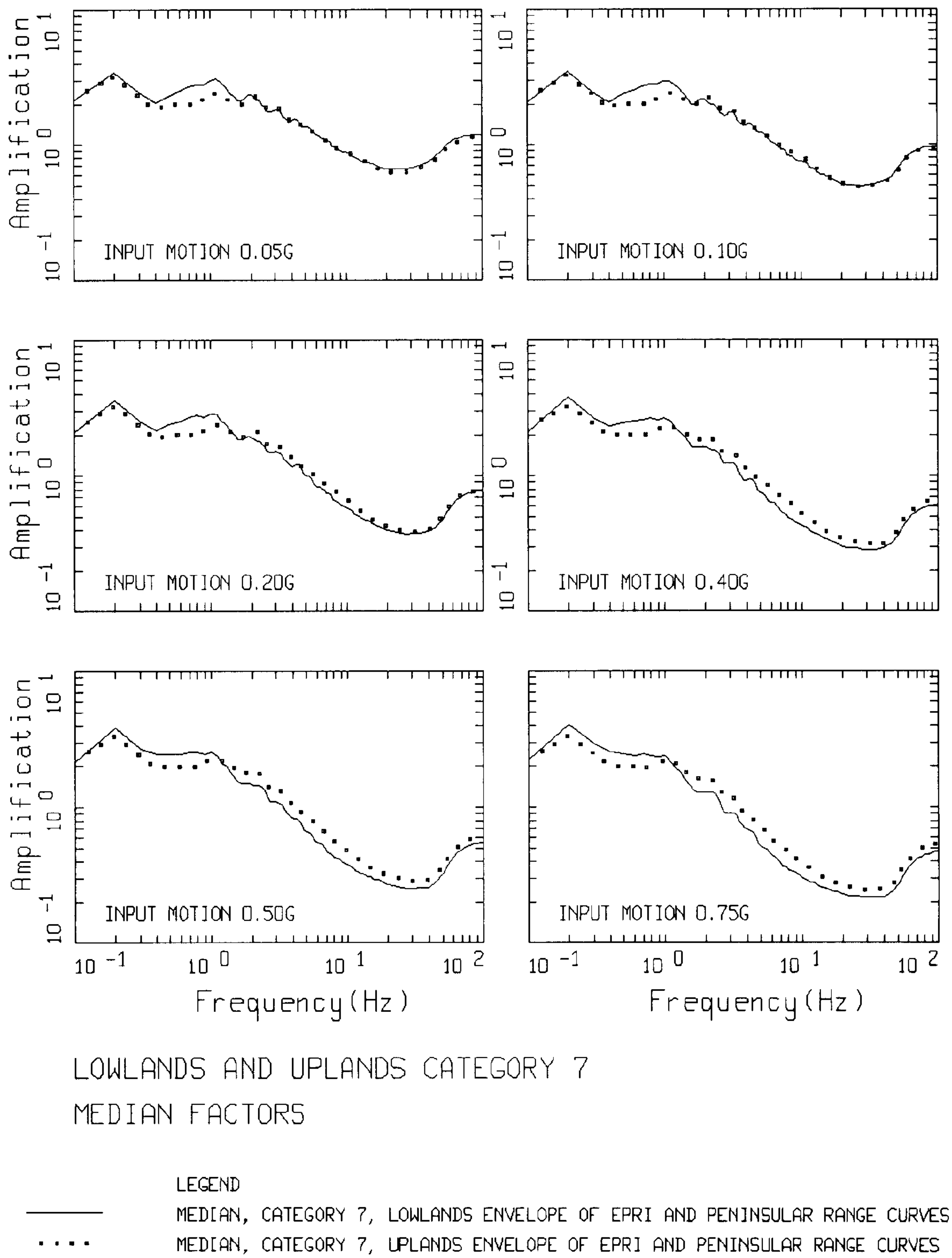

Figure 4-17g. Comparison of median amplification factors computed for the Lowlands and Uplands profiles. Lowlands and Uplands reflect envelopes using EPRI and Peninsular Range nonlinear dynamic material properties. Depth category 7 (2,001 to 4,000 ft).

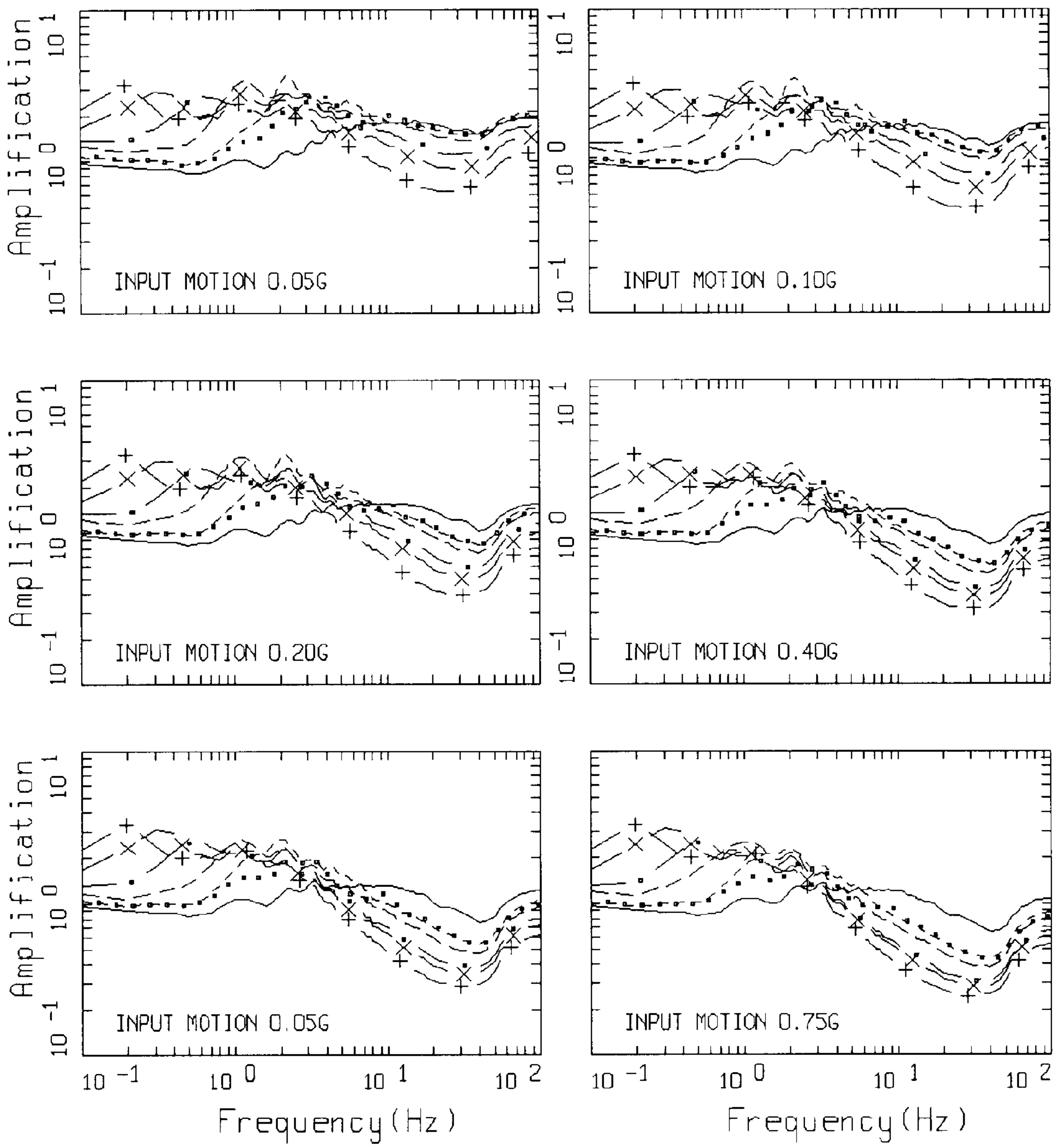

UPLANDS, CATEGORIES 1,2,3,4,5,6,7

ENVELOPE OF EPRI AND PENINSULAR RANGE CURVES

LEGEND

———	MEDIAN, CATEGORY 1
• • • •	MEDIAN, CATEGORY 2
- - - - -	MEDIAN, CATEGORY 3
— — — -	MEDIAN, CATEGORY 4
— • —	MEDIAN, CATEGORY 5
— × —	MEDIAN, CATEGORY 6
— + —	MEDIAN, CATEGORY 7

Figure 4-18a. Comparison of median envelope (EPRI and Peninsular Range nonlinear dynamic material properties) amplification factors for all depth categories (Table 4-6): Uplands profile.

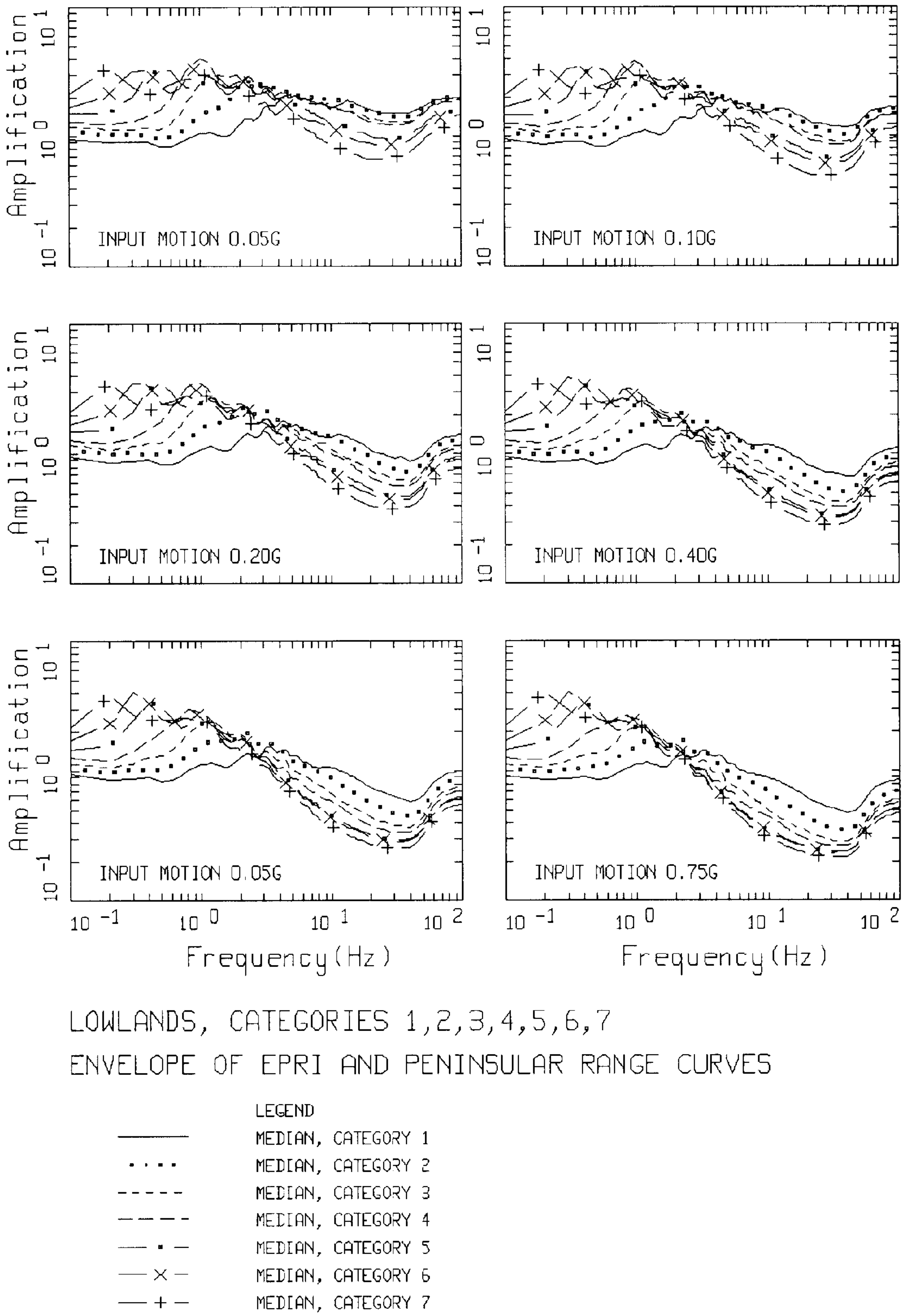

Figure 4-18b. Comparison of median envelope (EPRI and Peninsular Range nonlinear dynamic material properties) amplification factors for all depth categories (Table 4-6):Lowlands profile.

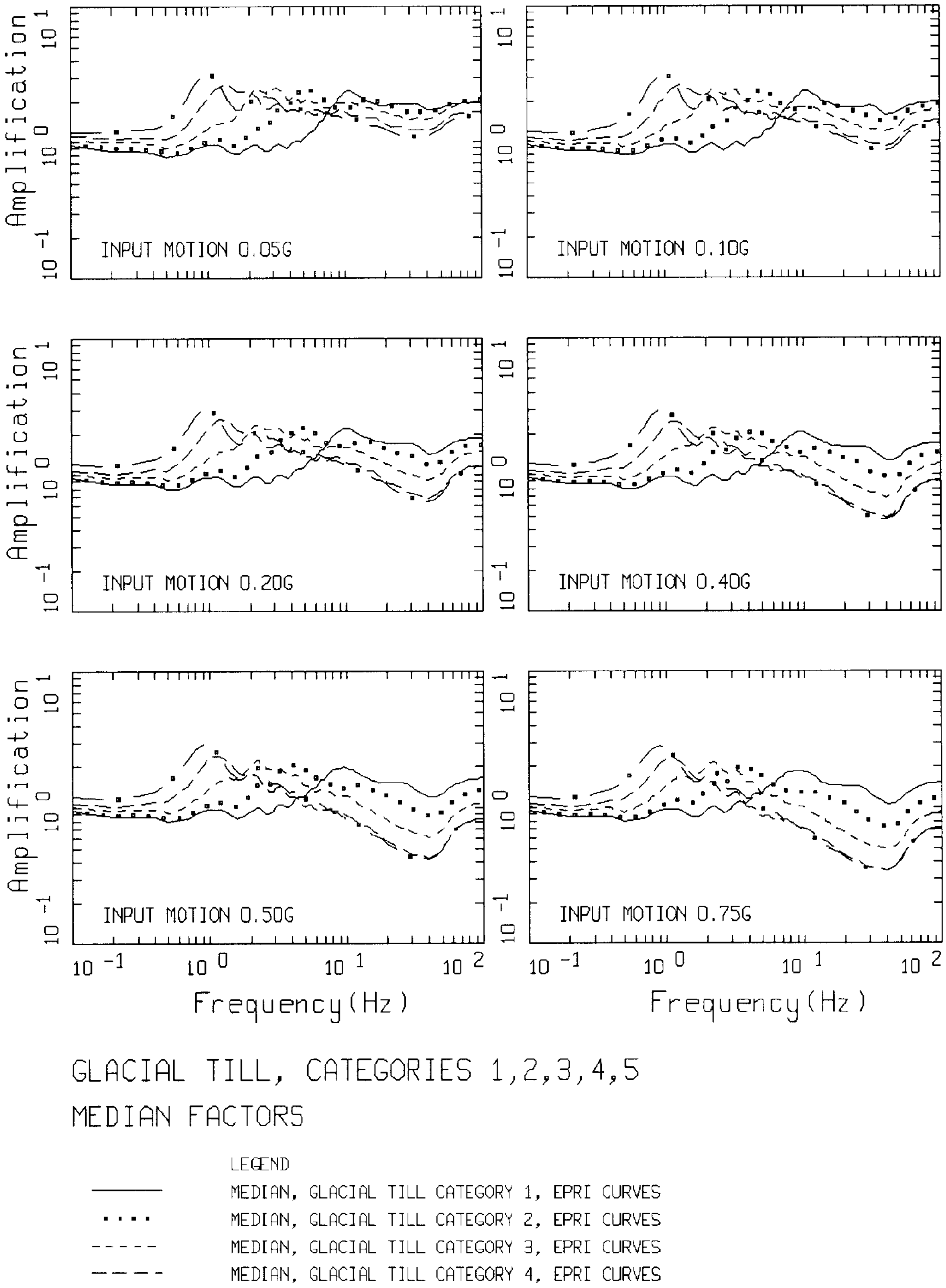

Figure 4-18c. Comparison of median amplification factors for all depth categories (Table 4-6): Glacial Till profile.

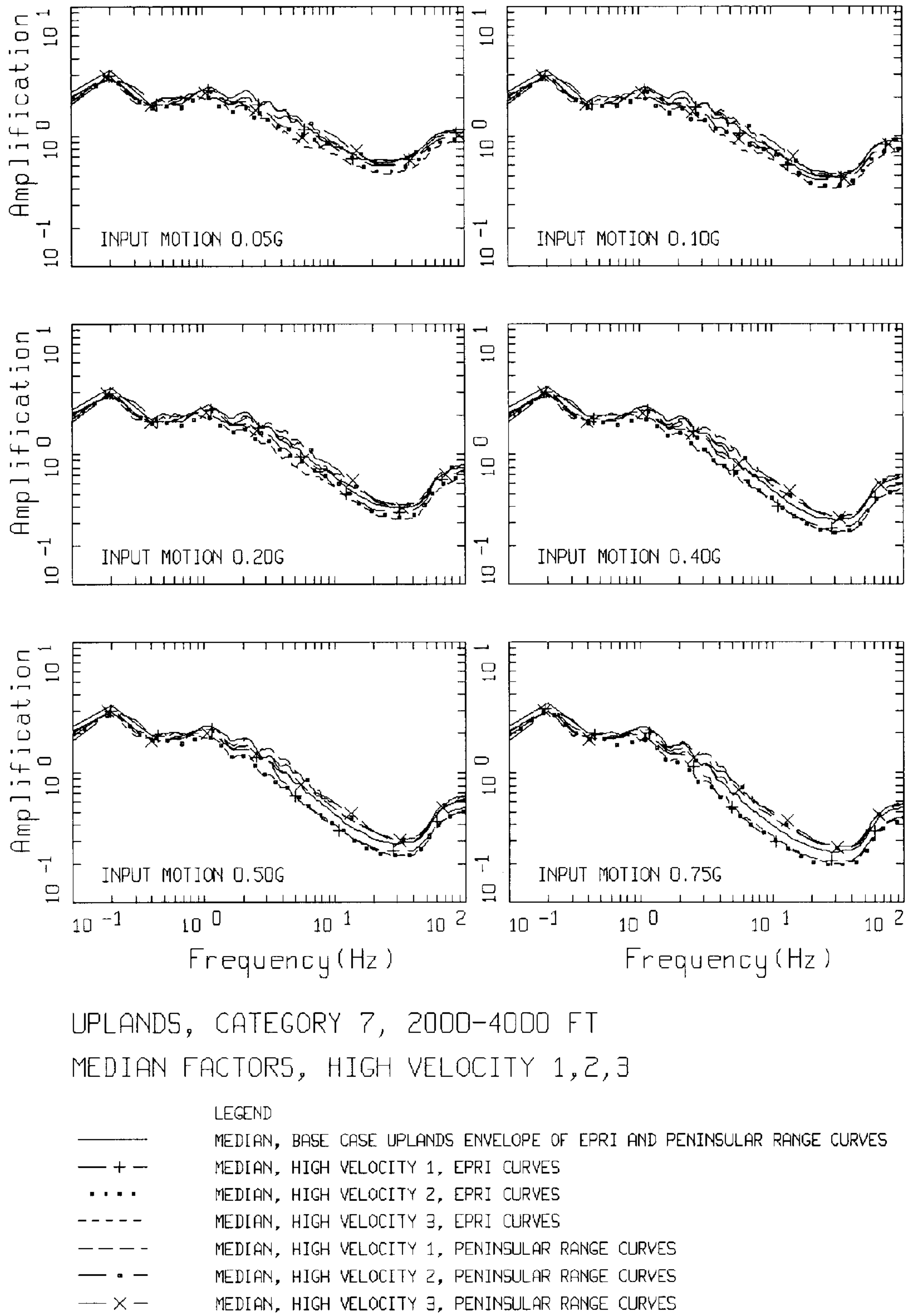

Figure 19. Comparison of median amplification factors for the shallow high velocity Uplands profiles (Figure 4-11). Results using both Peninsular Range and EPRI nonlinear dynamic material properties are shown. For reference, the base-case Uplands envelope amplification factors are included.

Section 5

SEISMIC HAZARD RESULTS AND PROBABILITY-BASED SCENARIO GROUND MOTIONS FOR MEMPHIS AND SAINT LOUIS

5.1 INTRODUCTION

This section presents the probabilistic seismic hazard results obtained for the metropolitan areas of Saint Louis and Memphis and uses those results to develop probability-based scenario spectra and the associated ground motions. The hazard calculations and the development of the scenarios events and their spectra are done for rock site conditions. The rock spectra are then converted to the soil site conditions typical of Saint Louis and Memphis. Finally, artificial ground motions are generated for each spectrum.

Two values of exceedence probability will be considered, namely 10% and 2% in 50 years. The value of 10% in 50 years is currently in use in building codes (e.g., BSSC, 1997). The value of 2% in 50 years is often used for important bridges, landfills, and other special facilities (e.g., EPA, 1995).

5.2 HAZARD AND DEAGGREGATION RESULTS

We performed probabilistic seismic hazard calculations for Saint Louis and Memphis using the source characterizations documented in Section 2 and the rock attenuation equations documented in Section 3, for 5%-damped spectral accelerations of 0.2, 0.5, 1.0, 2.0, 5.0, 10., 20., 50., and 100 Hz (the latter corresponding to peak ground acceleration or PGA). Figures 5-1 through 5-4 present the mean hazard curves.

The spread between the 0.15 and 0.85-fractile spectra indicate the uncertainty that results from incomplete knowledge about earthquakes in the central United States, and their associated ground motions. Analysis of variance on the hazard results indicates which parameter uncertainties are the most important contributors to uncertainty in the hazard. For low-frequency motions in Saint Louis, the most important contributors are the ground-motion models, the geographic extent and seismicity parameters of the Wabash Large source zone, the rate of characteristic events in the NMSZ faults, the maximum magnitude on the Reelfoot fault, and the maximum magnitude in Wabash Large. For high-frequency motions in Saint Louis, the most important contributors are the ground-motion models, and the geographic extent and seismicity parameters of the Wabash Large source zone. For Memphis, the most important contributors are the maximum magnitude on the Blytheville Arch fault, the ground-motion models, and the rate of characteristic events in the NMSZ. The relative importance of these contributors varies as a function of frequency and of exceedence probability, with the Blytheville Arch M_{max} becoming more important for low frequencies and low return periods.

Figures 5-5 through 5-8 show the mean hazard by source for the most important sources, for 1-Hz and PGA, as well as the combined hazard from all sources[1]. In Saint Louis, the largest contributions to hazard come from the Wabash source (Large and Proper combined), followed by the Ozarks background source and by the characteristic portion of the New Madrid sources (Reelfoot fault, East Prairie, and Eeast Prairie extension). The contribution from Wabash is roughly 60% for low frequencies and 80% for high frequencies. In Memphis, the largest contributions to hazard come from the SE Flank fault and the Blytheville arch[2]. At low frequencies, the contribution from the SE Flank fault is somewhat larger; at high frequencies, the contributions from the SE Flank fault and the Blytheville arch are roughly equal.

Figures 5-9 through 5-24 show the deaggregation results for Saint Louis and Memphis, for 1-Hz spectral acceleration and PGA, and for exceedence probabilities of 10% and 2% in 50 years. The 1-Hz results for Saint Louis indicate an almost uniform distribution of contributing magnitudes. The associated distance distribution is multimodal, showing important contributions from local events (from the Wabash Large source), as well as from the northern

[1]In Memphis, the combined hazard is not the sum of the hazards by source because of the clustering of events in the three New Madrid sources, as discussed in Section 2. The same clustering assumption is used for Saint Louis, but its effect is negligible there.

[2]Both the exponential and the characteristic portions of the Blytheville arch have significant contributions to hazard in Memphis.

portions of the NMSZ. The PGA results for Saint Louis indicate that moderate (5.0-6.5) magnitudes in the Wabash Large source are the most important contributors to hazard, but there are moderate contributions from large, distant events in the NMSZ. The results from Memphis show less of a difference between 1 Hz and PGA. For both frequencies, there is a broad distribution of contributing magnitudes, which shifts to higher magnitudes for the lower exceedence probability. The distribution of distance shows spikes associated with the SE Flank of the Reelfoot rift (~ 20 km), with the Blytheville Arch (~65 km), and with the Reelfoot fault (~100 km). The distributions of epsilon at both locations indicate that the 10% in 50 year results are typically associated with median+1σ motions, while the the 2% in 50 year results are typically associated with roughly median+1.5σ to median+2σ motions (where the higher value applies to Saint Louis).

5.3 SELECTION OF SCENARIO EVENTS

In a manner analogous to Appendix C of NRC 1.165 (1997), we define separate scenarios for low-frequency and high-frequency motion, using the 1-Hz and 10-Hz deaggregation results (the latter are essentially identical to the PGA results shown here).

The deaggregation results presented above indicate that, with the possible exception of high-frequency motions in Saint Louis, the hazard at the locations and exceedence probabilities of interest is due to events in broad range of magnitudes and distances. It is not appropriate, therefore, to represent this hazard for a given frequency by means of a single scenario event. After experimenting with approaches based on fractiles or moments of the magnitude and distance distributions (e.g., Lee et al., 1997), we decided to use a simpler and more intuitive approach where break up the sources into those near the site and those more distant ones. In essence, we break up the distribution of distance in Figures 5-9 through 5-24 and use the associated conditional magnitudes. For Saint Louis, the local sources consist of the Wabash large source plus all other regional area sources (only the former makes a significant contribution), and the distant sources consist of all NMSZ sources plus the Rough Creek graben. For Saint Louis, the local sources consist of the SE-Flank fault plus relatively unimportant local area sources (Reelfoot rift, SE U.S., and Arkansas), and the distant sources consist of all other sources. For each site and group of sources, we then compute the modal magnitude-distance-epsilon combination and we assign it a weight roughly equal to the relative contribution of that group of sources to the total hazard[3]. The resulting events are shown in Table 5-1.

Results for Saint Louis in Table 5-1 indicate that the ground motions associated with the exceedence probabilities in common use may be caused by very different events, namely a moderate earthquake with magnitude 5.1 to 5.6 at 10 to 34 km distance occurring in the Wabash Large seismic source, or a large earthquake with magnitude 7.4 to 7.75 at 236 km distance occurring in the northern portions of the NMSZ. Results are similar for Memphis, with the small-distance events occurring on the SE Flank fault, except that the contrast in distances is less pronounced and that in one case (the 1 Hz, 2% in 50 years case) the magnitude of the local event is 7.75.

5.4 SCENARIO SPECTRA FOR ROCK SITE CONDITIONS

We calculate the spectra associated with each scenario events using the following approach:

1. Use the two attenuation equations (one- and two-corner models) to calculate the median ground motions associated with the magnitude-distance combination of the scenario and average the two results[4].

---

[3]If the modal magnitude was greater than 7.75, it was reduced to this value and the associated distance and epsilon were set to their conditional modal values given a magnitude of 7.75. This is done because, in spite of the thoughtful arguments by Johnston (1996), there were concerns among members of the project team about the plausibility of having magnitude 8 or greater earthquakes on faults with lengths of 140 km or less. Thus, although we assign some weight to these larger magnitudes in the hazard calculations, and these magnitudes contribute significantly to the mean uniform-hazard spectrum, we do not generate scenario events with the durations associated with these larger magnitude. Questions remain about the magnitudes of the 1811-1812 events, and about the maximum magnitudes that are possible on the NMSZ faults. This will remain an issue of research and debate for many years to come.

[4]Use arithmetic averaging (on the amplitudes).

2. Modify the amplitude calculated for the effect of epsilon. At the frequency associated with this scenario (which is either 1 or 10 Hz), this implies multiplication by a factor of $\exp(\sigma\,\varepsilon)$, where σ is the ground-motion standard deviation given in Section 3.. At other frequencies, multiply by a smaller factor of $\exp[\sigma\,\varepsilon\,\rho(f,\tilde{f}_0)]$, where $\rho(f,\tilde{f}_0)$ is the correlation coefficient between epsilon values at the frequency f of interest and at the frequency $\tilde{f}_0$, where $\tilde{f}_0$ is defined as the frequency closest to f in the interval $[f_0/3\,,\,3f_0]$, and f_0 is the frequency associated with the scenario[5]. We use the correlation model by Inoue (see Risk Engineering, 1991), which takes the form:

$$\rho(f,\tilde{f}_0)=Max[1-\frac{1}{3}\ln|\frac{f}{\tilde{f}_0}|,0] \tag{5-1}$$

Figures 5-25 through 5-32 show the scenario spectra for rock. Each figure also shows the associated mean uniform hazard spectrum. The low-frequency scenarios are associated with 1-Hz spectral acceleration. The high frequency scenarios are associated with 1-Hz spectral acceleration.

The result of the above exercise is a set of four scenario events for each combination of city and exceedence probability. These scenario spectra, the scenario spectra to be derived in the next two sections, and the associated time histories, should be used as follows:

a. In design, the stresses or forces calculated under each scenario should be lower than the values allowed by code.

---

[5]We introduce the ρ term because the assumption that epsilon is consistently high for all frequencies may be too conservative. On the other hand, we use $\tilde{f}_0$ rather than f_0 to calculate this term because we want the scenario spectrum to be high over the frequency range for which the scenario applies (i.e., either 0.33 to 3 Hz for the low-frequency scenarios or 3.3 to 30 Hz for the high-frequency scenarios), not just at the discrete frequencies of 1 or 10 Hz.

b. In calculating economic losses, the loss given the occurrence of an event with 2% or 10% probability in 50 years is the weighted sum of the losses calculated with the four corresponding scenarios (using the weights in Table 5-1).

5.5 SCENARIO SPECTRA FOR SAINT LOUIS SITE CONDITIONS

In this Sections 5.5 and 5.6, we select several typical profiles for each city of interest and use the amplification factors developed in Section 4 to generate the associated scenario spectra.

For Saint Louis, we use the surface-geology characterization, bedrock topography, and typical profiles compiled by McCaskie (personal communication, 11/30/1999) to define the following representative categories:

Floodplains. The floodplains of the Missouri and Mississippi Rivers are relatively flat and made up of extensive deposits of alluvial materials filling a deep bedrock valley. High groundwater levels that fluctuate with the river stage are observed across the flood plains. The Florissant Basin, a localized area of low relief in north St. Louis County, is also included in this category. These categories are represented by symbols Ia and Ic by Lutzen and Rockaway (1971). Because there are no velocity measurements for profiles in this region, we represent this category by means of the Lowlands profile from Section 4, using a depth of 100 feet.

Loess Sites. This category includes two types of loess sites. One area, the rolling uplands, covers a widespread area throughout the City of St. Louis and St. Louis County and consists of windblown deposits (loess) covering a rugged bedrock topography. The upland areas are characterized by a relatively steep and rugged terrain at the bluffs grading to undulating hills behind the bluff lines. Another area, located in southwest St. Louis County, is fairly rugged with slopes greater than 5 percent and topographic relief often more than 200 feet. This area generally has a thin cover of loessial and residual soils and bedrock outcrops are common. These soils are represented by symbols Xb and IIb by Lutzen and Rockaway (1971). For the purposes of site-response, we will represent this category by means of the Uplands profile. We will consider two values of the depth to bedrock, namely 30 feet (which we denote as **Loess1**) and 60 feet (which we denote as **Loess2**).

Figure 5-33 shows the contours of loess thickness in Saint Louis. This map may also be used to identify the boundaries of the flood plain area, which extends beyond the bluffs. The Florissant basin, which consists of a narrow (~ 2km wide) strip extending from the International Airport to the NNE, is not resolved by this map.

For the calculation of the scenario spectra for a soil type, we multiply each ordinate of the rock spectrum by the amplification factor (from Section 4) corresponding to that frequency and rock amplitude[6]. The scenario spectra corresponding to the Saint Louis Floodplains, Loess1, and Loess2 site conditions are shown in Figures 5-34 through 5-37, 5-38 through 5-41, and 5-42 through 5-45, respectively. It is noted that all three Saint Louis site categories exhibit significant amplification of high-frequency energy as a result of their shallow soil columns. The response Loess1 and Loess2 categories differ only at frequencies near 3 Hz.

5.6 SCENARIO SPECTRA FOR MEMPHIS SITE CONDITIONS

For Memphis, we use the work of Romero and Rix (2000), as well as additional insights and data provided by them. Based on this information, we use the following three representative categories:

Holocene Deposits. These consist of Holocene deposits along the major rivers and meanders in the Memphis metropolitan area (see Figure 5-46). Romero and Rix find that their characteristic profile for this category is consistent with Hwang's Soil Profile 1. For the purposes of site-response, we will represent this category by means of the Lowlands profile (which is based, in part, on Romero and Rix's data for these sites), with a depth of 3,000 feet.

[6] In calculating the soil amplitudes by simply multiplying by the median amplification factor, we neglect the uncertainty in site response, as well as other effects. A more refined, recently developed procedure is provided in McGuire et al. (2000). This new procedure accounts for the combined effects of site-response uncertainty and increasing soil nonlinearity.

Pleistocene Upland Deposits. Profiles in the area are generally composed of loess deposits, underlain by some of the same formations seen in the Lowlands profiles. Romero and Rix (2000) separate the available profiles into several categories based primarily on geographical location and elevation (see Figure 5-46). These authors also observe more variability among the Pleistocene profiles than among the Holocene profiles. One significant feature in some of the Pleistocene profiles is the presence of a high-velocity layer at depths of 10 to 25 m (with velocities significantly higher than those of the strata immediately above and below this layer), which has been identified as a sandy gravel with varying degrees of cementation. The profiles with high-velocity layers are identified by large circles in Figure 5-46. We note that the profiles with a high-velocity layer include all profiles in Shelby Farms, a large number of the profiles in "Memphis", as well as three profiles in the vicinity of "Memphis."

We consider two representative Pleistocene profiles for the development of scenario spectra. The first (which we denote as **Pleistocene1**) has no high-velocity layer and is represented in the site-response calculations by the Uplands profile, with a depth of 3,000 feet. The second (which we denote as **Pleistocene2**) has a high-velocity layer and is represented in the site-response calculations by the worst (at each individual frequency) of the Uplands profile and the three high-velocity profiles considered in Section 4, with a depth of 3,000 feet. Pleistocene1 is applicable to the Shelby Forest and "Memphis" areas in Figure 5-46, as well as to locations near the boundaries of the latter.

The scenario spectra corresponding to the Memphis Holocene, Pleistocene1, and Pleistocene2 site conditions are shown in Figures 5-47 through 5-50, 5-51 through 5-53, and 5-54 through 5-57, respectively. It is noted that all three Memphis site categories exhibit significant amplification of low-frequency energy as a result of their very thick soil columns. Although PGA values differ little from the rock values, all energy above 15 Hz is filtered out by the effect of anelastic attenuation through the thick soil column. The high-frequency portions of some of these spectra show minor anomalies in shape, which will be removed prior to the generation of artificial time histories. Differences in amplification between the three representative Memphis profiles is small.

5.7 SCENARIO TIME HISTORIES

We have generated artificial time histories corresponding to the scenario spectra obtained in Sections 5.4 through 5.6 Downloadable files with these time histories, as well as a description of the simulation approach used, are available at the web site http://www.riskeng.com.

5.8 REFERENCES

Building Science Safety Council (1997). NEHRP *Recommended Provisions for Seismic Regulations for New Buildings and Other Structures*. FEMA 302 and 303.

EPA (1995). *RCRA Subtitle D (258) Seismic Design Guidance for Municipal Soild Waste Landfill Facilities.* Prepared by G. Richardson, E. Kavazanjian, and N. Matasovi. EPA Risk Reduction Engineering Laboratory.

Johnston, A.C., 1996. Seismic moment assessment of earthquakes in stable continental regions III. New Madrid 1811-1812, Charleston 1886 and Lisbon 1755. *Geophys. Jour. International*, 126: 314-344.

Lee, R.C.; Maryak, M.E.; and McHood, M.D. 1997. SRS Seismic Response Analysis and Design Basis Guidelines. WSRC-TR-97-0085, Rev. 0. Aiken, South Carolina: Westinghouse Savannah River Company.

Lutzen, Edwin E. and John D. Rockaway, Jr., (1971), "Engineering Geology of St. Louis County, Missouri", Engineering Geology Series No. 4, Missouri Geological Survey and Water Resources.

McGuire, R.K., W. J. Silva, and C. Costantino (2000). "Technical Basis for Revision of Regulatory Guidance on Design Ground Motions." Report to US Nuclear Regulatory Commission, in press.

Nuclear Regulatory Commission (1997). *Regulatory Guide 1.165--Identification and Characterization of Seismic Sources and Determination of Safe Shutdown Earthquake Ground Motion*, March.

Risk Engineering, Inc. (1991). *Impact of Ground Motion Characterization on Conservatism and Variability in Seismic Risk Estimates,* prepared for U.S. Nuclear Regulatory Commission, Final Report, May.

Romero, S., and G.J. Rix (2000). "Regional Variation of Shear Wave Velocity in the Greater Memphis Area," manuscript submitted to *Engineering Geology*.

Table 5-1. Probability-Based Scenario Events

Site	Freq (Hz)	P[exc., 50yr]	Weight	Target Ampl (g)	M	R (km)	epsilon†	Source
St. Louis	1	10%	0.6	0.031	5.2	26	0.90	Wabash Large (area src.)
St. Louis	1	10%	0.4	0.031	7.4	236	0.95	E. Prairie Flt. (NMSZ)
St. Louis	1	2%	0.66	0.079	5.6	26	1.23	Wabash Large (area src.)
St. Louis	1	2%	0.33	0.079	7.75	236	1.84	E. Prairie Flt. (NMSZ)
St. Louis	10	10%	0.8	0.13	5.1	34	0.48	Wabash Large (area src.)
St. Louis	10	10%	0.2	0.13	7.75	236	1.43	E. Prairie Flt. (NMSZ)
St. Louis	10	2%	0.9	0.35	5.1	11	0.34	Wabash Large (area src.)
St. Louis	10	2%	0.1	0.35	7.75	236	2.66	E. Prairie Flt. (NMSZ)
Memphis	1	10%	0.25	0.038	5.4	26	0.74	S.E. Flank
Memphis	1	10%	0.75	0.038	7.4	101	-0.01	Blytheville Arch (NMSZ)
Memphis	1	2%	0.3	0.12	7.75	19	-0.62	S.E. Flank
Memphis	1	2%	0.7	0.12	7.75	64	0.60	Blytheville Arch (NMSZ)
Memphis	10	10%	0.4	0.14	5.1	26	0.17	S.E. Flank
Memphis	10	10%	0.6	0.14	7.4	101	0.38	Blytheville Arch (NMSZ)
Memphis	10	2%	0.4	0.37	5.2	26	1.28	S.E. Flank
Memphis	10	2%	0.6	0.37	7.75	64	0.68	Blytheville Arch (NMSZ)

† The modal epsilon value is modified (usually by a small amount) so that the ground-motion amplitude at the frequency of interest matches the mean uniform-hazard spectrum.

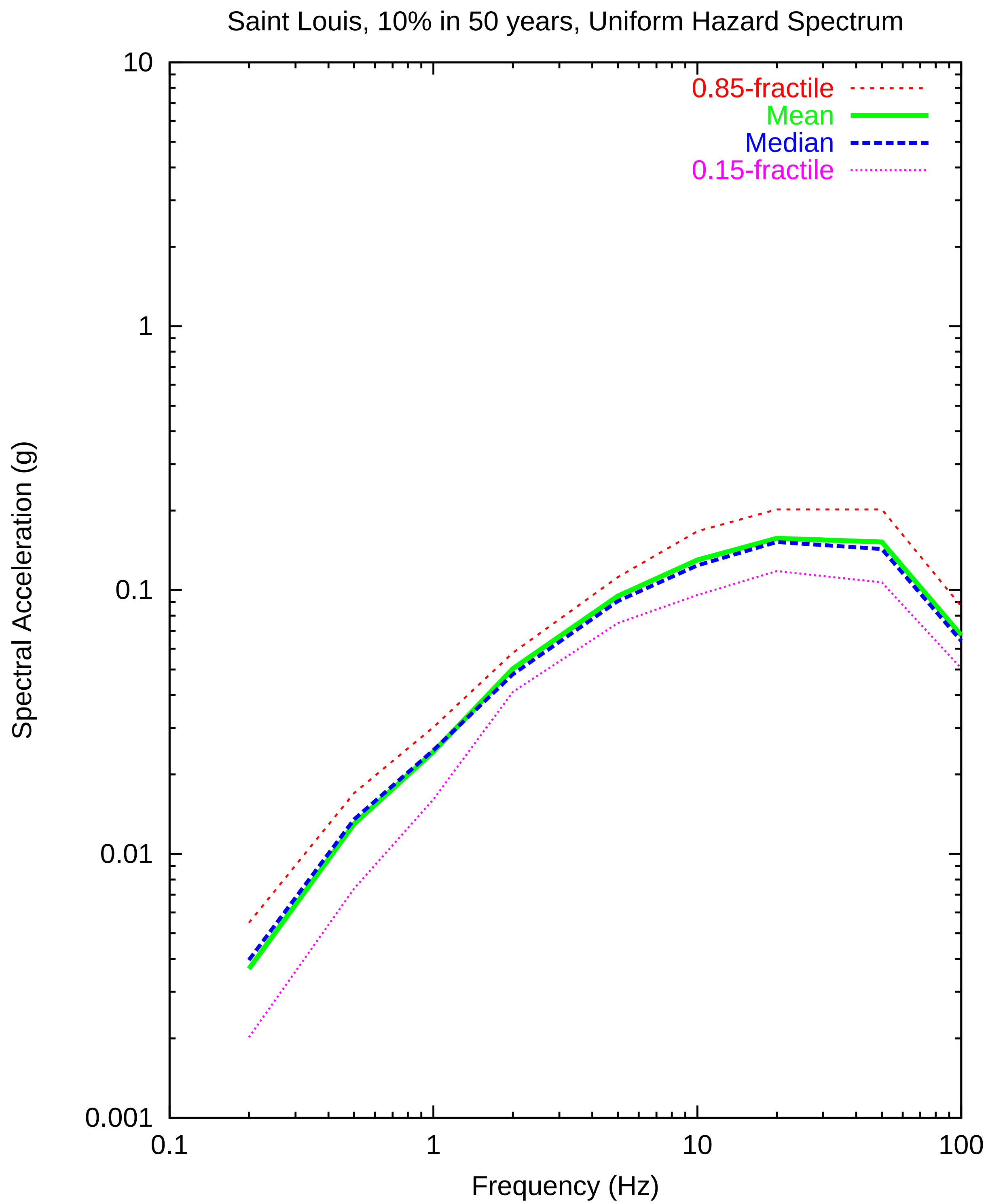

Figure 5-1. Uniform-hazard spectrum for Saint Louis (rock site conditions), for an exceedence probability of 10% in 50 years. The spread between the 0.15 and 0.85 fractiles indicate epistemic uncertainty.

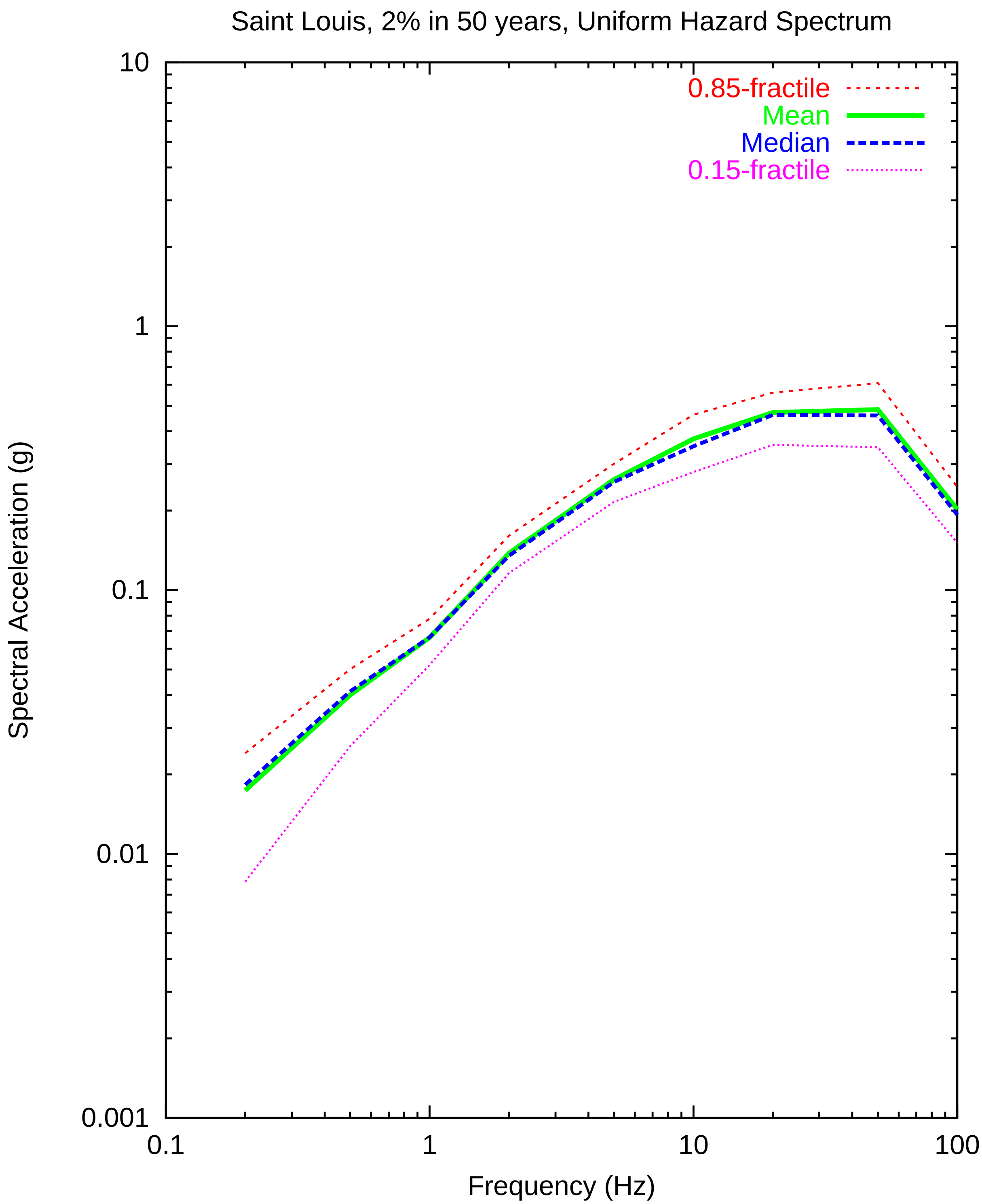

Figure 5-2. Uniform-hazard spectrum for Saint Louis (rock site conditions), for an exceedence probability of 2% in 50 years. The spread between the 0.15 and 0.85 fractiles indicate epistemic uncertainty.

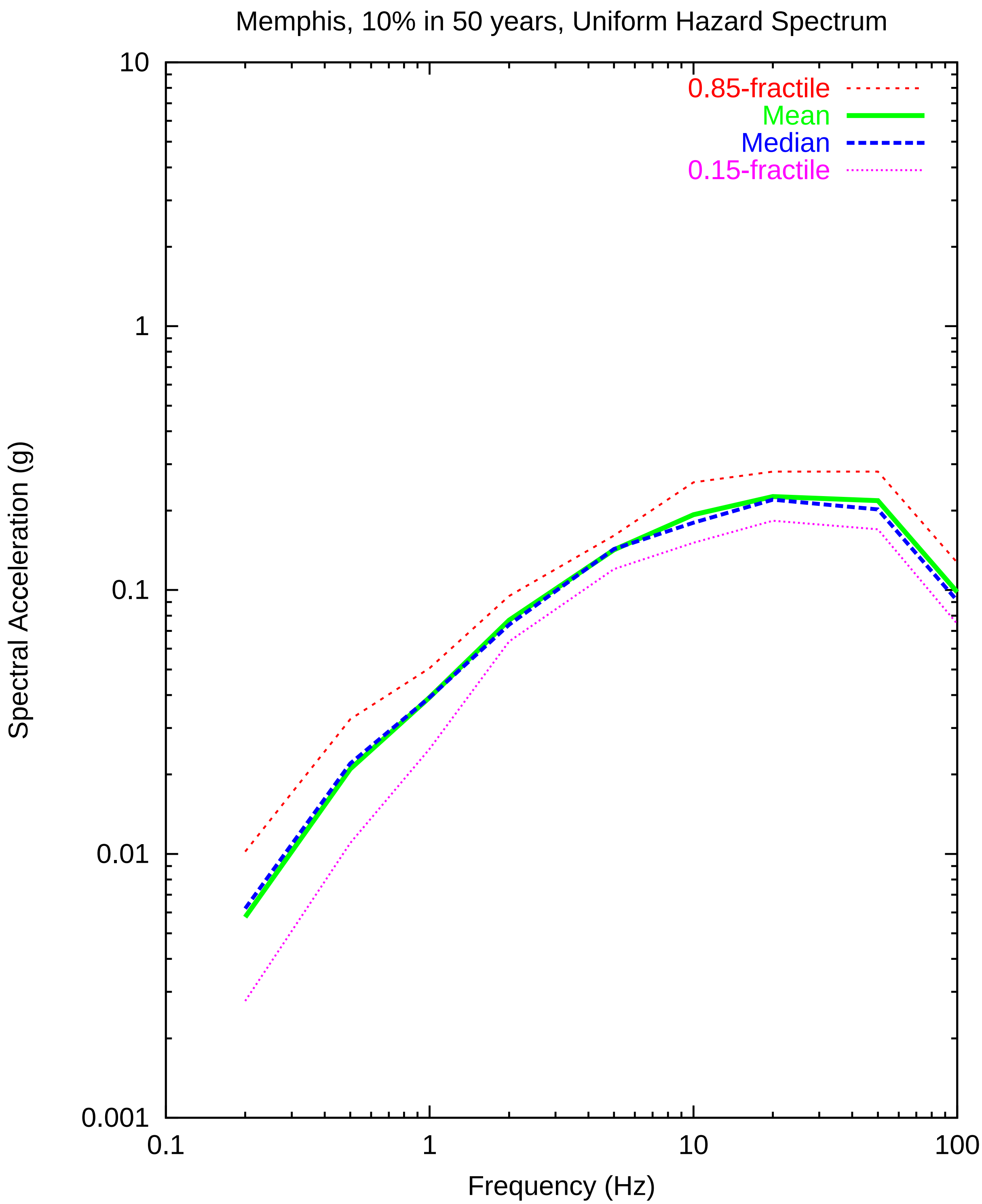

Figure 5-3. Uniform-hazard spectrum for Memphis (rock site conditions), for an exceedence probability of 10% in 50 years. The spread between the 0.15 and 0.85 fractiles indicate epistemic uncertainty.

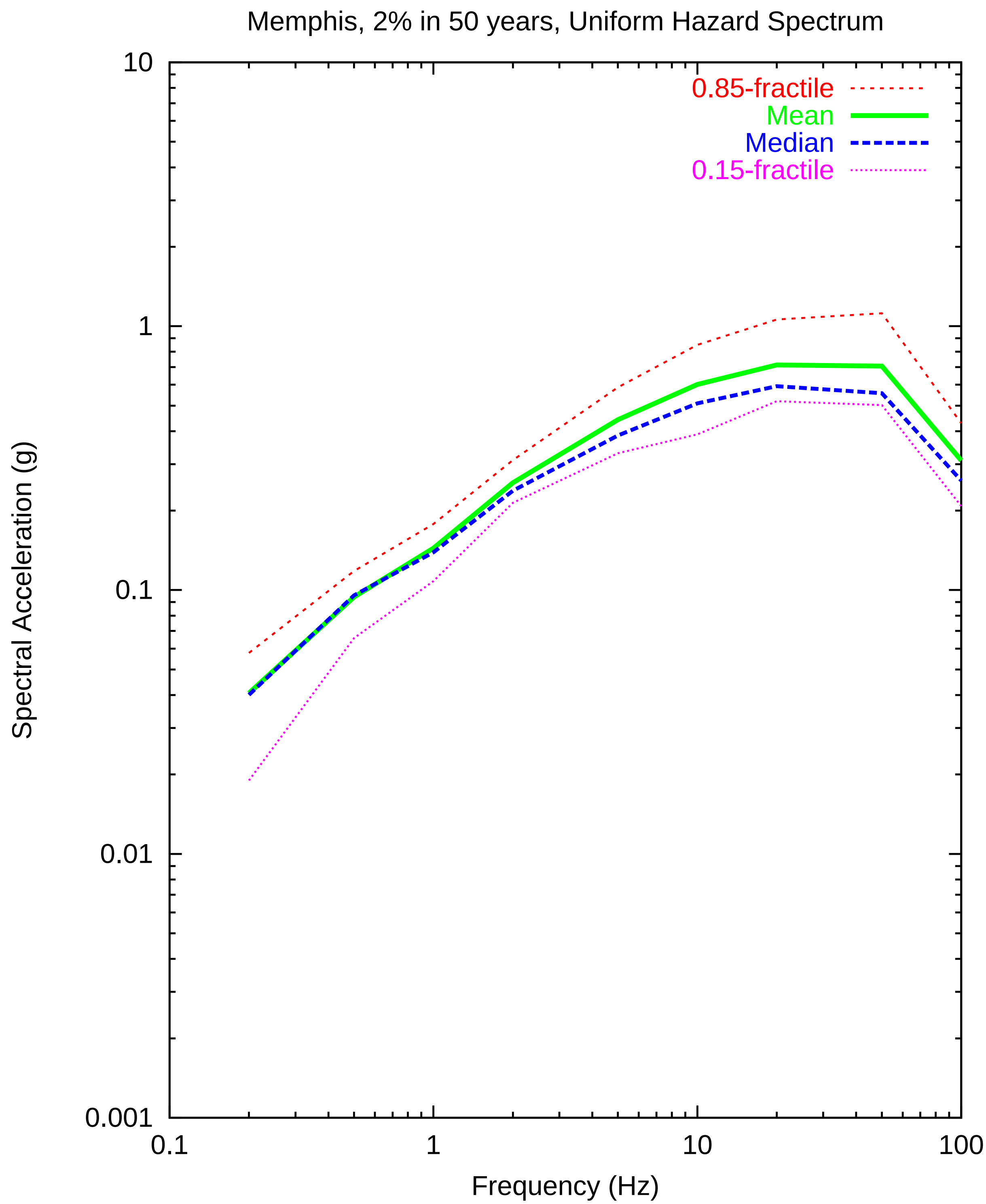

Figure 5-4. Uniform-hazard spectrum for Memphis (rock site conditions), for an exceedence probability of 2% in 50 years. The spread between the 0.15 and 0.85 fractiles indicate epistemic uncertainty.

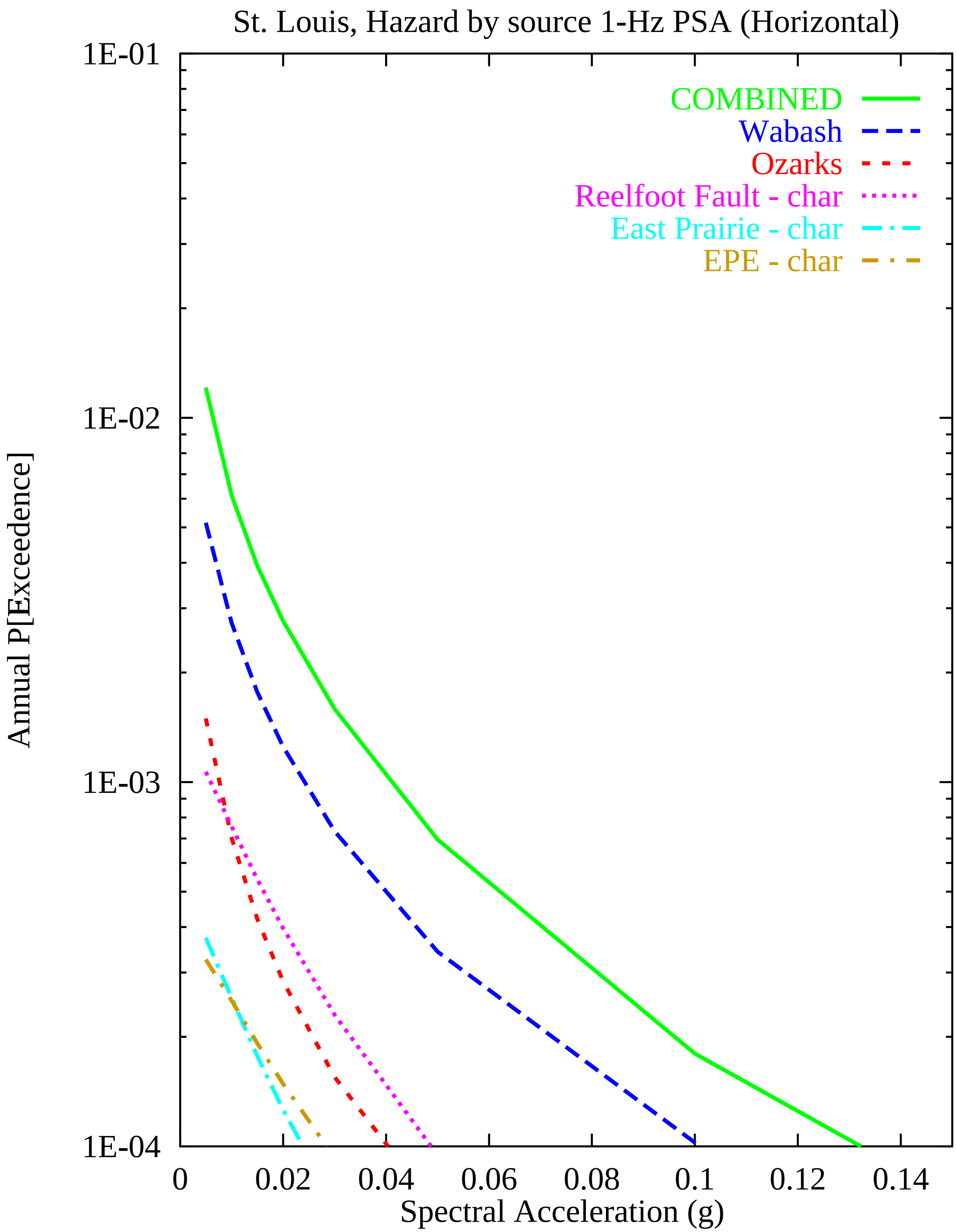

Figure 5-5. Seismic hazard in Saint Louis: contributions by source for 1-Hz spectral acceleration.

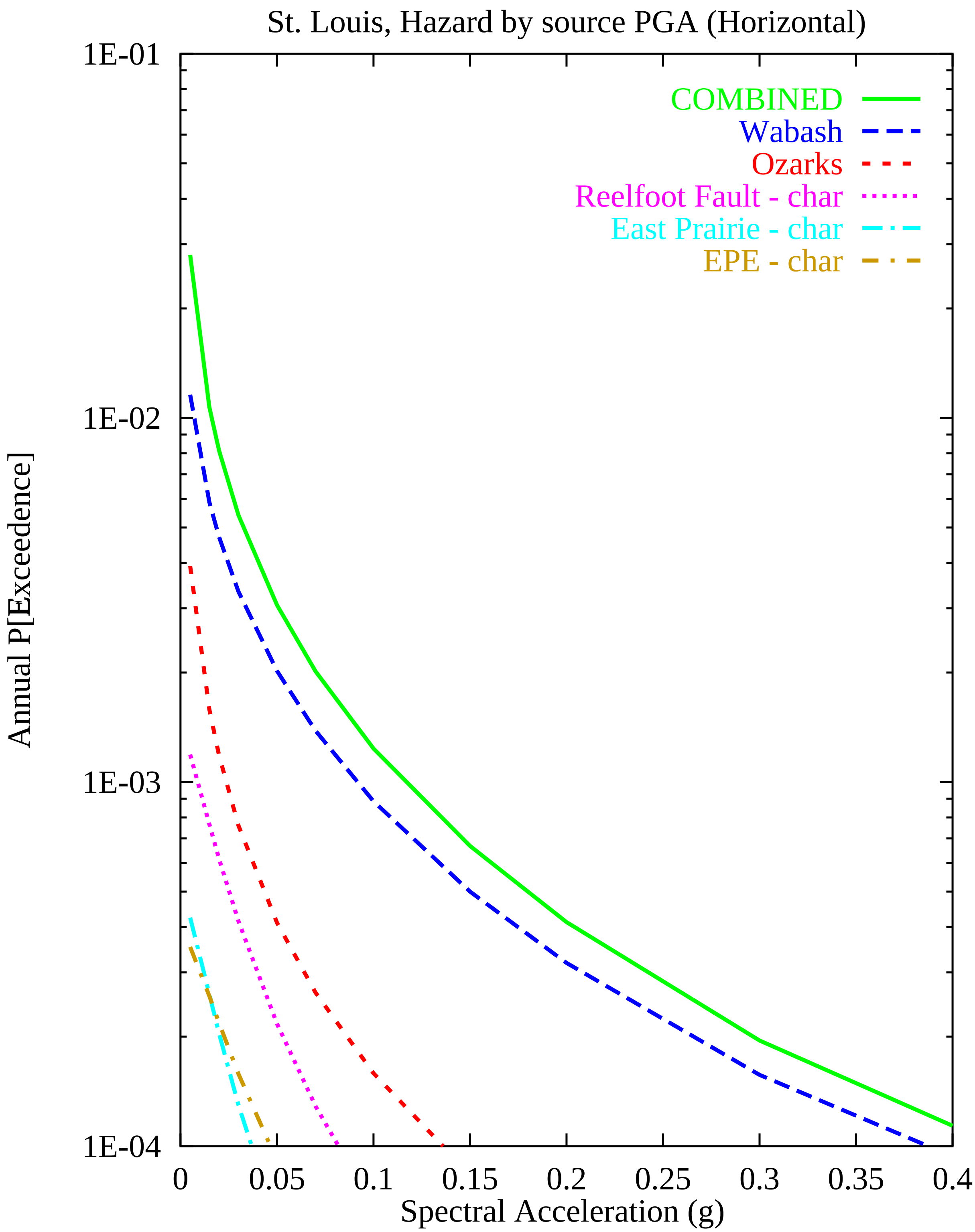

Figure 5-6. Seismic hazard in Saint Louis: contributions by source for PGA.

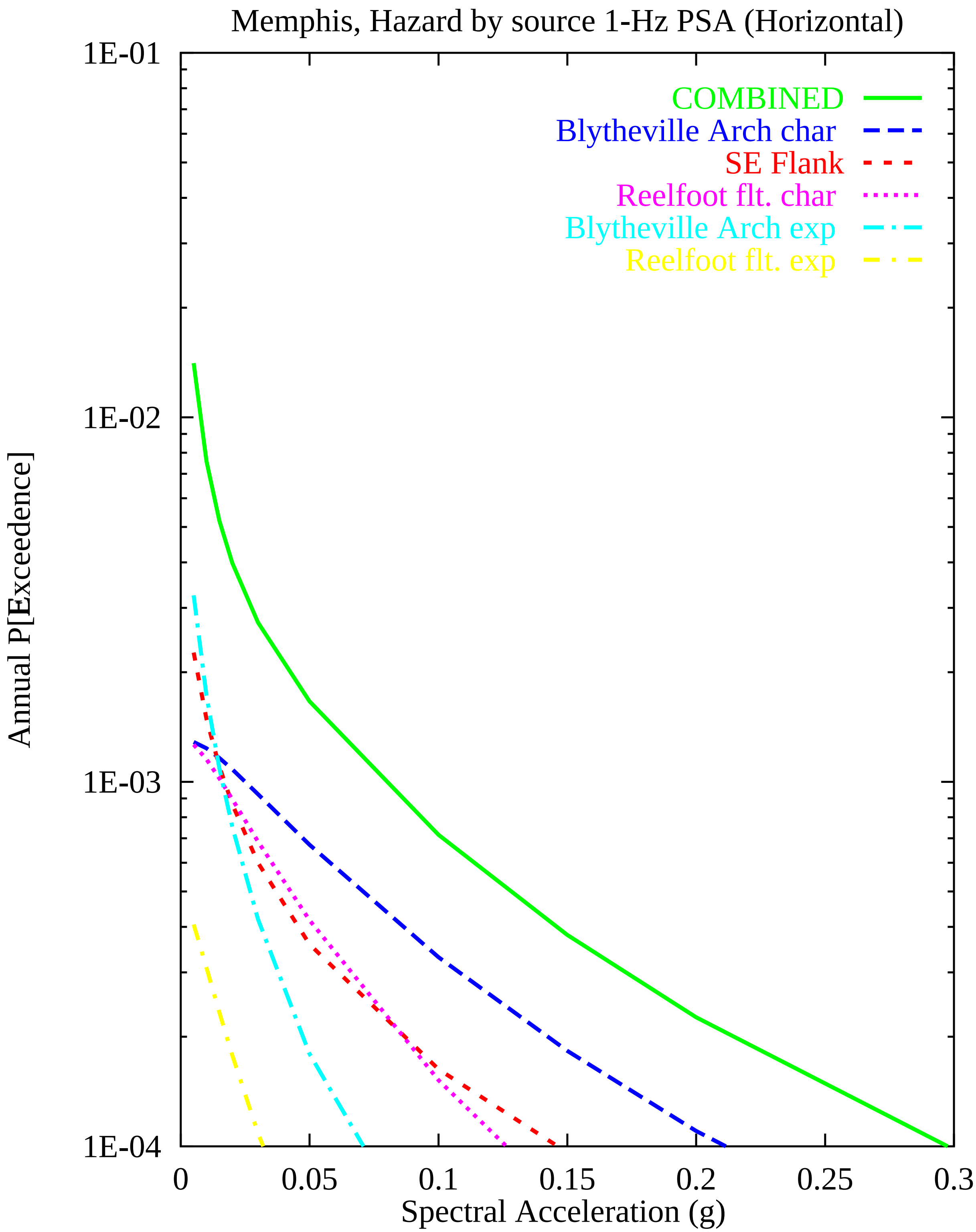

Figure 5-7. Seismic hazard in Memphis: contributions by source for 1-Hz spectral acceleration.

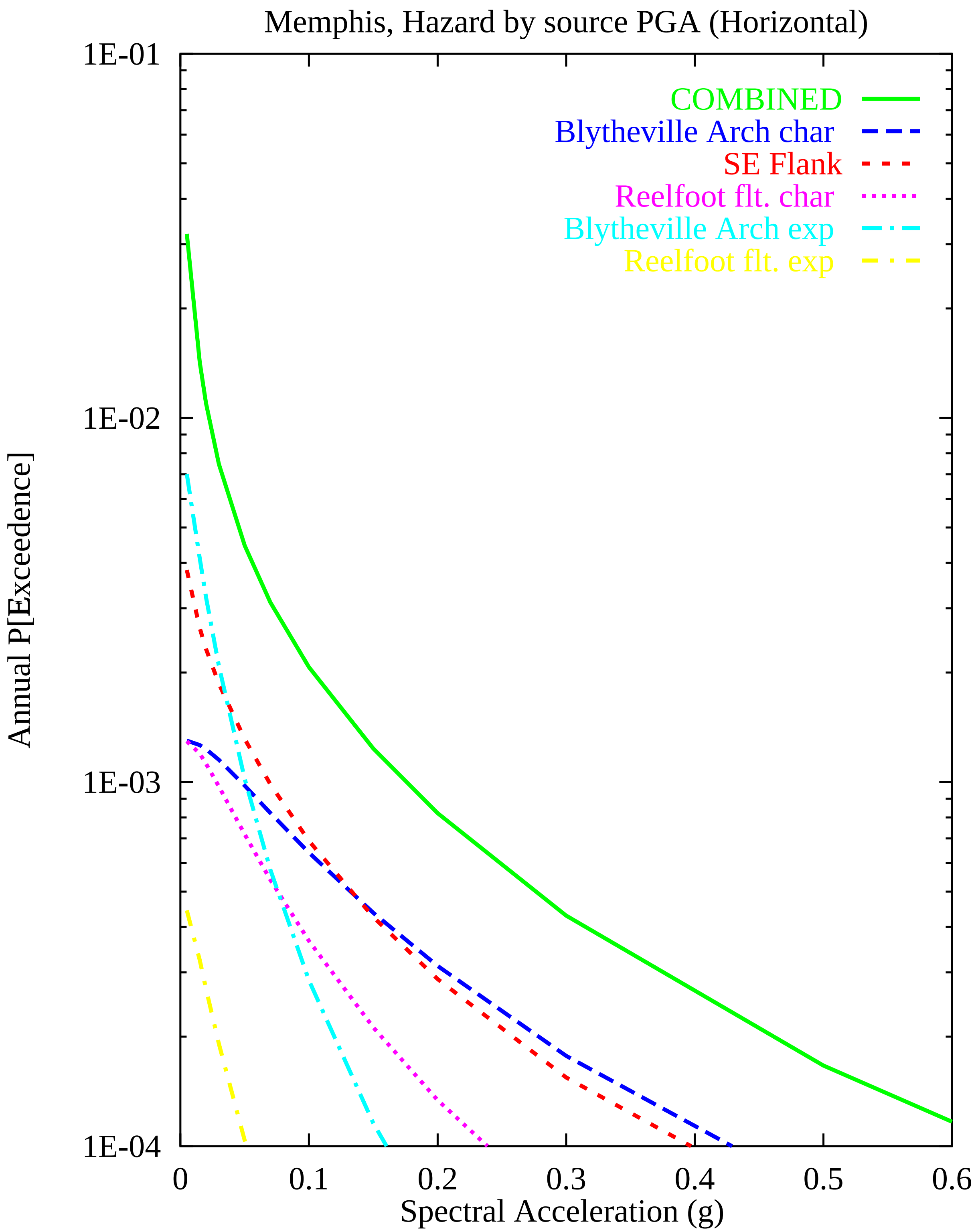

Figure 5-8. Seismic hazard in Memphis: contributions by source for PGA.

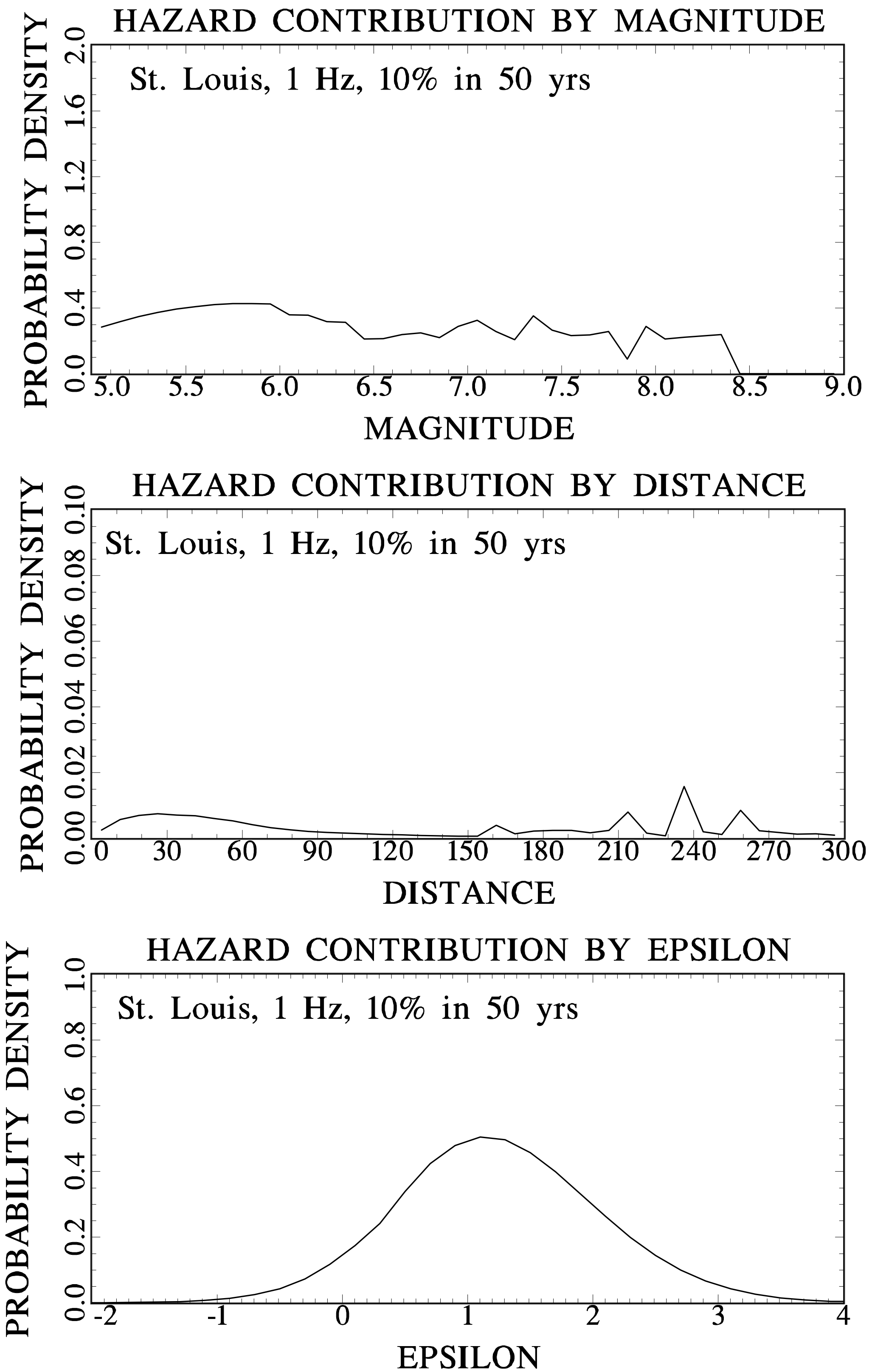

Figure 5-9. Marginal magnitude-distance-epsilon deaggregation for 1-Hz spectral acceleration in Saint Louis; 10% in 50 years exceedence probability.

St. Louis, 1 Hz, 10% in 50 yrs

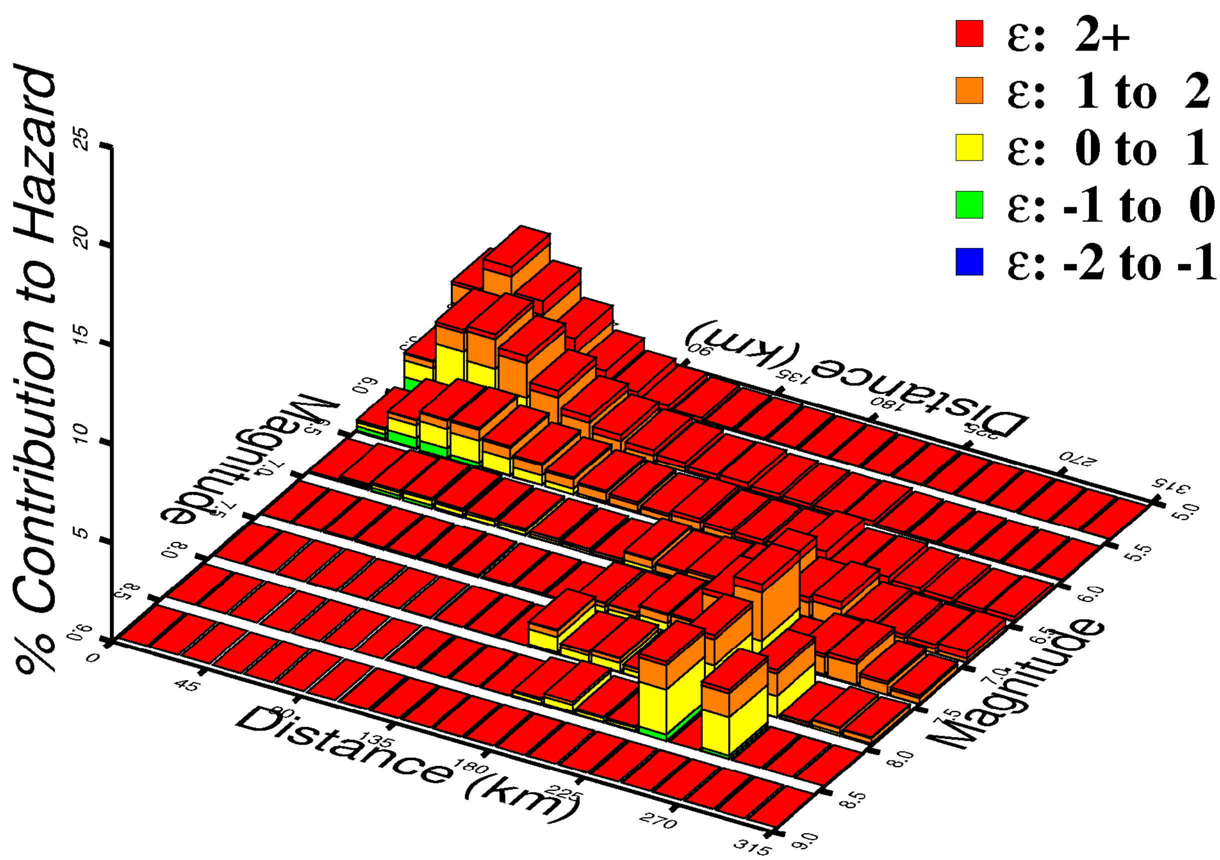

Figure 5-10. Joint magnitude-distance-epsilon deaggregation for 1-Hz spectral acceleration in Saint Louis; 10% in 50 years exceedence probability.

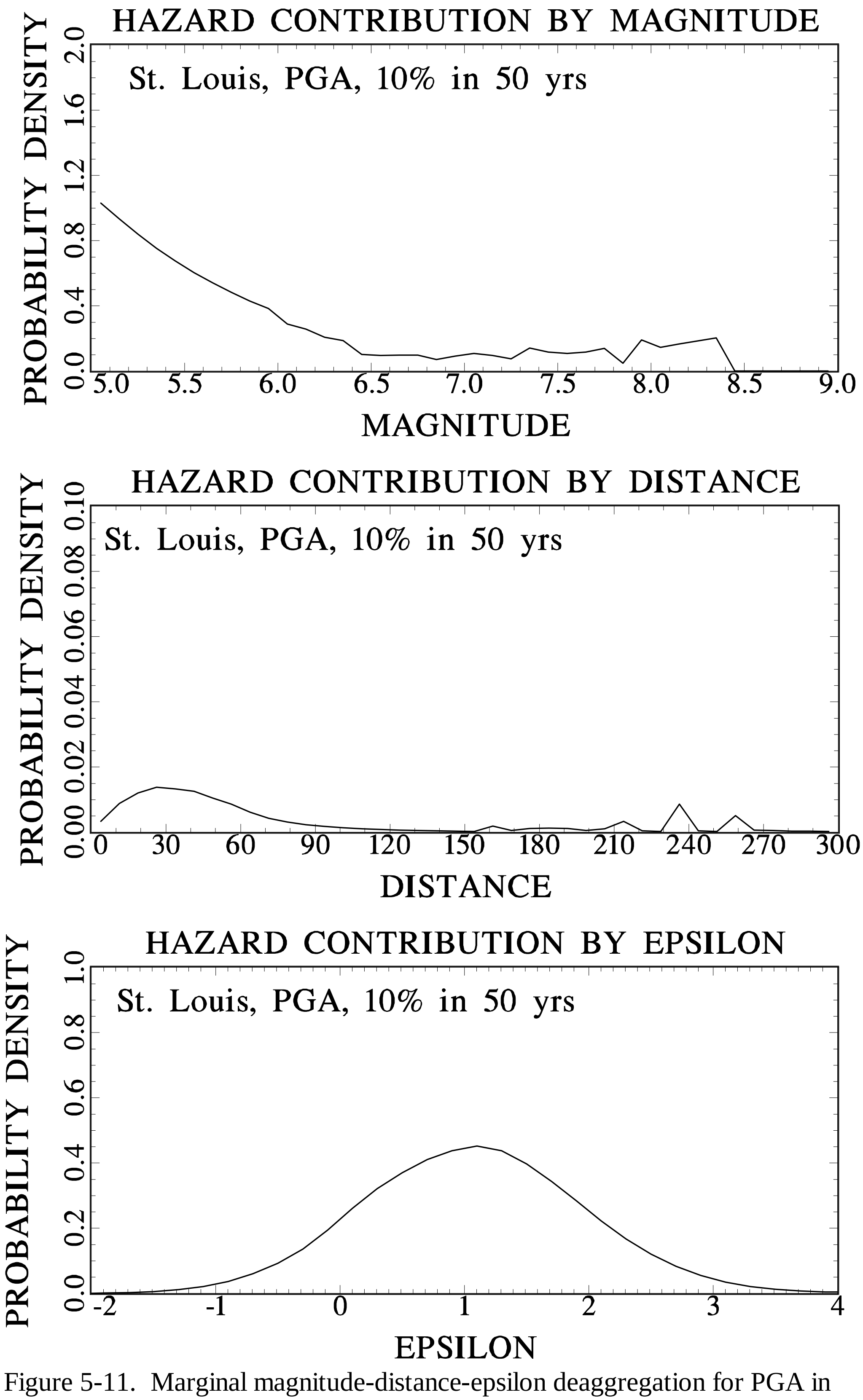

Figure 5-11. Marginal magnitude-distance-epsilon deaggregation for PGA in Saint Louis; 10% in 50 years exceedence probability.

St. Louis, PGA, 10% in 50 yrs

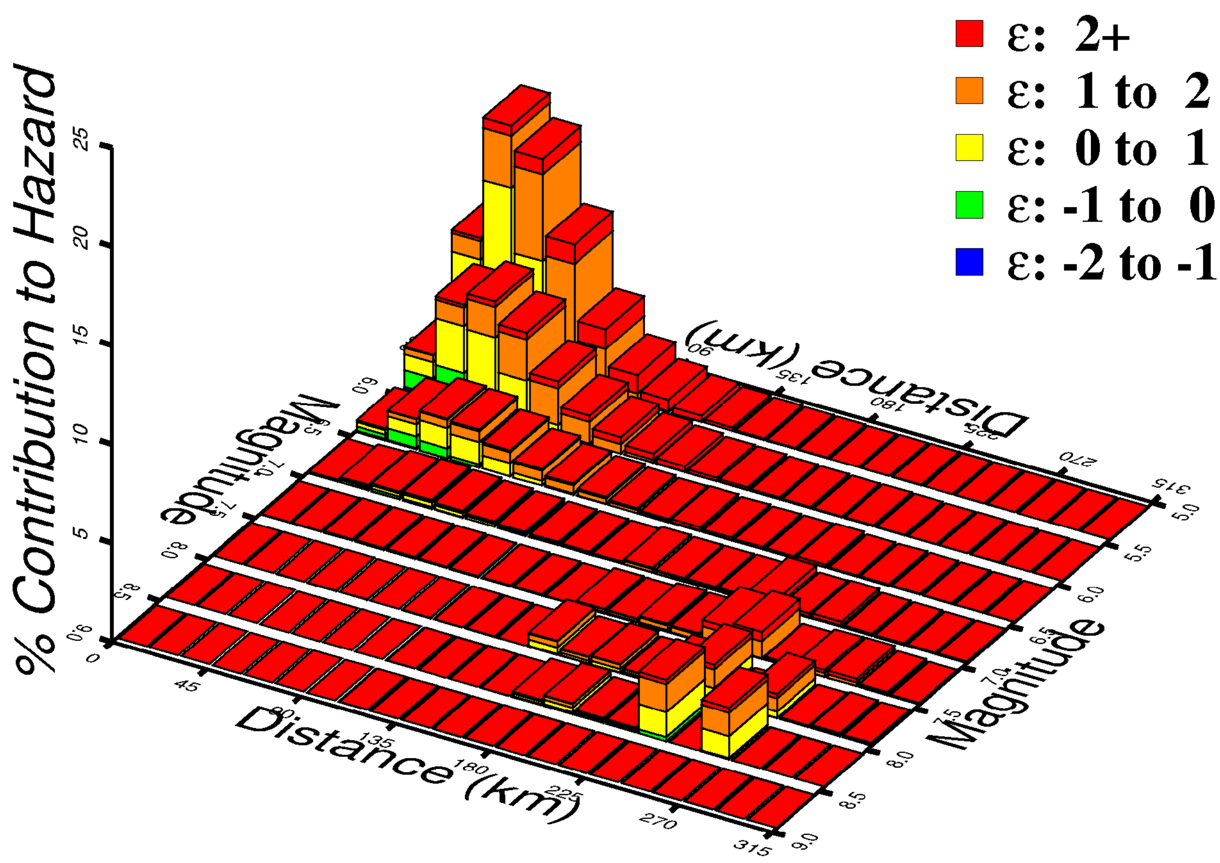

Figure 5-12. Joint magnitude-distance-epsilon deaggregation for PGA in Saint Louis; 10% in 50 years exceedence probability.

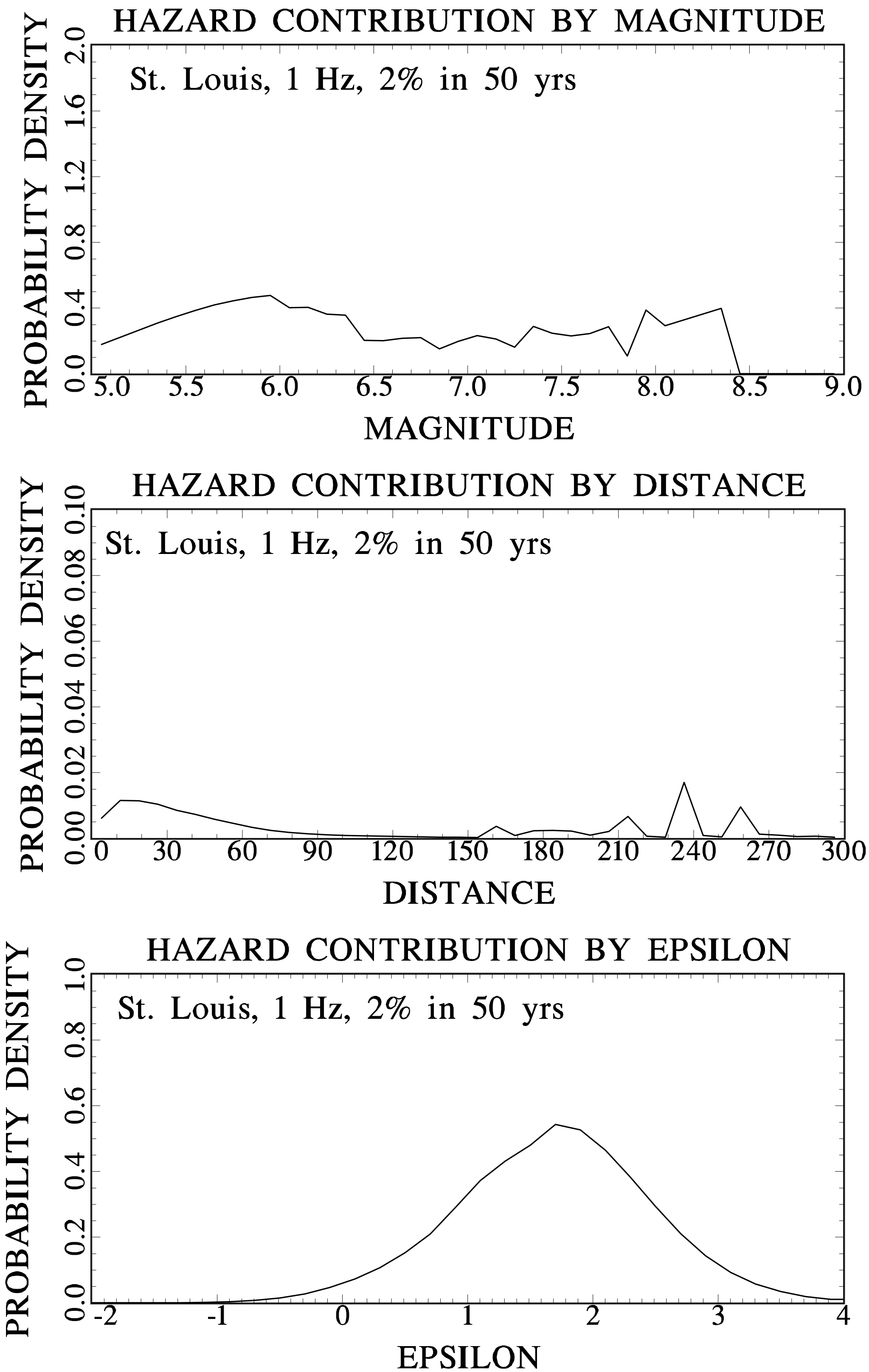

Figure 5-13. Marginal magnitude-distance-epsilon deaggregation for 1-Hz spectral acceleration in Saint Louis; 2% in 50 years exceedence probability.

St. Louis, 1 Hz, 2% in 50 yrs

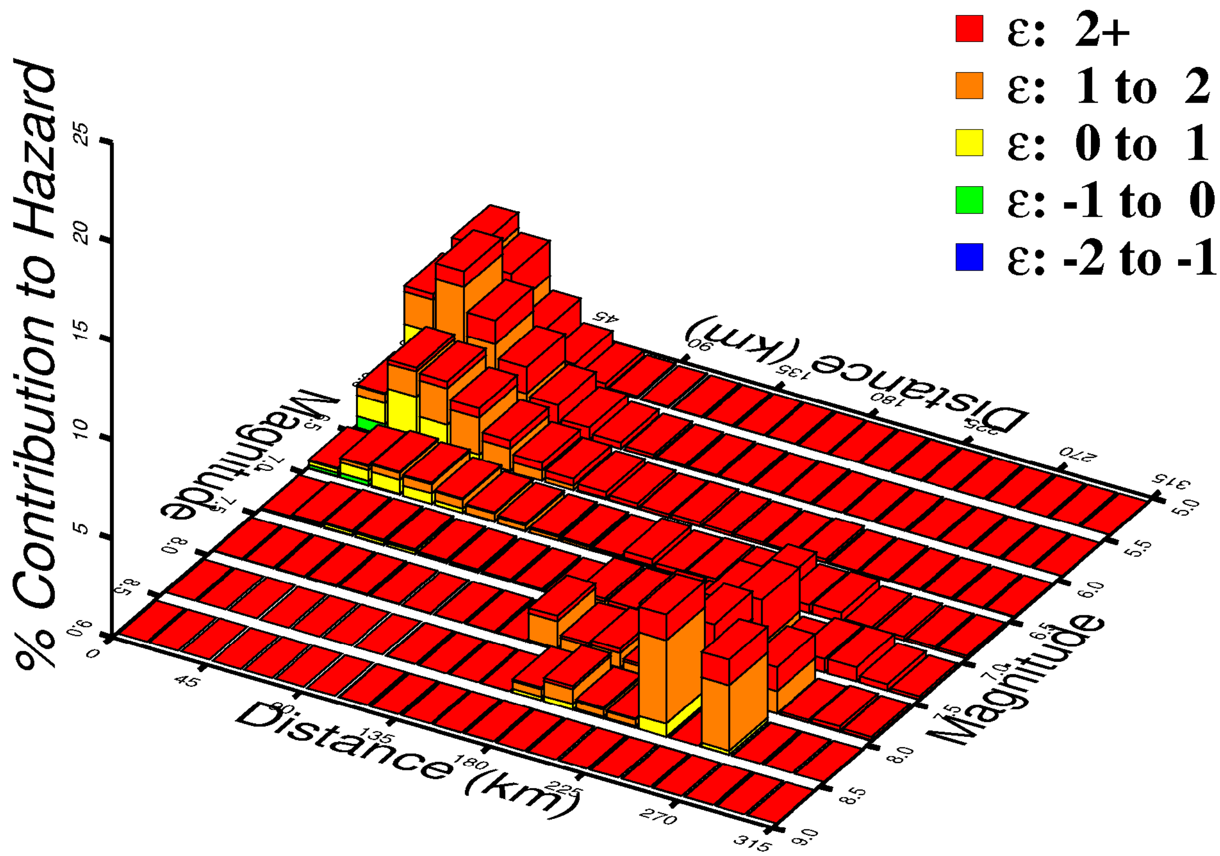

Figure 5-14. Joint magnitude-distance-epsilon deaggregation for 1-Hz spectral acceleration in Saint Louis; 2% in 50 years exceedence probability.

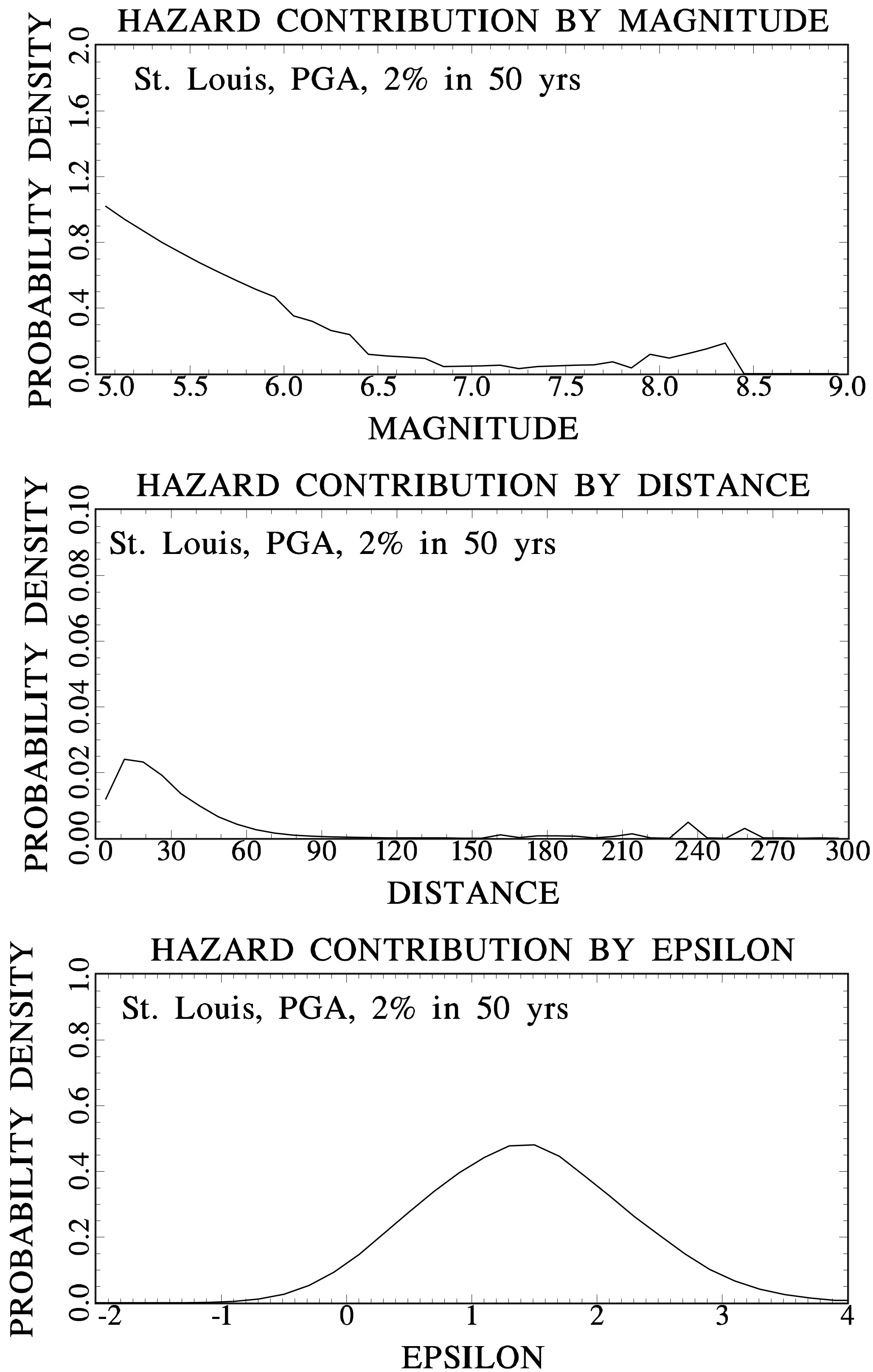

Figure 5-15. Marginal magnitude-distance-epsilon deaggregation for PGA in Saint Louis; 2% in 50 years exceedence probability.

St. Louis, PGA, 2% in 50 yrs

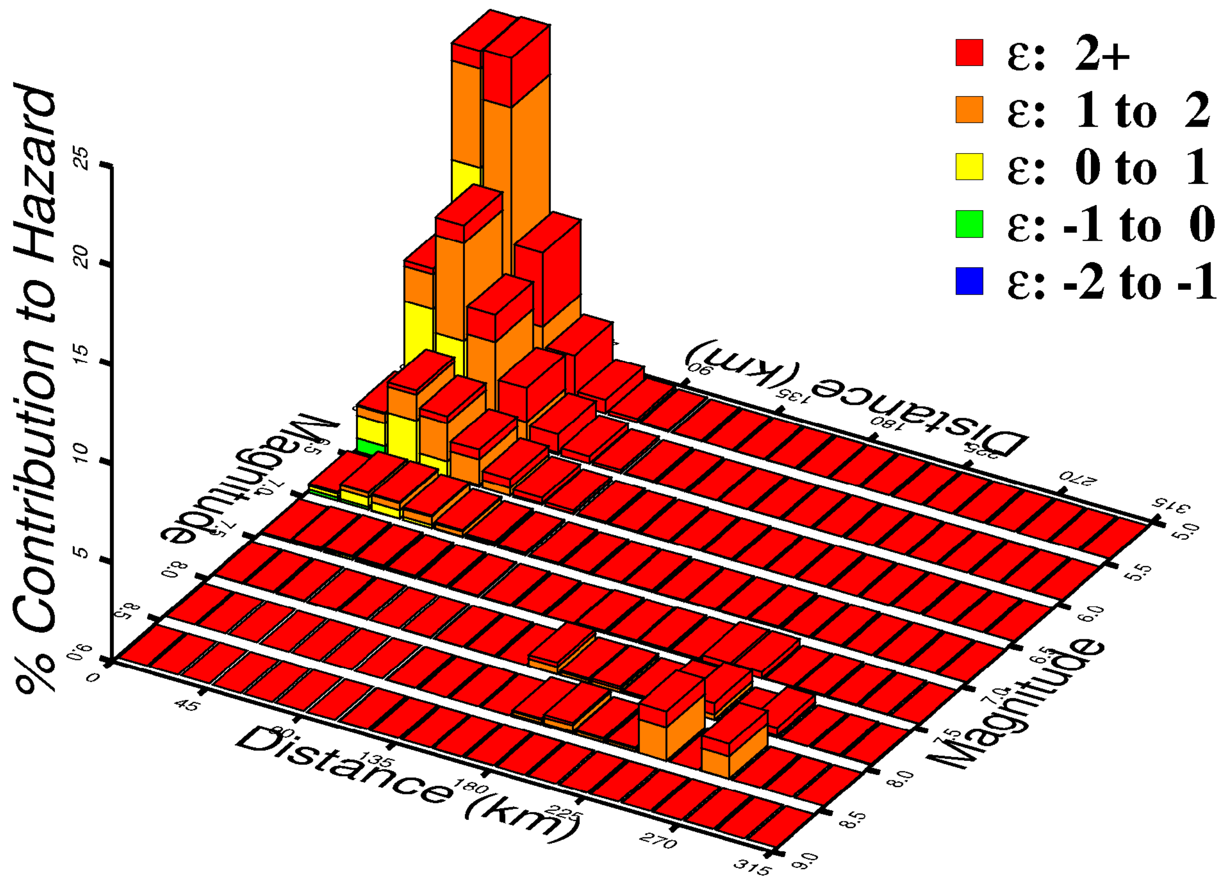

Figure 5-16. Joint magnitude-distance-epsilon deaggregation for PGA in Saint Louis; 2% in 50 years exceedence probability.

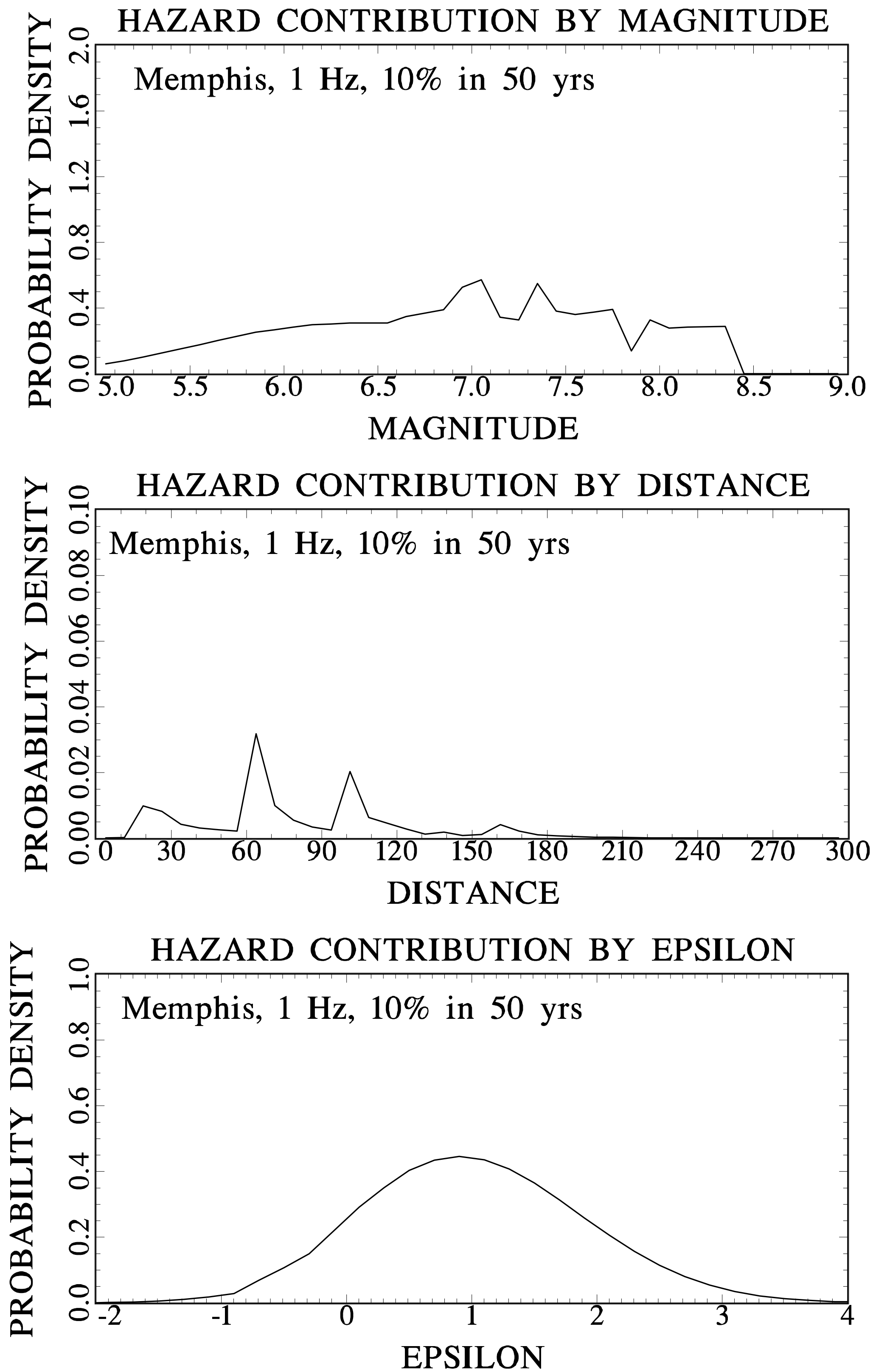

Figure 5-17. Marginal magnitude-distance-epsilon deaggregation for 1-Hz spectral acceleration in Memphis; 10% in 50 years exceedence probability.

Memphis, 1 Hz, 10% in 50 yrs

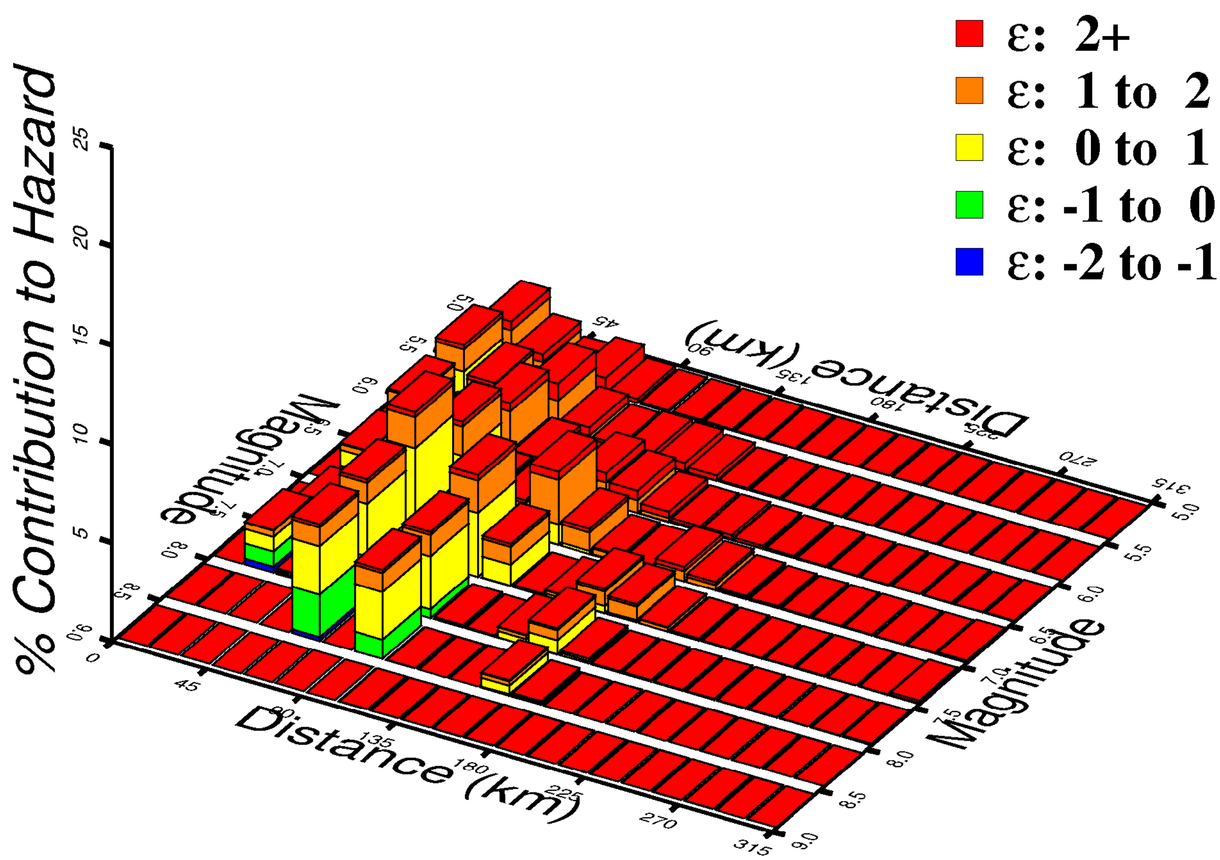

Figure 5-18. Joint magnitude-distance-epsilon deaggregation for 1-Hz spectral acceleration in Memphis; 10% in 50 years exceedence probability.

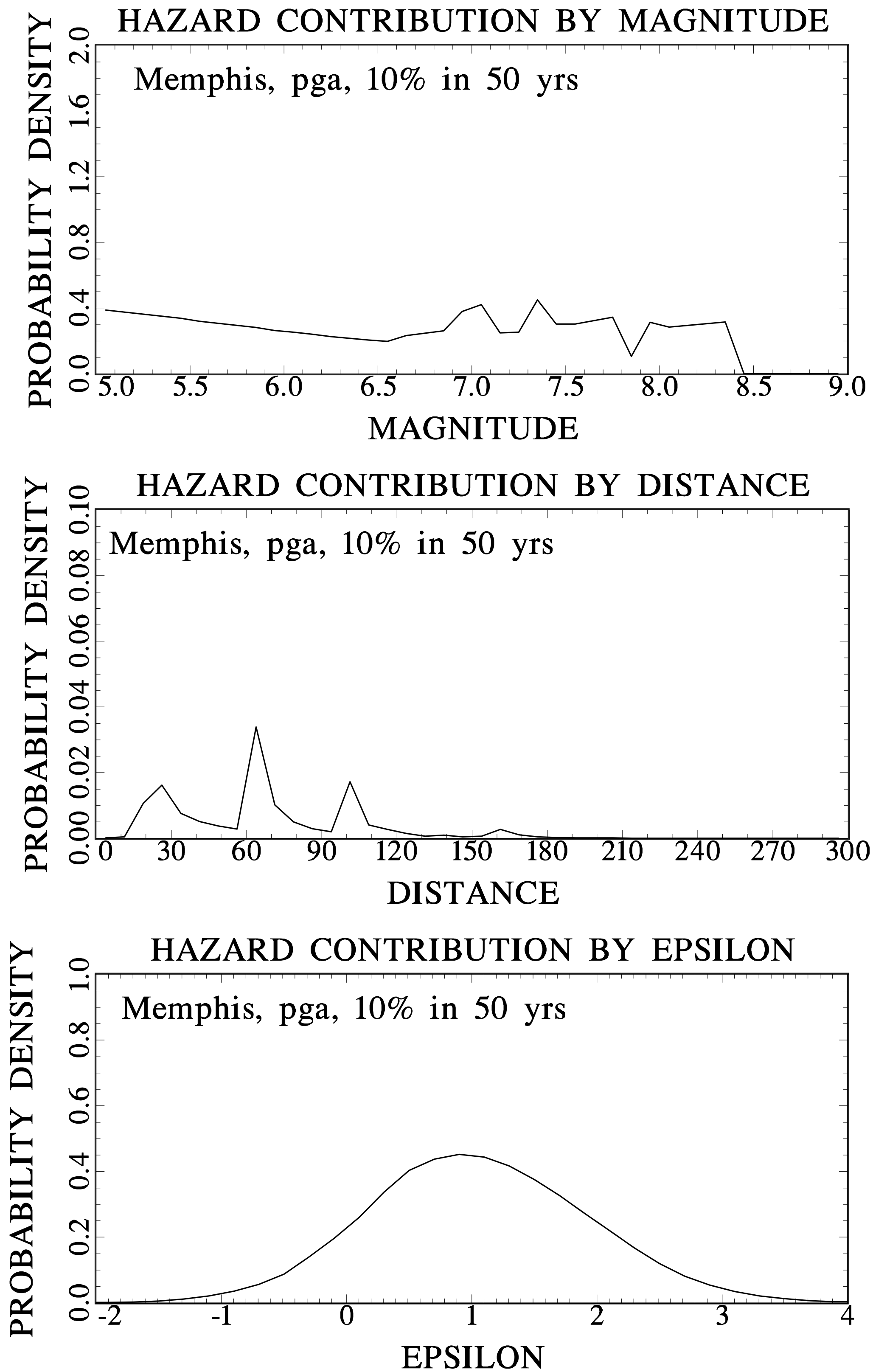

Figure 5-19. Marginal magnitude-distance-epsilon deaggregation for PGA in Memphis; 10% in 50 years exceedence probability.

Memphis, pga, 10% in 50 yrs

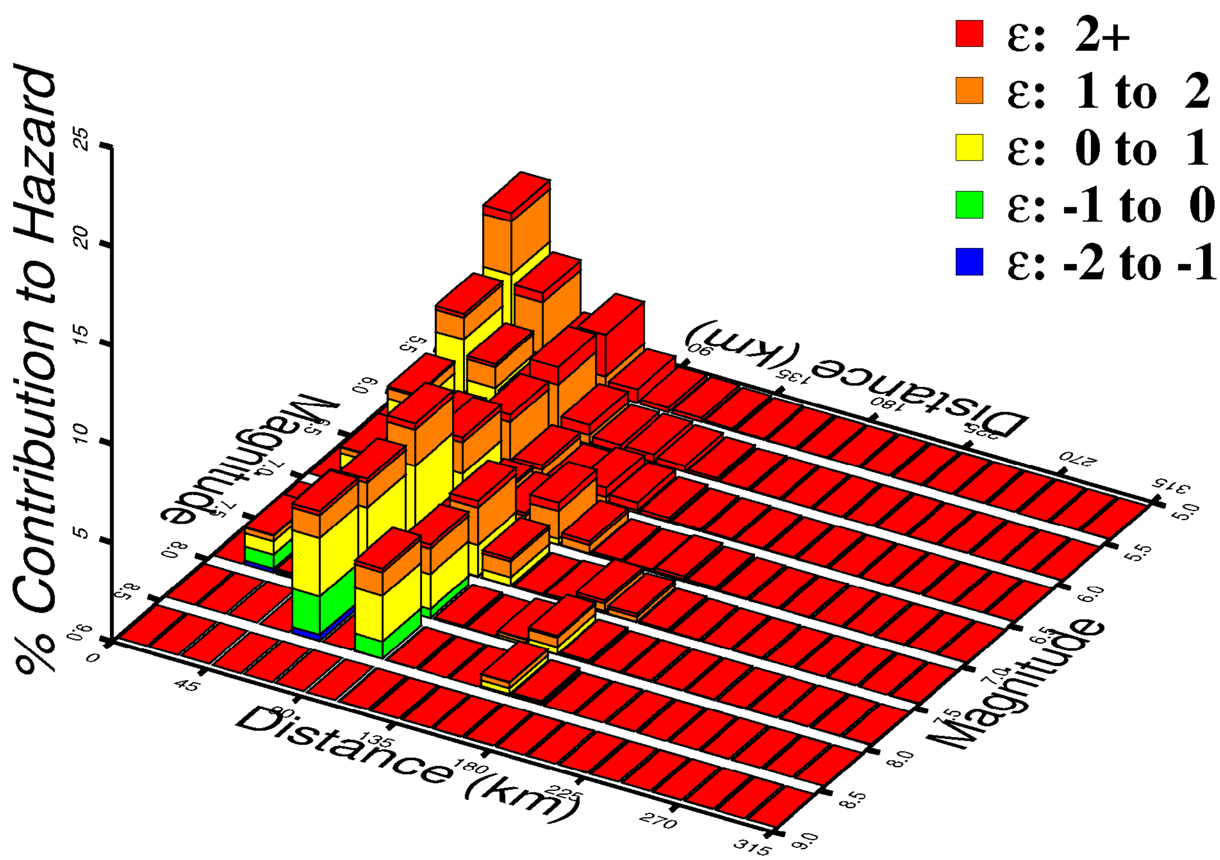

Figure 5-20. Joint magnitude-distance-epsilon deaggregation for PGA in Memphis; 10% in 50 years exceedence probability.

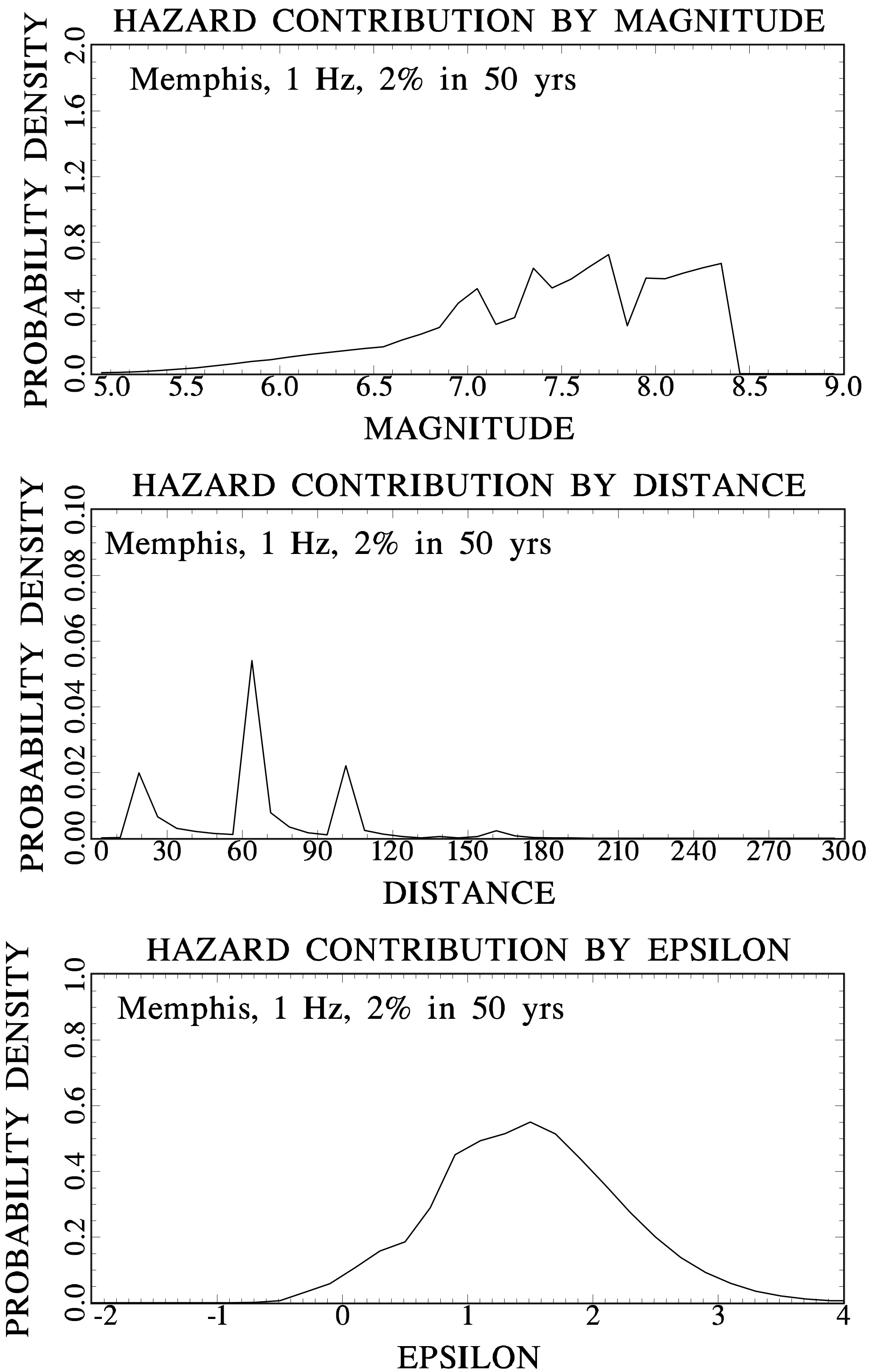

Figure 5-21. Marginal magnitude-distance-epsilon deaggregation for 1-Hz spectral acceleration in Memphis; 2% in 50 years exceedence probability.

Memphis, 1 Hz, 2% in 50 yrs

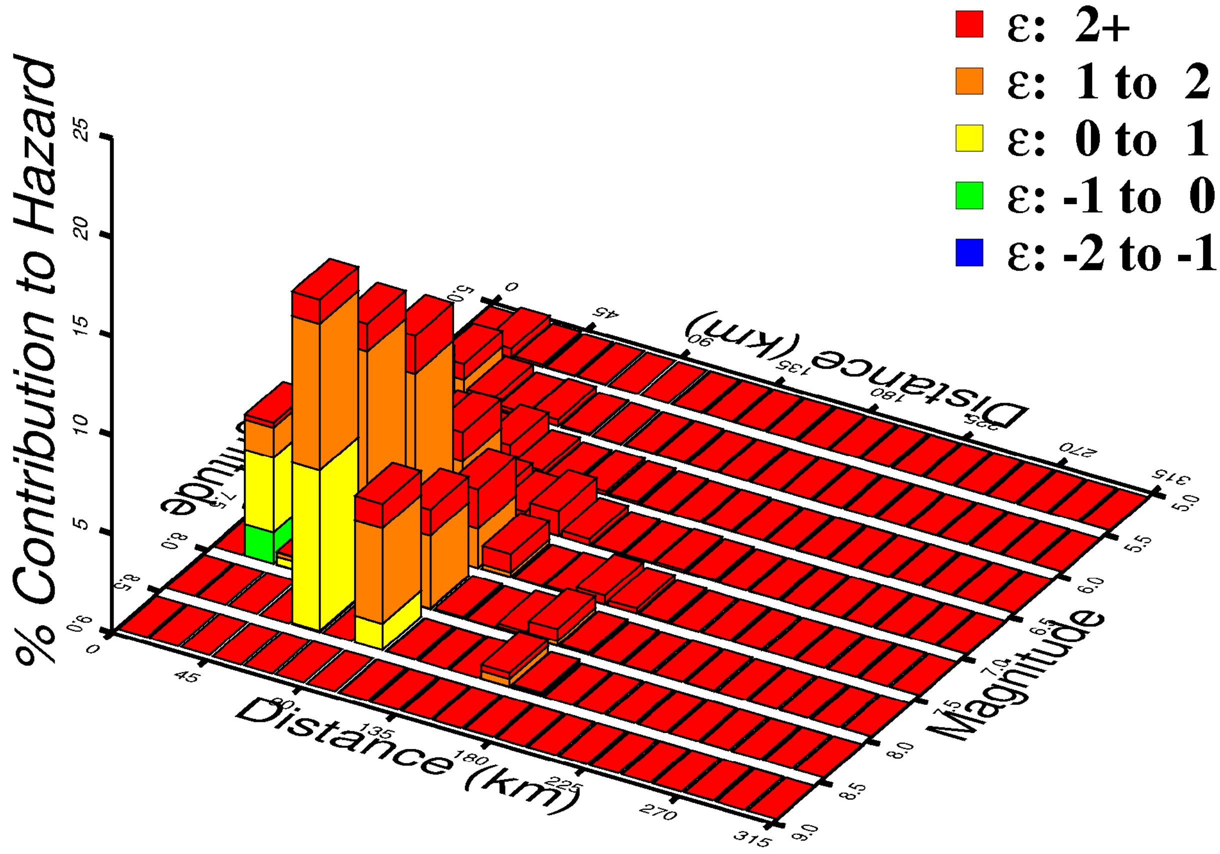

Figure 5-22. Joint magnitude-distance-epsilon deaggregation for 1-Hz spectral acceleration in Memphis; 2% in 50 years exceedence probability.

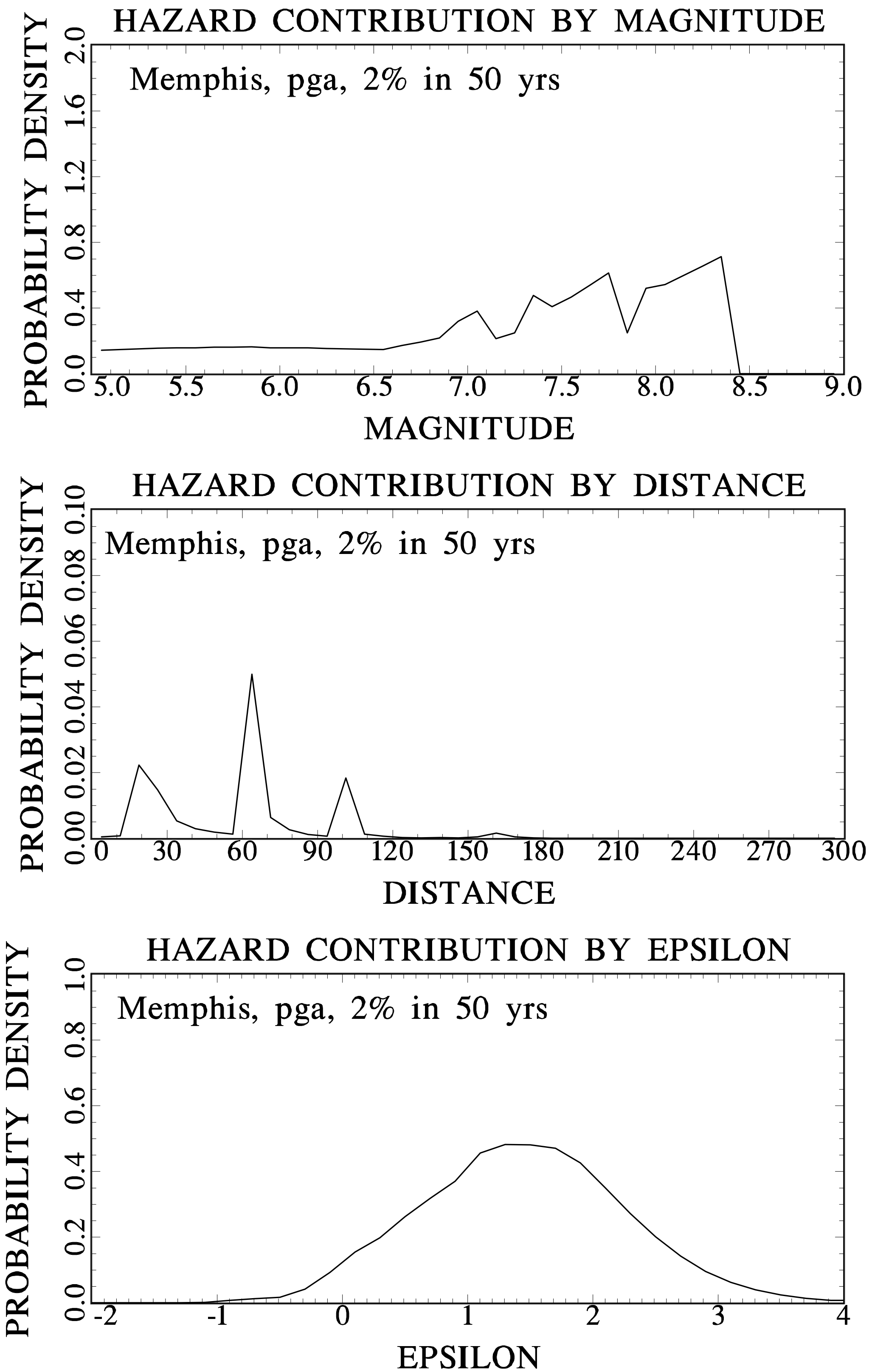

Figure 5-23. Marginal magnitude-distance-epsilon deaggregation for PGA in Memphis; 2% in 50 years exceedence probability.

Memphis, pga, 2% in 50 yrs

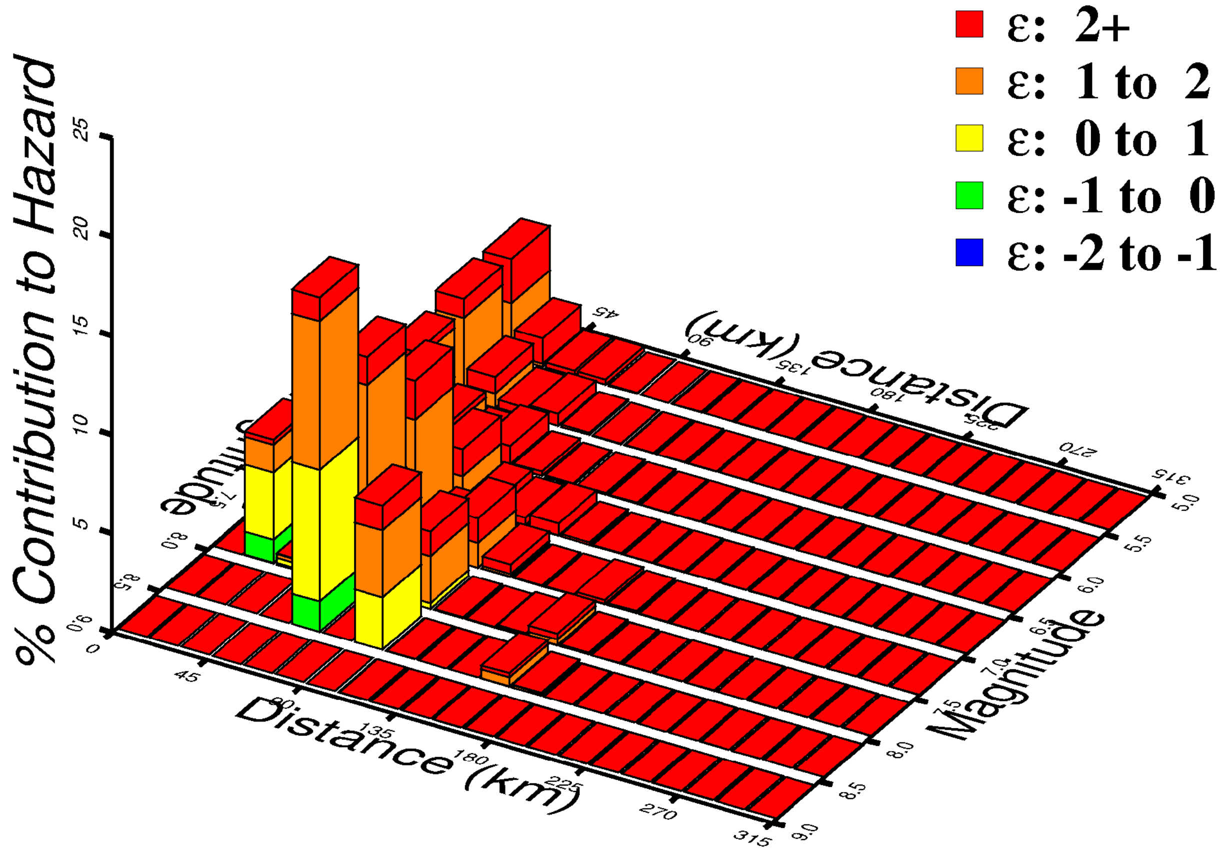

Figure 5-24. Joint magnitude-distance-epsilon deaggregation for PGA in Memphis; 2% in 50 years exceedence probability.

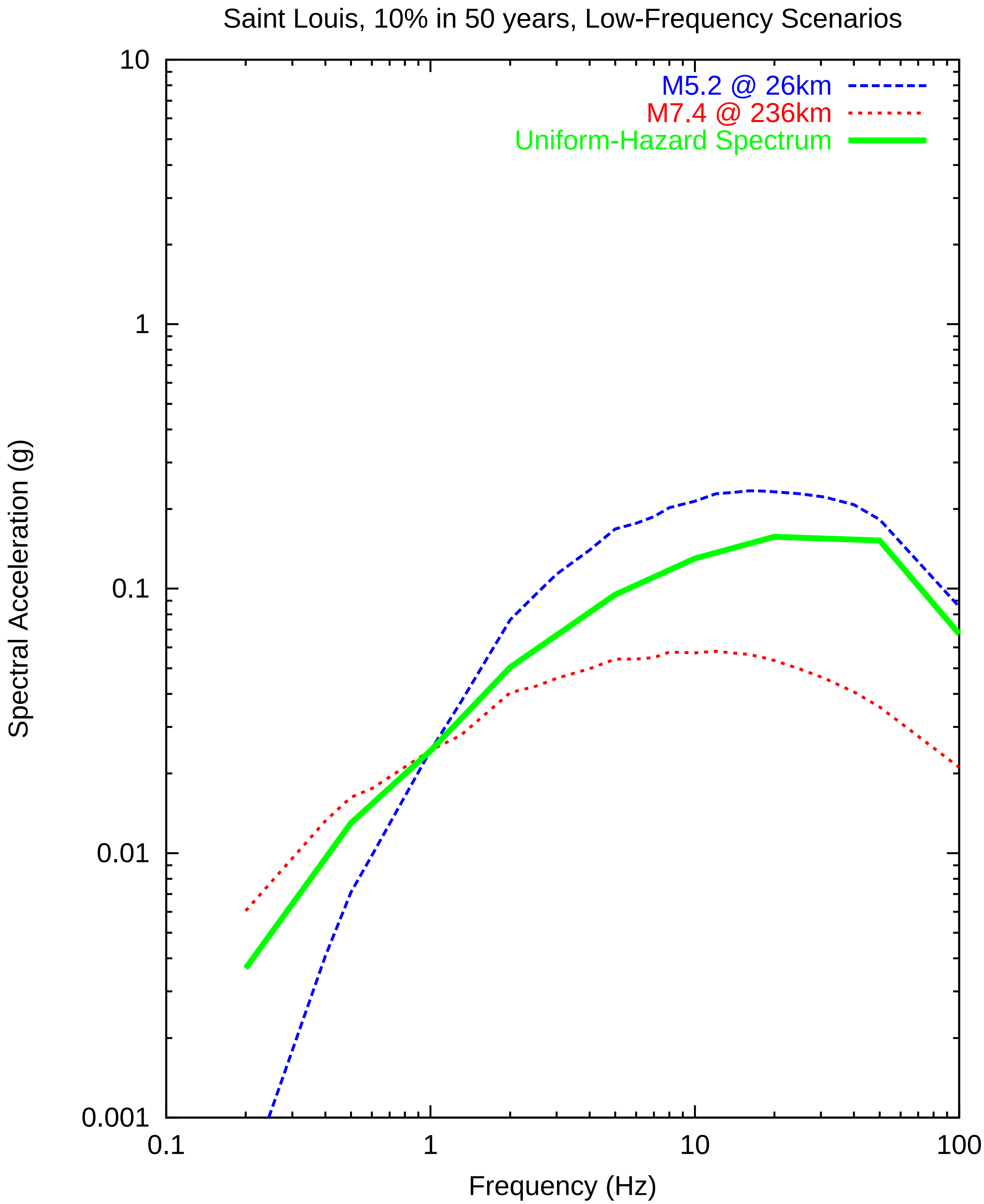

Figure 5-25. Spectra of low-frequency scenarios for Saint Louis, for an annual exceedence probability of 10% in 50 years.

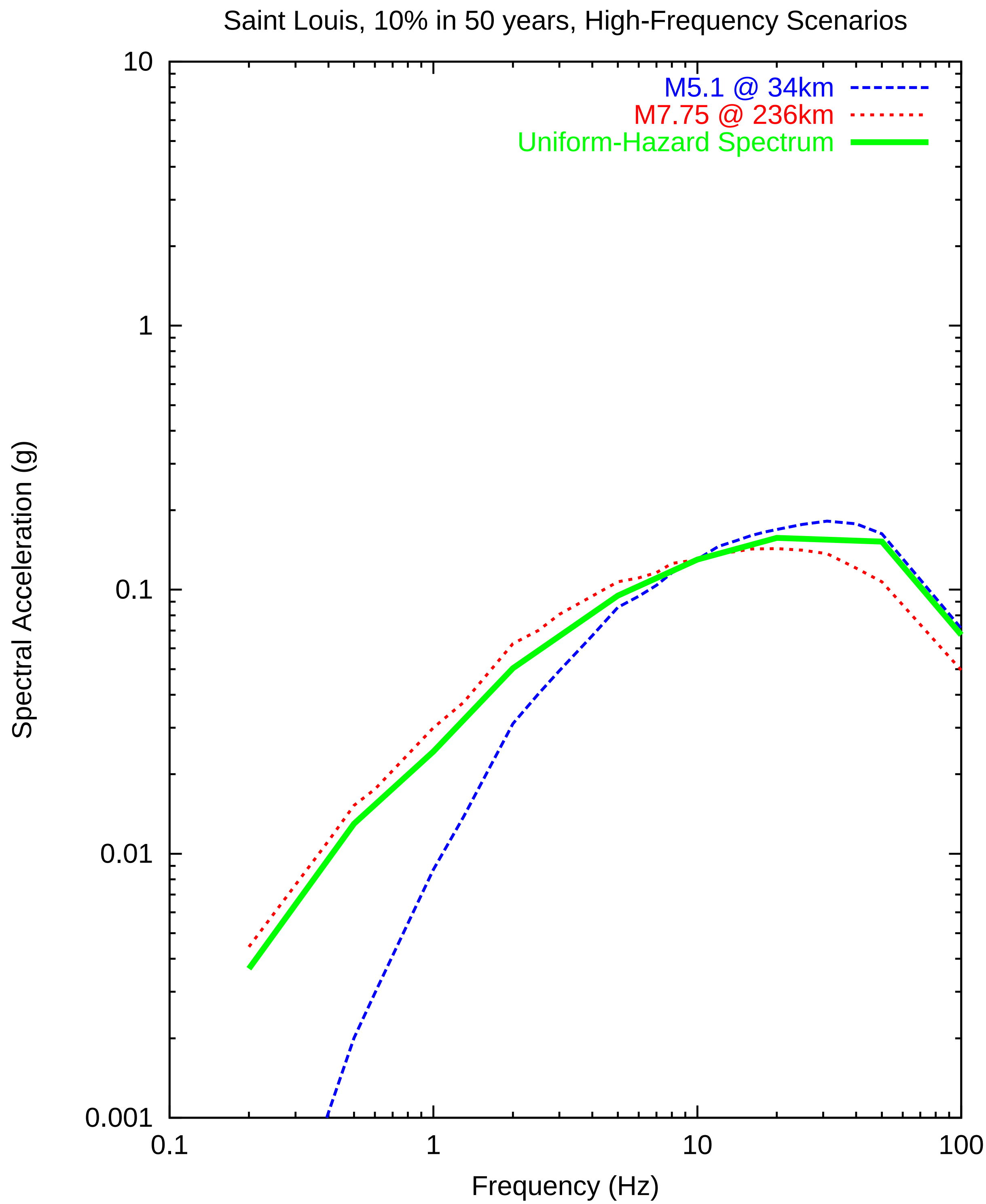

Figure 5-26. Spectra of high-frequency scenarios for Saint Louis, for an annual exceedence probability of 10% in 50 years.

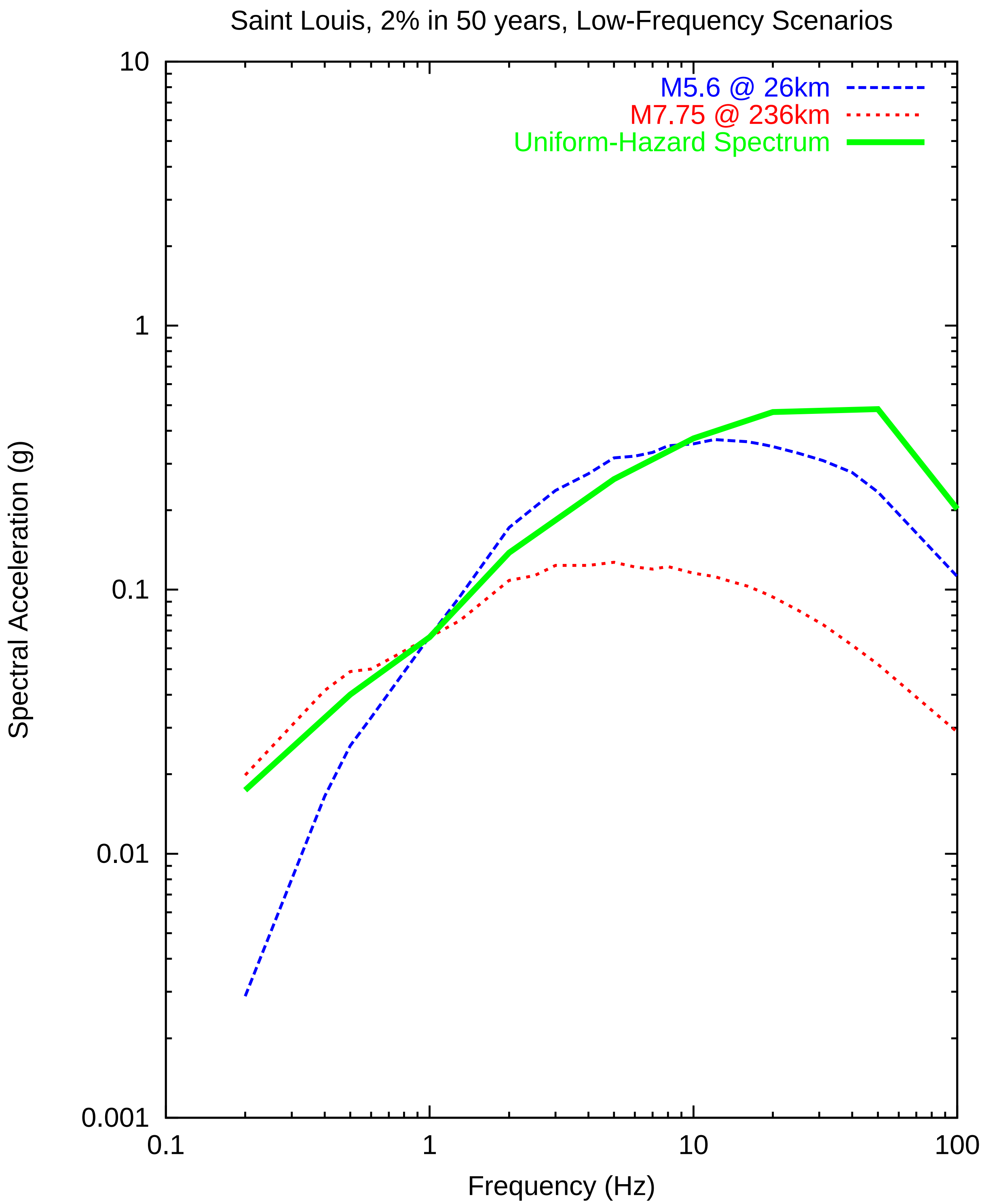

Figure 5-27. Spectra of low-frequency scenarios for Saint Louis, for an annual exceedence probability of 2% in 50 years.

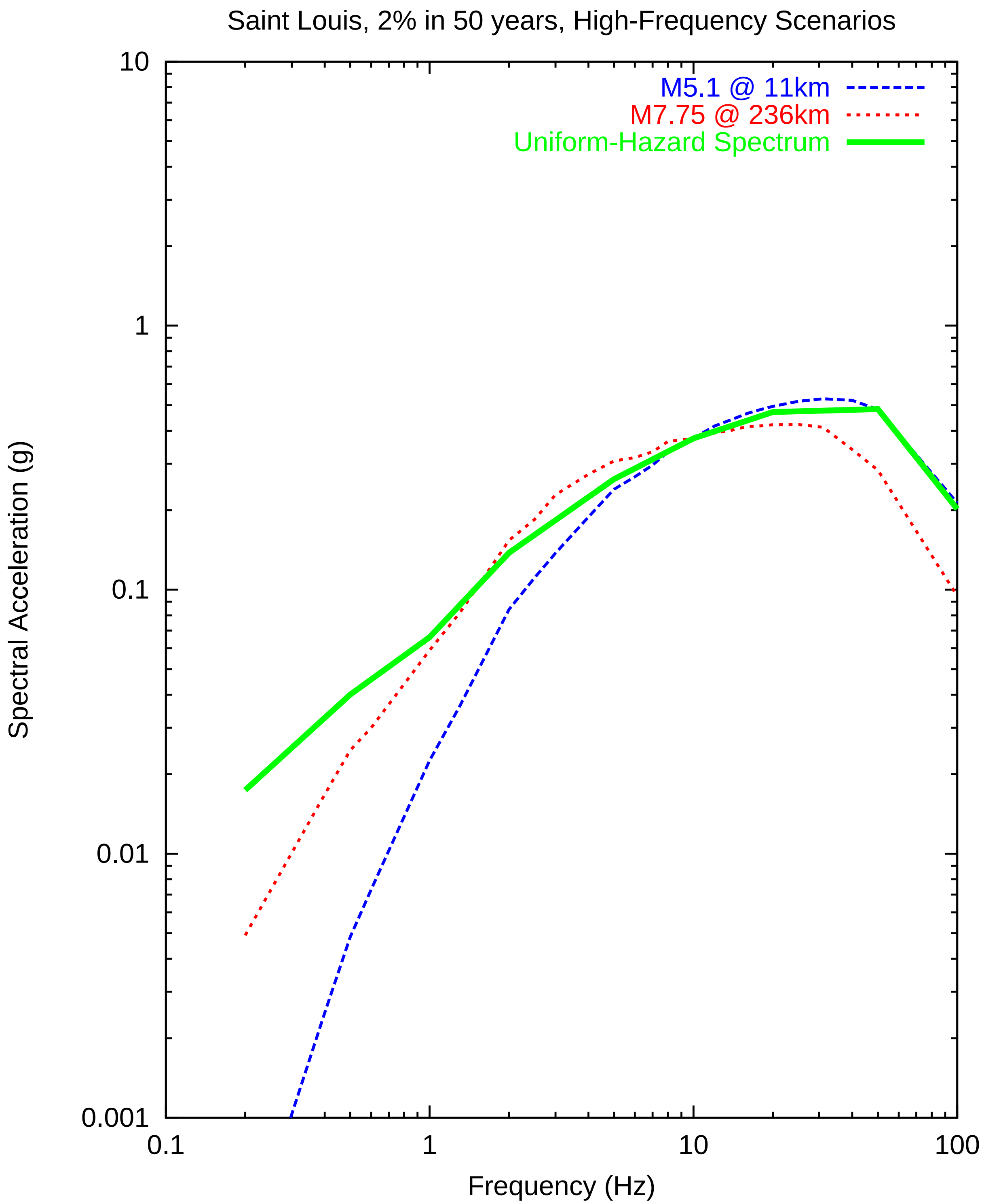

Figure 5-28. Spectra of high-frequency scenarios for Saint Louis, for an annual exceedence probability of 2% in 50 years.

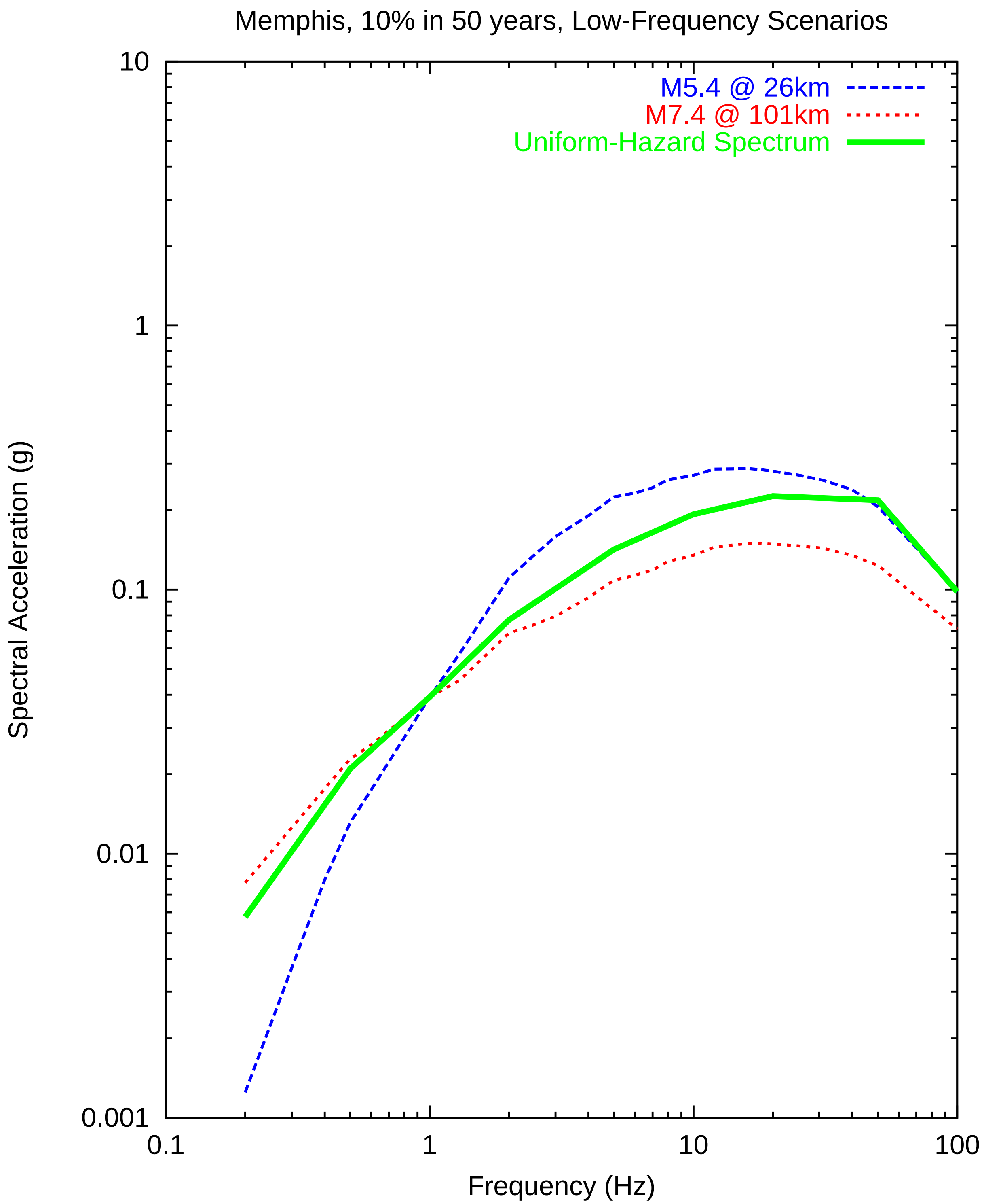

Figure 5-29. Spectra of low-frequency scenarios for Memphis, for an annual exceedence probability of 10% in 50 years.

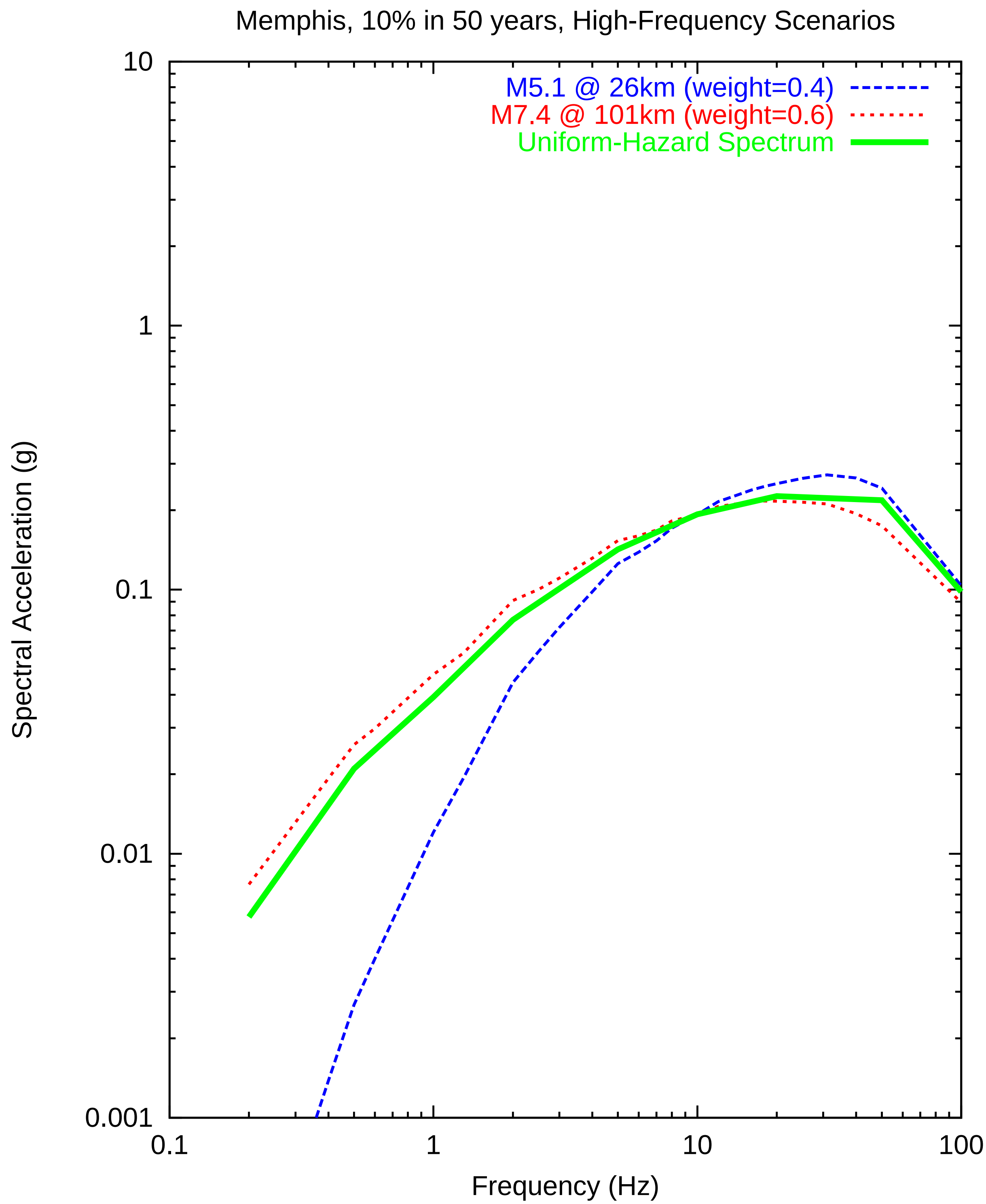

Figure 5-30. Spectra of high-frequency scenarios for Memphis, for an annual exceedence probability of 10% in 50 years.

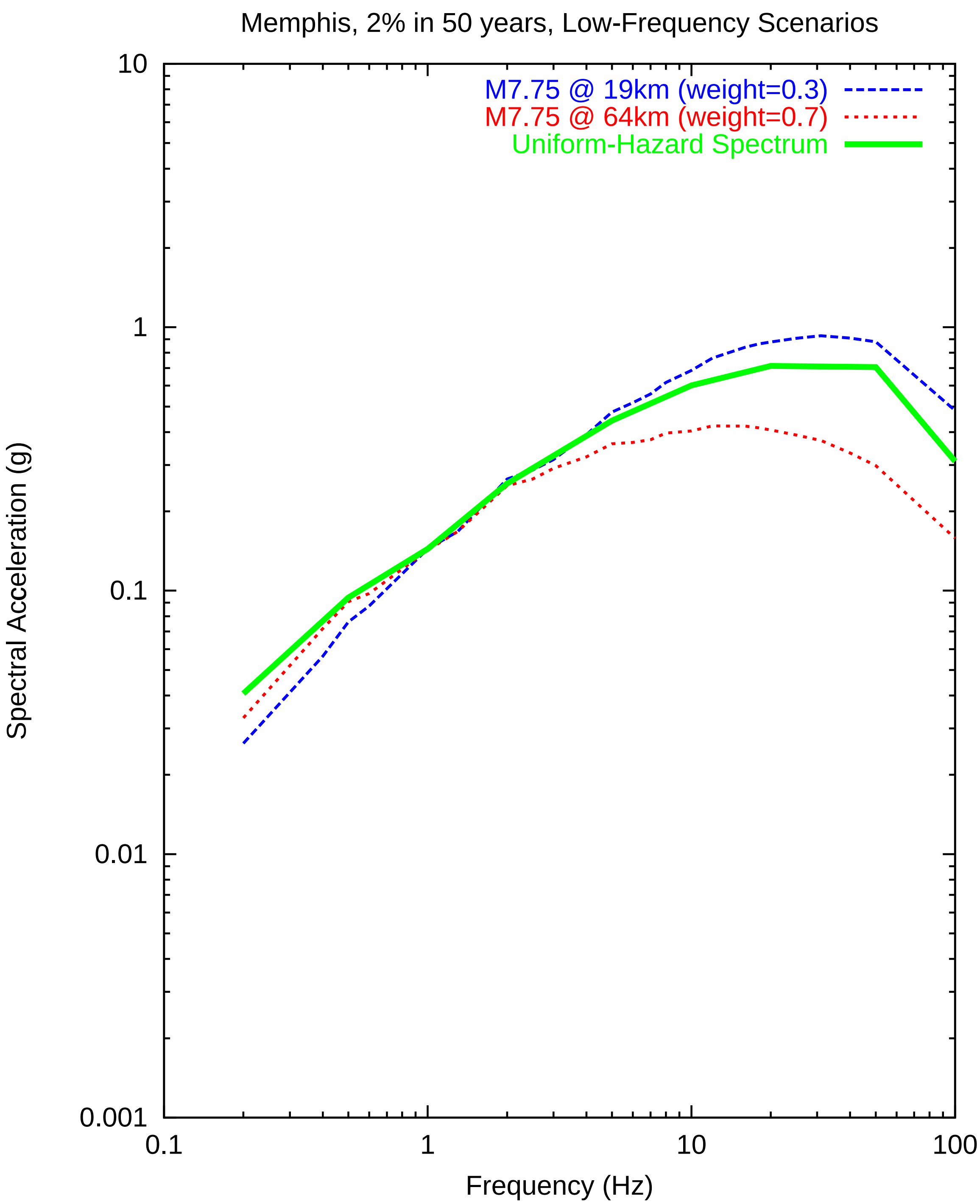

Figure 5-31. Spectra of low-frequency scenarios for Memphis, for an annual exceedence probability of 2% in 50 years.

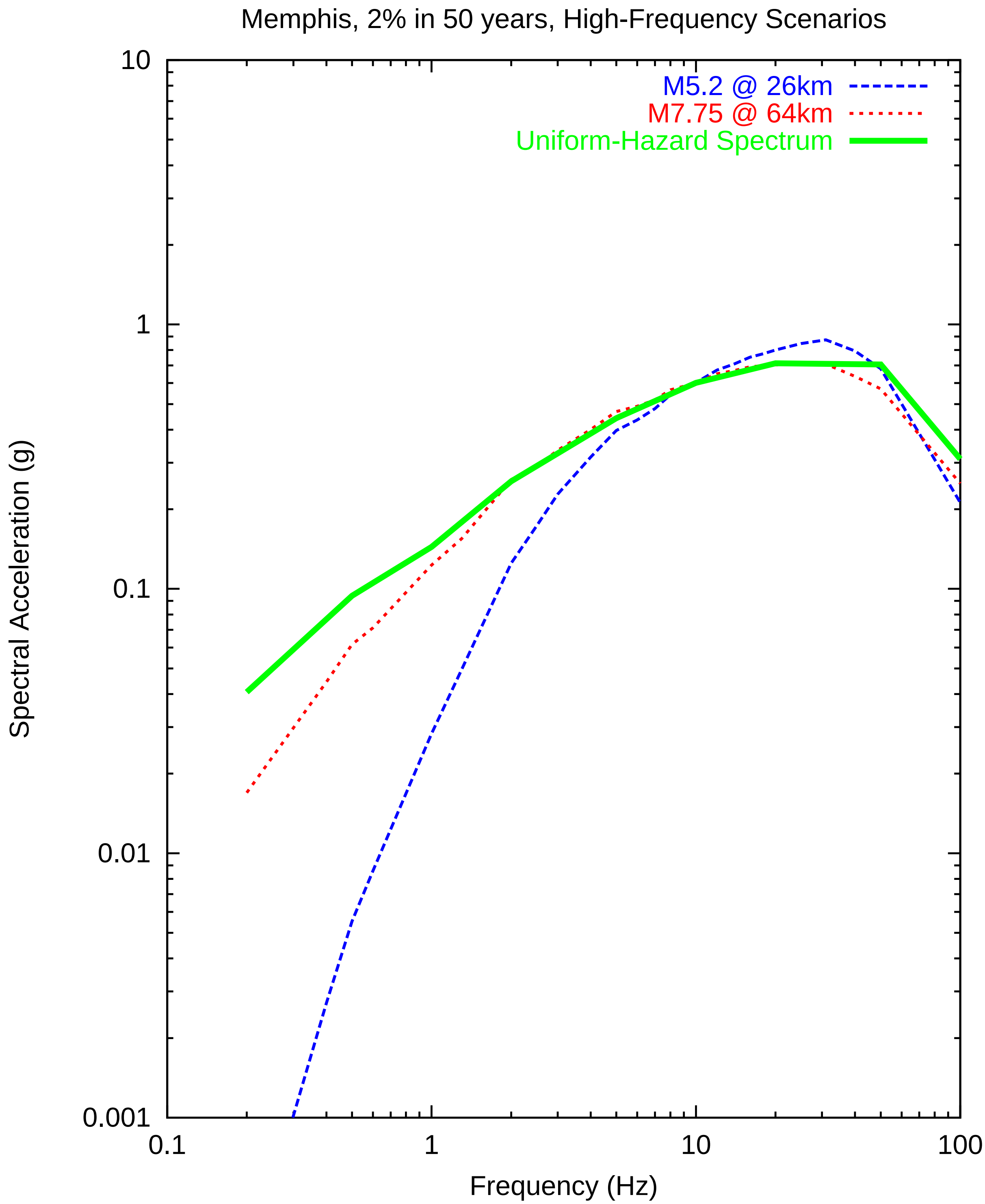

Figure 5-32. Spectra of high-frequency scenarios for Memphis, for an annual exceedence probability of 2% in 50 years.

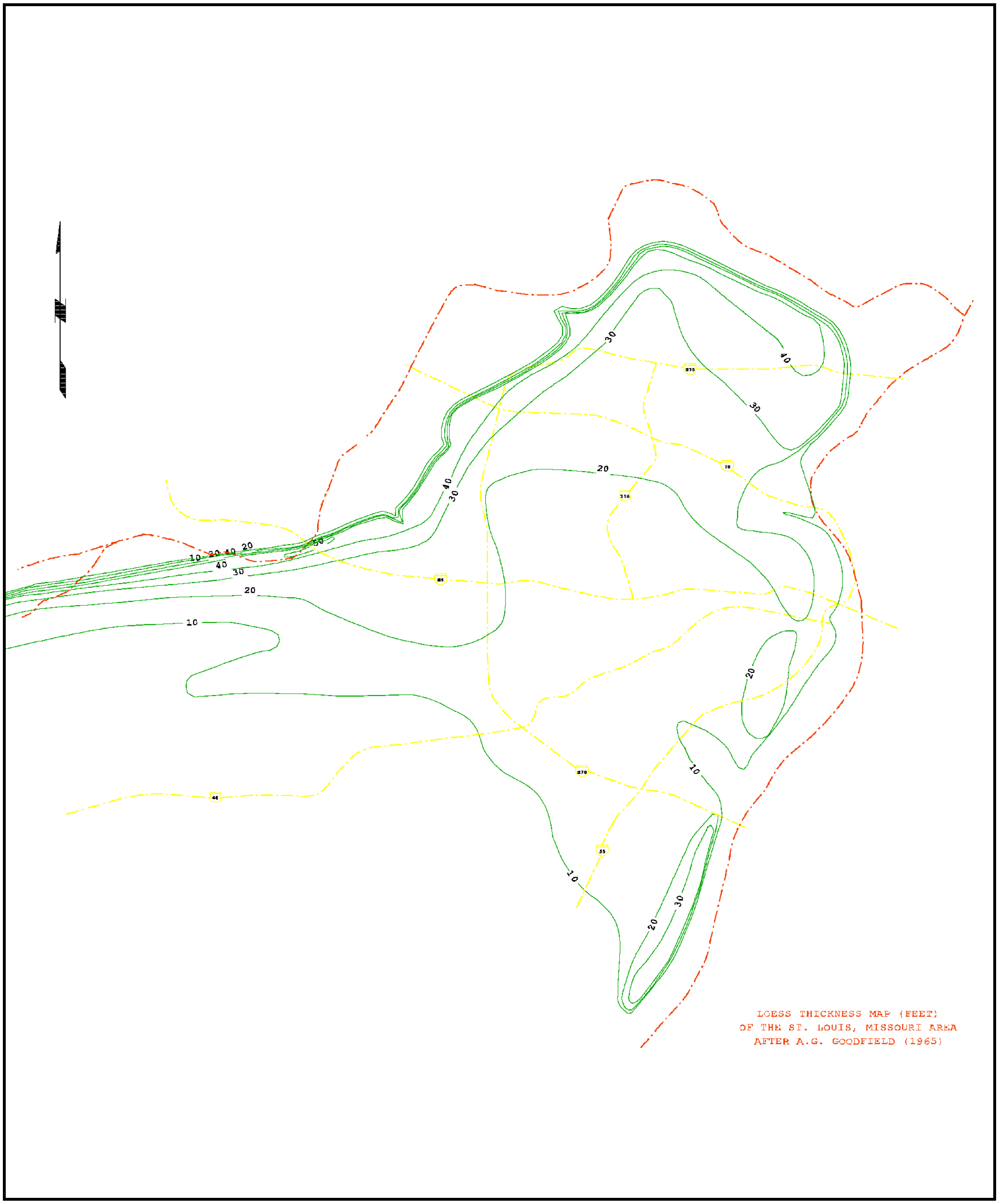

Figure 5-33. Map showing loess thickness in Saint Louis and vicinity. Source: Goodfiled (1964).

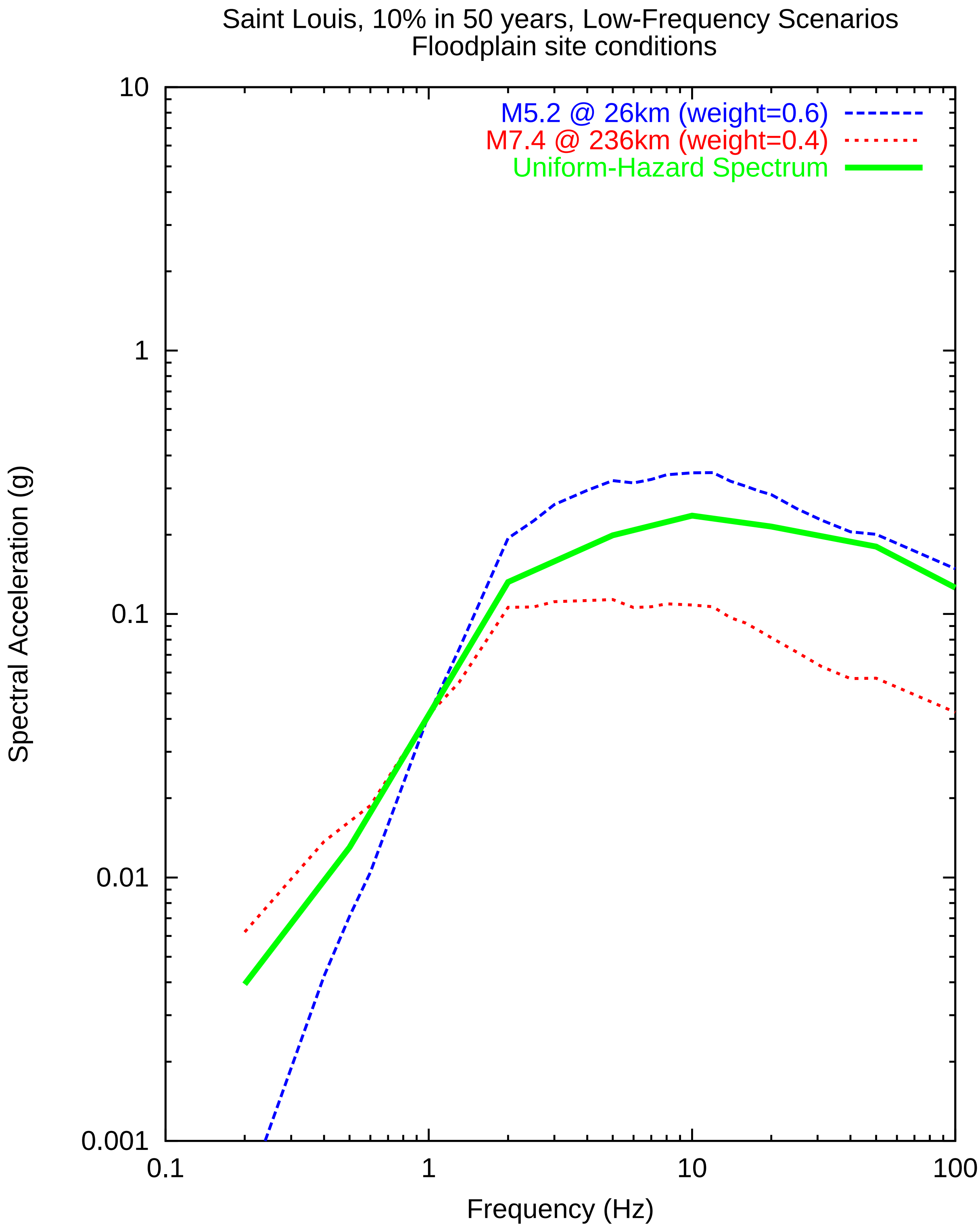

Figure 5-34. Spectra of low-frequency scenarios for Floodplain site conditions in Saint Louis, for an annual exceedence probability of 10% in 50 years.

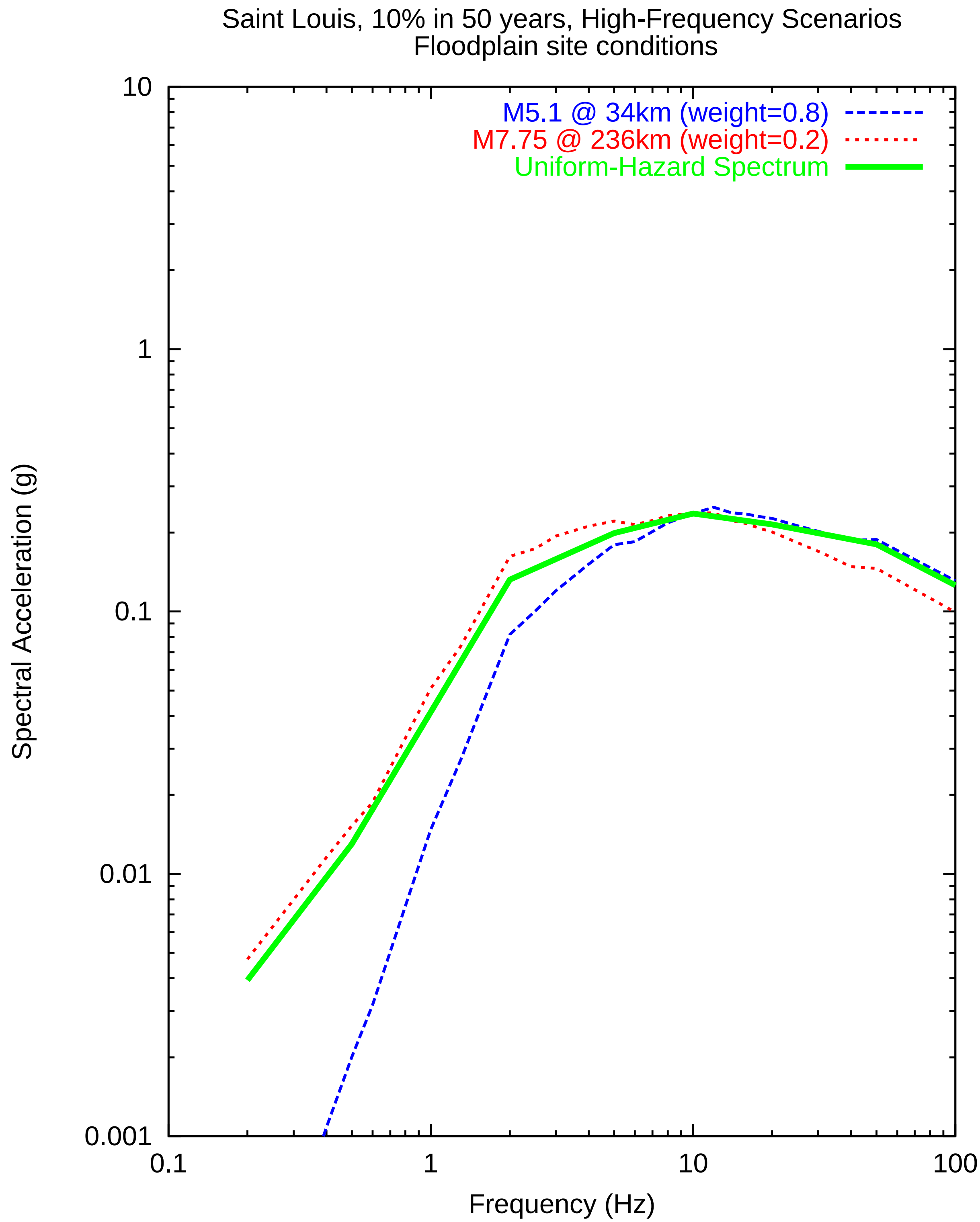

Figure 5-35. Spectra of high-frequency scenarios for Floodplain site conditions in Saint Louis, for an annual exceedence probability of 10% in 50 years.

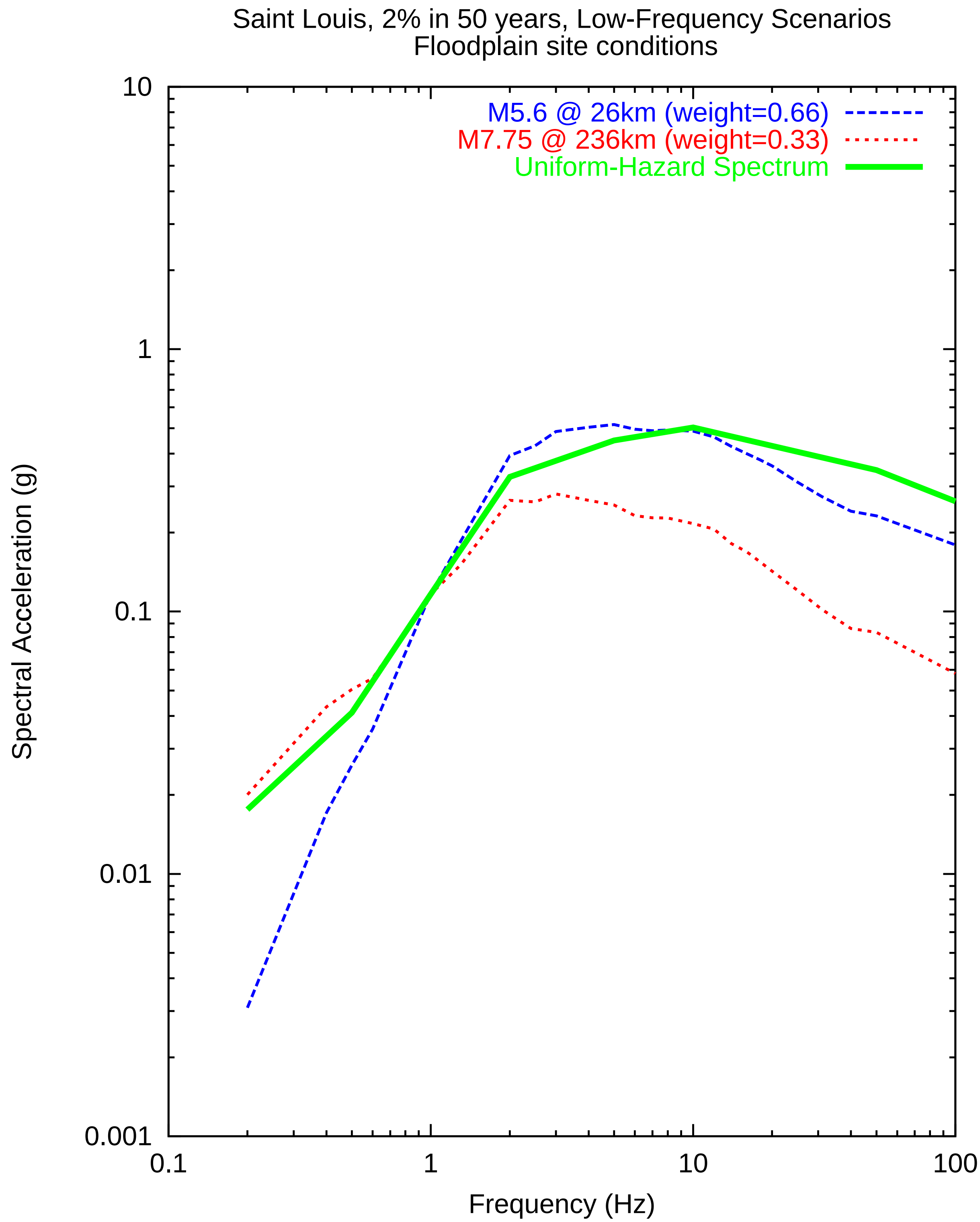

Figure 5-36. Spectra of low-frequency scenarios for Floodplain site conditions in Saint Louis, for an annual exceedence probability of 2% in 50 years.

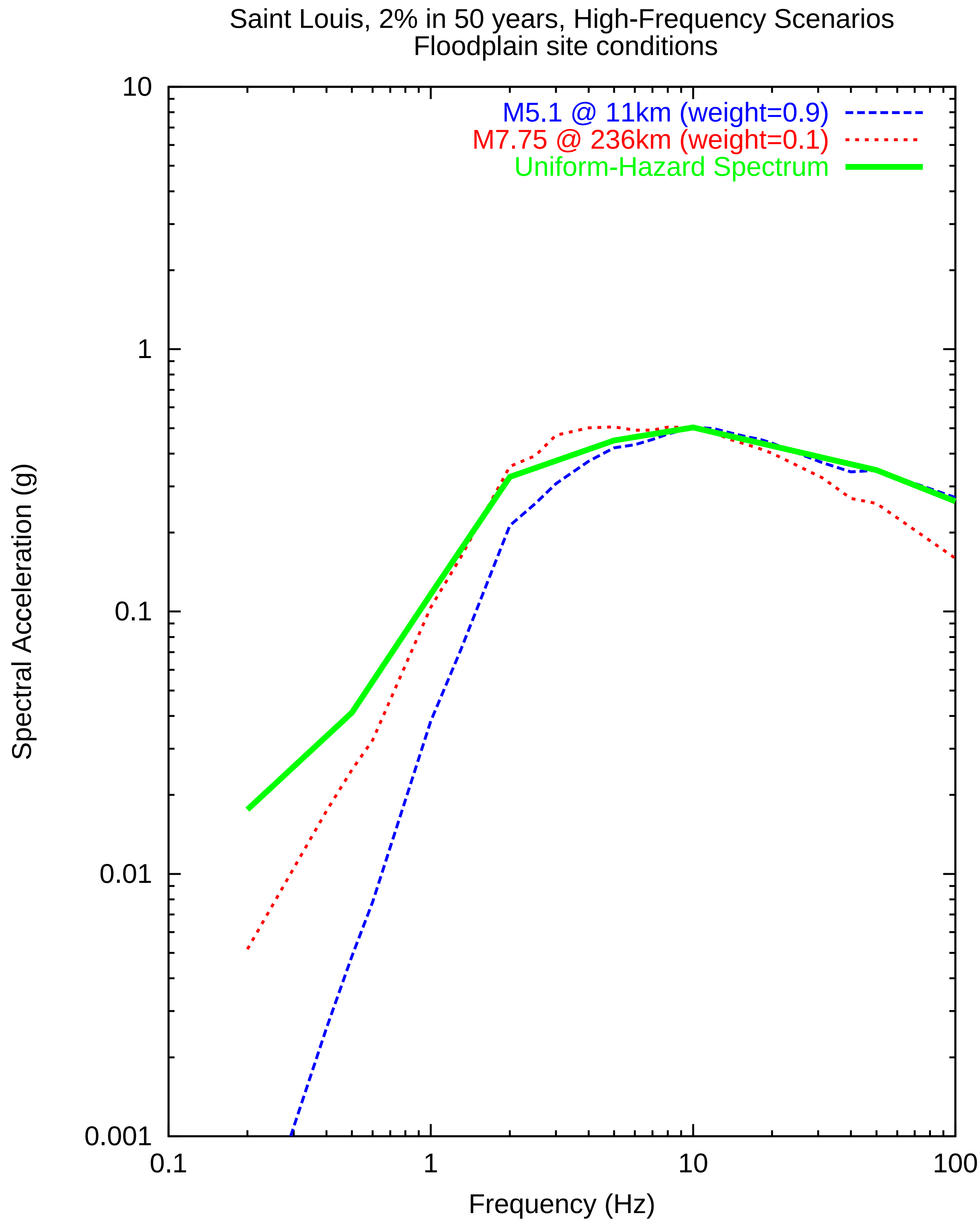

Figure 5-37. Spectra of high-frequency scenarios for Floodplain site conditions in Saint Louis, for an annual exceedence probability of 2% in 50 years.

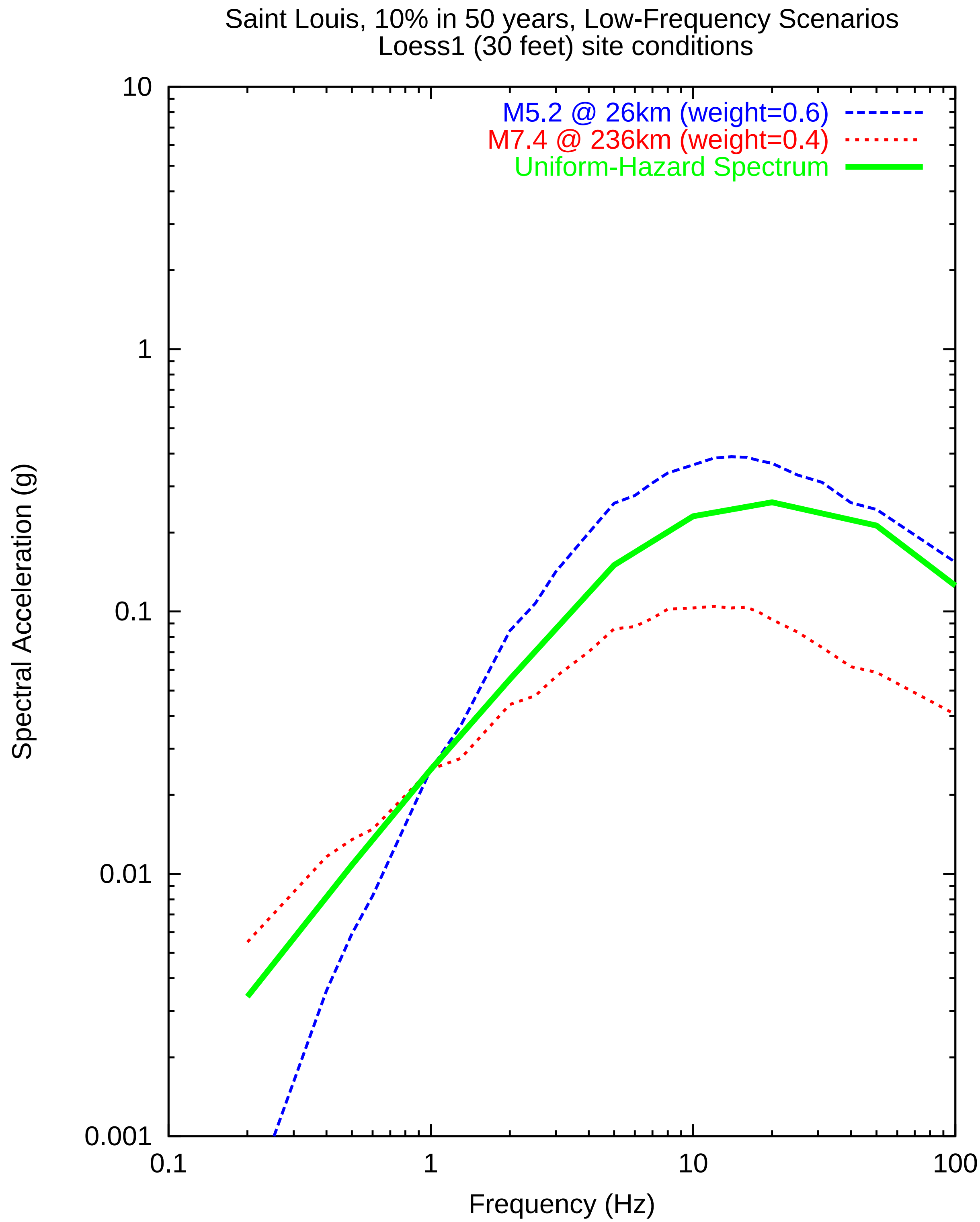

Figure 5-38. Spectra of low-frequency scenarios for Loess1 (30 feet) site conditions in Saint Louis, for an annual exceedence probability of 10% in 50 years.

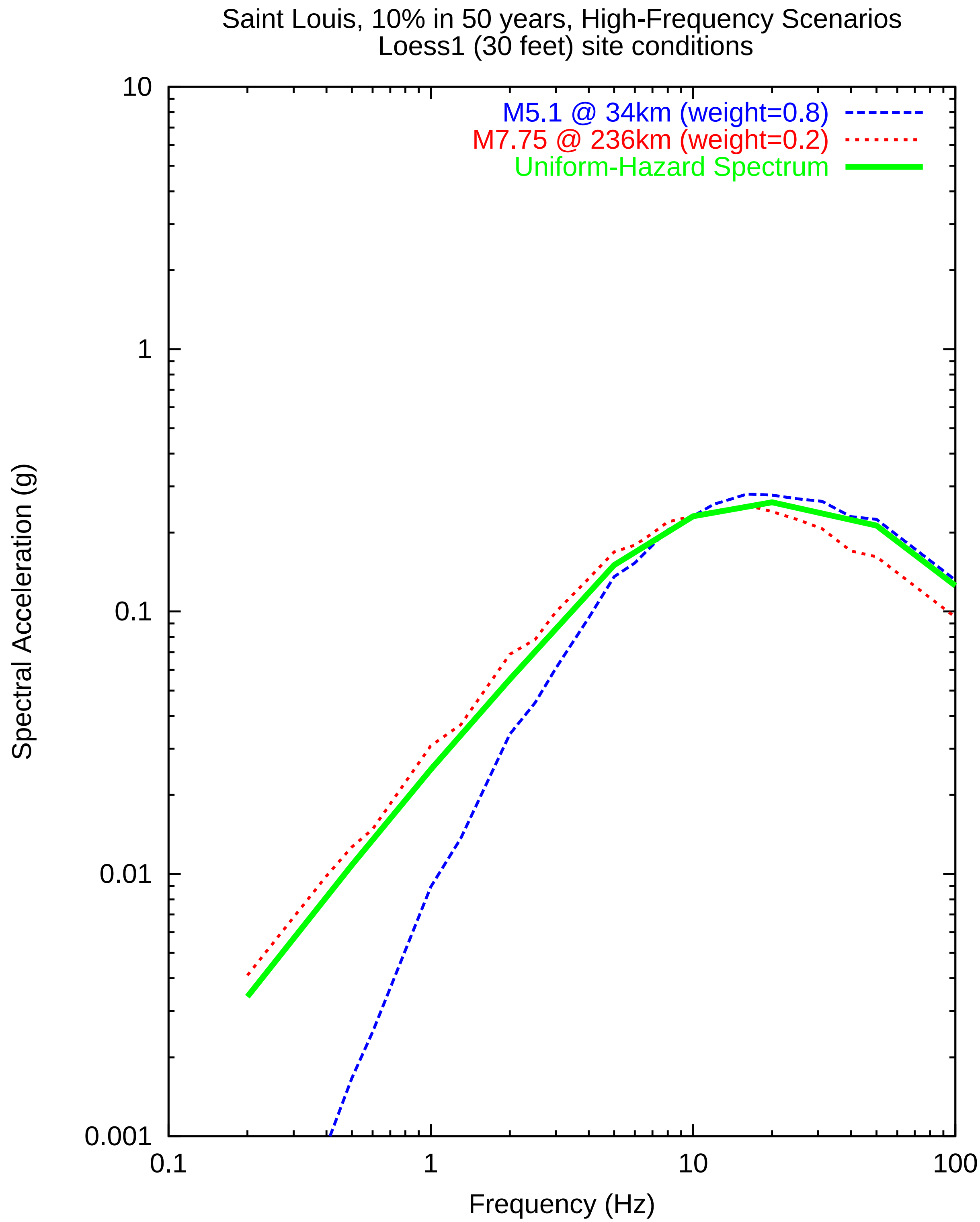

Figure 5-39. Spectra of high-frequency scenarios for Loess1 (30 feet) site conditions in Saint Louis, for an annual exceedence probability of 10% in 50 years.

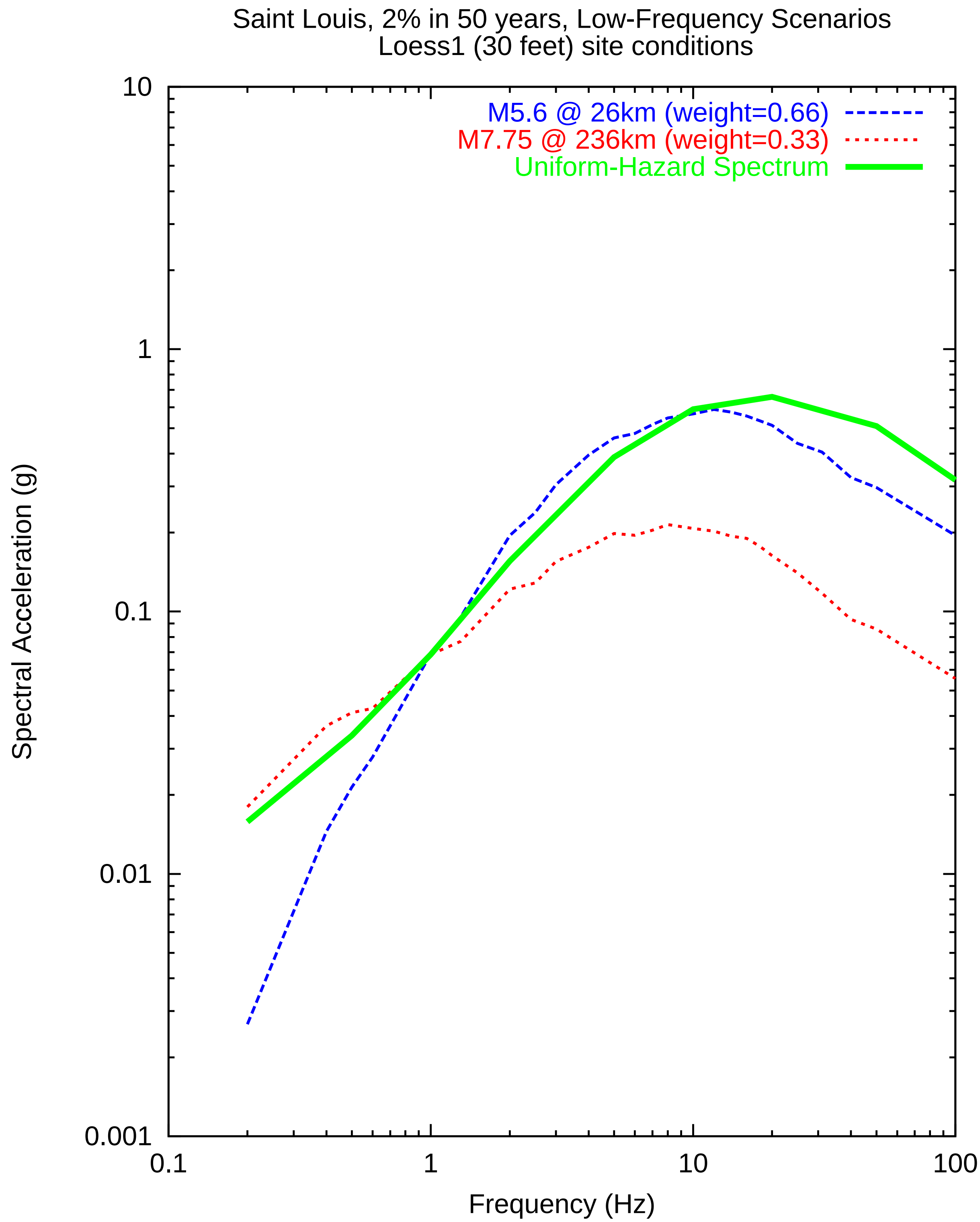

Figure 5-40. Spectra of low-frequency scenarios for Loess1 (30 feet) site conditions in Saint Louis, for an annual exceedence probability of 2% in 50 years.

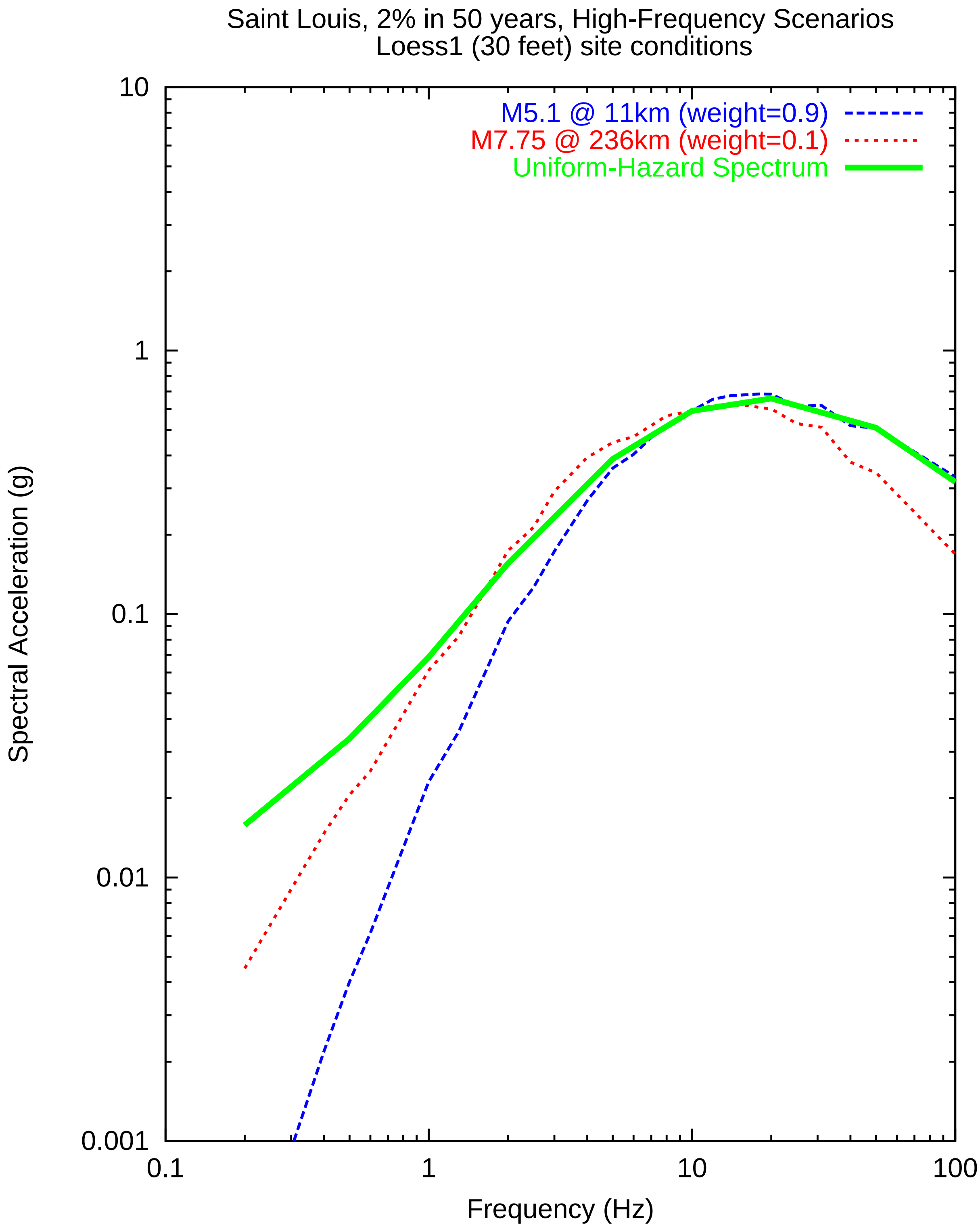

Figure 5-41. Spectra of high-frequency scenarios for Loess1 (30 feet) site conditions in Saint Louis, for an annual exceedence probability of 2% in 50 years.

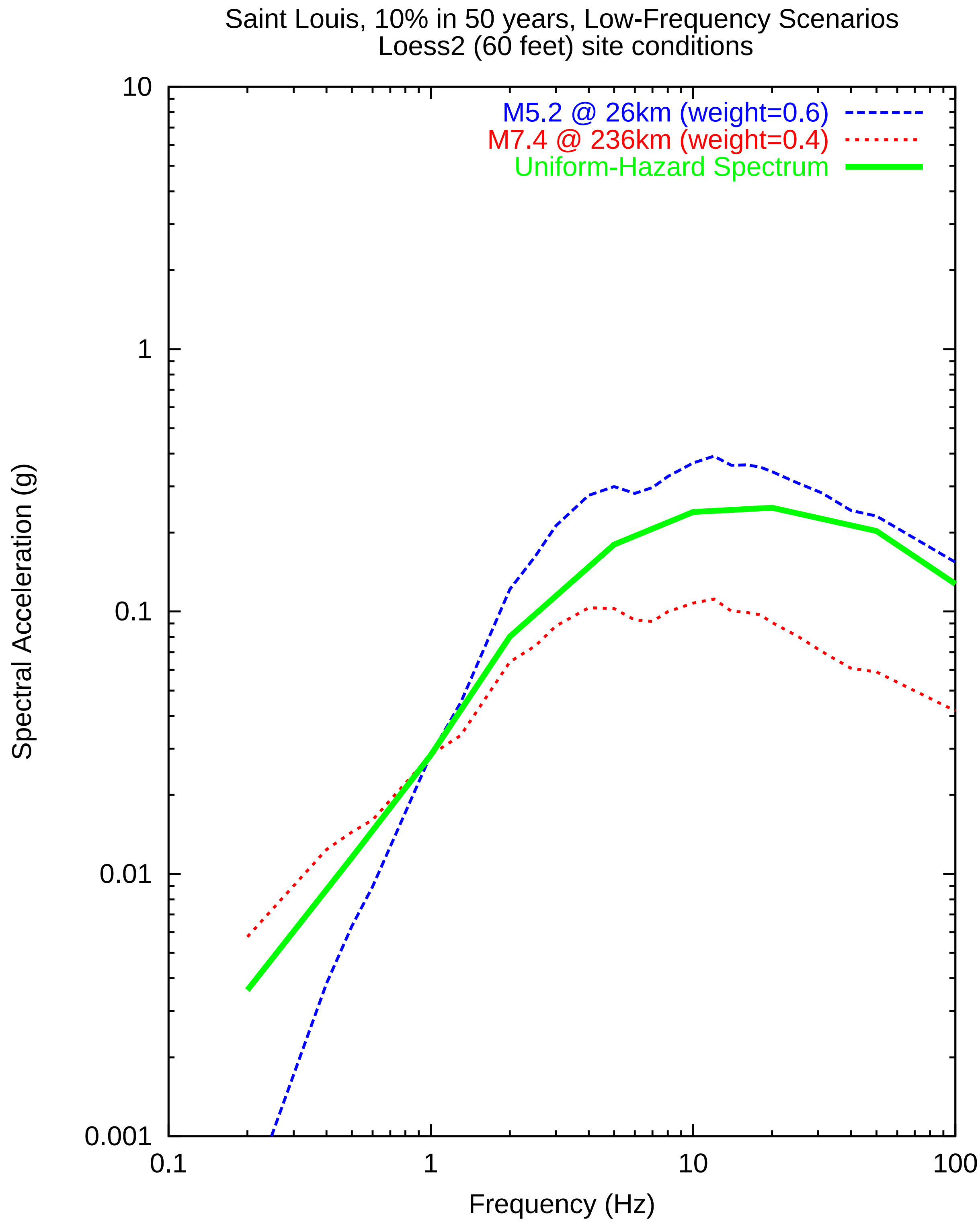

Figure 5-42. Spectra of low-frequency scenarios for Loess2 (60 feet) site conditions in Saint Louis, for an annual exceedence probability of 10% in 50 years.

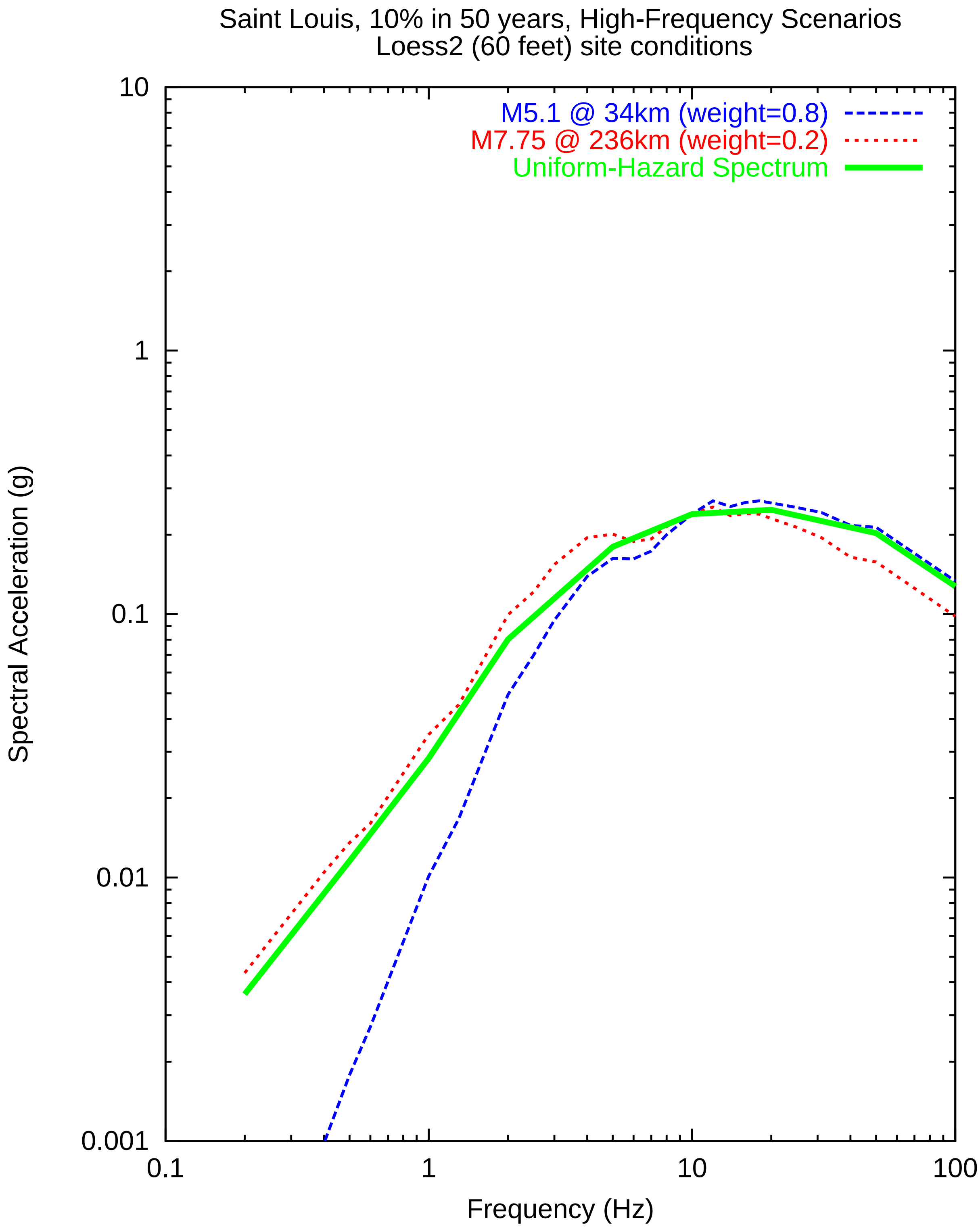

Figure 5-43. Spectra of high-frequency scenarios for Loess2 (60 feet) site conditions in Saint Louis, for an annual exceedence probability of 10% in 50 years.

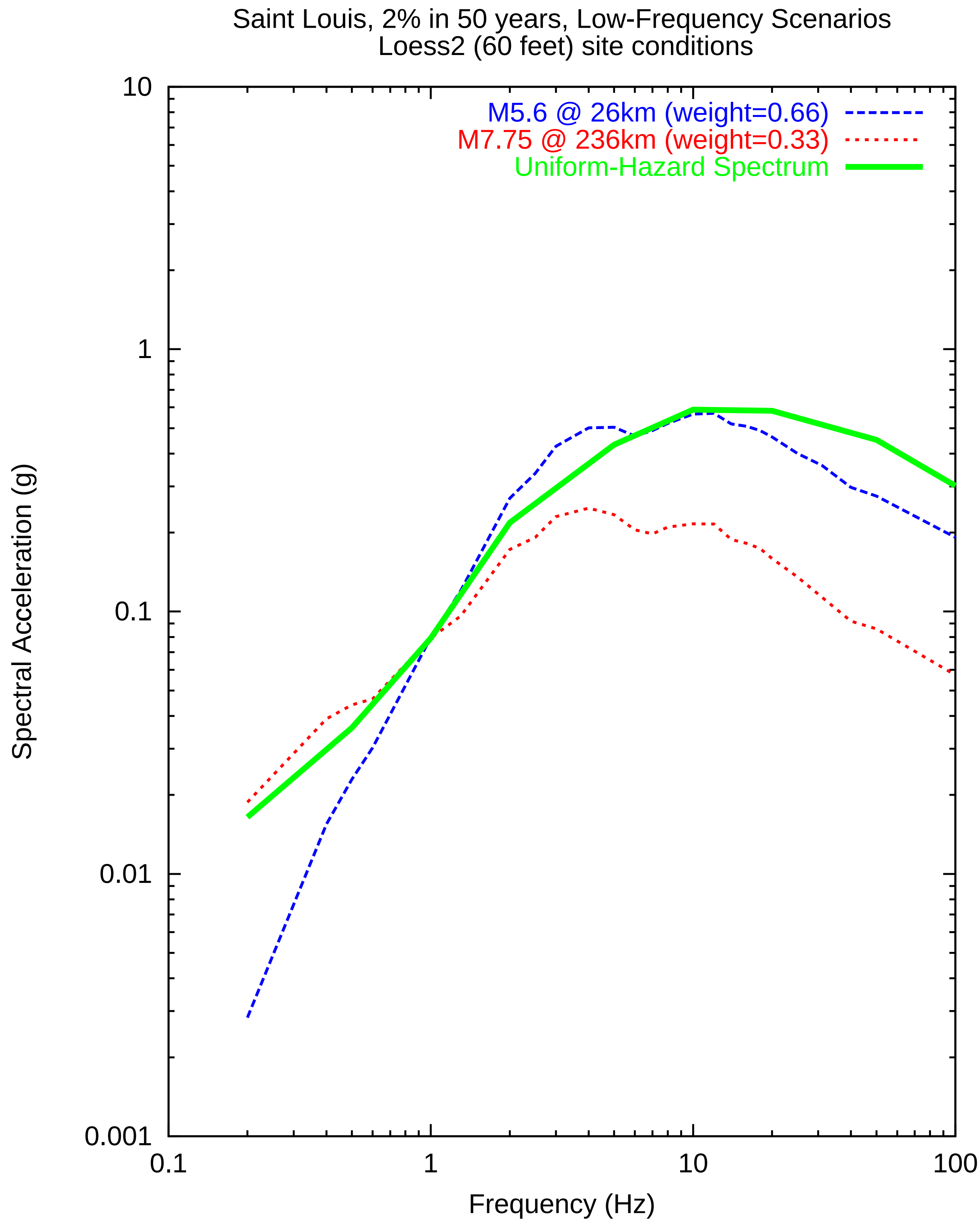

Figure 5-44. Spectra of low-frequency scenarios for Loess2 (60 feet) site conditions in Saint Louis, for an annual exceedence probability of 2% in 50 years.

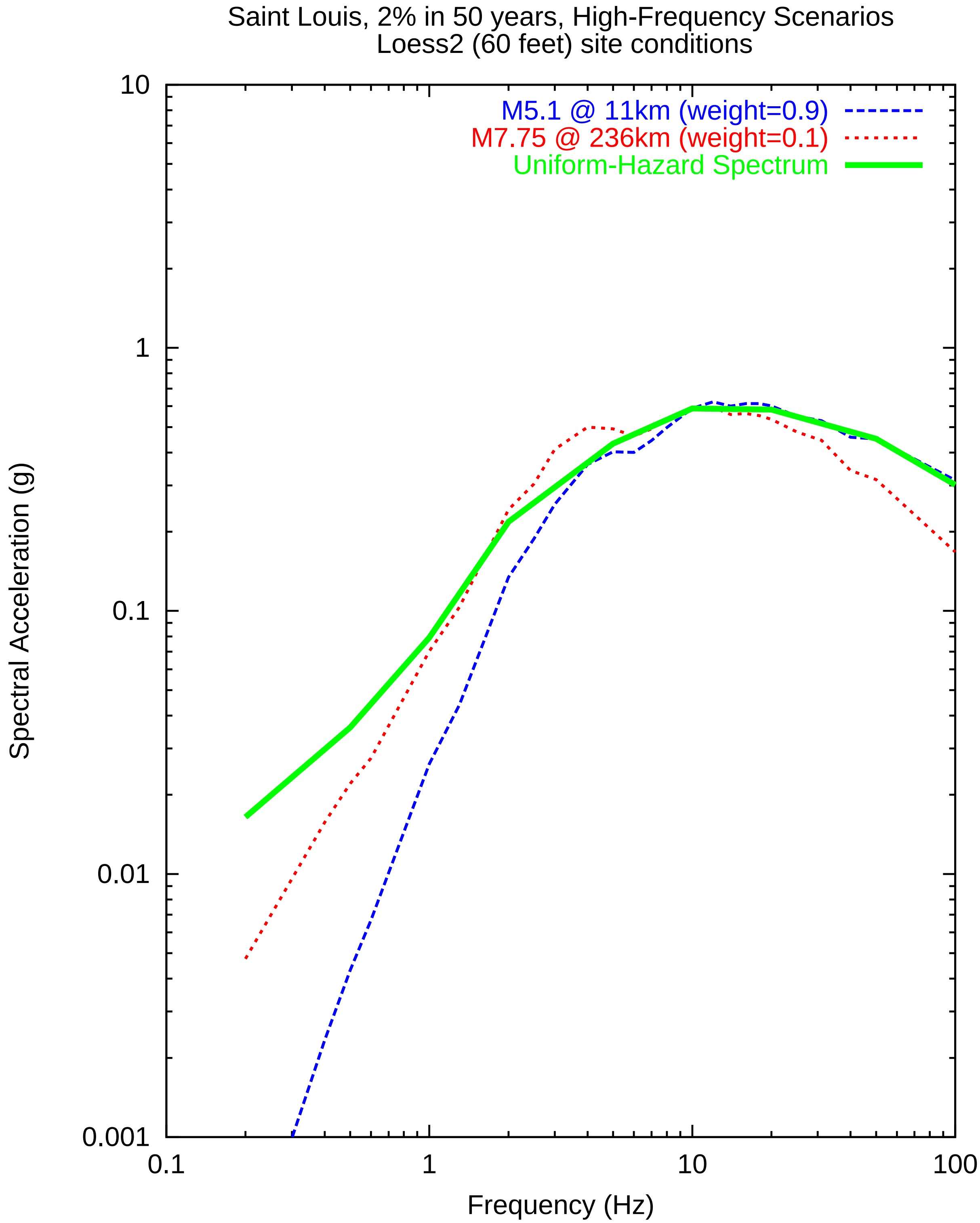

Figure 5-45. Spectra of high-frequency scenarios for Loess2 (60 feet) site conditions in Saint Louis, for an annual exceedence probability of 2% in 50 years.

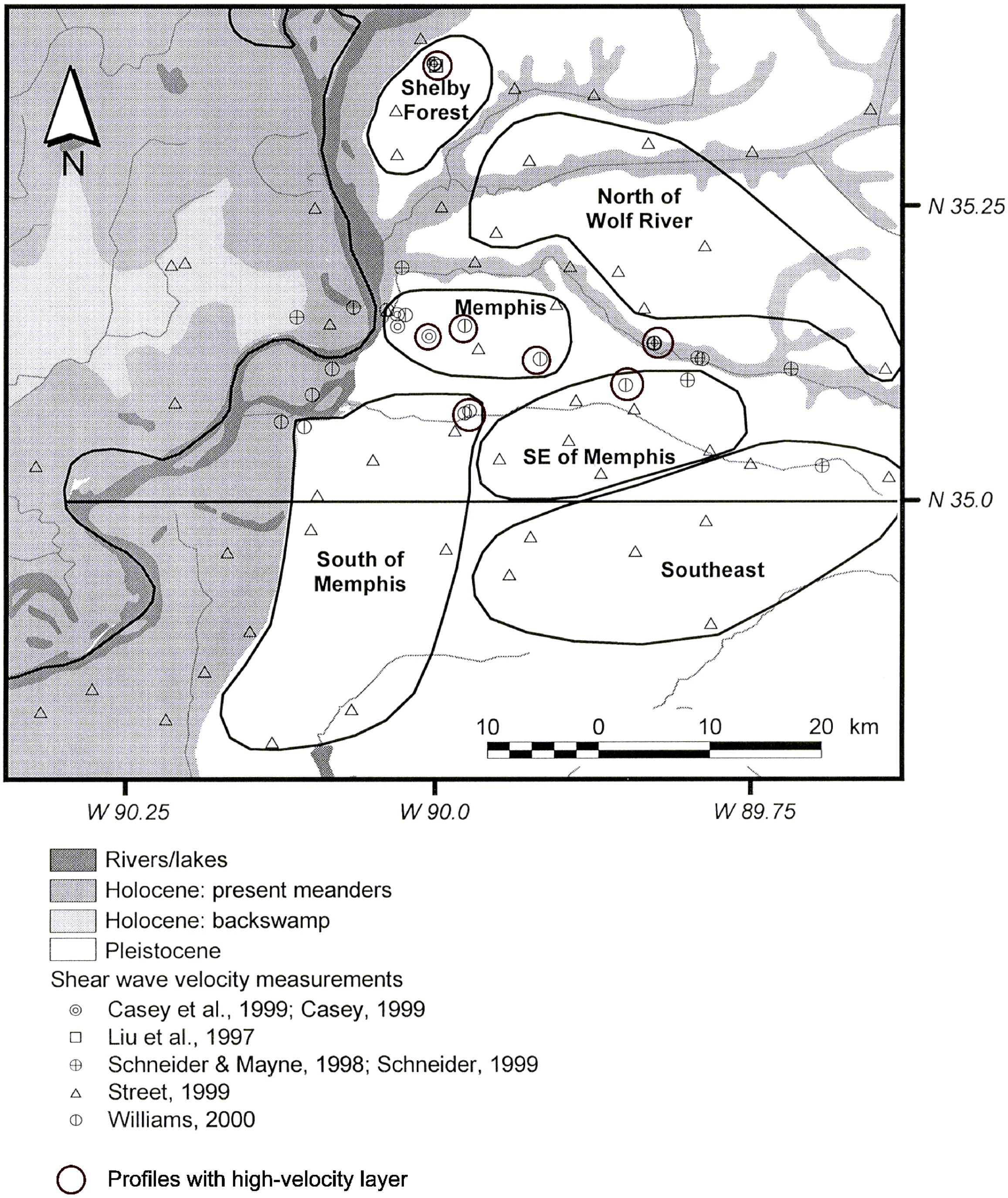

Figure 5-46. Map showing the locations in the Memphis metropolitan are with Holocene and Pleistocene deposits, as well as the locations of velocity profiles and the geographic locations considered by Romero and Rix. The large circles indicate profiles with high velocity layers. Modified from Romero and Rix (2000) using information provided by S. Romero, personal communication of 11/9/2000.

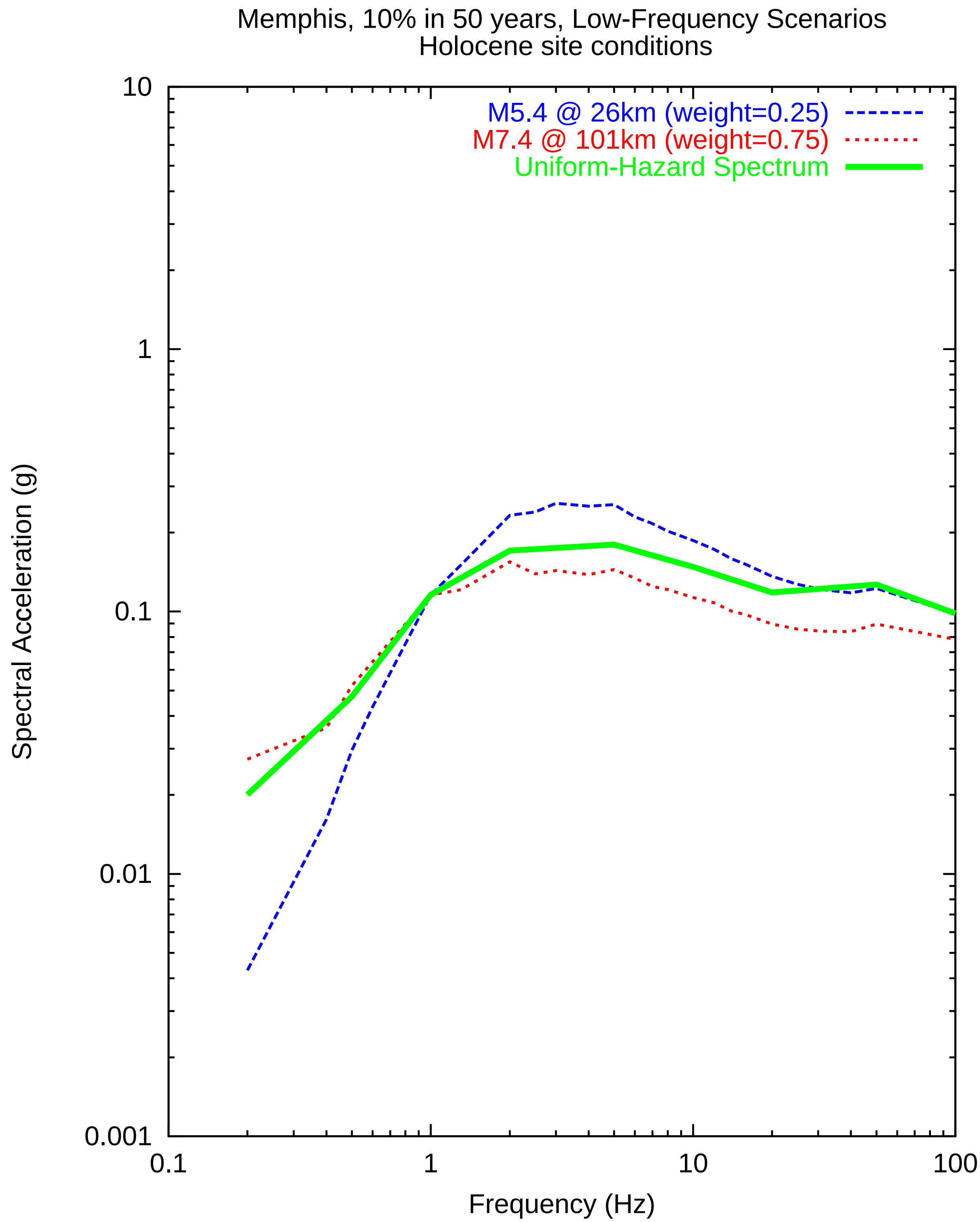

Figure 5-47. Spectra of low-frequency scenarios for Holocene site conditions in Memphis, for an annual exceedence probability of 10% in 50 years.

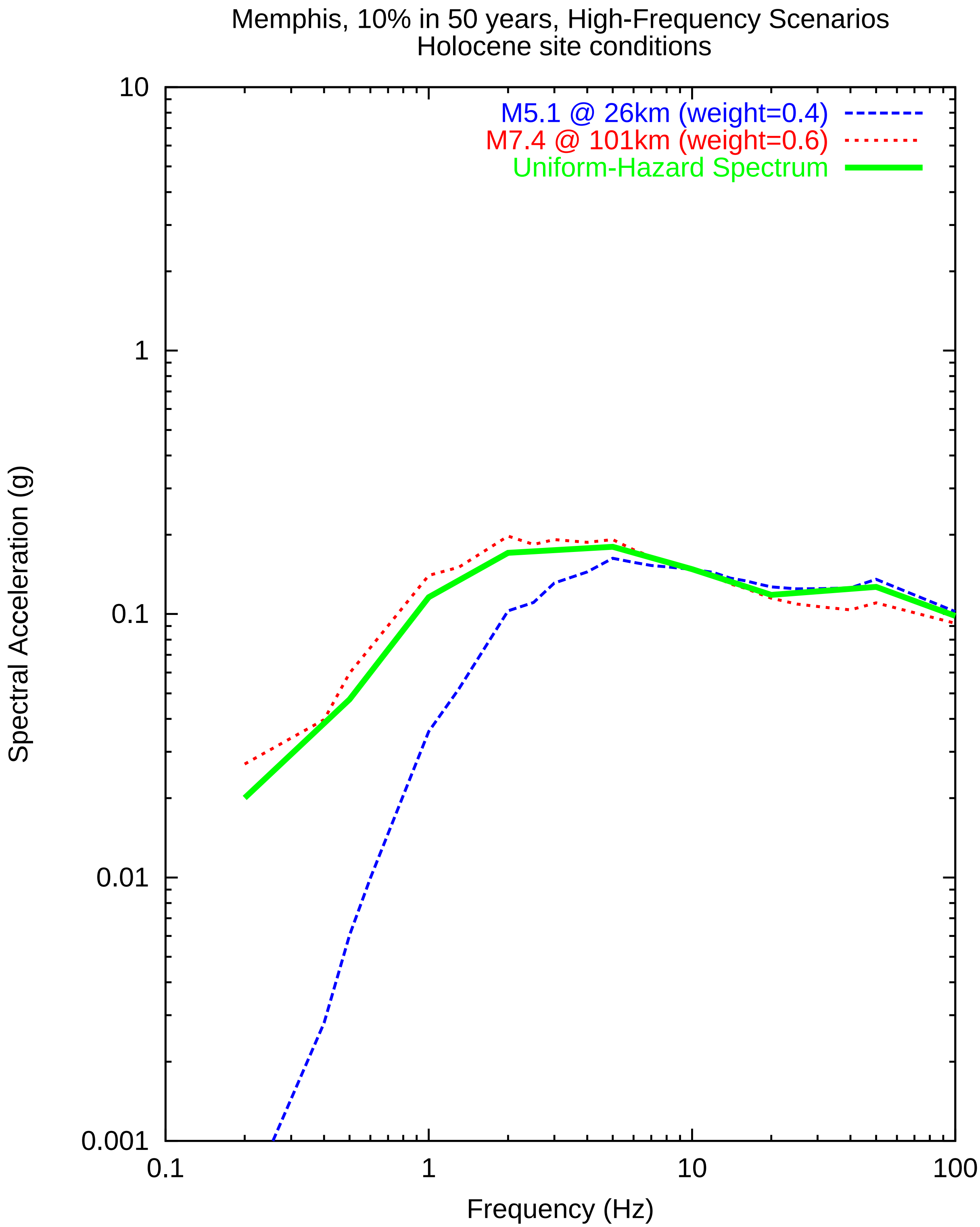

Figure 5-48. Spectra of high-frequency scenarios for Holocene site conditions in Memphis, for an annual exceedence probability of 10% in 50 years.

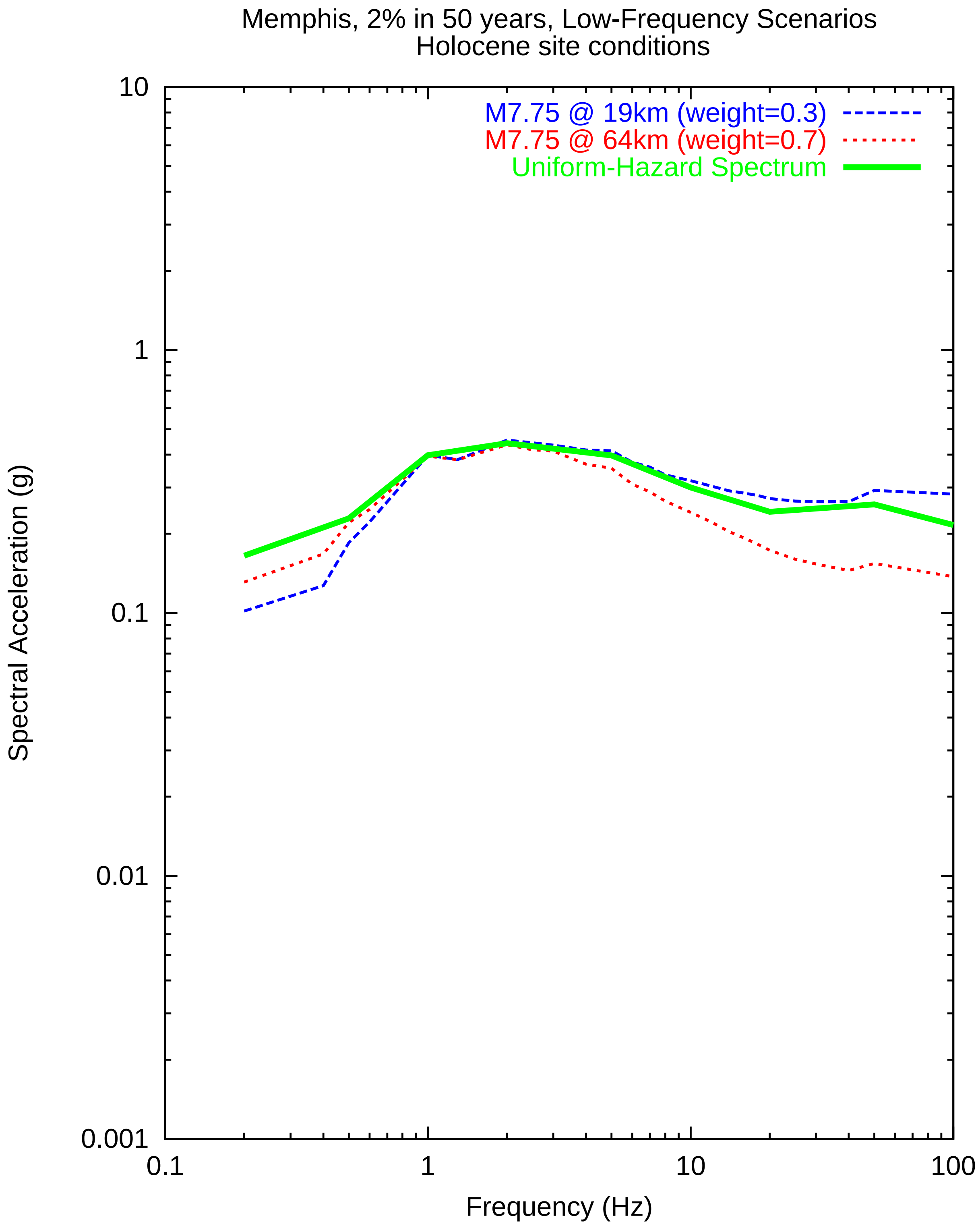

Figure 5-49. Spectra of low-frequency scenarios for Holocene site conditions in Memphis, for an annual exceedence probability of 2% in 50 years.

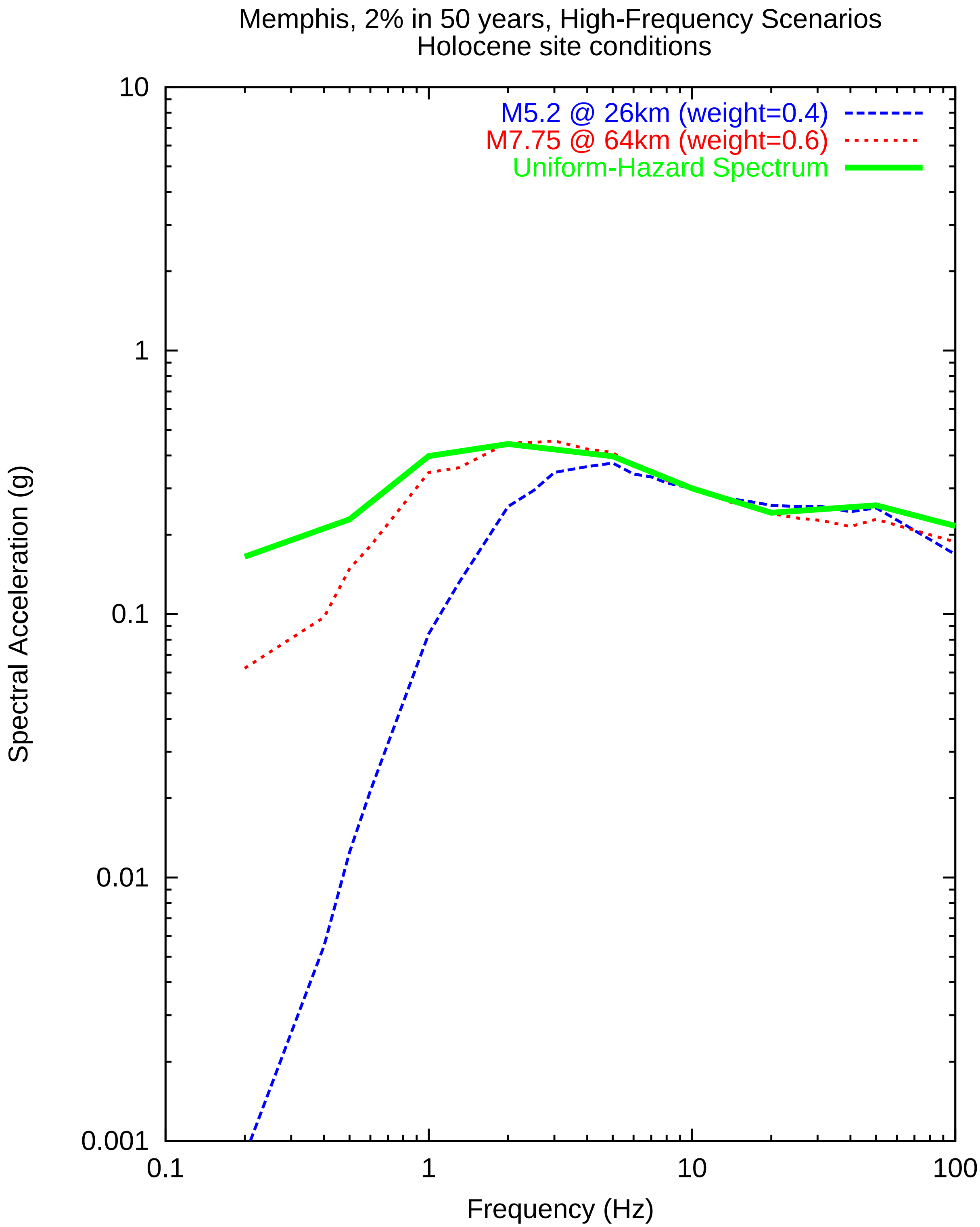

Figure 5-50. Spectra of high-frequency scenarios for Holocene site conditions in Memphis, for an annual exceedence probability of 2% in 50 years.

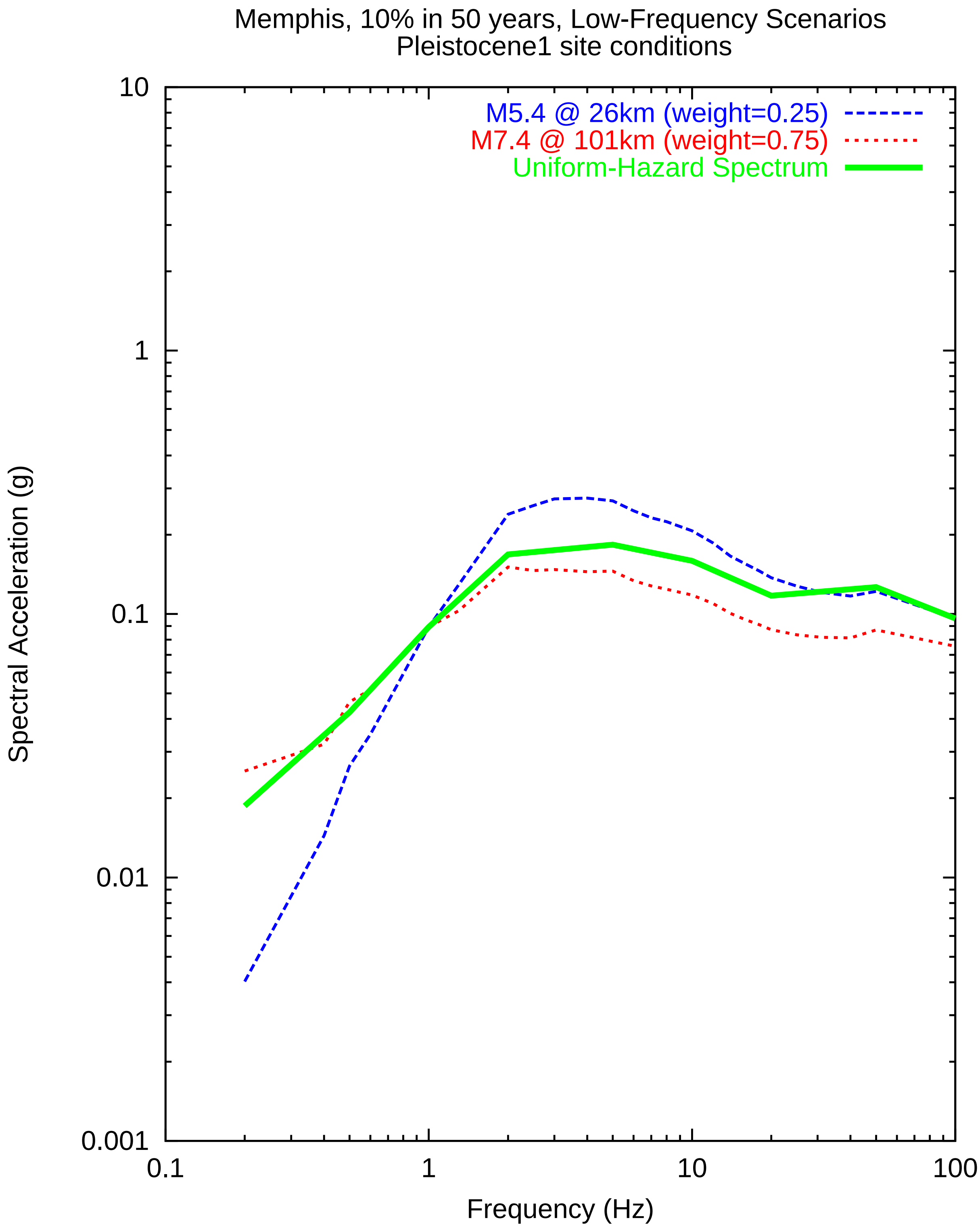

Figure 5-51. Spectra of low-frequency scenarios for Pleistocene1 site conditions in Memphis, for an annual exceedence probability of 10% in 50 years.

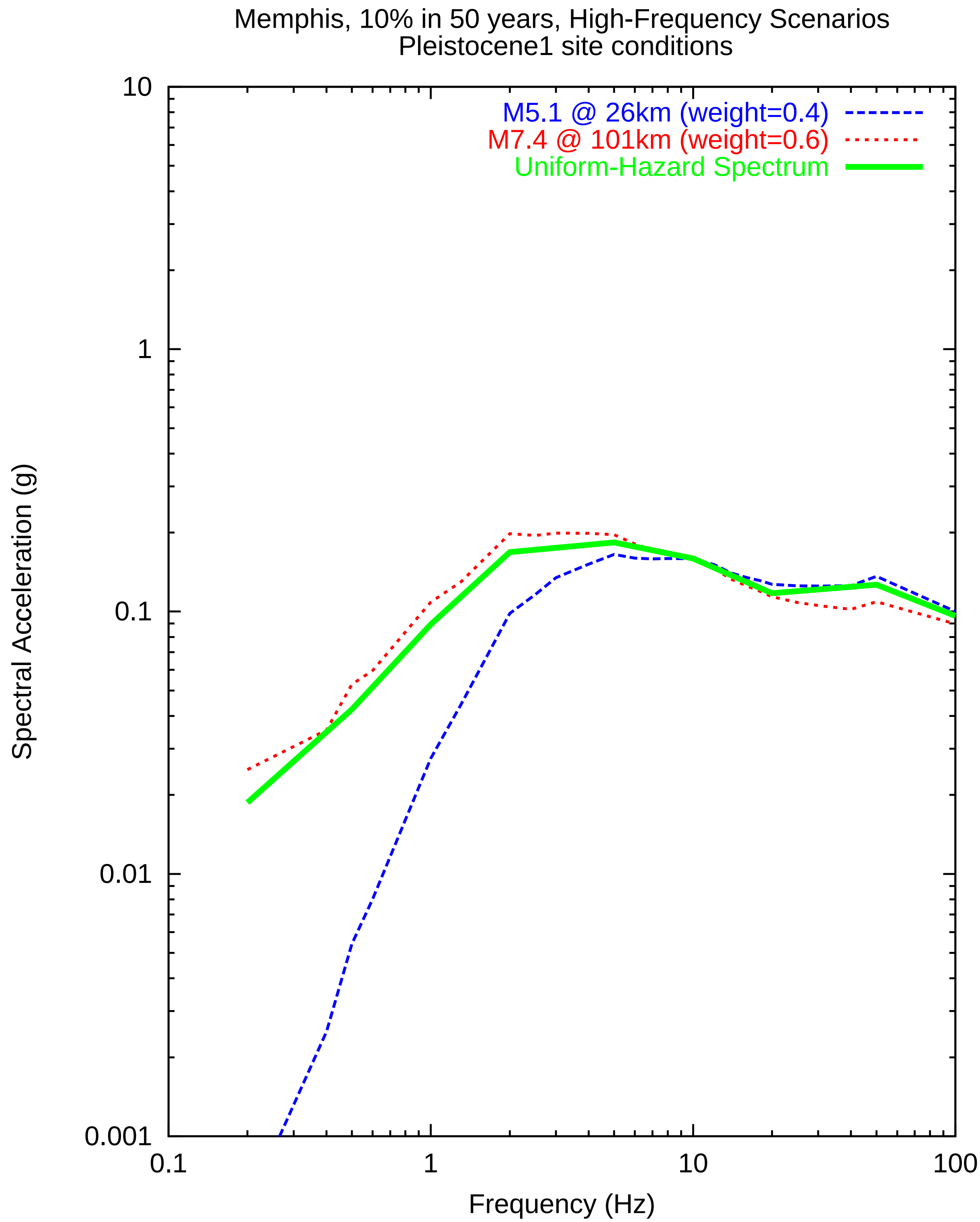

Figure 5-52. Spectra of high-frequency scenarios for Pleistocene1 site conditions in Memphis, for an annual exceedence probability of 10% in 50 years.

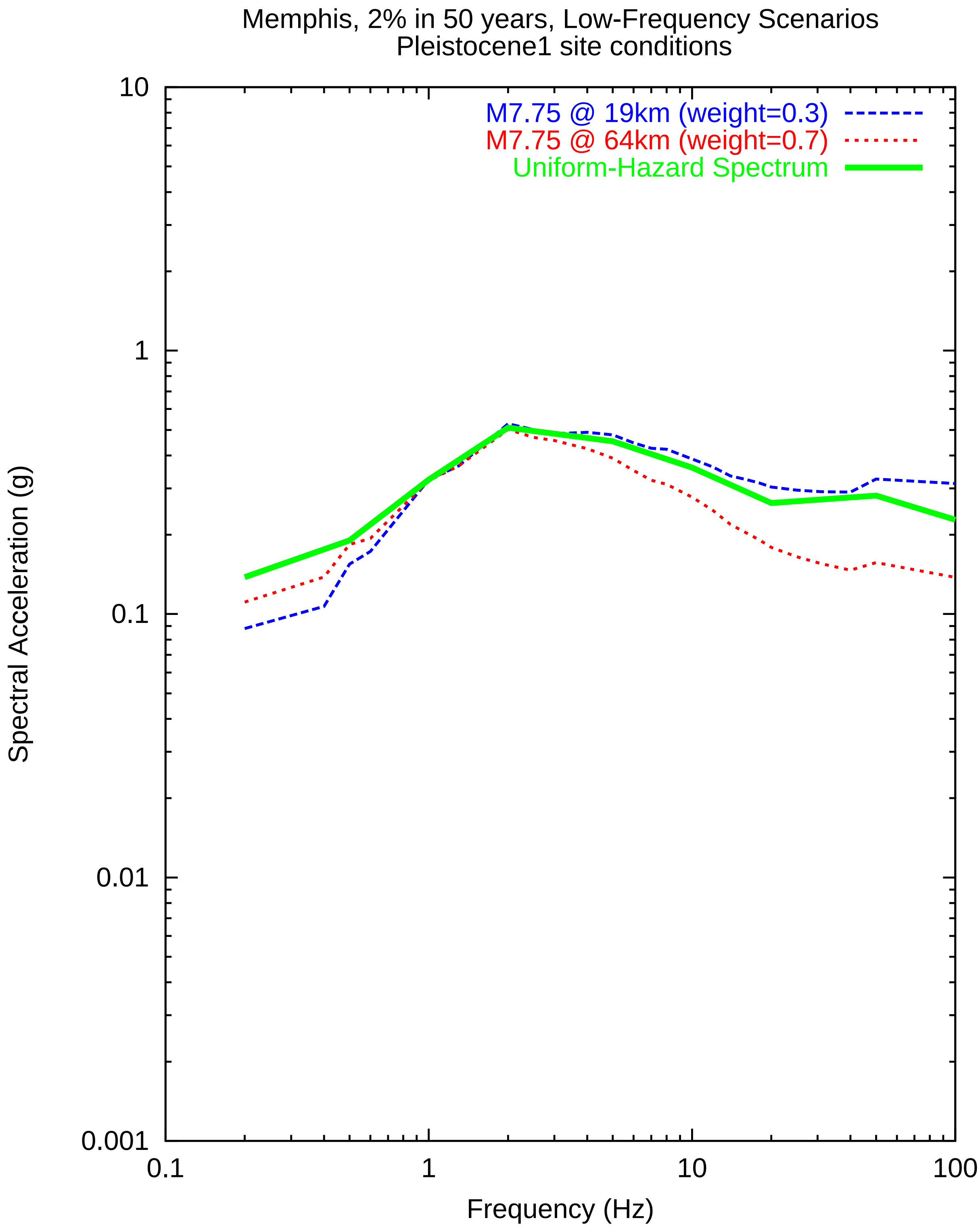

Figure 5-53. Spectra of low-frequency scenarios for Pleistocene1 site conditions in Memphis, for an annual exceedence probability of 2% in 50 years.

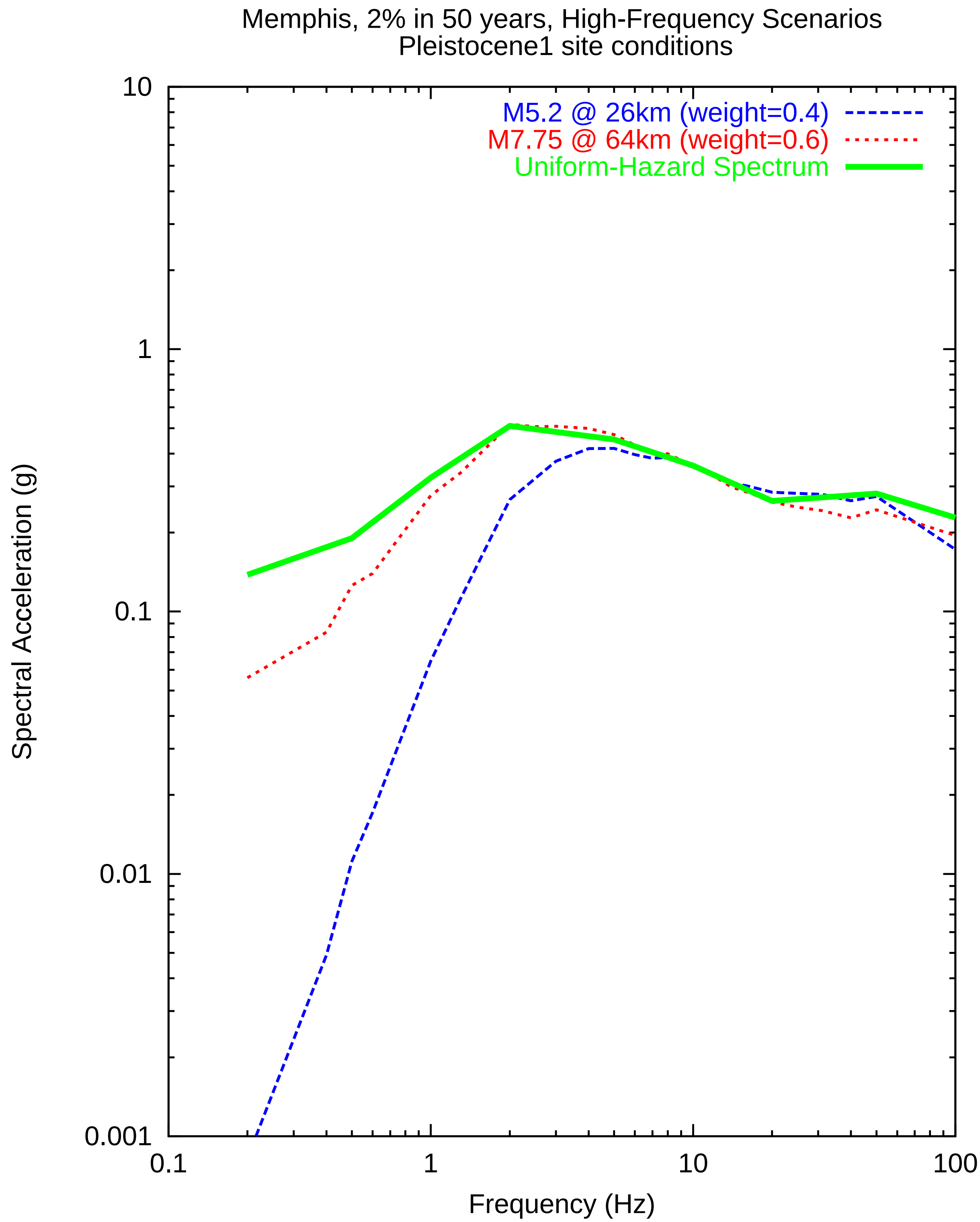

Figure 5-54. Spectra of high-frequency scenarios for Pleistocene1 site conditions in Memphis, for an annual exceedence probability of 2% in 50 years.

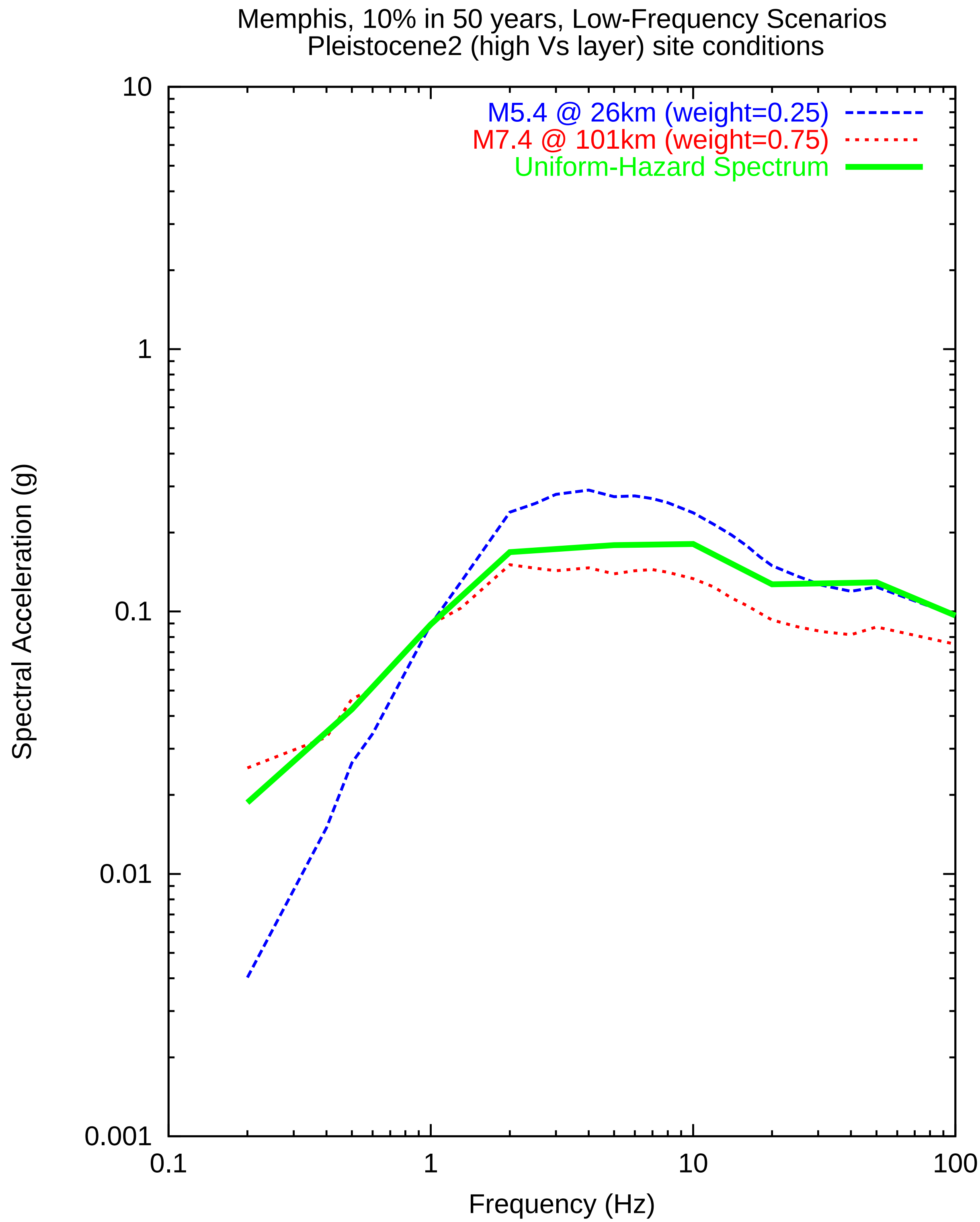

Figure 5-55. Spectra of low-frequency scenarios for Pleistocene2 (high Vs layer) site conditions in Memphis, for an annual exceedence probability of 10% in 50 years.

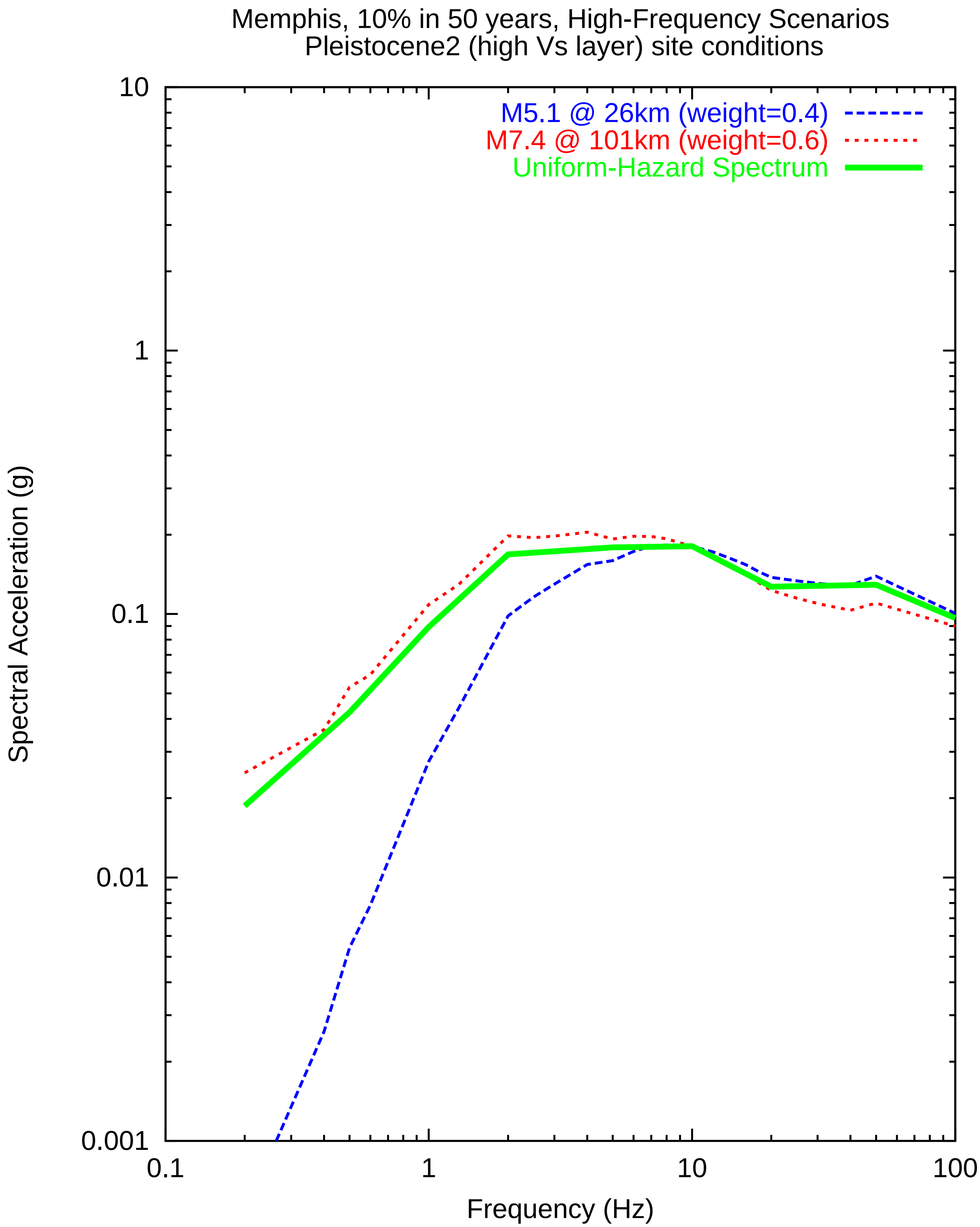

Figure 5-56. Spectra of high-frequency scenarios for Pleistocene2 (high Vs layer) site conditions in Memphis, for an annual exceedence probability of 10% in 50 years.

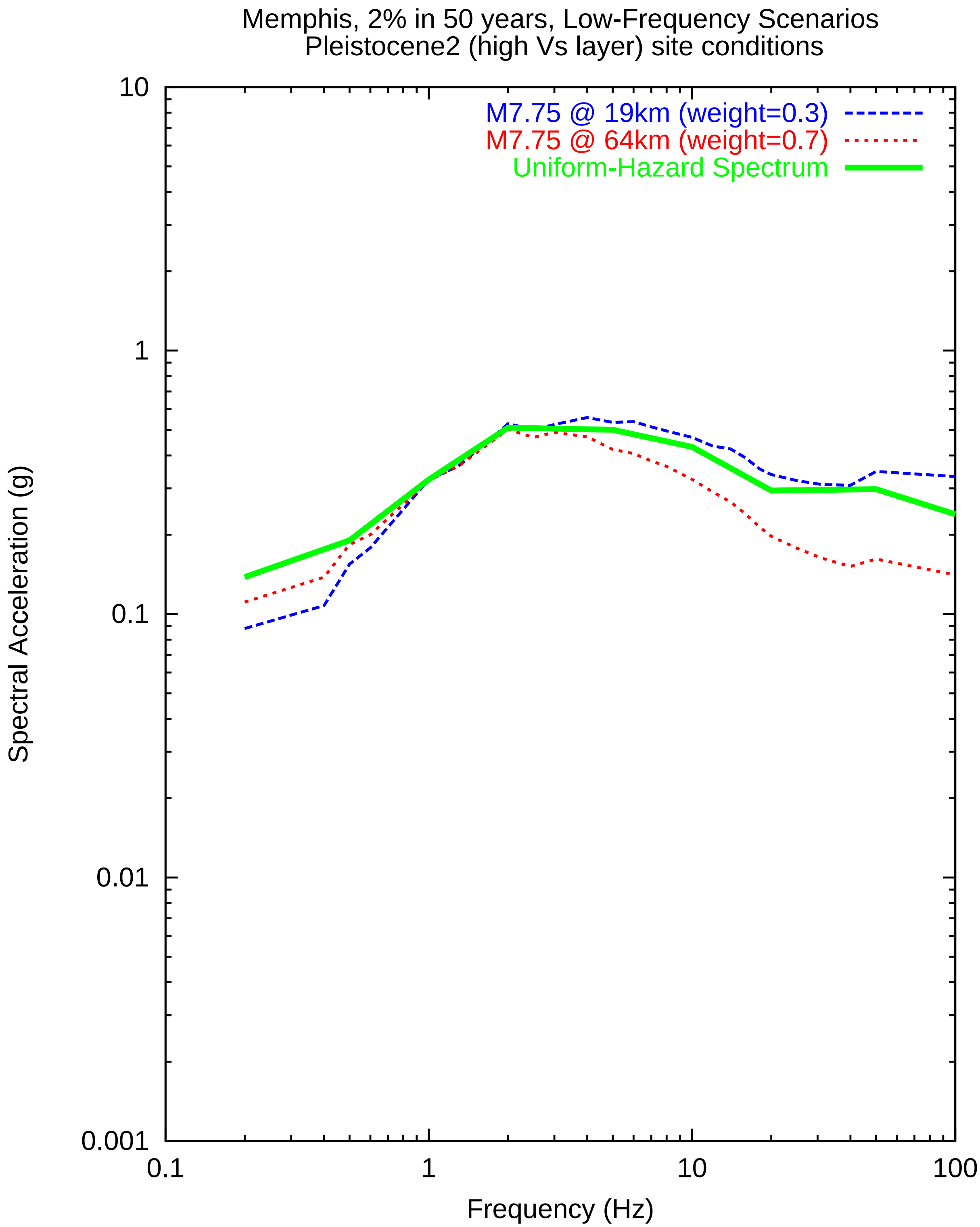

Figure 5-57. Spectra of low-frequency scenarios for Pleistocene2 (high Vs layer) site conditions in Memphis, for an annual exceedence probability of 2% in 50 years.

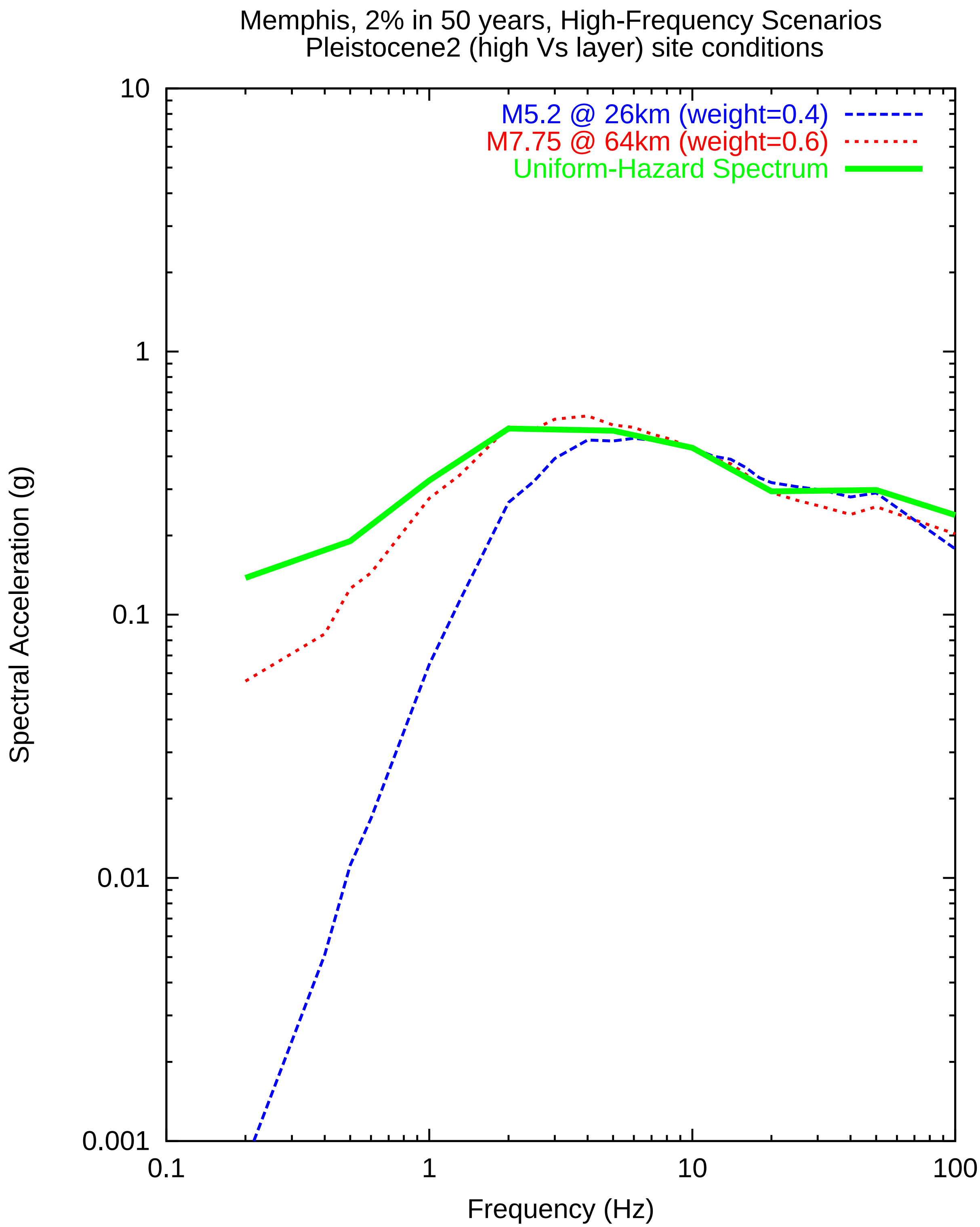

Figure 5-58. Spectra of high-frequency scenarios for Pleistocene2 (high Vs layer) site conditions in Memphis, for an annual exceedence probability of 2% in 50 years.

Section 6

REGIONAL SEISMIC HAZARD MAPS FOR THE CENTRAL UNITED STATES

6.1 INTRODUCTION

This section presents the developments of regional hazard maps for the region between latitudes 34 and 39 degrees North and longitudes 87 to 93 degrees West, using the source characterizations presented in Section 2, the attenuation equations presented in Section 3, the site-response models developed an Section 4, and information about the thickness of the soil column to be presented below. Hazard maps are presented for rock[1] and for the actual site conditions in the region.

6.2 DATA ON SOIL-COLUMN THICKNESS

Soil-column thickness is an important parameter in the calculation of site response, particularly for the study region, where thickness may vary from 20 feet or less in the Ozarks region to more than 3,000 feet in the Mississippi embayment. This study uses two sources of thickness data. For the Mississippi embayment, we use the CERI model. Another model for the embayment has been developed by Dart and Swolfs (1998) using the same data set of well logs and reflection profiles. For the portion north of 37 degrees latitude, we use the depth contours published by Soller and Packard (1998). The variation of thickness in this northern portion of the study region is much more subdued than in the Mississippi embayment. For locations where data was not available from either source (generally upland locations), a depth of 30 feet was assumed. Figure 6-1 shows the resulting thickness model.

6.3 HAZARD MAPS FOR ROCK

Figures 6-2 through 6-9 show the hazard maps for rock, for four ground-motion measures ranging from 0.2-Hz spectral acceleration to PGA, and for exceedence probabilities of 10%

---

[1]The hazard maps for rock are an intermediate result obtained in the process of calculating the hazard maps that include regional information on site response. They are also useful for comparison to other hazard maps which do not consider regional information on site response.

and 2% in 50 years. These maps show that the highest amplitudes are limited to a small region centered on the Reelfoot fault, particularly for the high-frequency motions. Although the 10% in 50 years PGA for New Madrid, MO is 0.4 g, the corresponding value for Memphis is 0.1. The contours for high-frequency motions are elongated to the Northeast, as a result of the Wabash sources, and to the Southwest, as a result of the SE Flank fault.

6.4 HAZARD MAPS FOR SOIL

For the calculation of the hazard maps for soil, we multiply the spectral acceleration at each grid point by the amplification factor (from Section 4) corresponding to that frequency and rock amplitude, soil type and soil-column depth[2]. Figures 6-10 through 6-17 show the hazard maps for soil, for four ground-motion measures, and for exceedence probabilities of 10% and 2% in 50 years. The contours for low-frequency motions are strongly affected by the amplification introduced by thick Mississippi embayment soils (with thickness that increases to the SW). High-frequency motions, particularly the 10-Hz spectral acceleration, are strongly amplified by the shallow soils in southern Illinois and in the Ozarks. This effect is strong enough to shift the highest 10-Hz contours to southern Illinois.

6.5 REFERENCES

Dart, R.L. and H.S. Swolfs, Contour mapping of relic structures in the Precambrian basement of the Reelfoot rift, North American Midcontinent, *Tectonics*, 17, 235-249, 1998.

McGuire, R.K., W. J. Silva, and C. Costantino (2000). "Technical Basis for Revision of Regulatory Guidance on Design Ground Motions." Report to US Nuclear Regulatory Commission, in press.

Soller, D.R., and Packard, P.H., 1998, Digital representation of a map showing the thickness and character of Quaternary sediments in the glaciated United States east of the Rocky

---

[2] In calculating the soil amplitudes by simply multiplying by the median amplification factor, we neglect the uncertainty in site response, as well as other effects. A more refined, recently developed procedure is provided in McGuire et al. (2000). This new procedure accounts for the combined effects of site-response uncertainty and increasing soil nonlinearity.

Mountains: U.S. Geological Survey Digital Data Series DDS #38 [Digital version of USGS map I-1970-A, B, C, D and OFR 93-543.] . Available online at http://pubs.usgs.gov/dds/dds38/ (accessed on 11/15/2000).

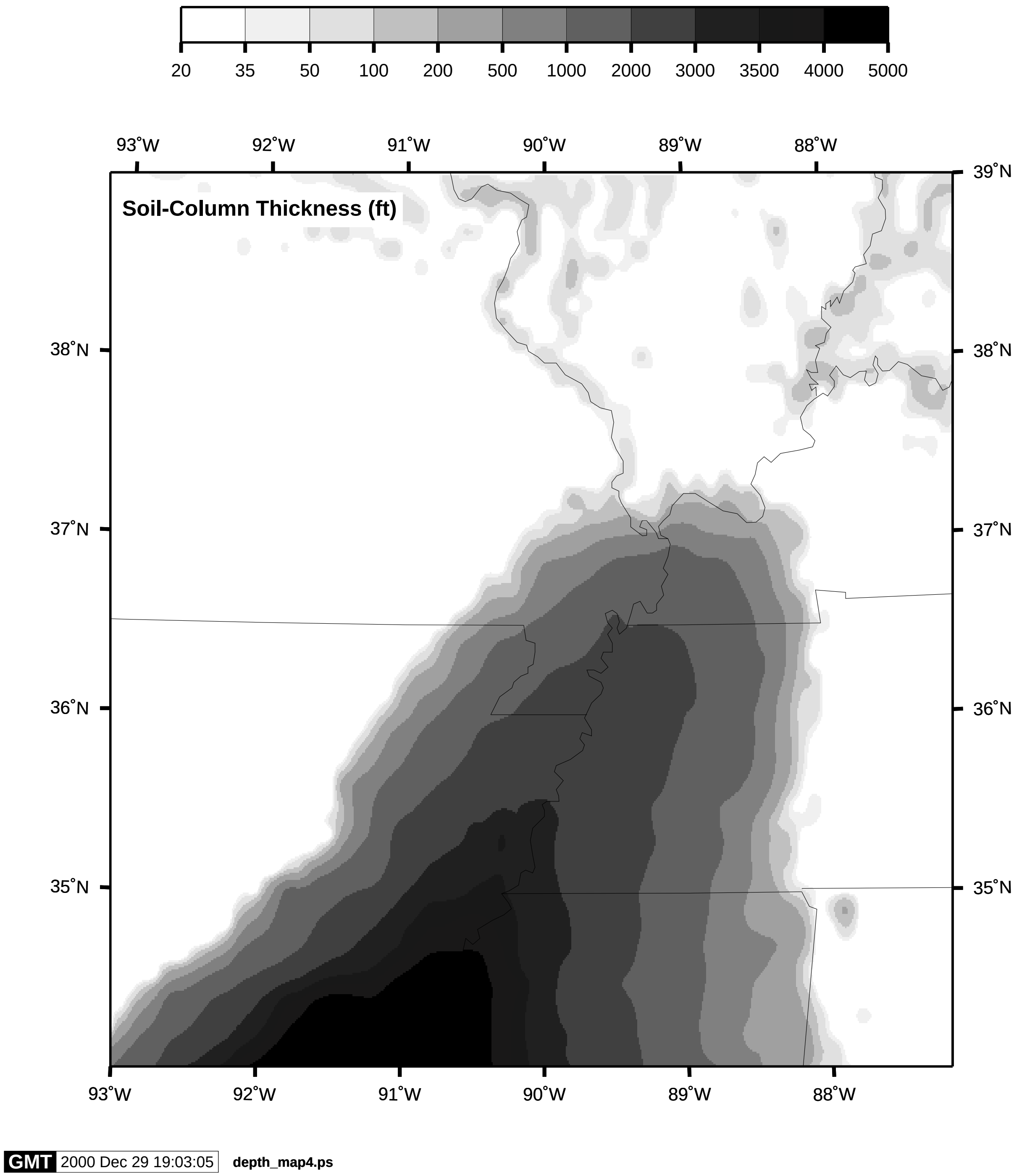

Figure 6-1. Model of soil-column thickness used for the seismic-hazard mapping calculations.

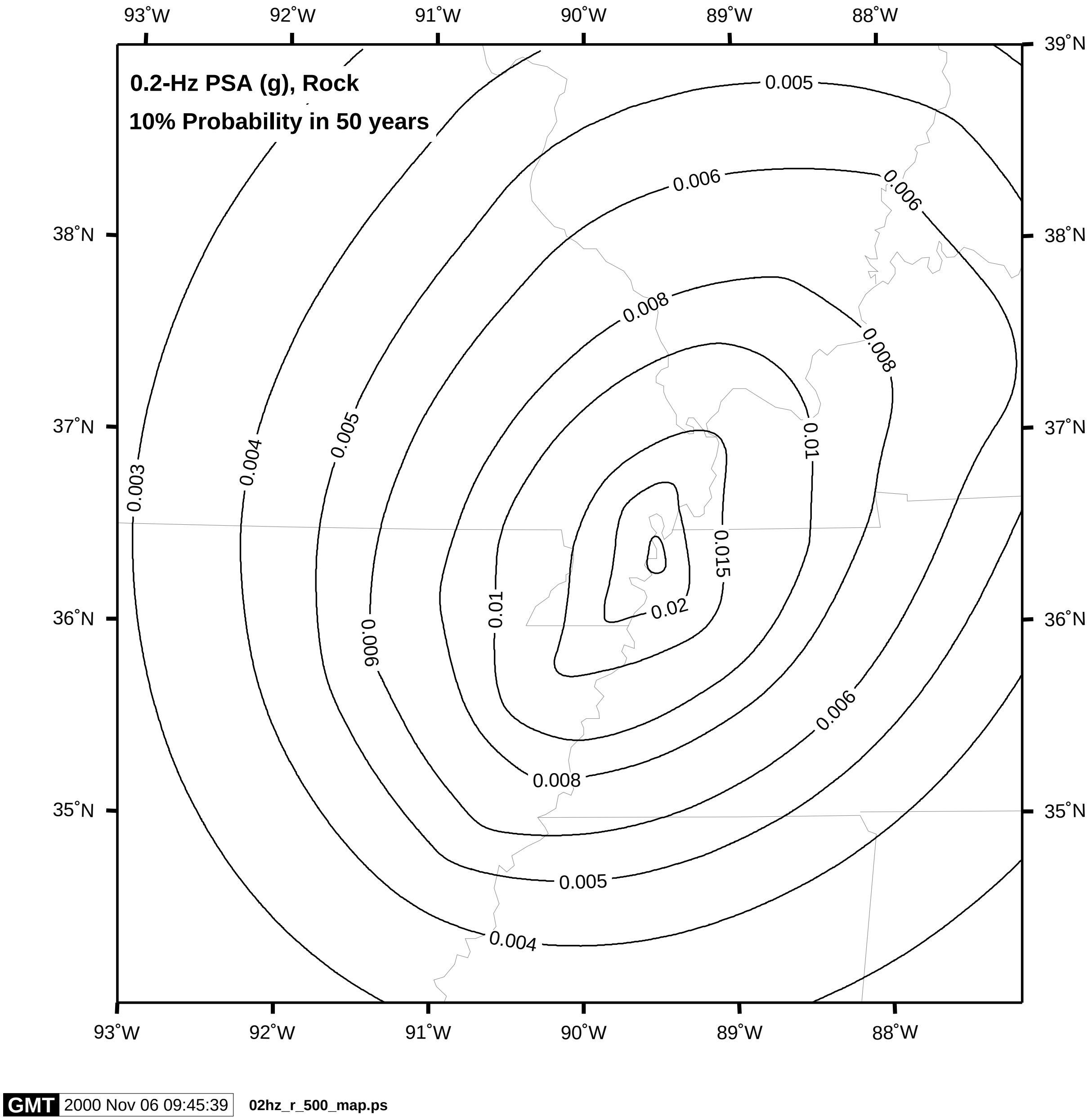

Figure 6-2. Seismic hazard map for 0.2-Hz spectral acceleration. Rock site conditions, 10% exceedence probability in 50 years.

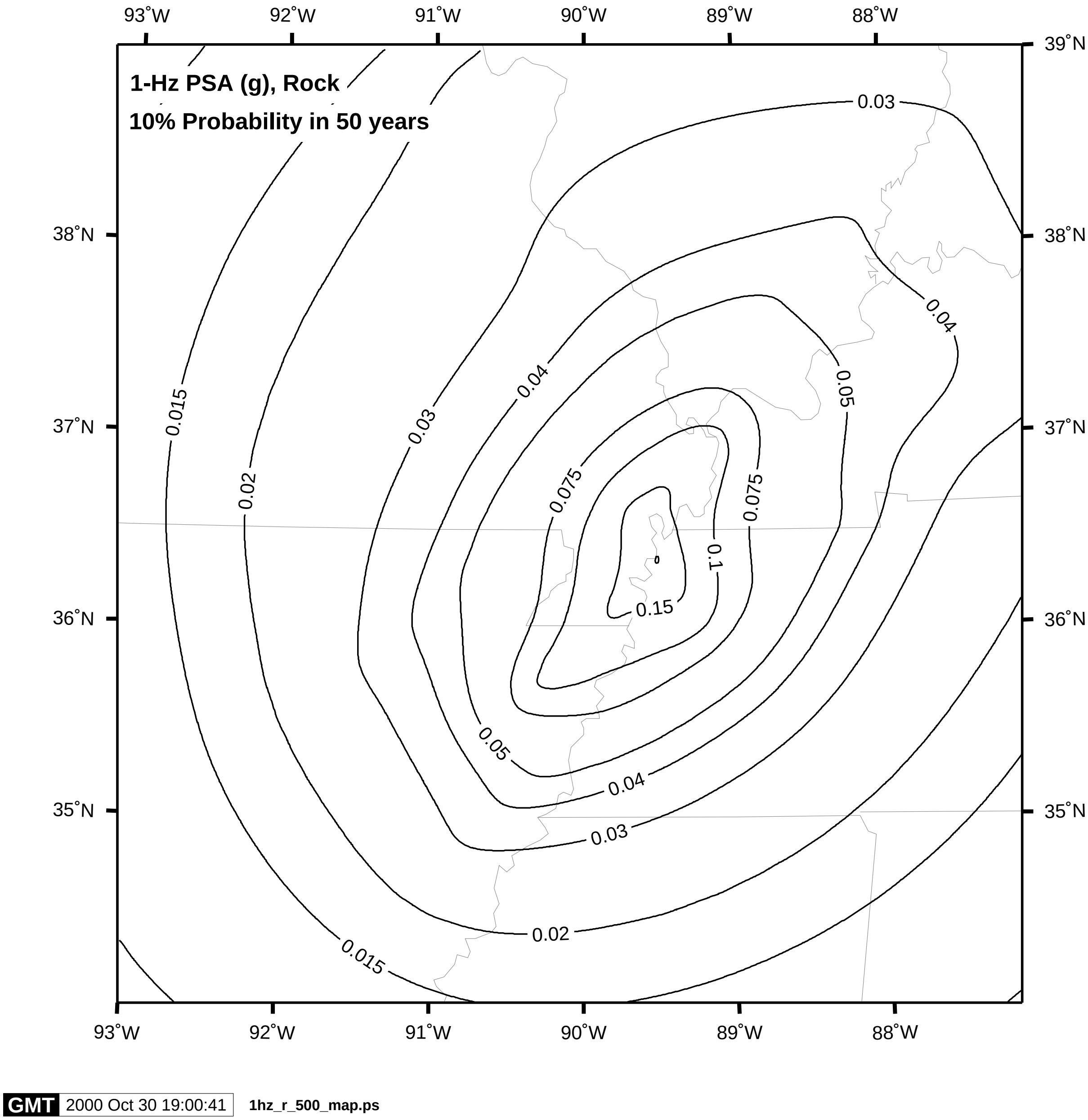

Figure 6-3. Seismic hazard map for 1-Hz spectral acceleration. Rock site conditions, 10% exceedence probability in 50 years.

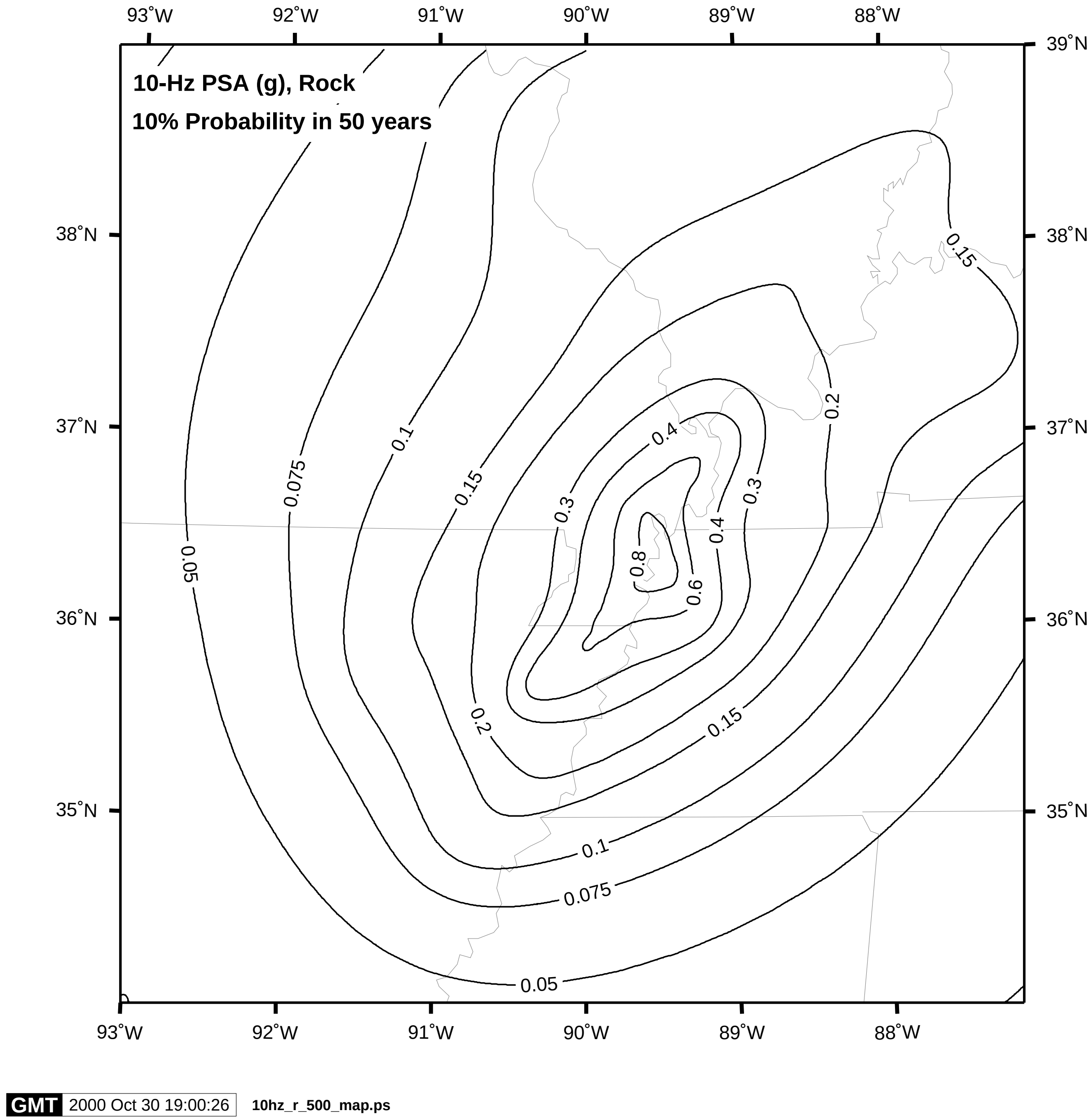

Figure 6-4. Seismic hazard map for 10-Hz spectral acceleration. Rock site conditions, 10% exceedence probability in 50 years.

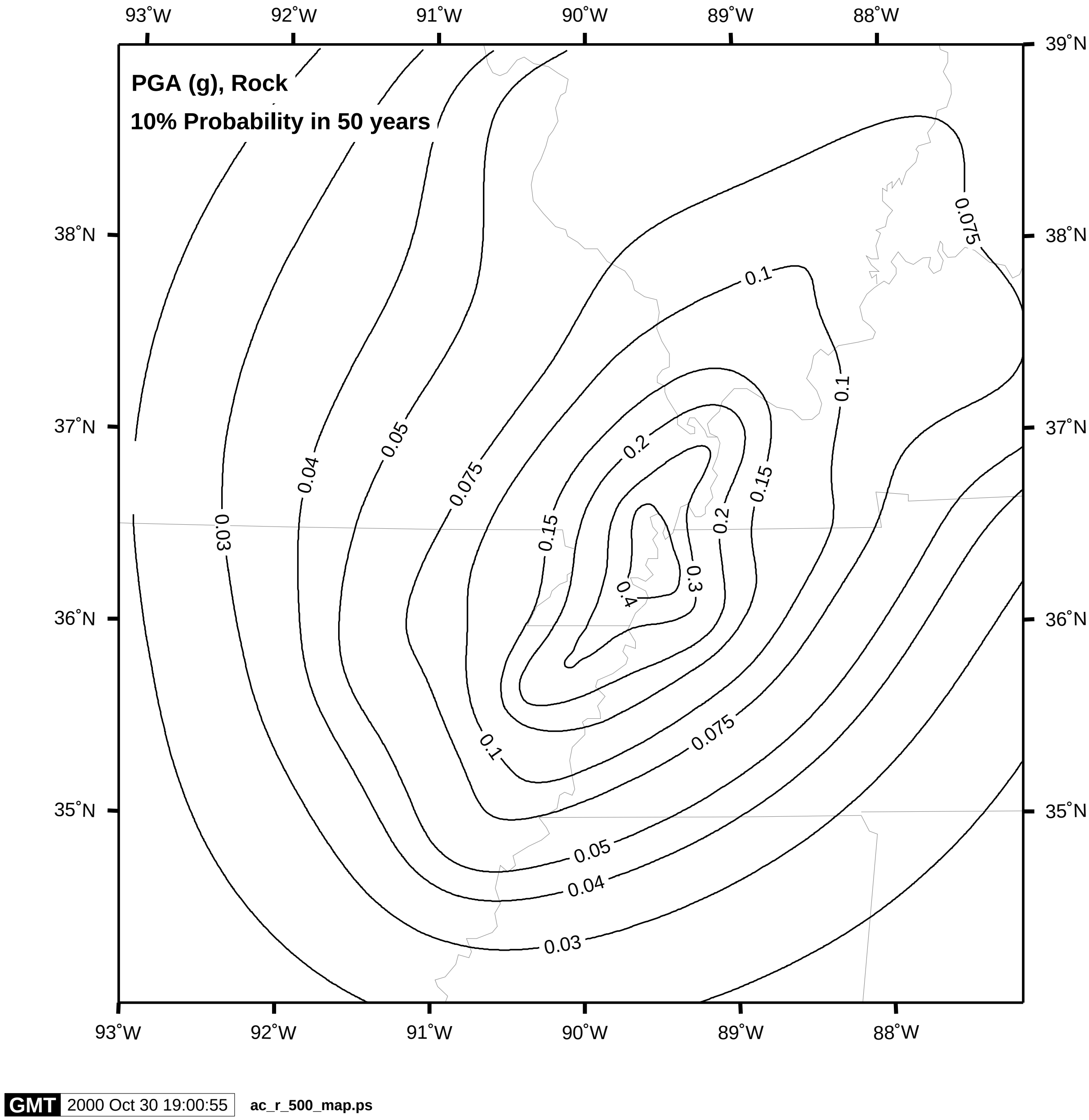

Figure 6-5. Seismic hazard map for PGA. Rock site conditions, 10% exceedence probability in 50 years.

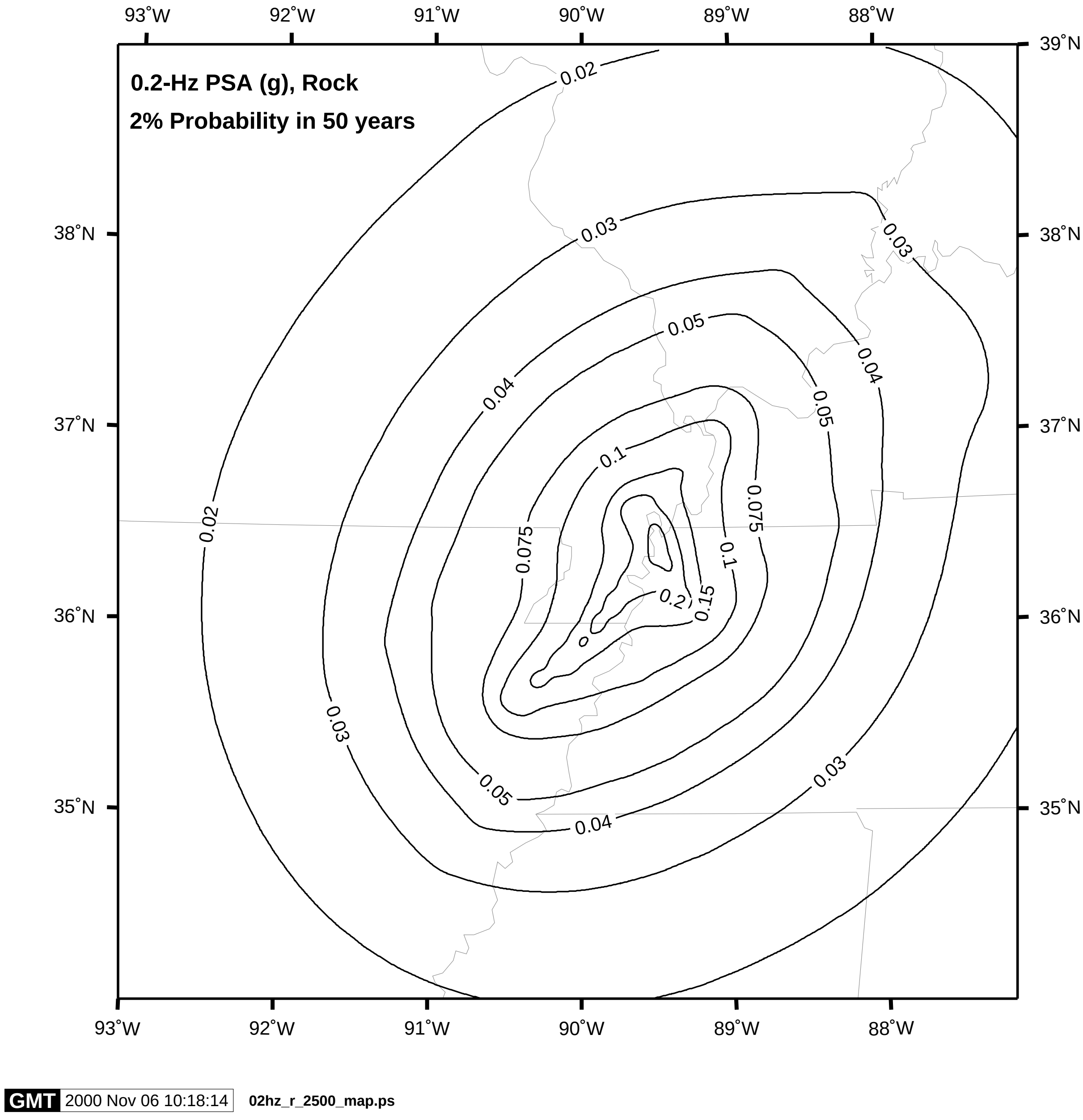

Figure 6-6. Seismic hazard map for 0.2-Hz spectral acceleration. Rock site conditions, 2% exceedence probability in 50 years.

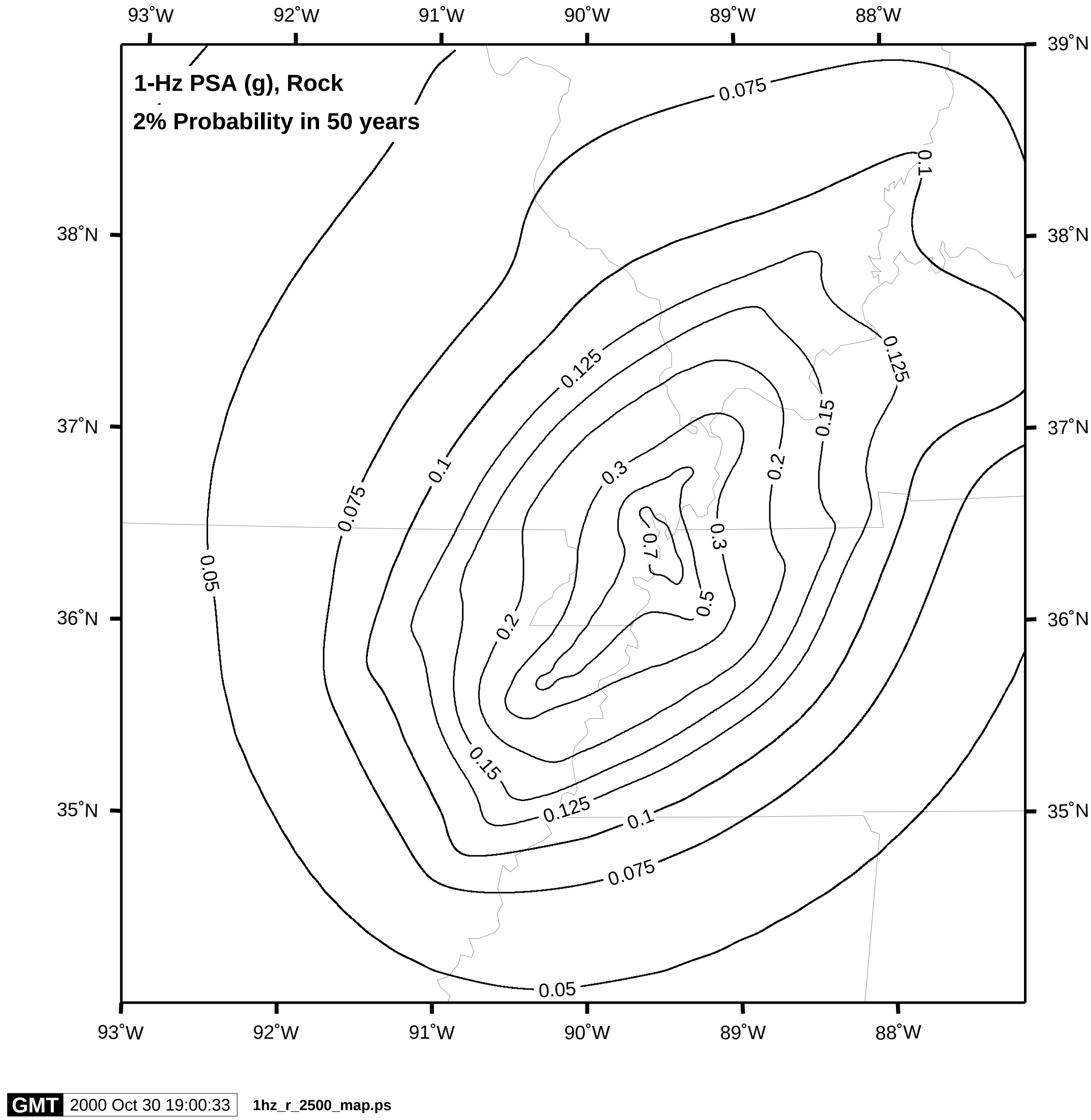

Figure 6-7. Seismic hazard map for 1-Hz spectral acceleration. Rock site conditions, 2% exceedence probability in 50 years.

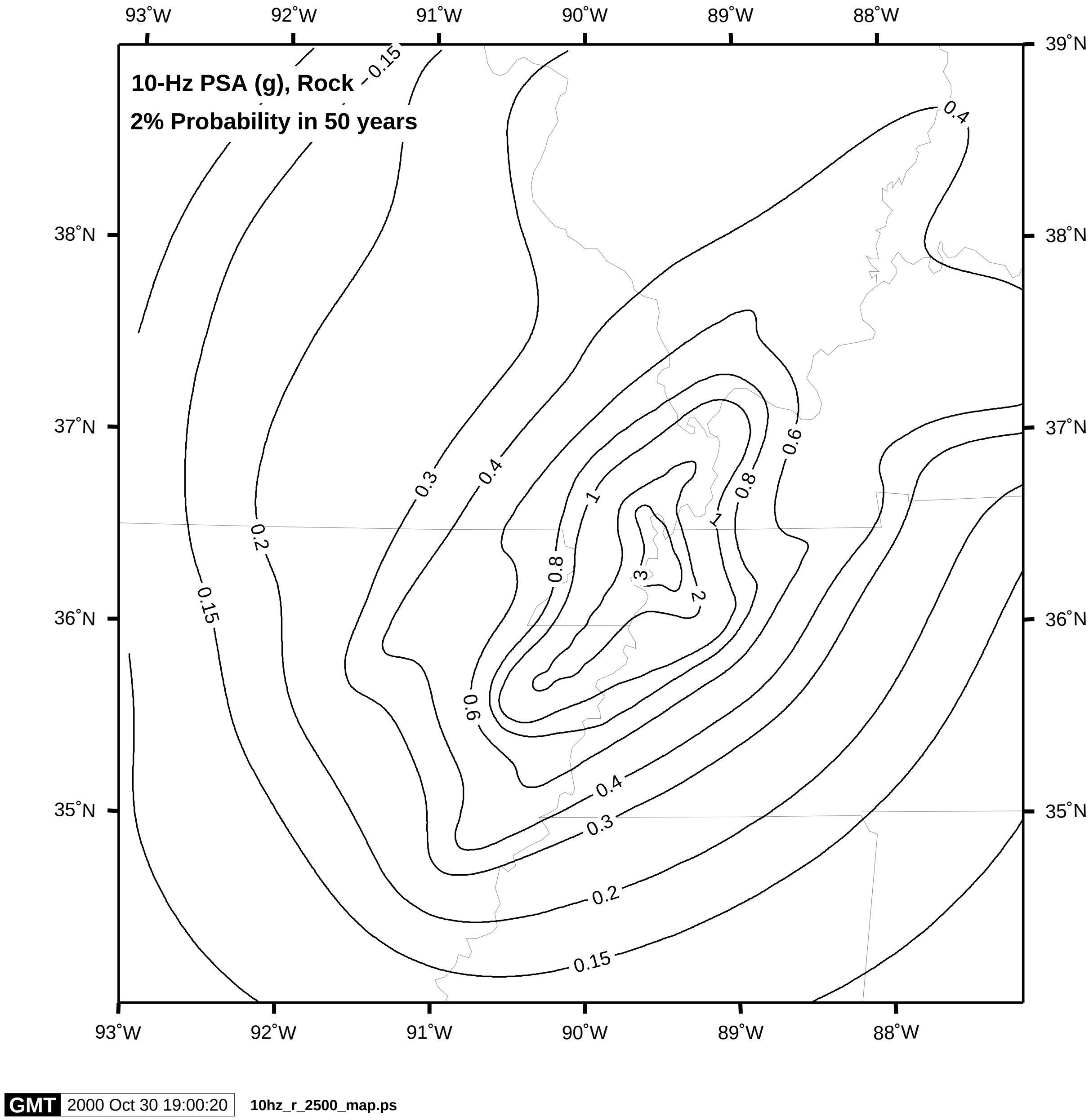

Figure 6-8. Seismic hazard map for 10-Hz spectral acceleration. Rock site conditions, 2% exceedence probability in 50 years.

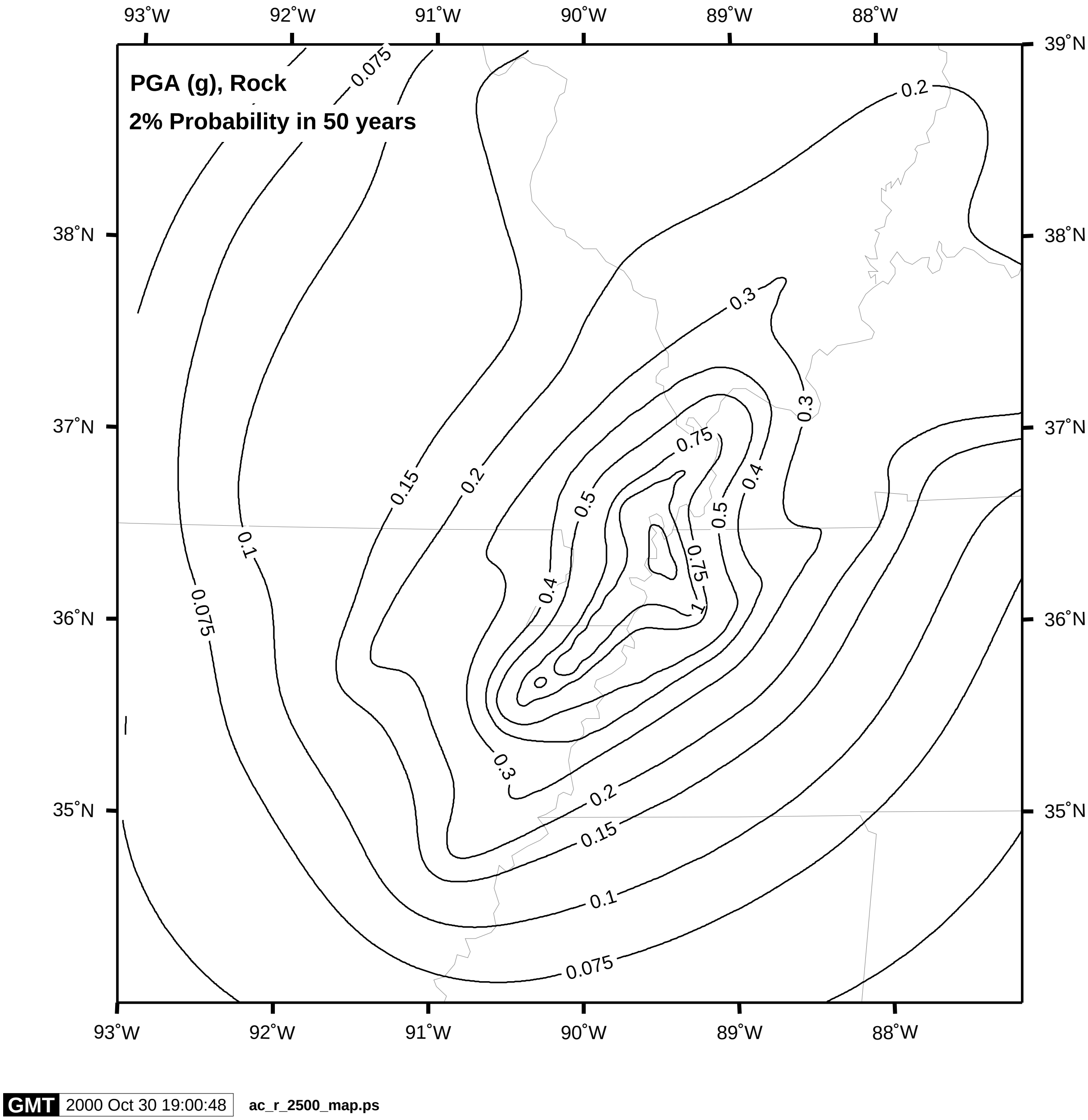

Figure 6-9. Seismic hazard map for PGA. Rock site conditions, 2% exceedence probability in 50 years.

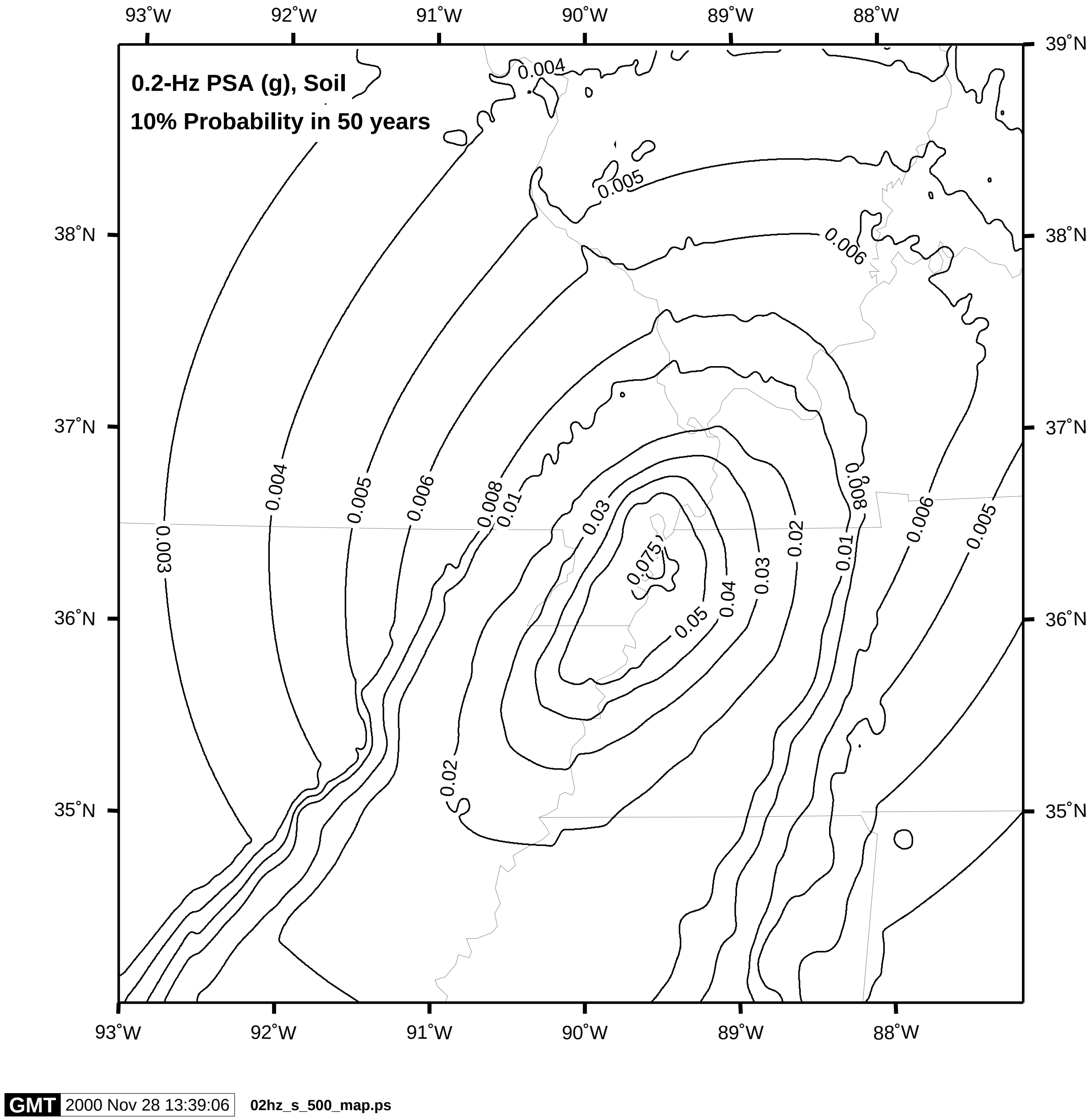

Figure 6-10. Seismic hazard map for 0.2-Hz spectral acceleration. Soil site conditions, 10% exceedence probability in 50 years.

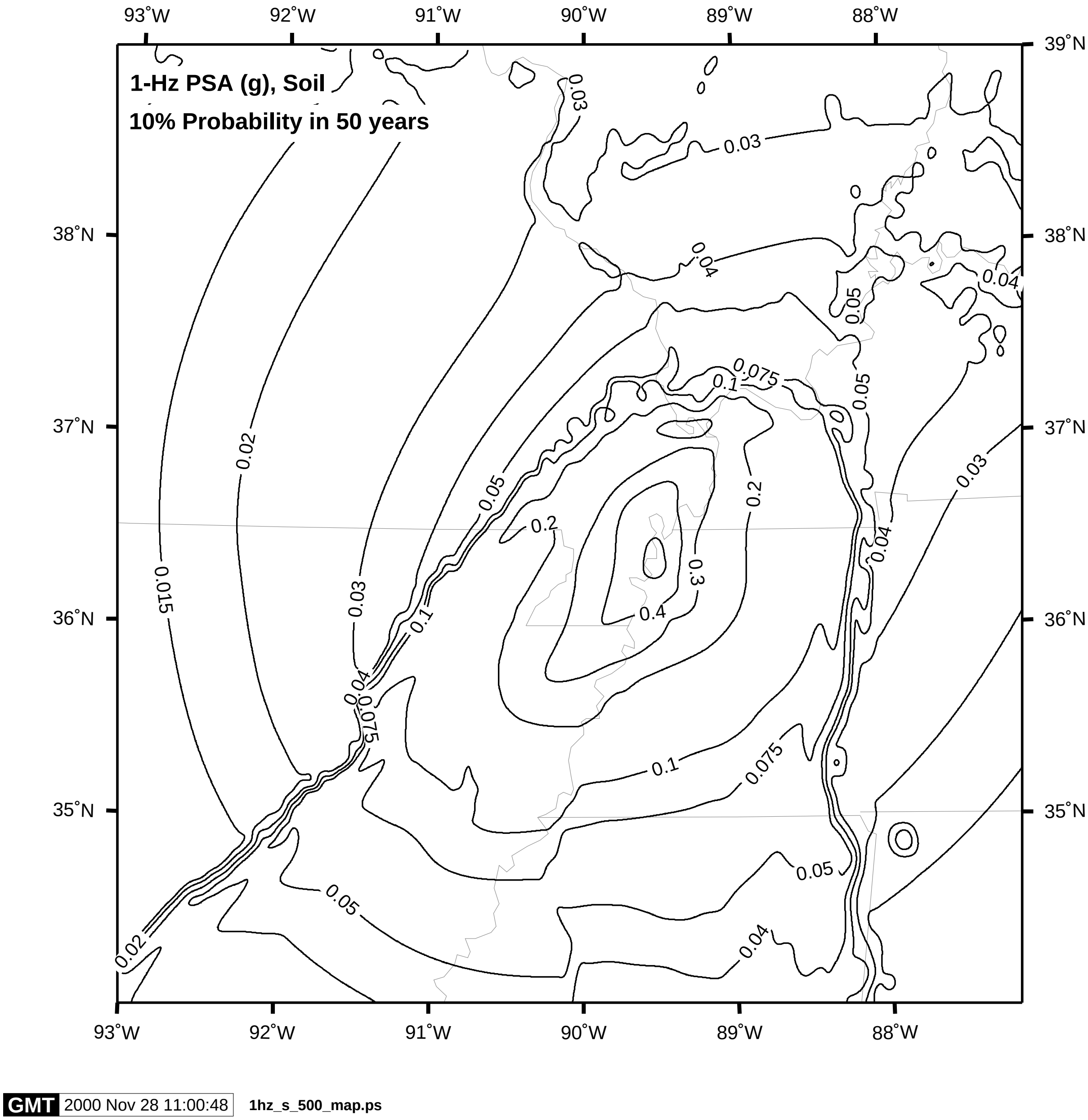

Figure 6-11. Seismic hazard map for 1-Hz spectral acceleration. Soil site conditions, 10% exceedence probability in 50 years.

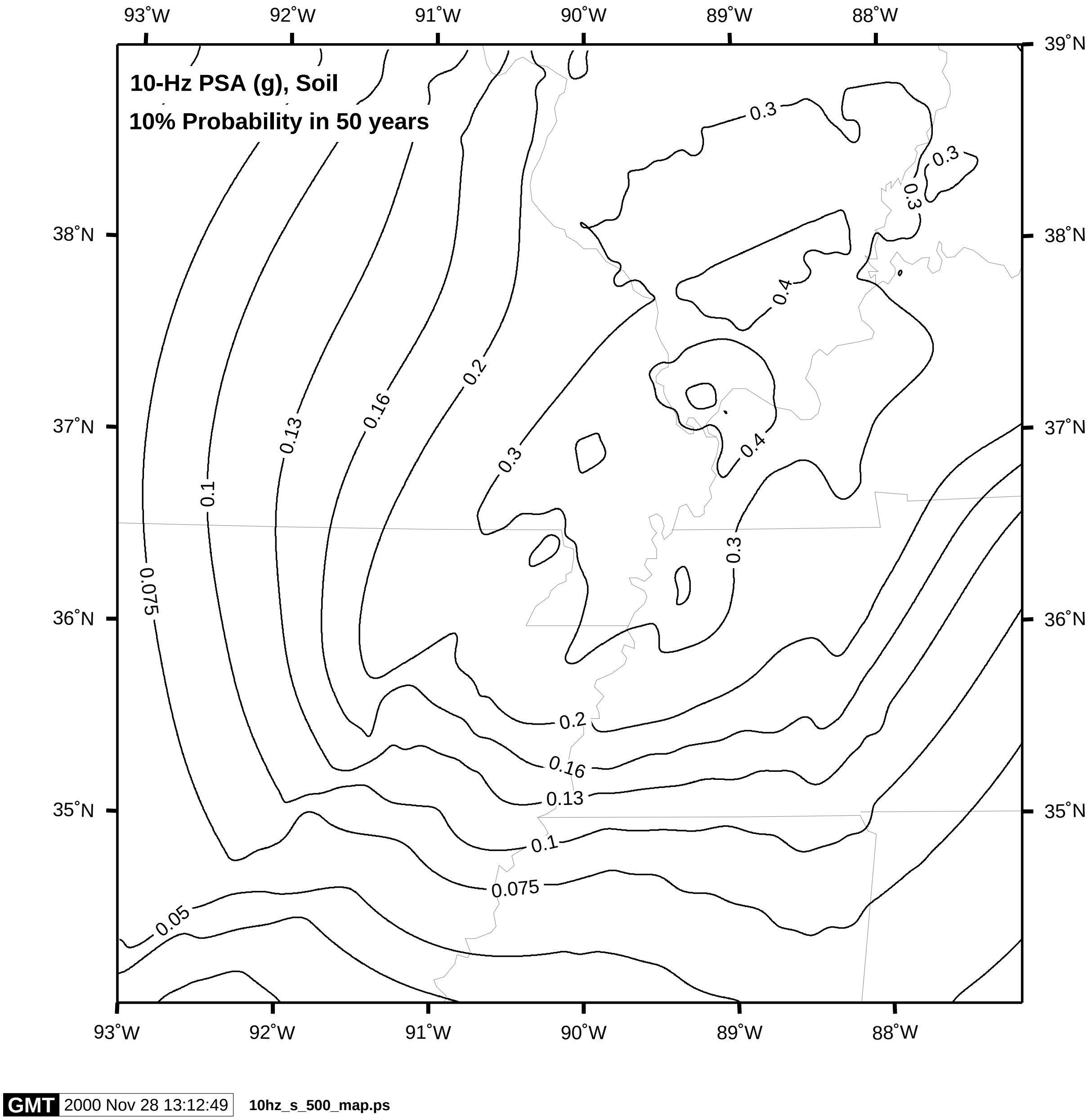

Figure 6-12. Seismic hazard map for 10-Hz spectral acceleration. Soil site conditions, 10% exceedence probability in 50 years.

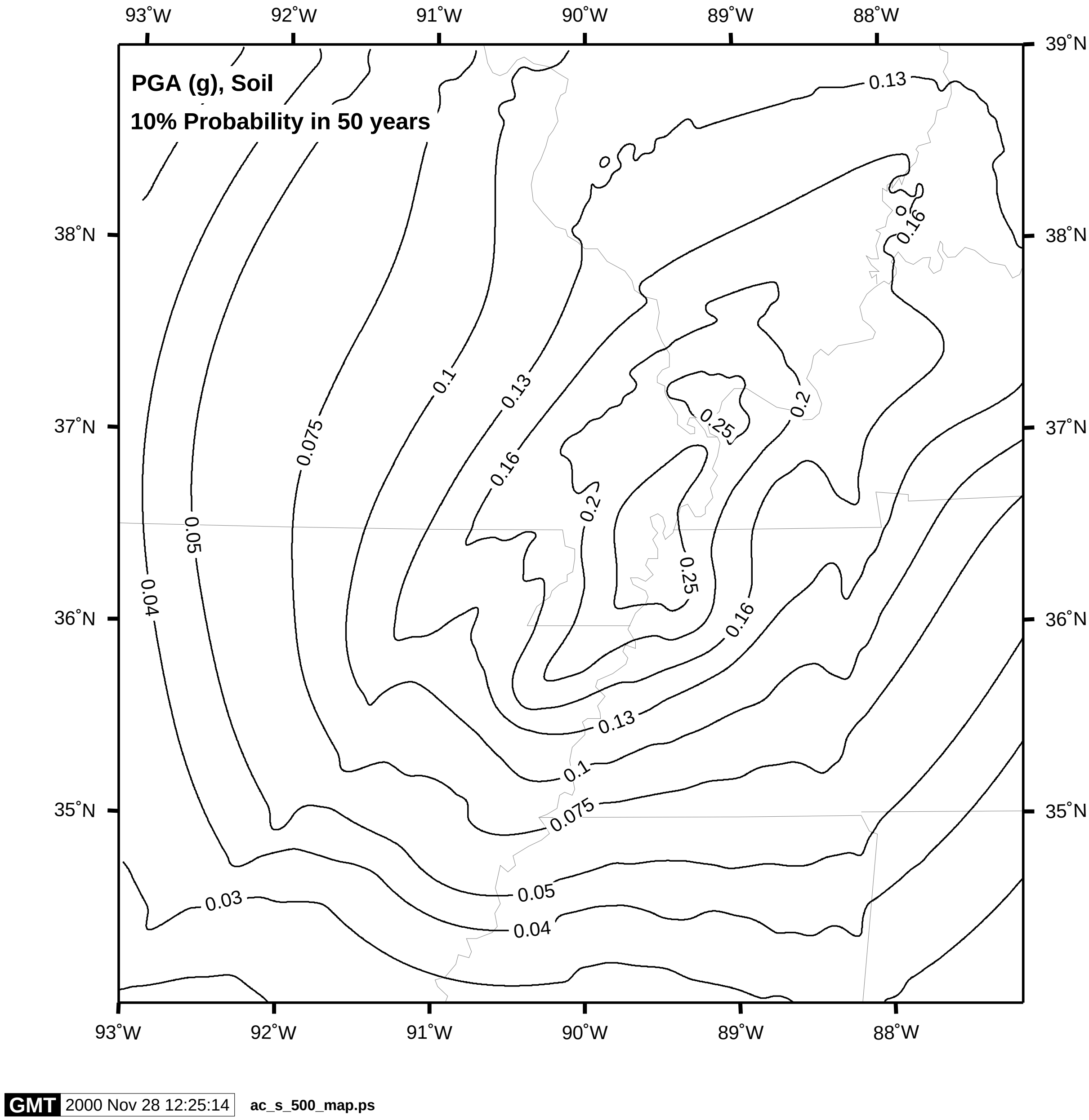

Figure 6-13. Seismic hazard map for PGA. Soil site conditions, 10% exceedence probability in 50 years.

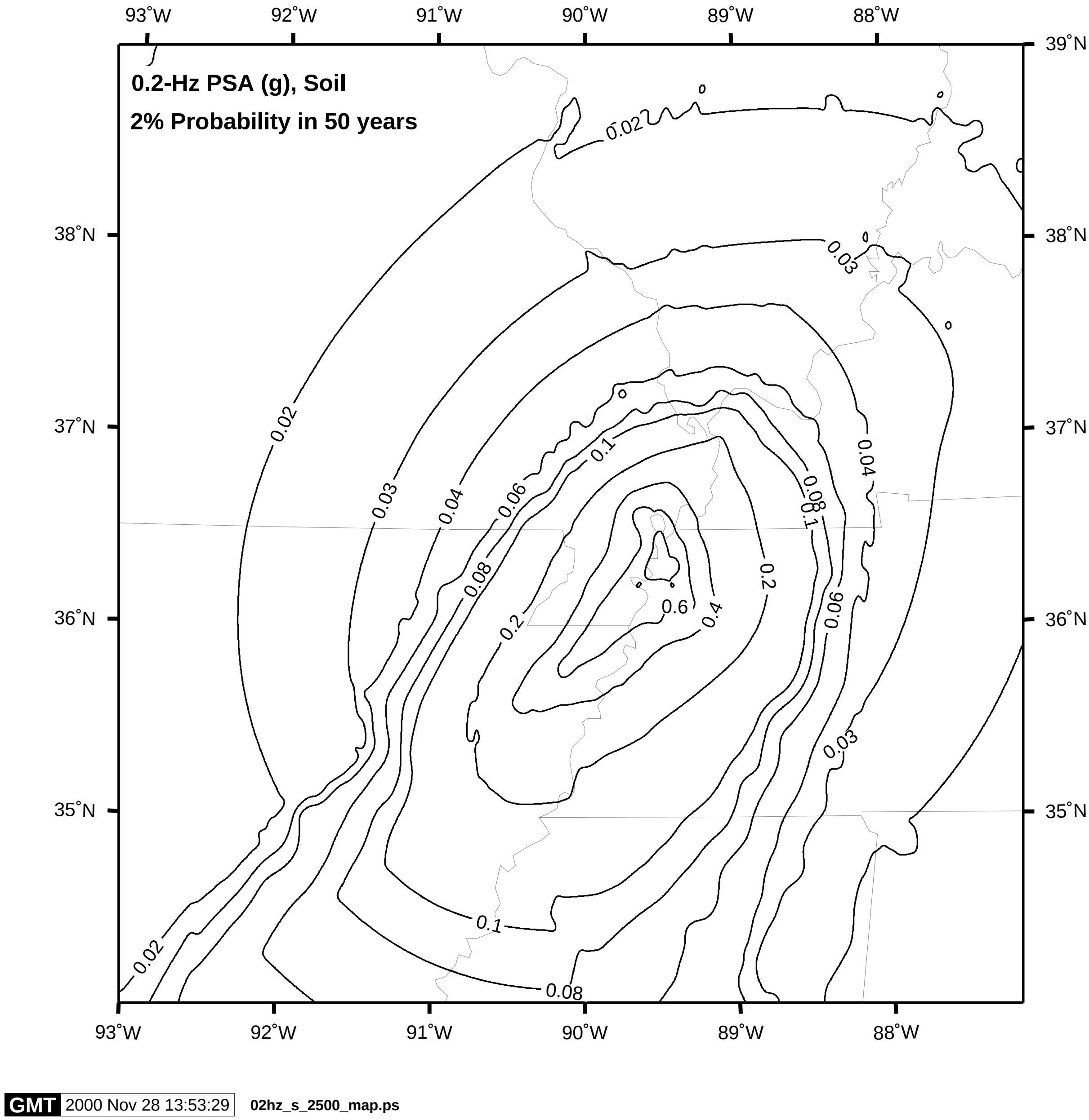

Figure 6-14. Seismic hazard map for 0.2-Hz spectral acceleration. Soil site conditions, 2% exceedence probability in 50 years.

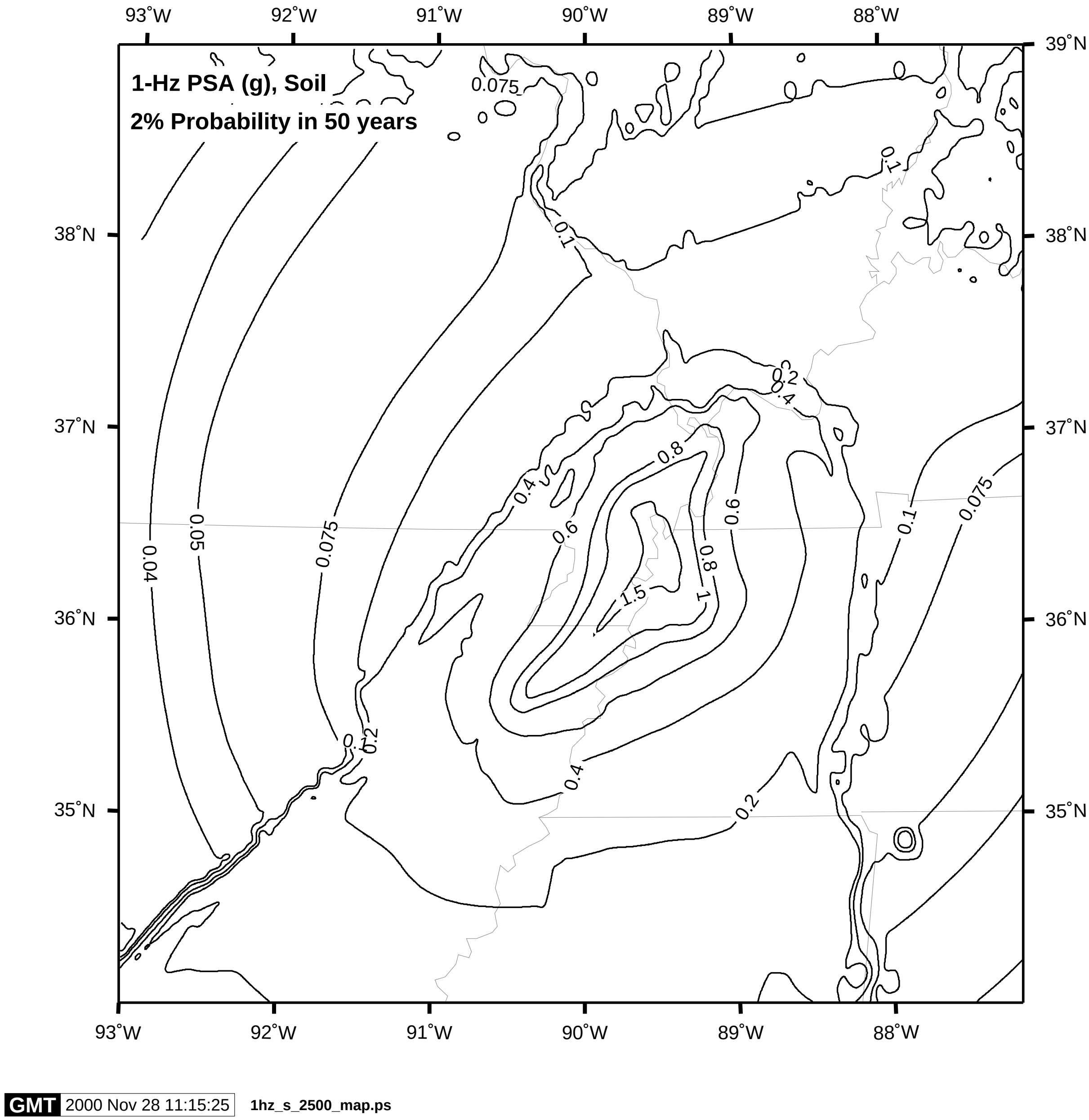

Figure 6-15. Seismic hazard map for 1-Hz spectral acceleration. Soil site conditions, 2% exceedence probability in 50 years.

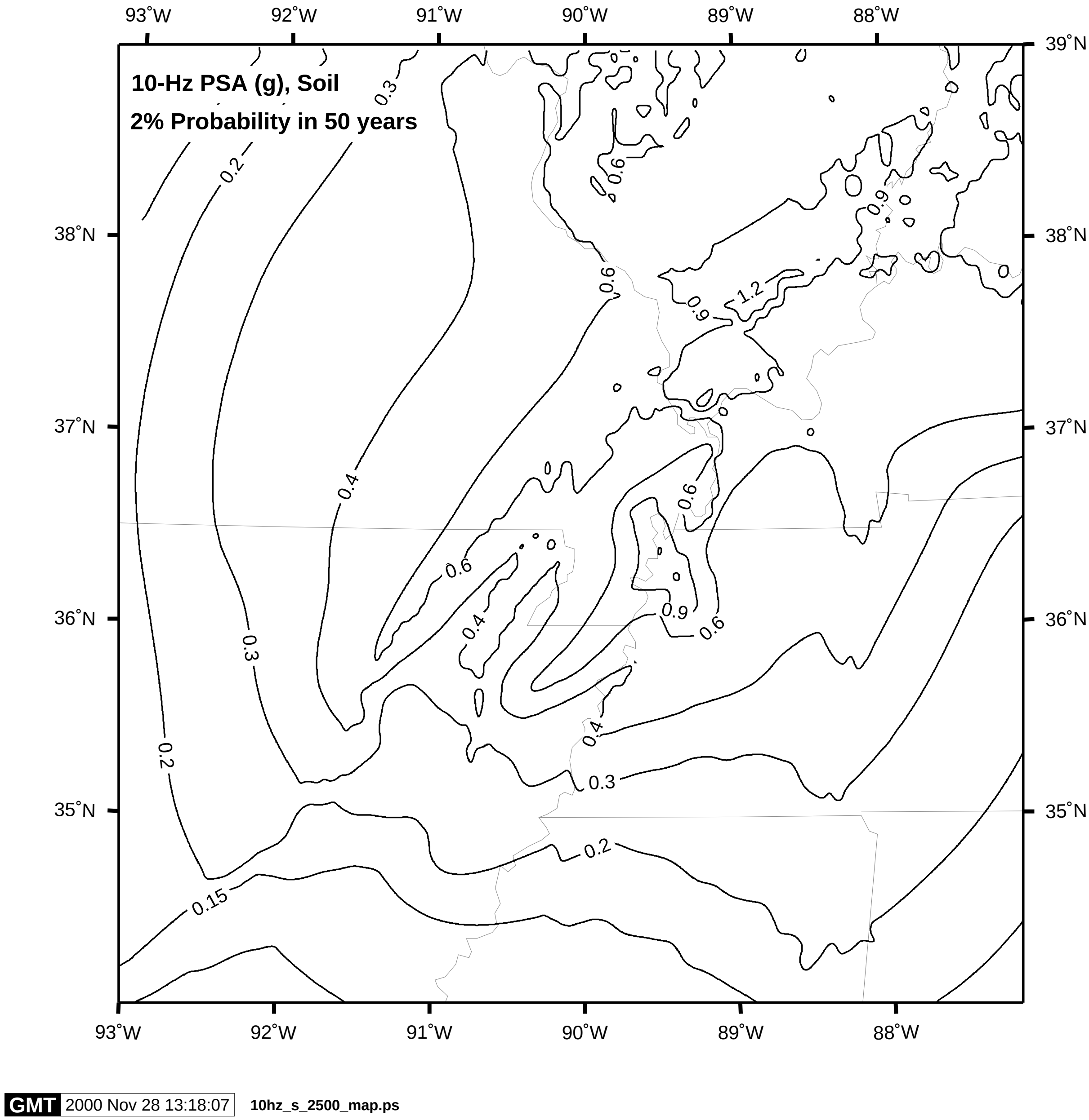

Figure 6-16. Seismic hazard map for 10-Hz spectral acceleration. Soil site conditions, 2% exceedence probability in 50 years.

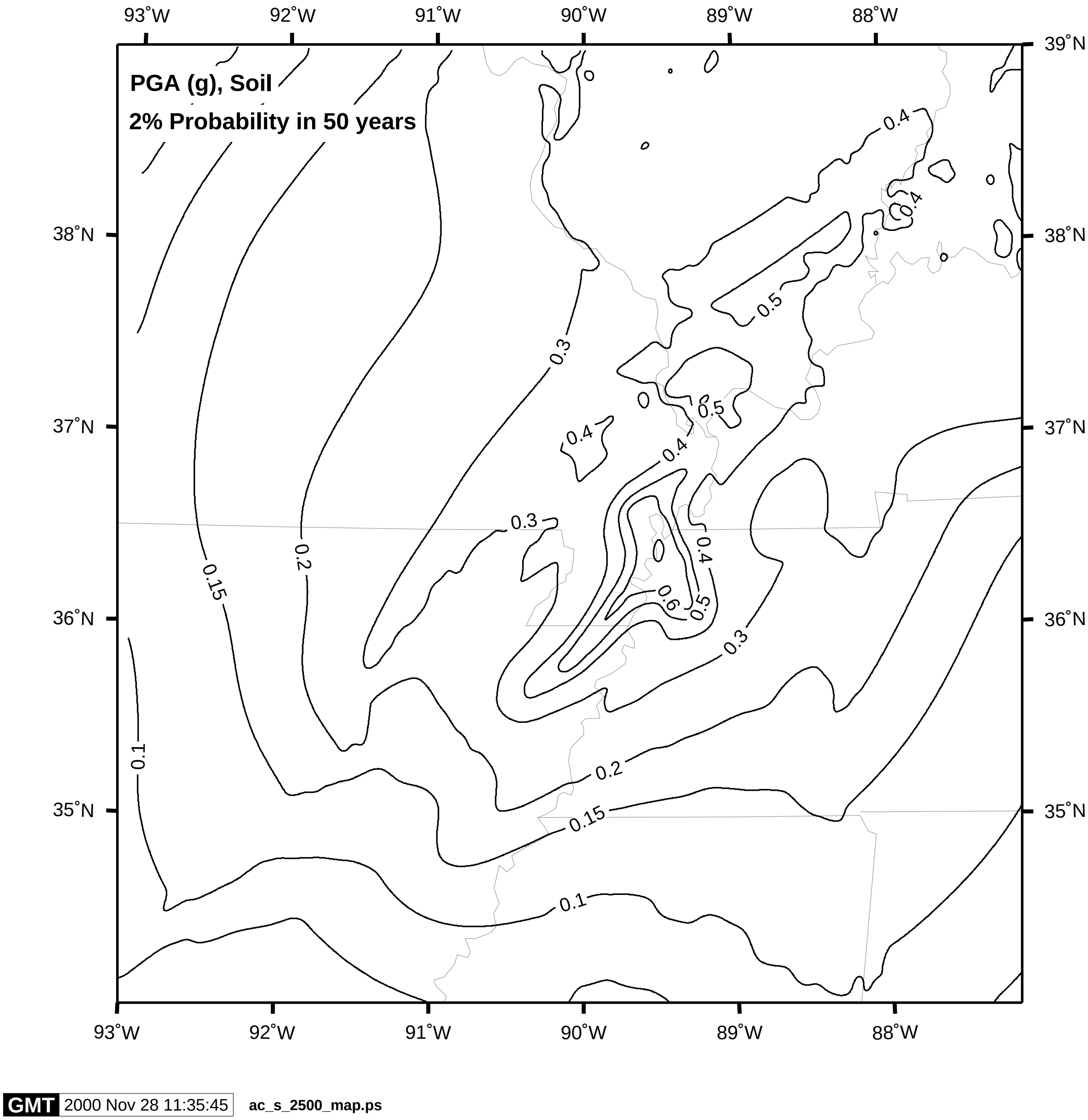

Figure 6-17. Seismic hazard map for PGA. Soil site conditions, 2% exceedence probability in 50 years.

Section 7
SUMMARY AND CONCLUSIONS

This study has utilized models that represent the current state of knowledge--and associated uncertainties--on the rates and severity of earthquakes in the New Madrid and Wabash Valley seismic zones, and on ground motions and site response characteristics in the central and eastern United States, to construct probabilistic scenarios for Saint Louis and Memphis and seismic hazard maps for the entire region.

In Saint Louis, most of the seismic hazard is contributed by the Wabash and New Madrid seismic zones. The effect of the thin soil column underneath Saint Louis (less than100 feet) on the ground motions is to amplify high-frequency motions. In Memphis, most of the seismic hazard is contributed by the New Madrid seismic zone and by the nearby Southeast Flank faut (also known as the Crittenden County fault). The effect of the thick Mississippi embayment soils underneath Memphis (approximately 3,000 feet) is to amplify low-frequency motions and attenuate high-frequency motions. The net effect of different seismic environments and site conditions between the two cities is a very large difference in response-spectral shape, despite similar values of peak ground acceleration. These differences are reflected in the probability-based scenarios and associated time histories developed here.

Another useful by-product of the hazard calculations for Saint Louis and Memphis is an understanding of which parameter uncertainties are the most important contributors to uncertainty in seismic hazard. For Saint Louis, the most important contributors are the ground-motion models, the characterization of seismicity in the Wabash Valley and elsewhere in Southern Illinois and nearby portions of Missouri, the rate and maximum magnitude of characteristic events in the NMSZ faults. For high-frequency motions in Saint Louis, the most important contributors are the ground-motion models, and the geographic extent and seismicity parameters of the Wabash Large source zone. For Memphis, the most important contributors are the maximum magnitude on the NMSZ, the ground-motion and site-response models, and the rate of characteristic events in the NMSZ.

The geographical variation of soil-column thickness and mechanical properties throughout the study region also have a substantial effect on the seismic-hazard maps. Low-frequency motions are amplified by the thick Mississippi embayment soils and are virtually unaffected by the thin soils in the Ozarks and in the northern portion of the study region. High-frequency motions, on the other hand, are attenuated by the thick embayment soils and strongly amplified by the thin soils.

Appendix A

AMPLIFICATION FACTORS FOR LOWLANDS PROFILE

Amplification factors, median and $\pm$ 1σ 5% damped response spectra, for the Lowlands generic profile depth categories 1, 2, 3, 4, 5, 6, 7. Peninsular Range and EPRI nonlinear dynamic material properties.

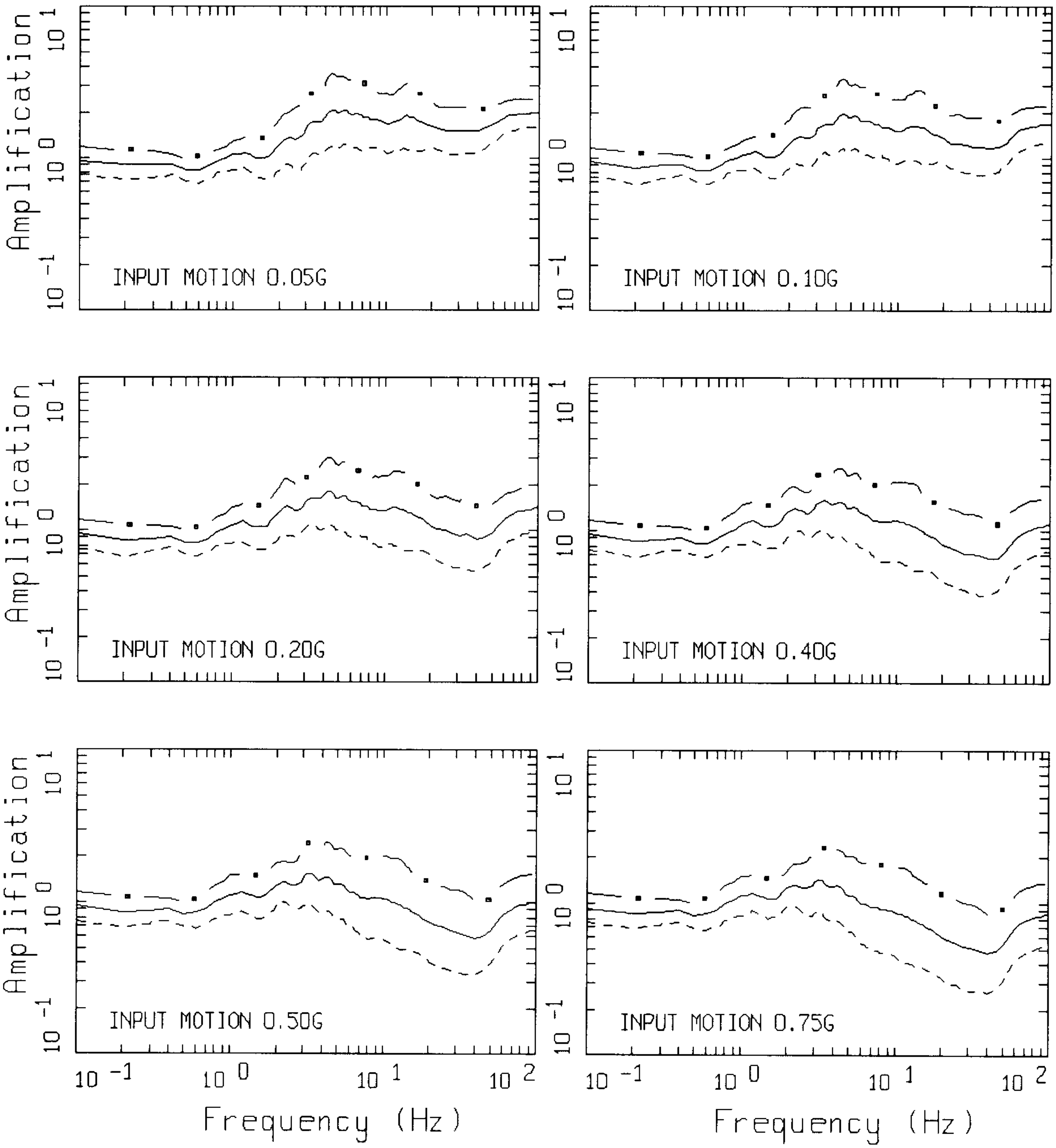

LOWLANDS, CATEGORY 1, 10-50 FT

PENINSULAR RANGE CURVES

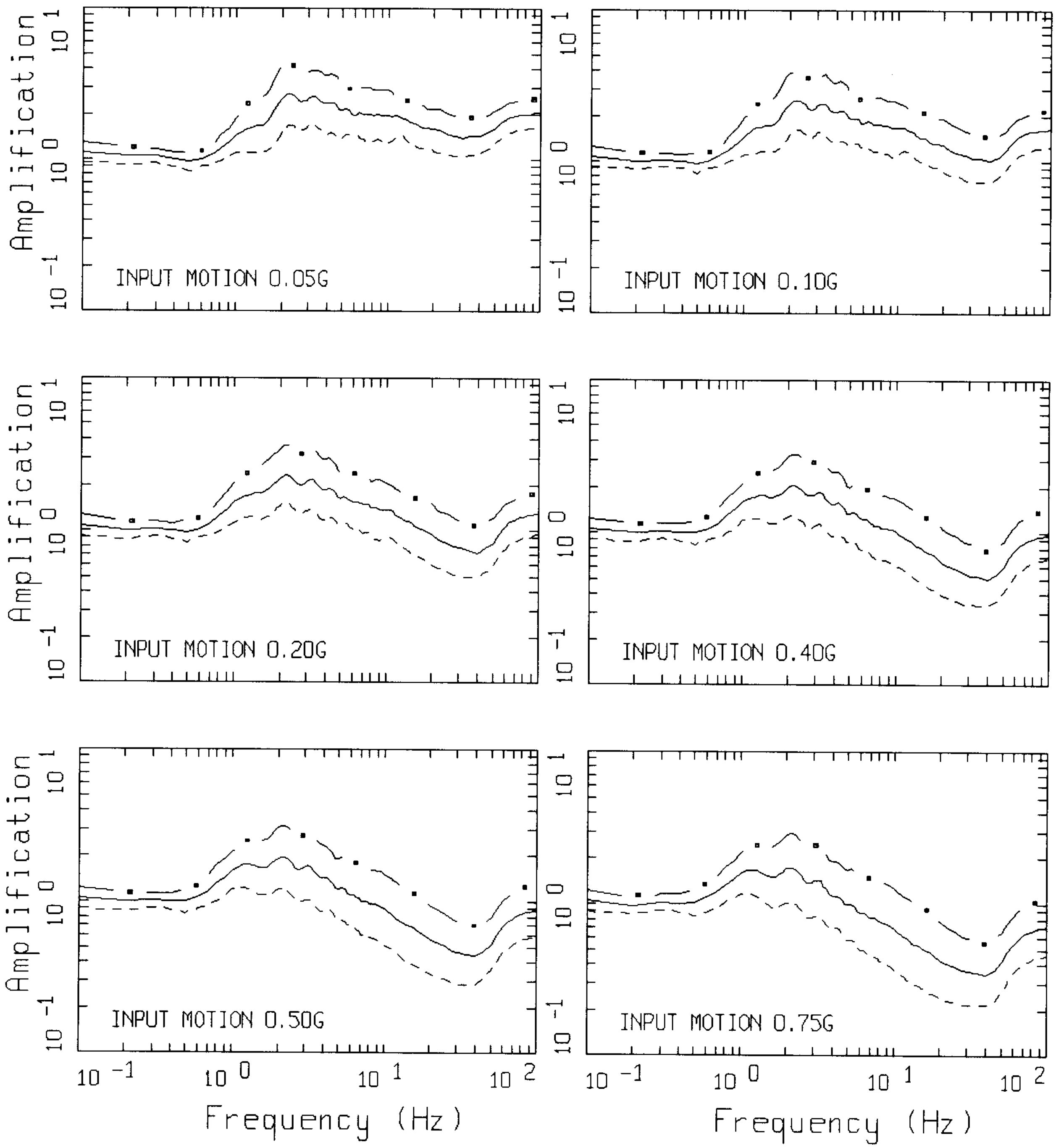

LOWLANDS, CATEGORY 2, 50-100 FT
PENINSULAR RANGE CURVES

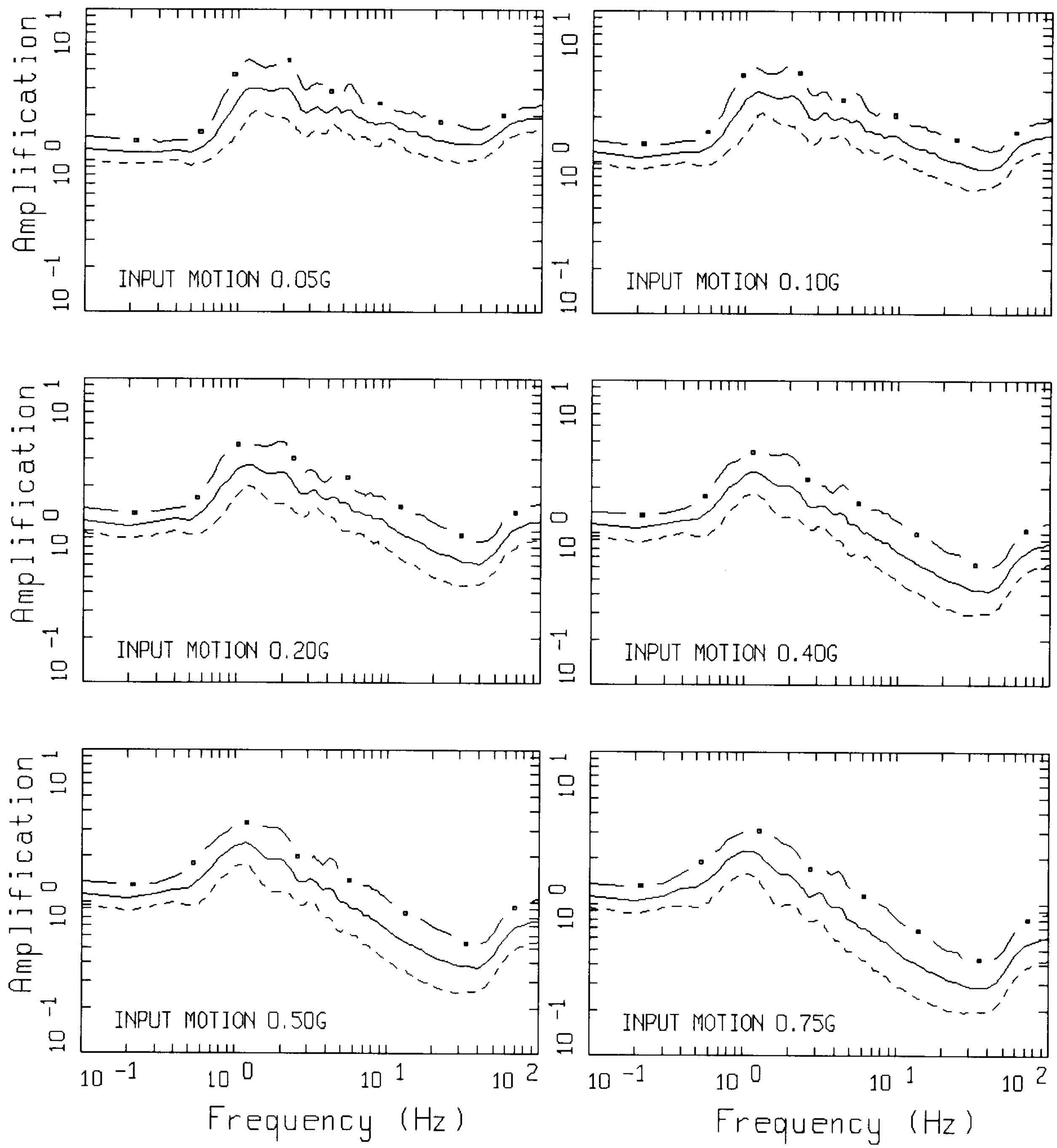

LOWLANDS, CATEGORY 3, 100-200 FT
PENINSULAR RANGE CURVES

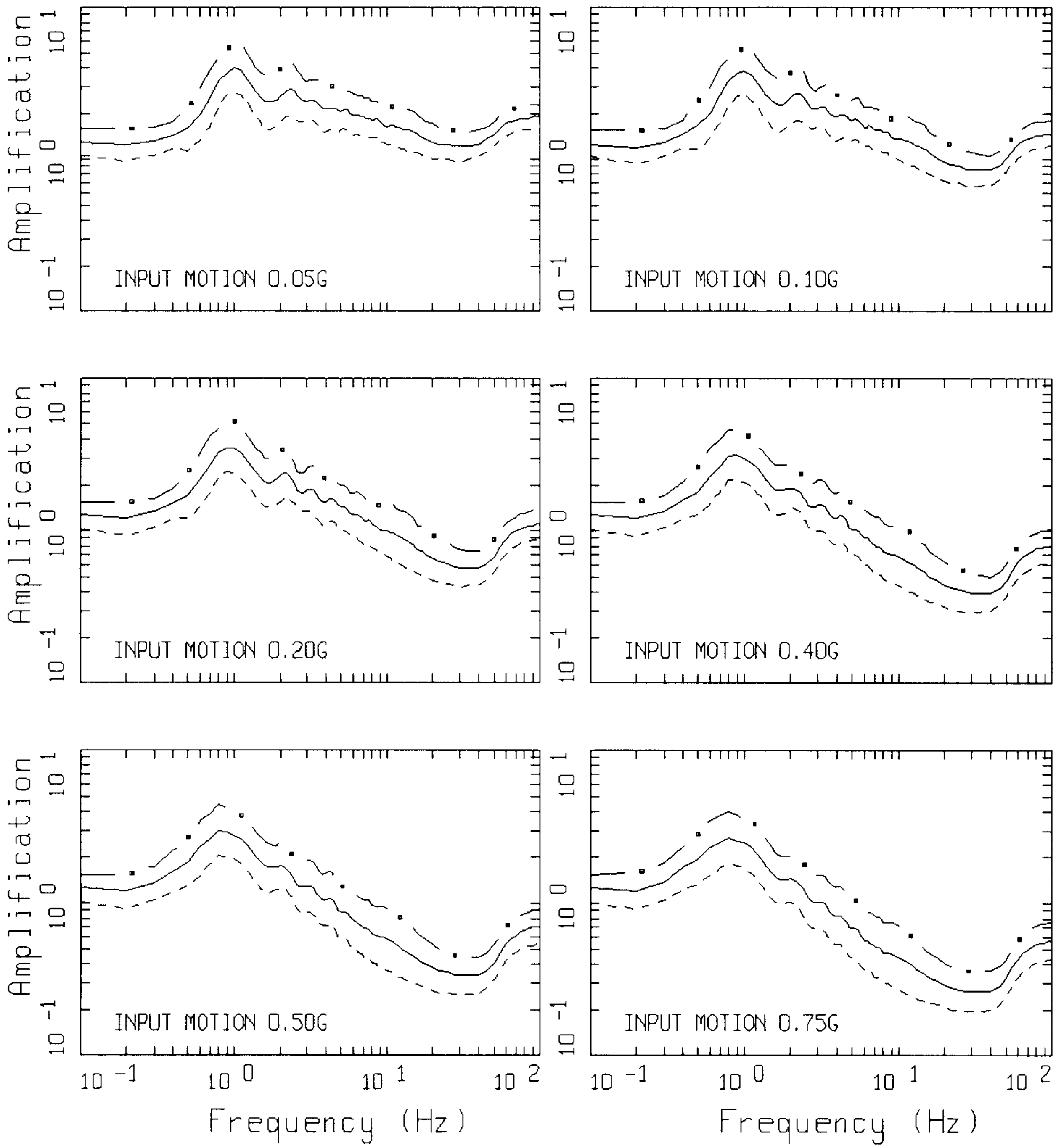

LOWLANDS, CATEGORY 4, 200-500 FT

PENINSULAR RANGE CURVES

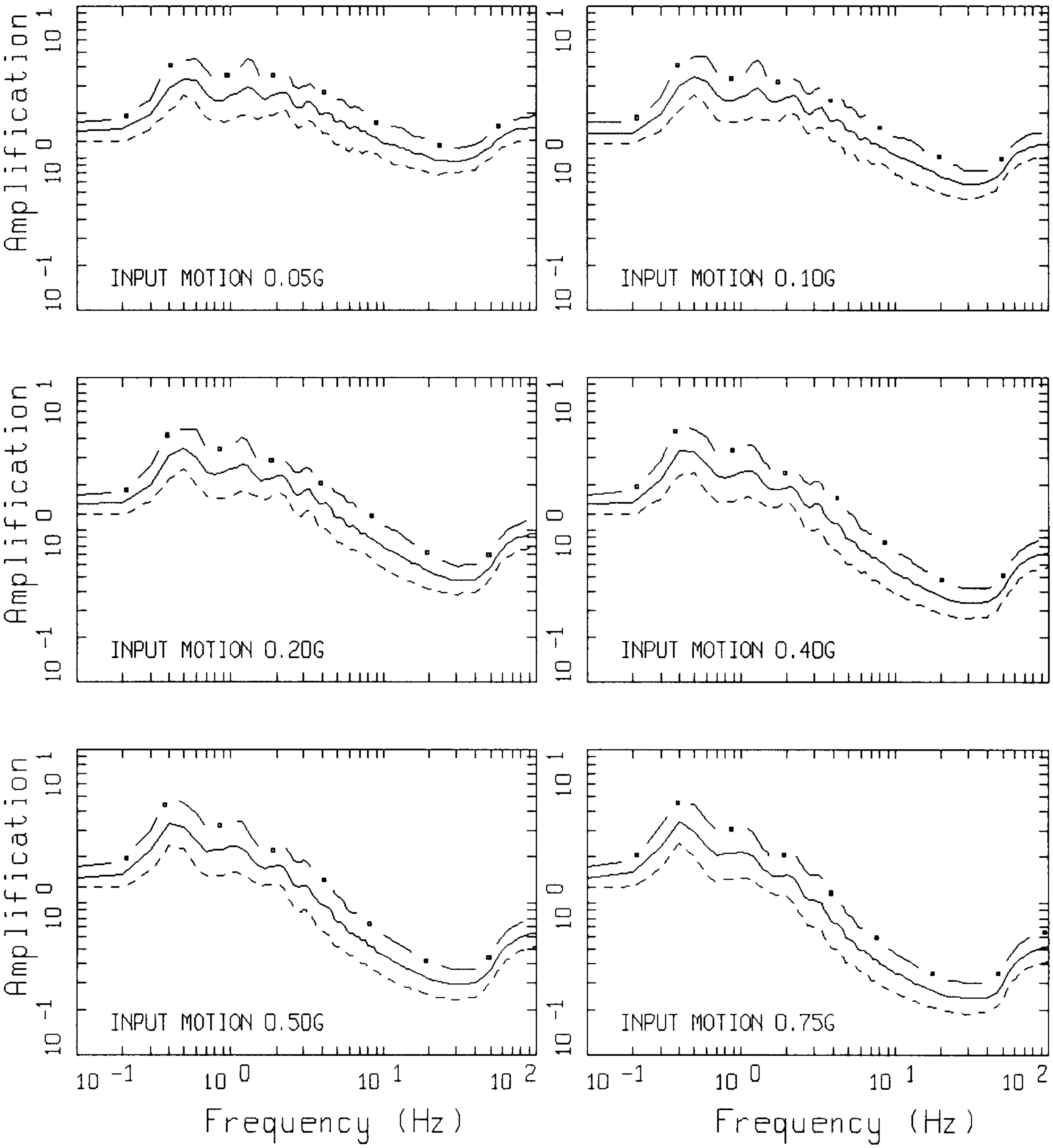

LOWLANDS, CATEGORY 5, 500-1000 FT

PENINSULAR RANGE CURVES

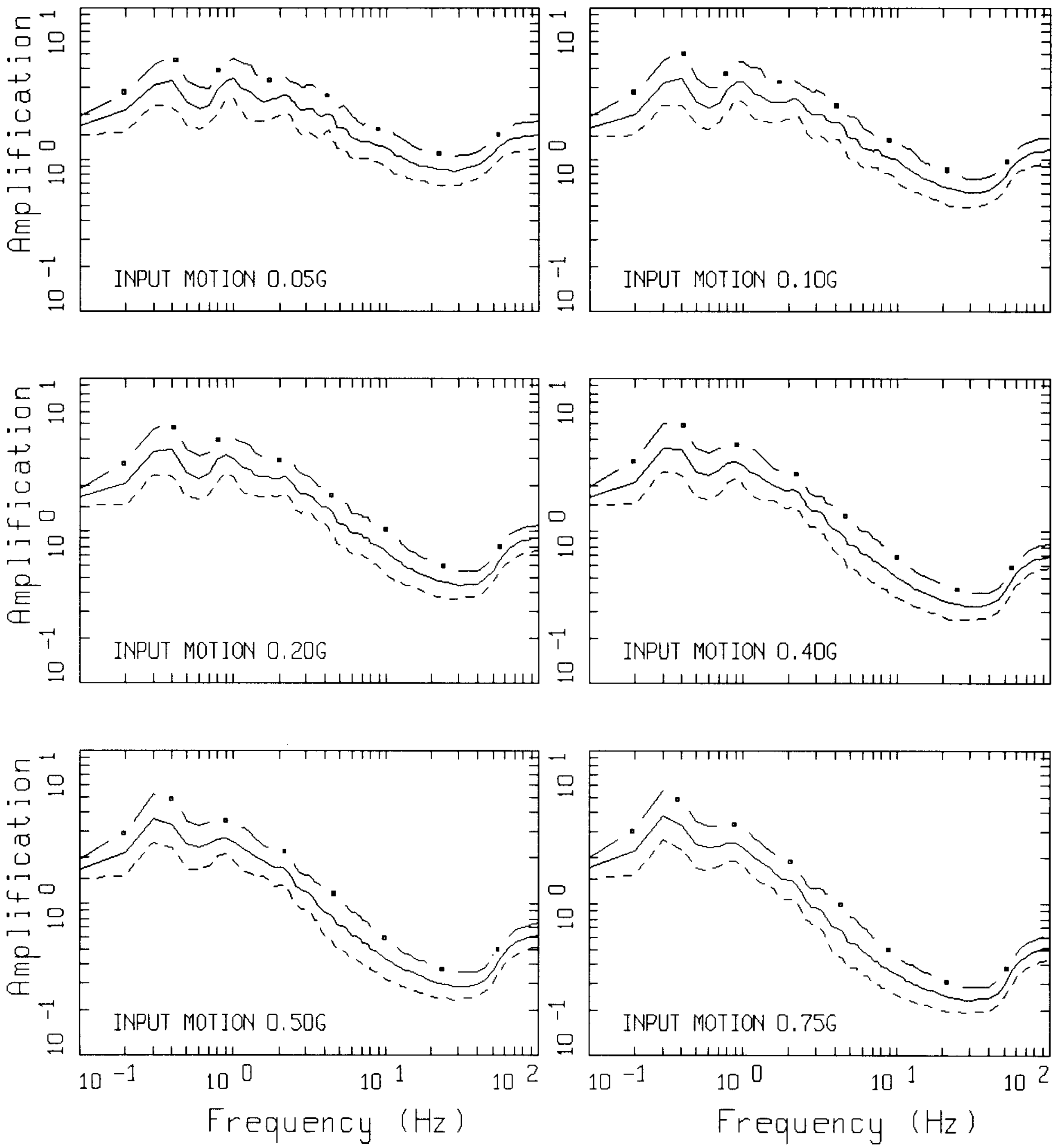

LOWLANDS, CATEGORY 6, 1000-2000 FT

PENINSULAR RANGE CURVES

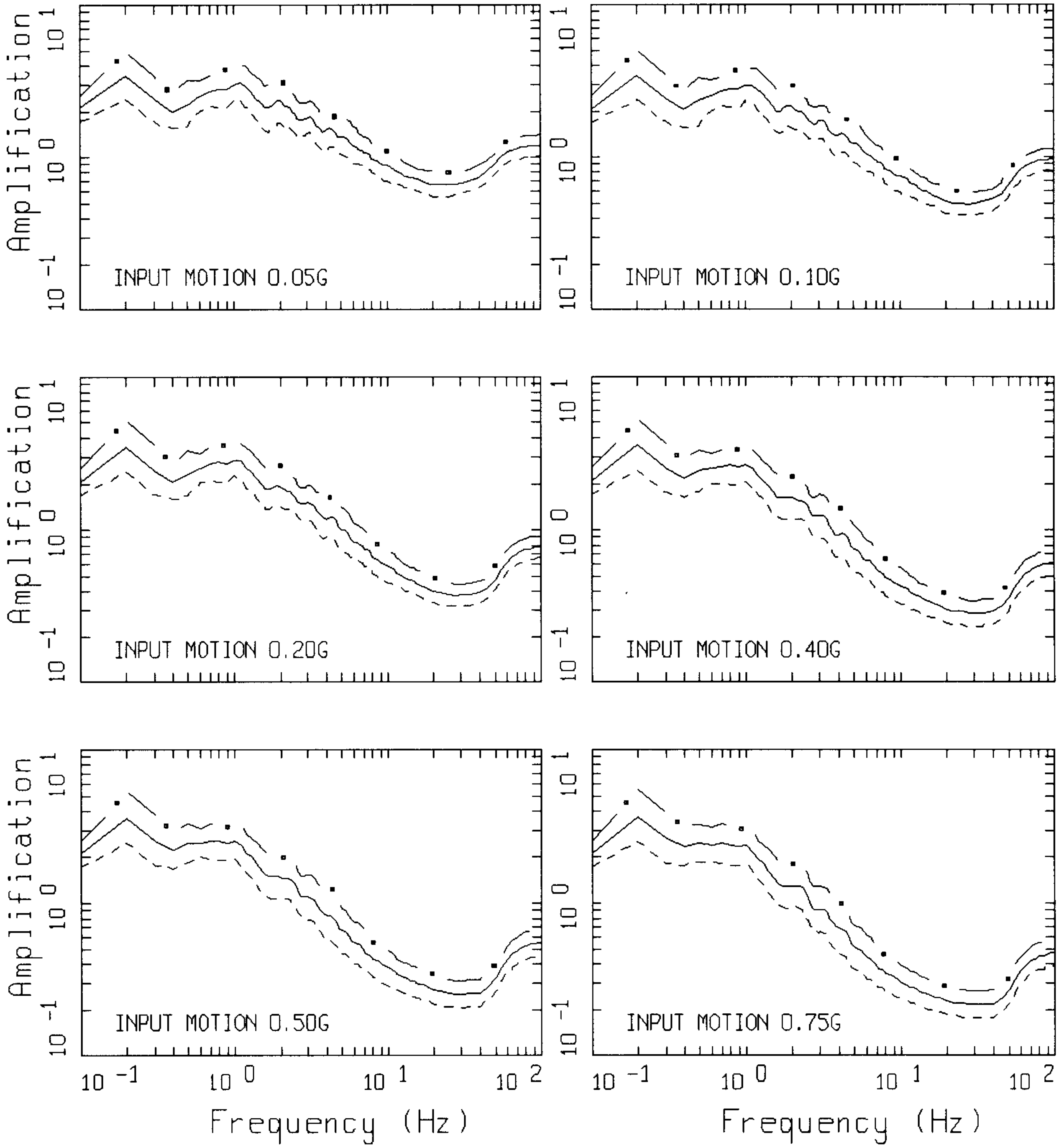

LOWLANDS, CATEGORY 7, 2000-4000 FT

PENINSULAR RANGE CURVES

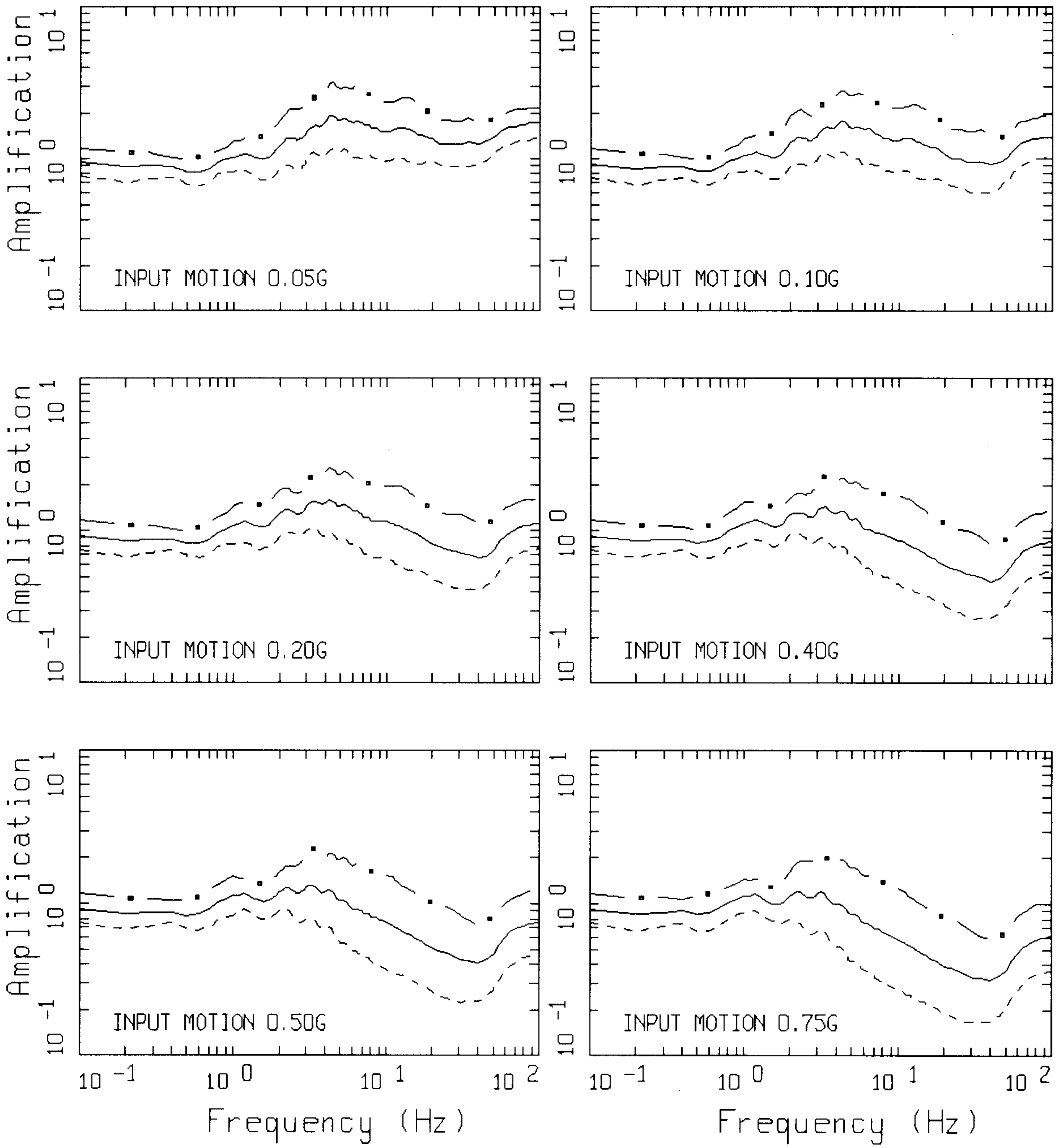

LOWLANDS, CATEGORY 1, 10-50 FT

EPRI CURVES

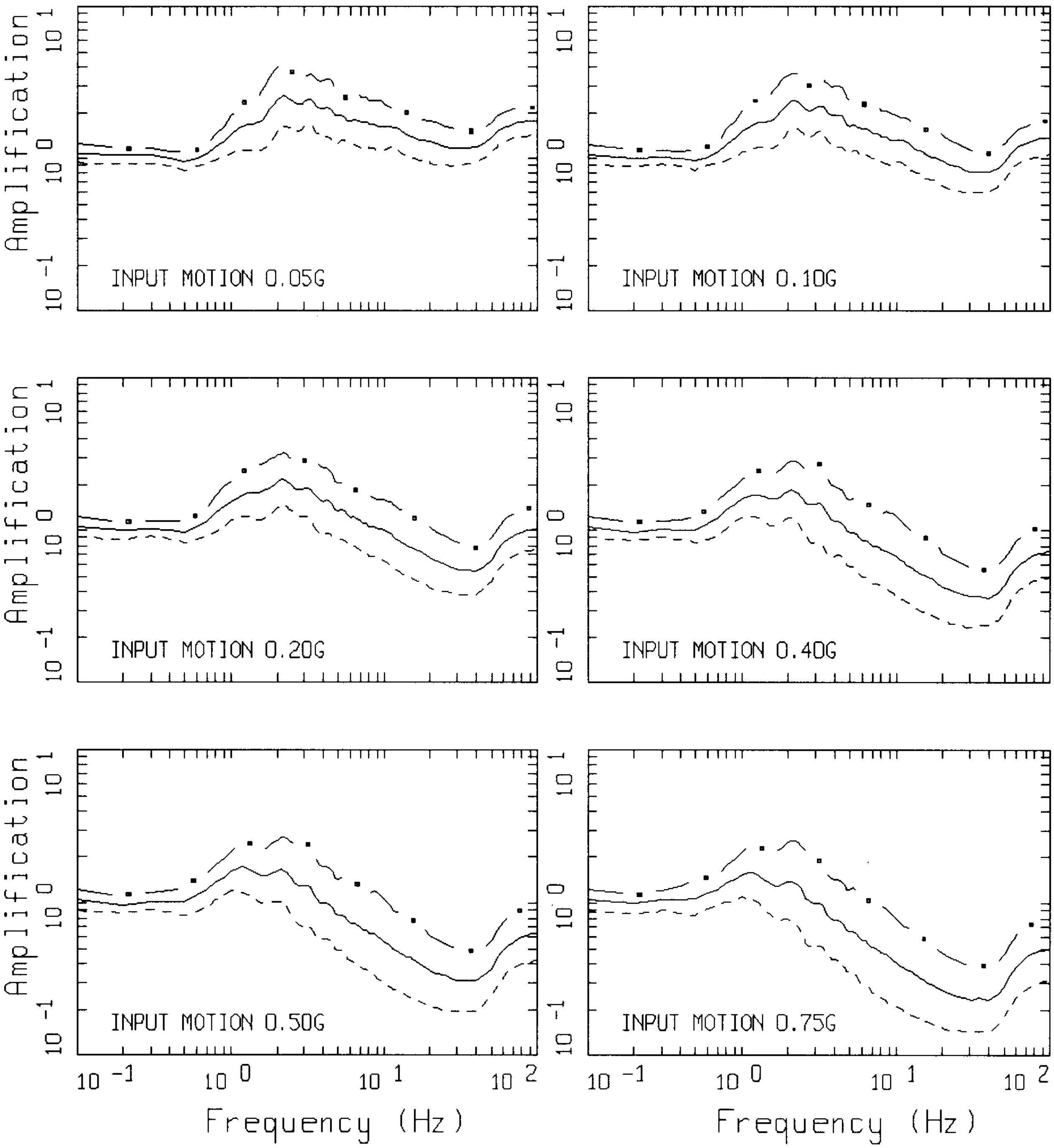

LOWLANDS, CATEGORY 2, 50-100 FT

EPRI CURVES

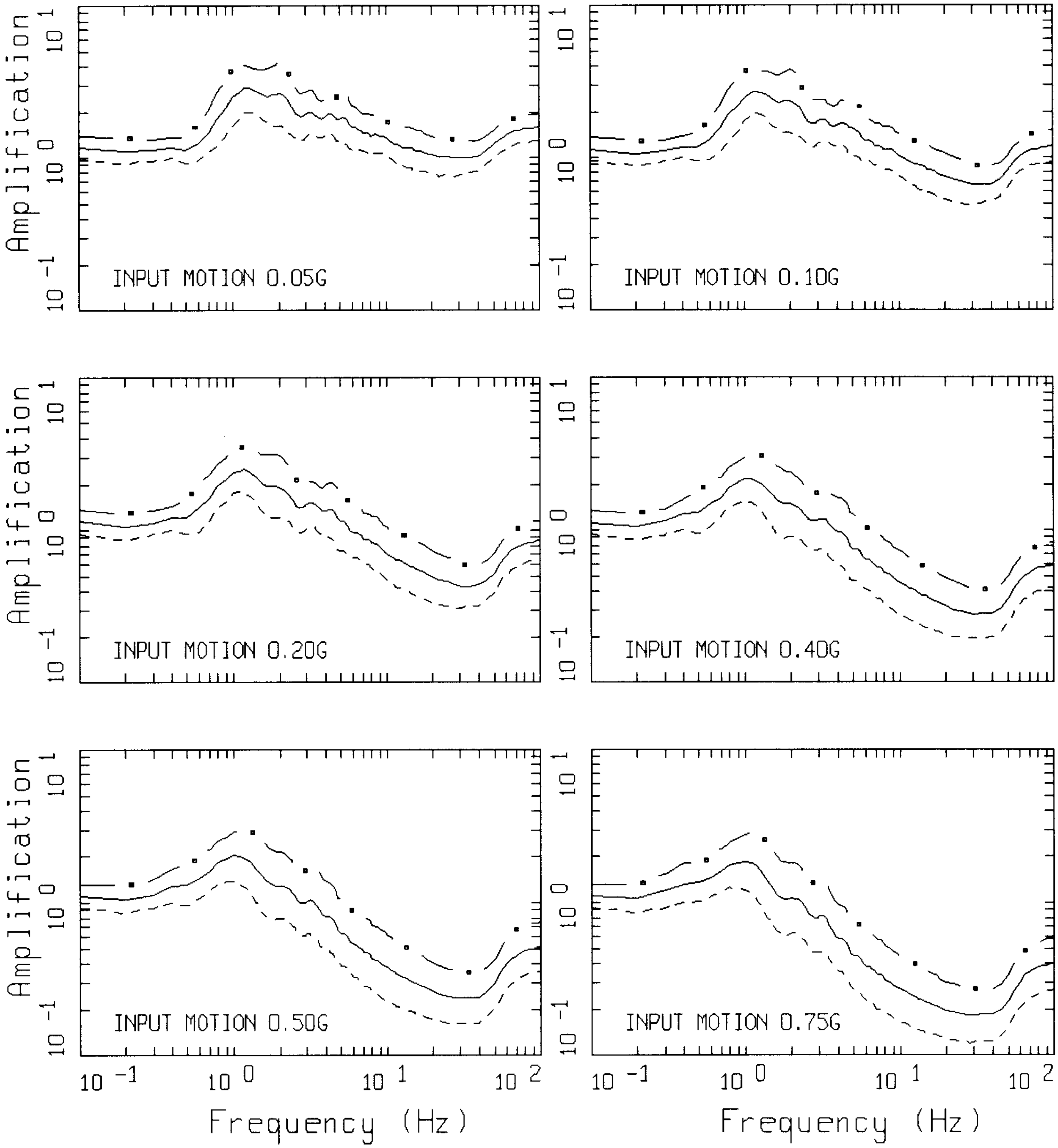

LOWLANDS, CATEGORY 3, 100-200 FT

EPRI CURVES

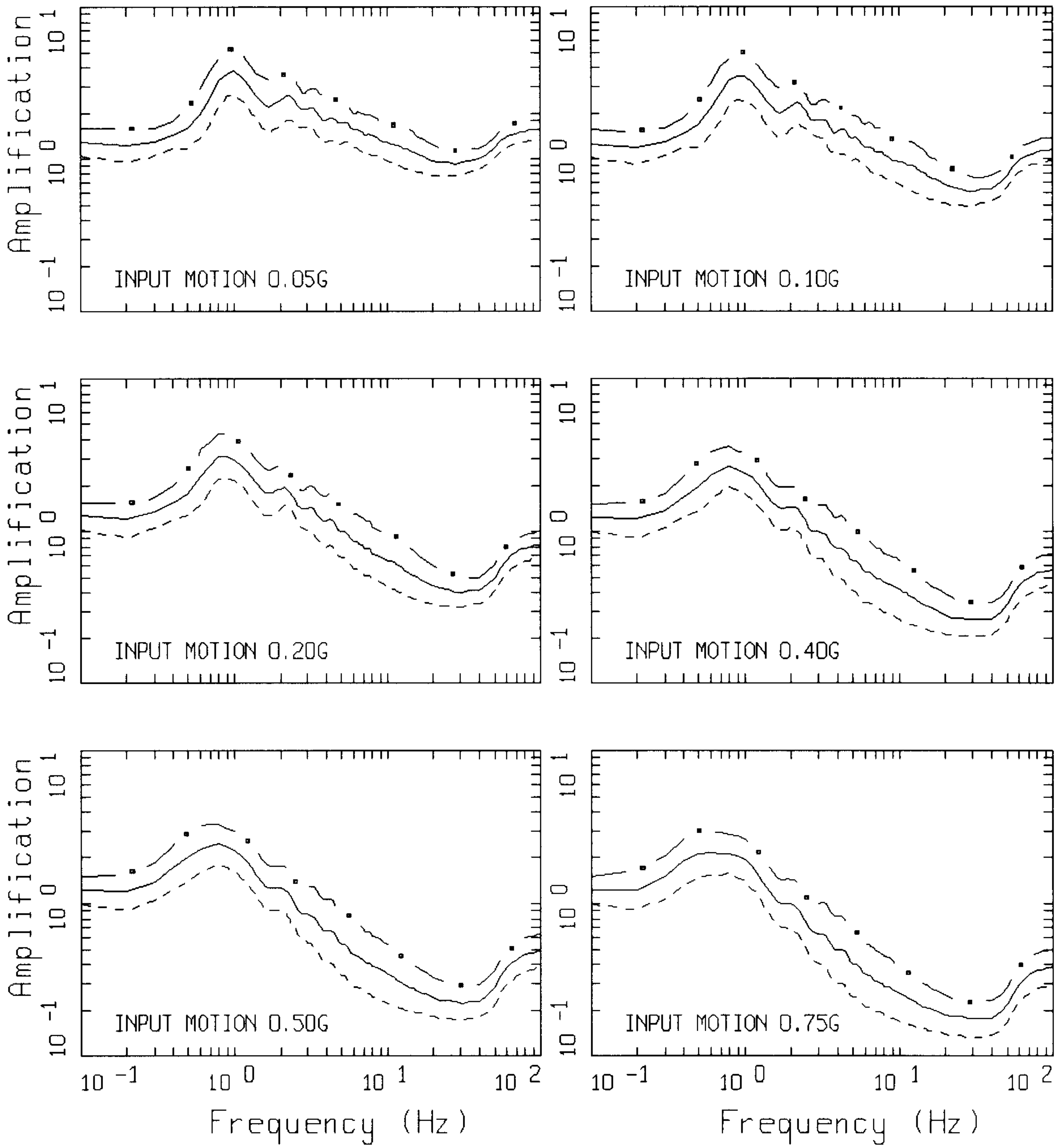

LOWLANDS, CATEGORY 4, 200-500 FT

EPRI CURVES

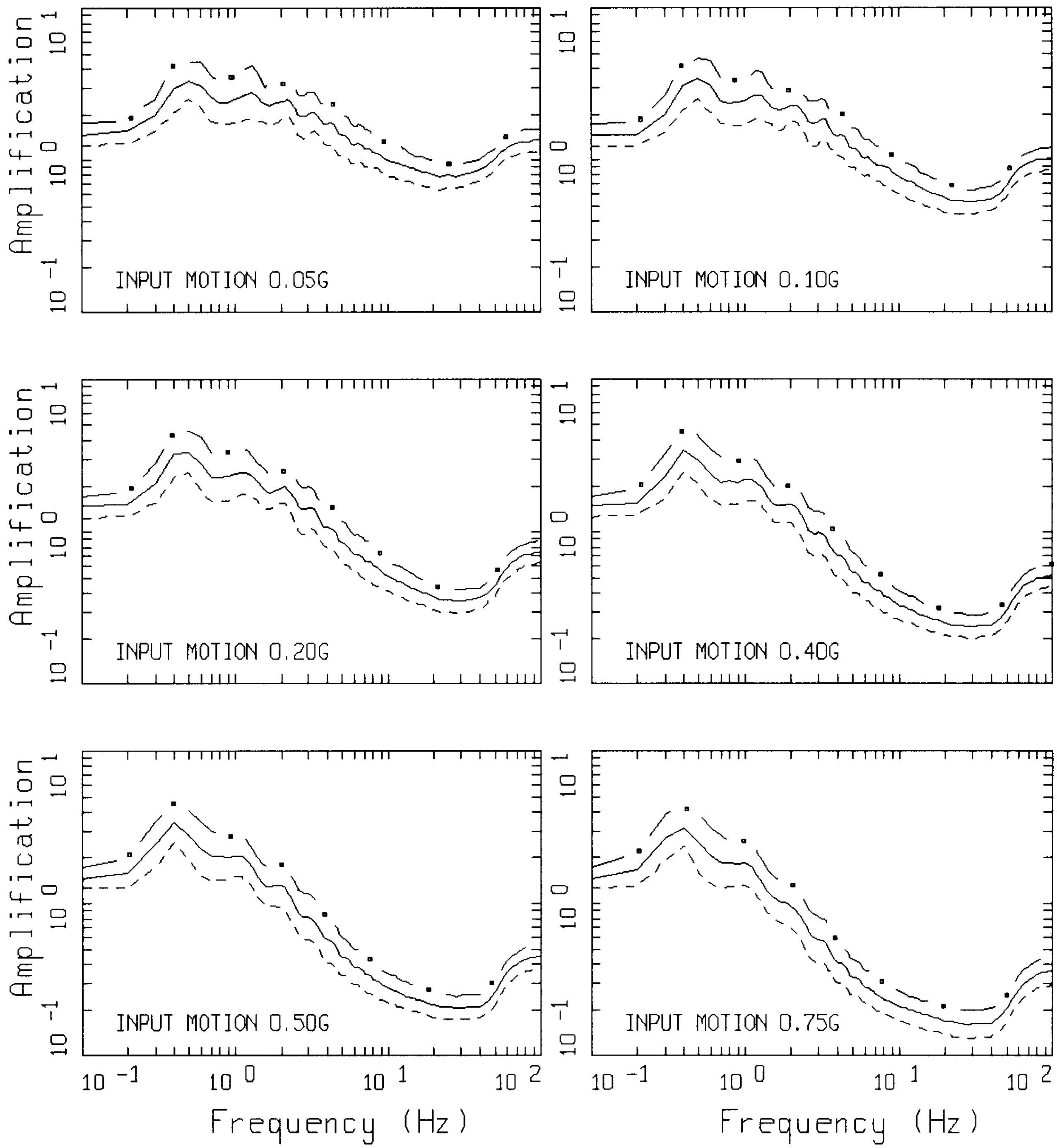

LOWLANDS, CATEGORY 5, 500-1000 FT

EPRI CURVES

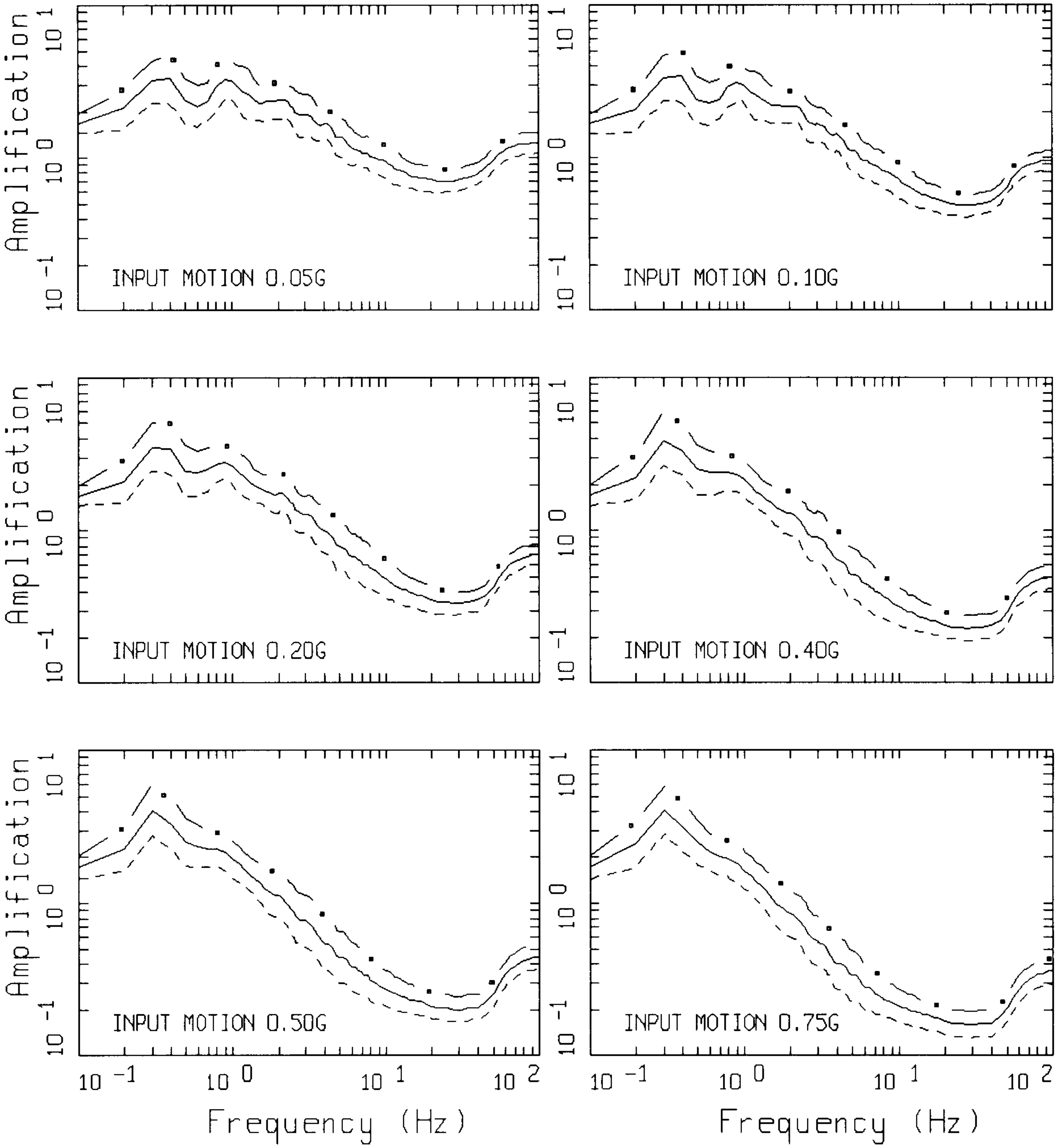

LOWLANDS, CATEGORY 6, 1000-2000 FT

EPRI CURVES

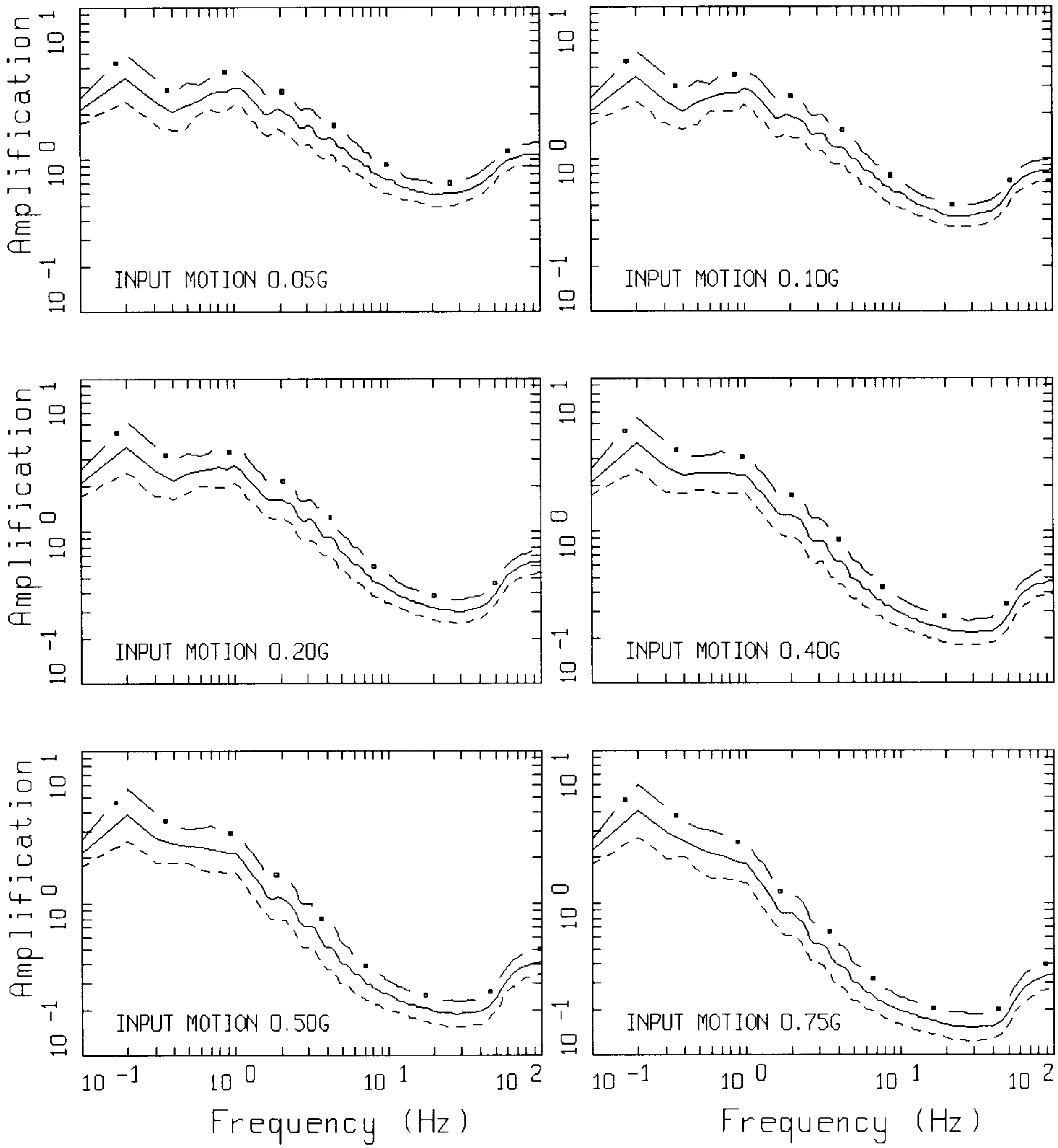

LOWLANDS, CATEGORY 7, 2000-4000 FT

EPRI CURVES

Appendix B

AMPLIFICATION FACTORS FOR UPLANDS PROFILE

Amplification factors, median and ± 1σ 5% damped response spectra, for the Uplands generic profile depth categories 1, 2, 3, 4, 5, 6, 7. Peninsular Range and EPRI nonlinear dynamic material properties.

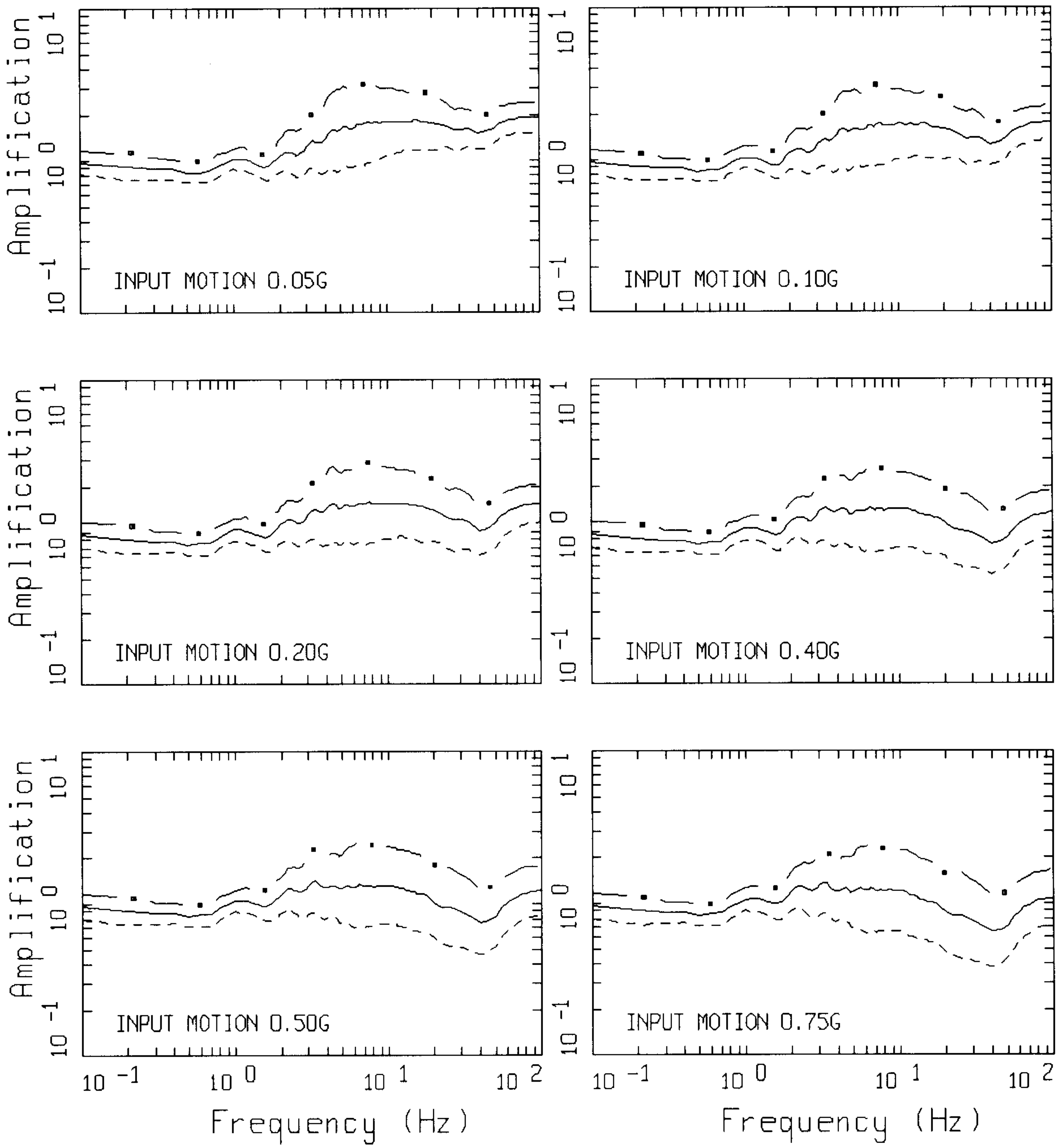

UPLANDS, CATEGORY 1, 10-50 FT

PENINSULAR RANGE CURVES

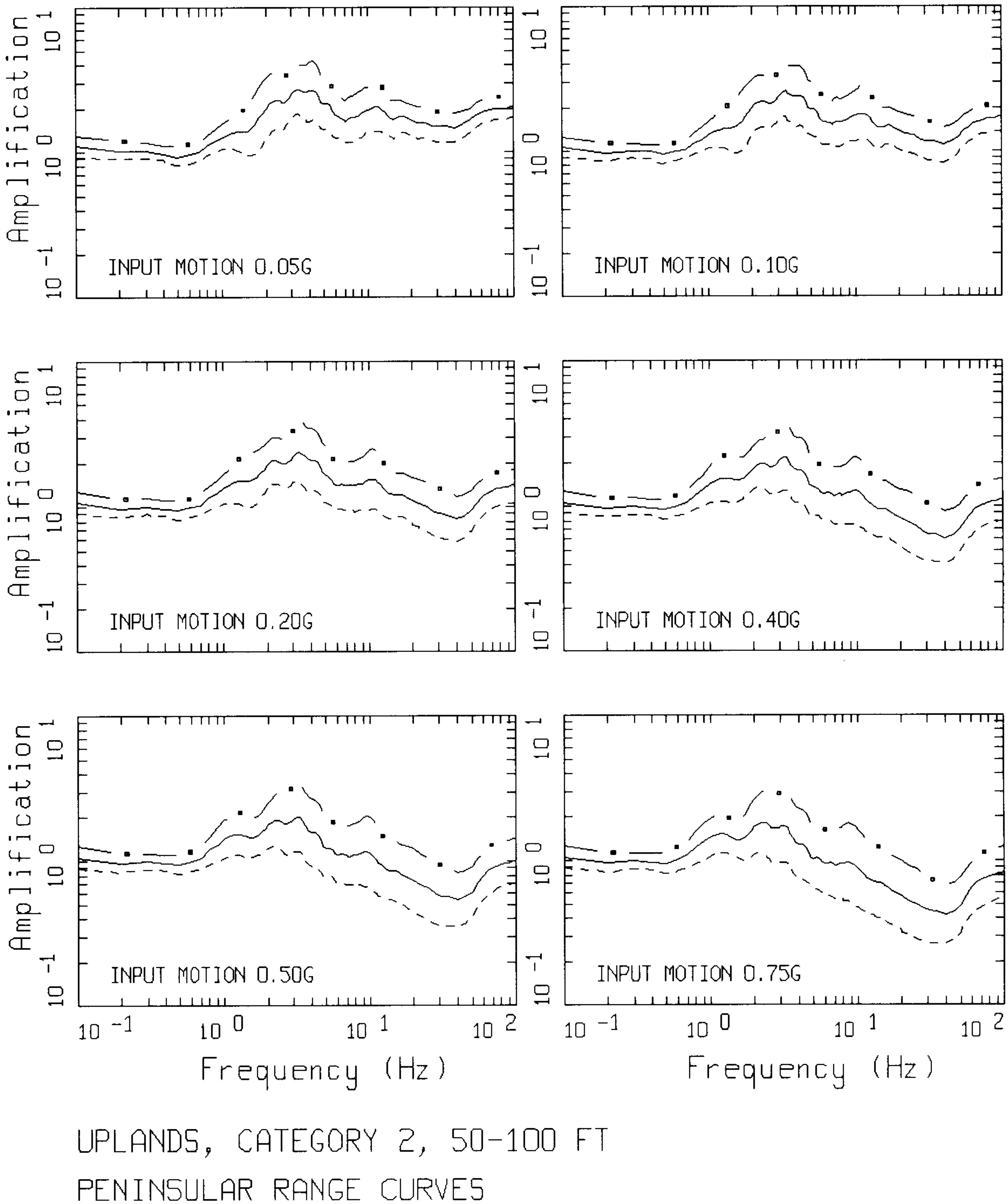
Amplification
INPUT MOTION 0.05G
INPUT MOTION 0.10G
INPUT MOTION 0.20G
INPUT MOTION 0.40G
INPUT MOTION 0.50G
INPUT MOTION 0.75G
Frequency (Hz)
UPLANDS, CATEGORY 2, 50-100 FT
PENINSULAR RANGE CURVES

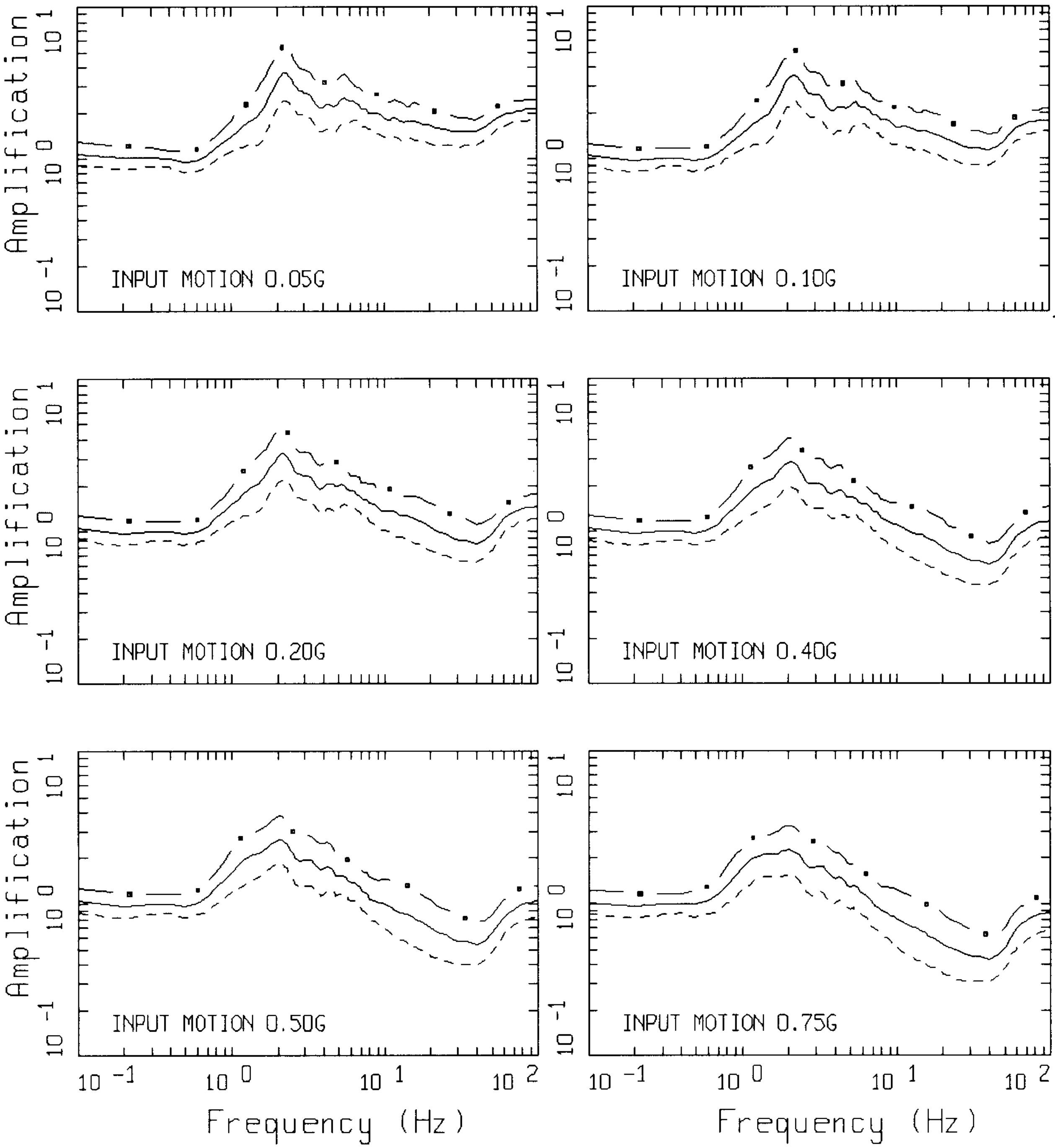

UPLANDS, CATEGORY 3, 100-200 FT

PENINSULAR RANGE CURVES

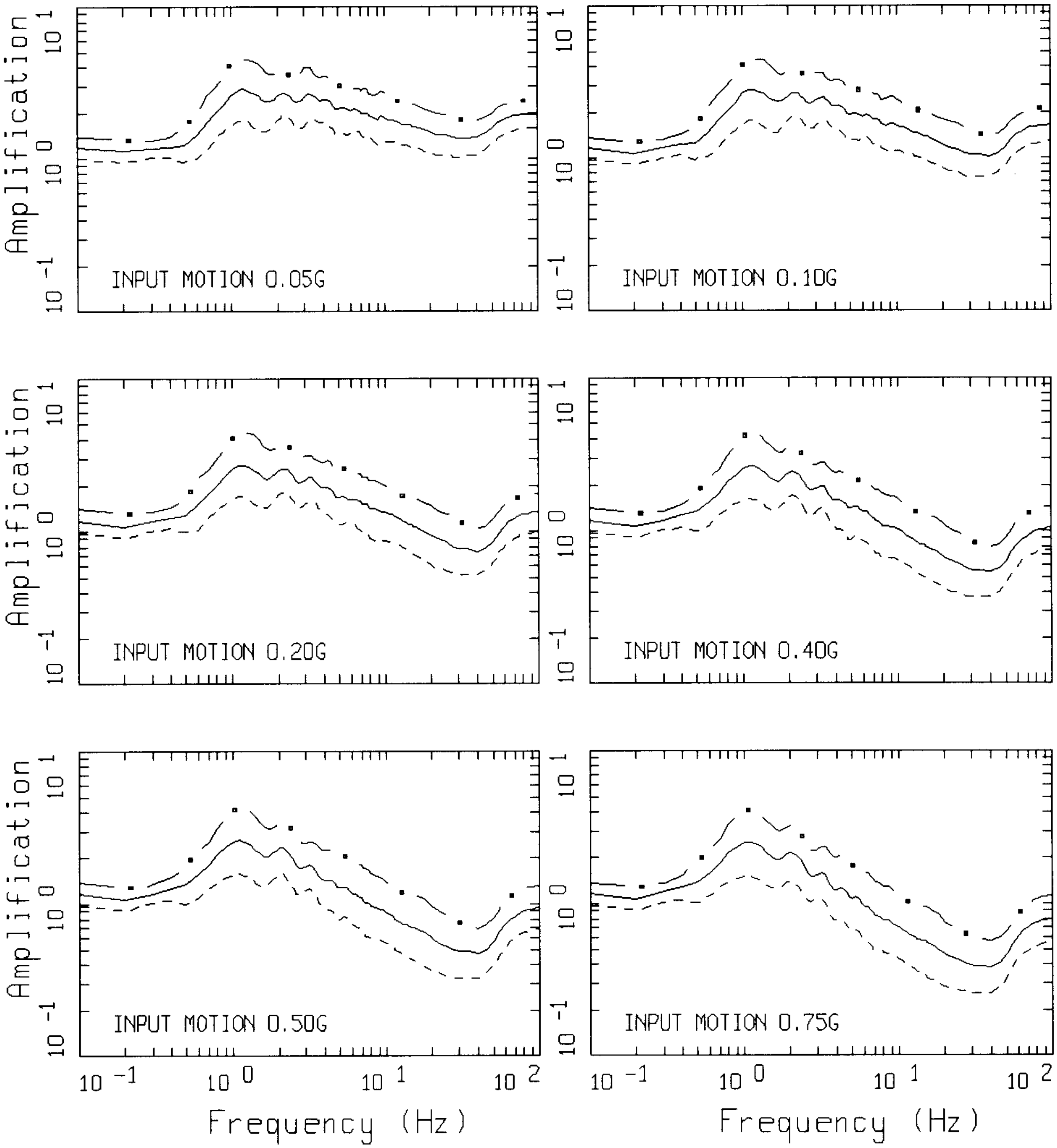

UPLANDS, CATEGORY 4, 200-500 FT

PENINSULAR RANGE CURVES

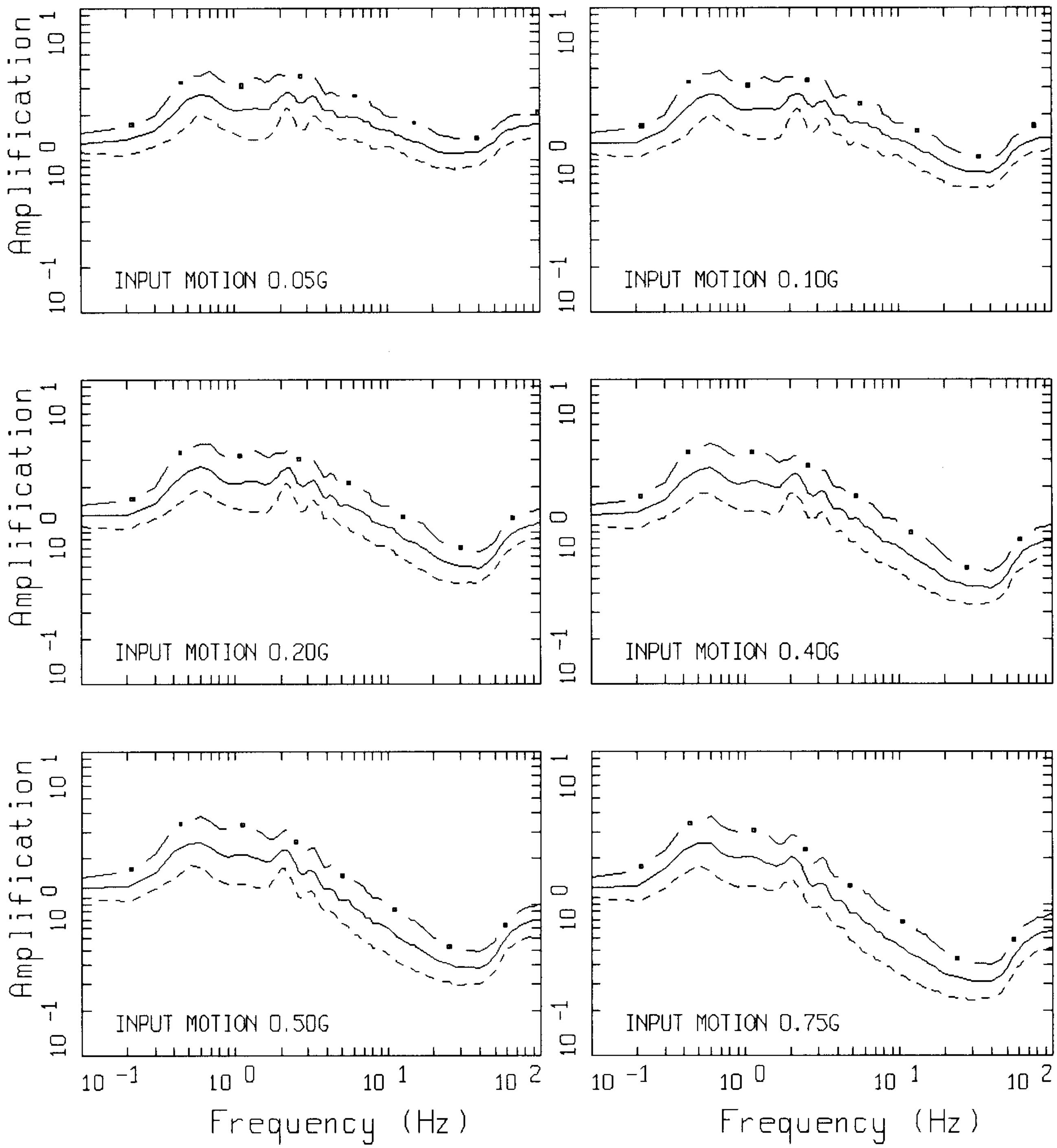

UPLANDS, CATEGORY 5, 500-1000 FT

PENINSULAR RANGE CURVES

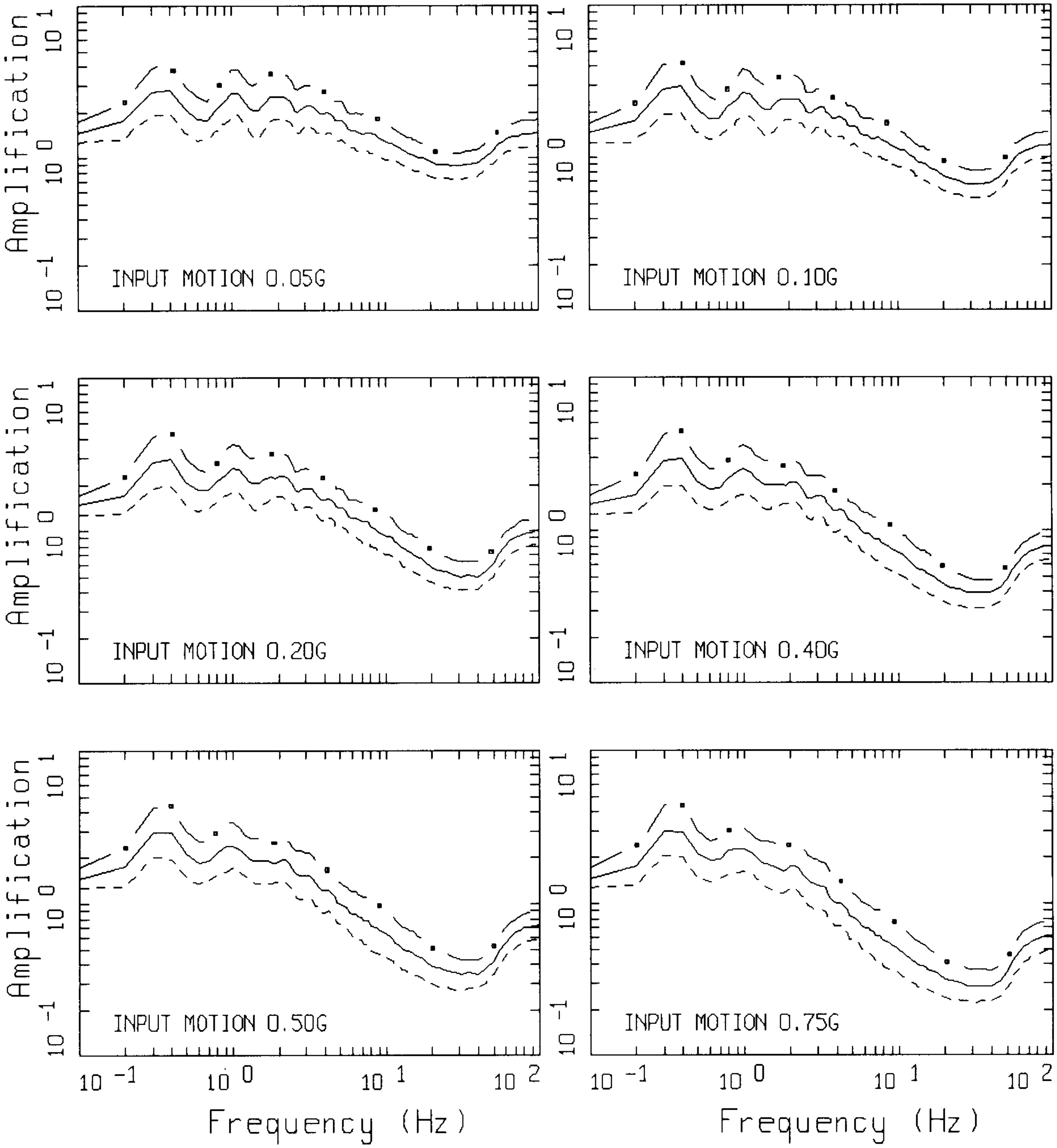

UPLANDS, CATEGORY 6, 1000-2000 FT

PENINSULAR RANGE CURVES

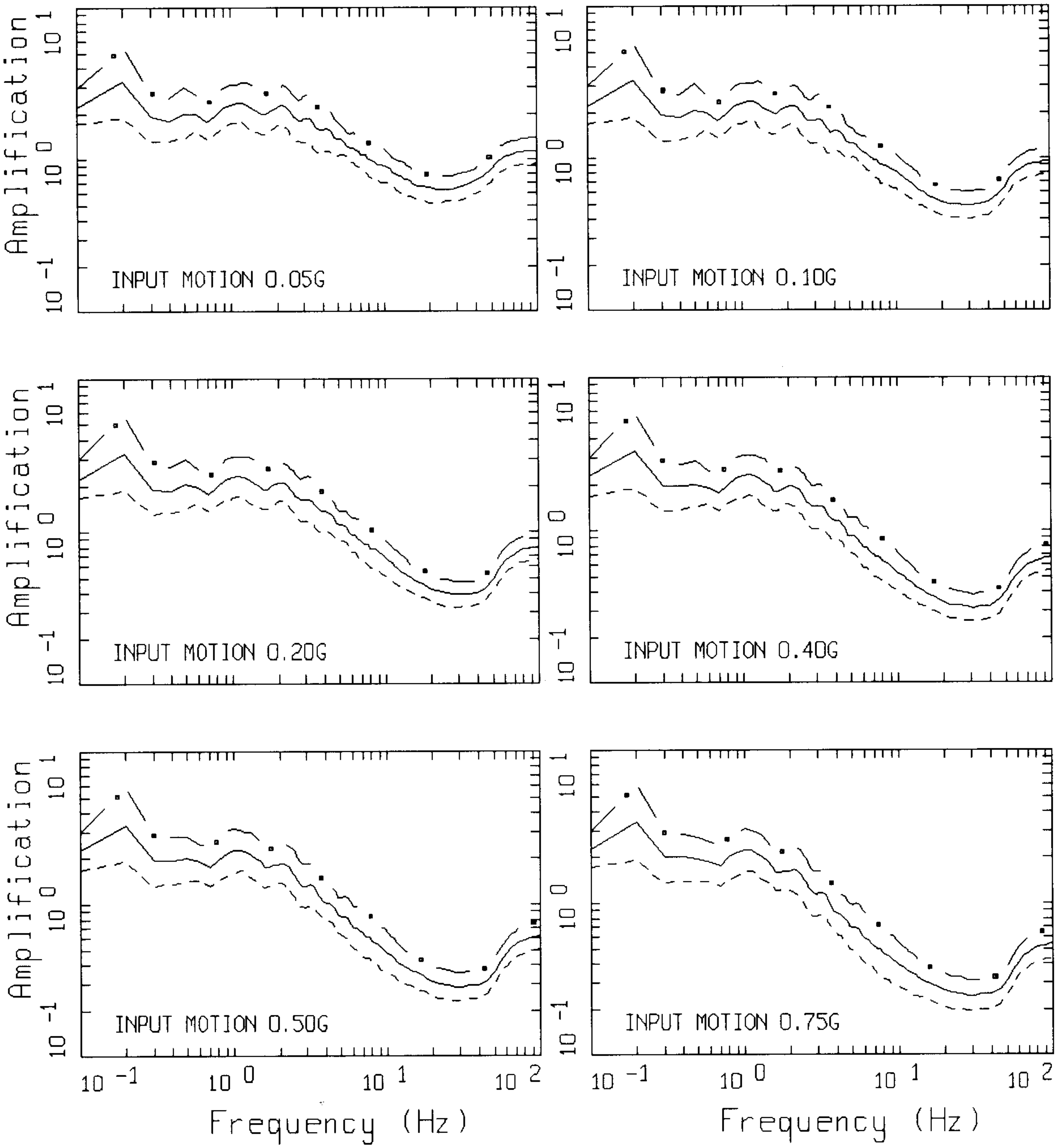

UPLANDS, CATEGORY 7, 2000-4000 FT

PENINSULAR RANGE CURVES

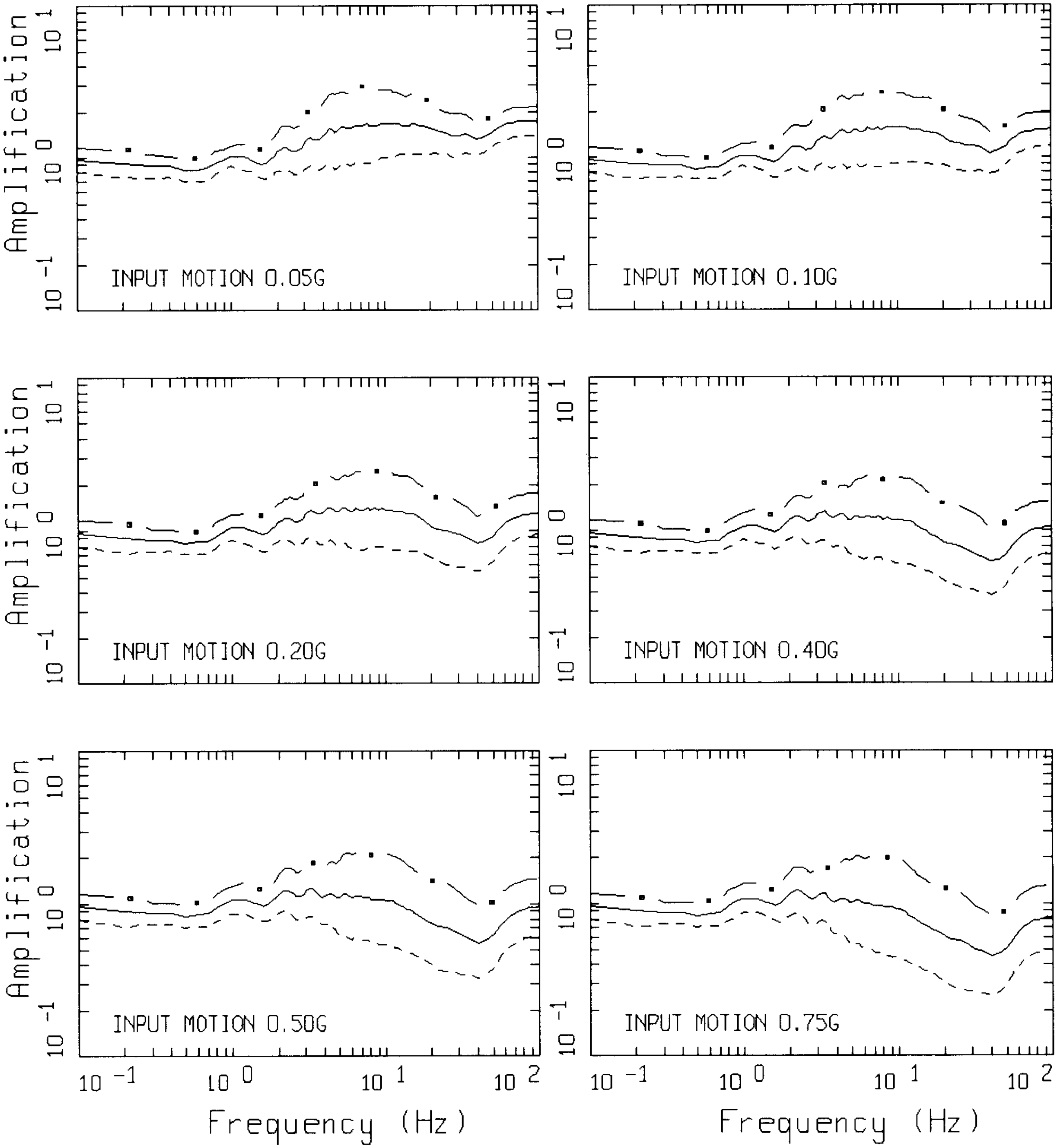

UPLANDS, CATEGORY 1, 10-50 FT

EPRI CURVES

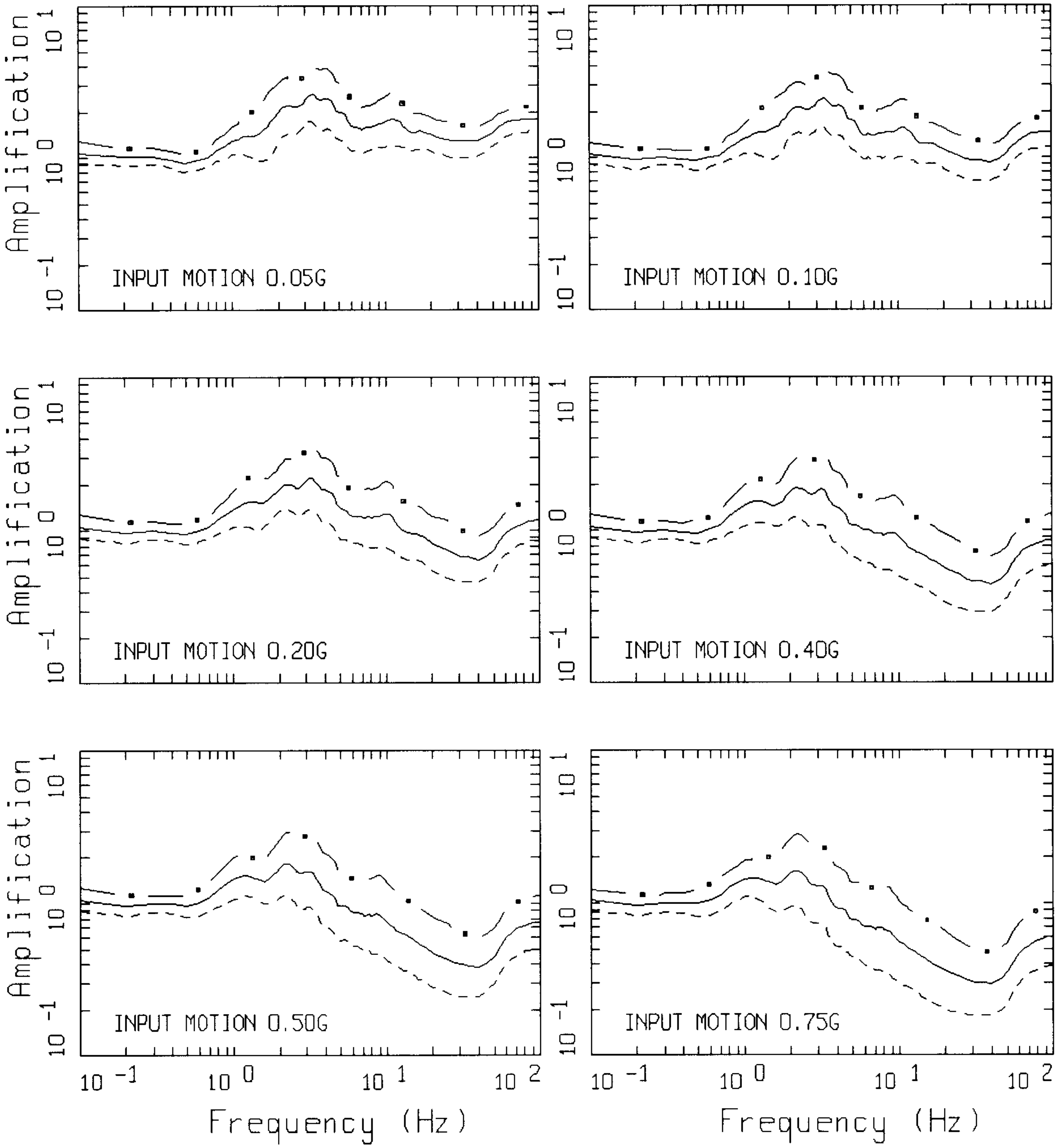

UPLANDS, CATEGORY 2, 50-100 FT

EPRI CURVES

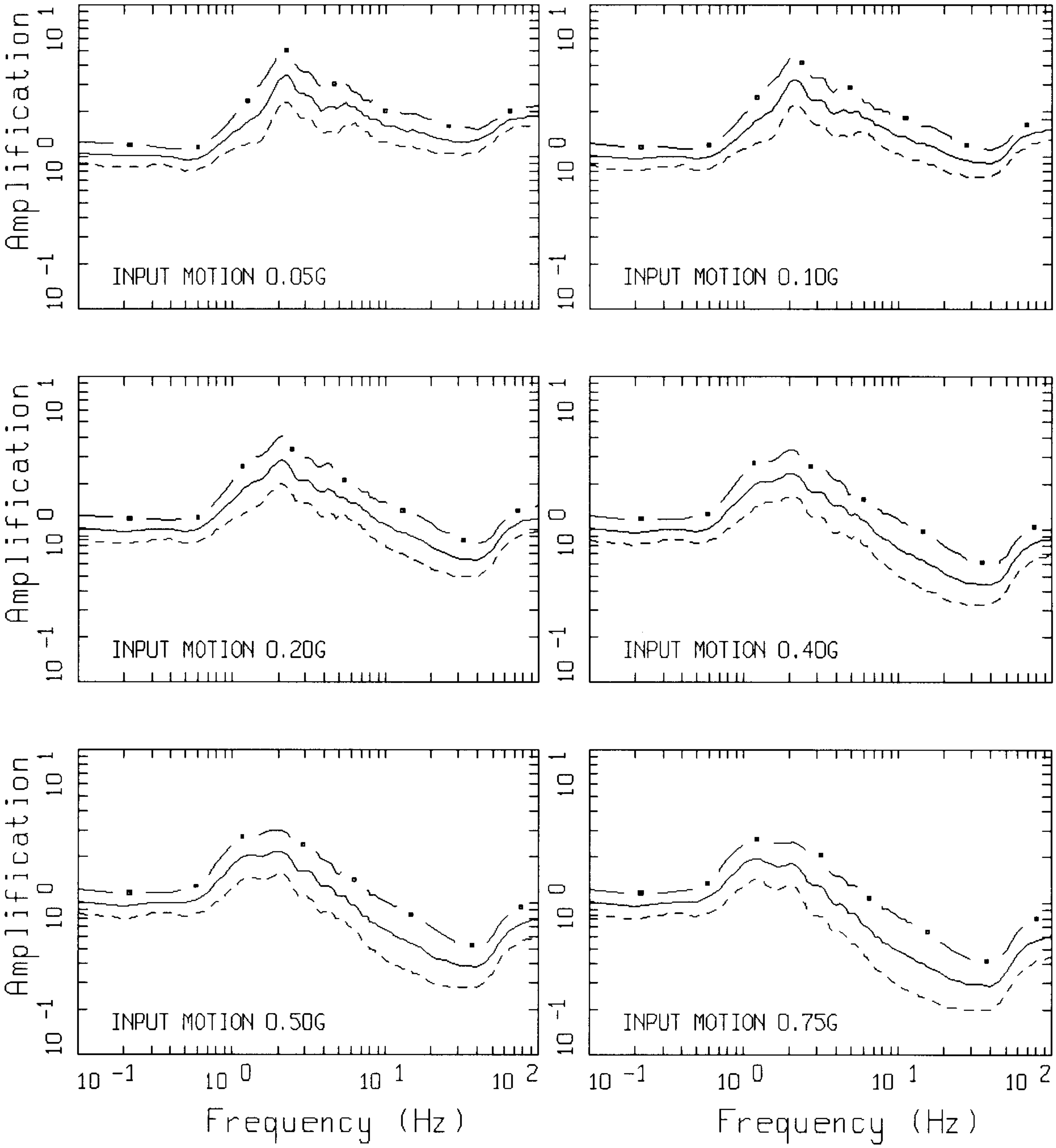

UPLANDS, CATEGORY 3, 100-200 FT

EPRI CURVES

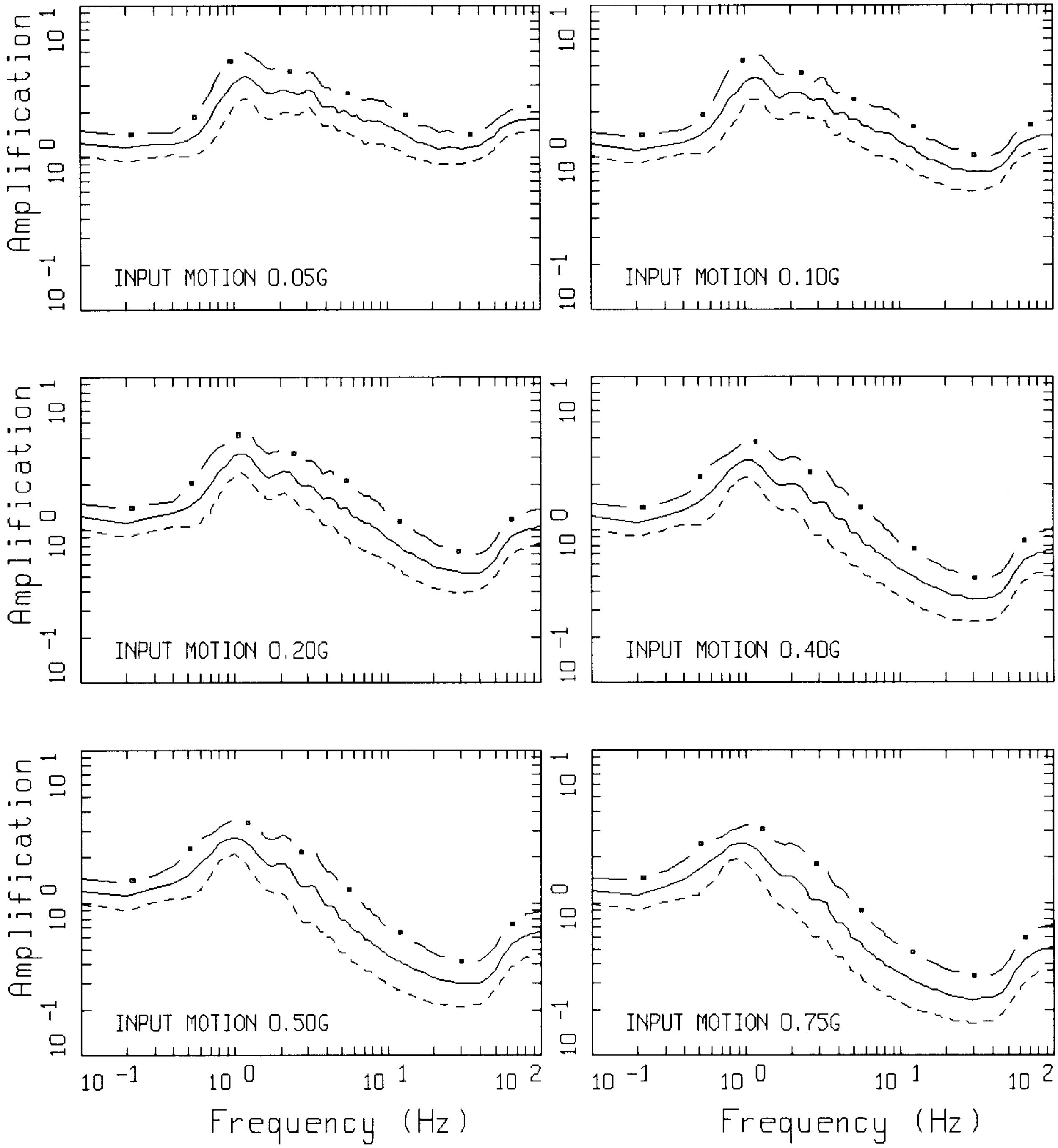

UPLANDS, CATEGORY 4, 200-500 FT

EPRI CURVES

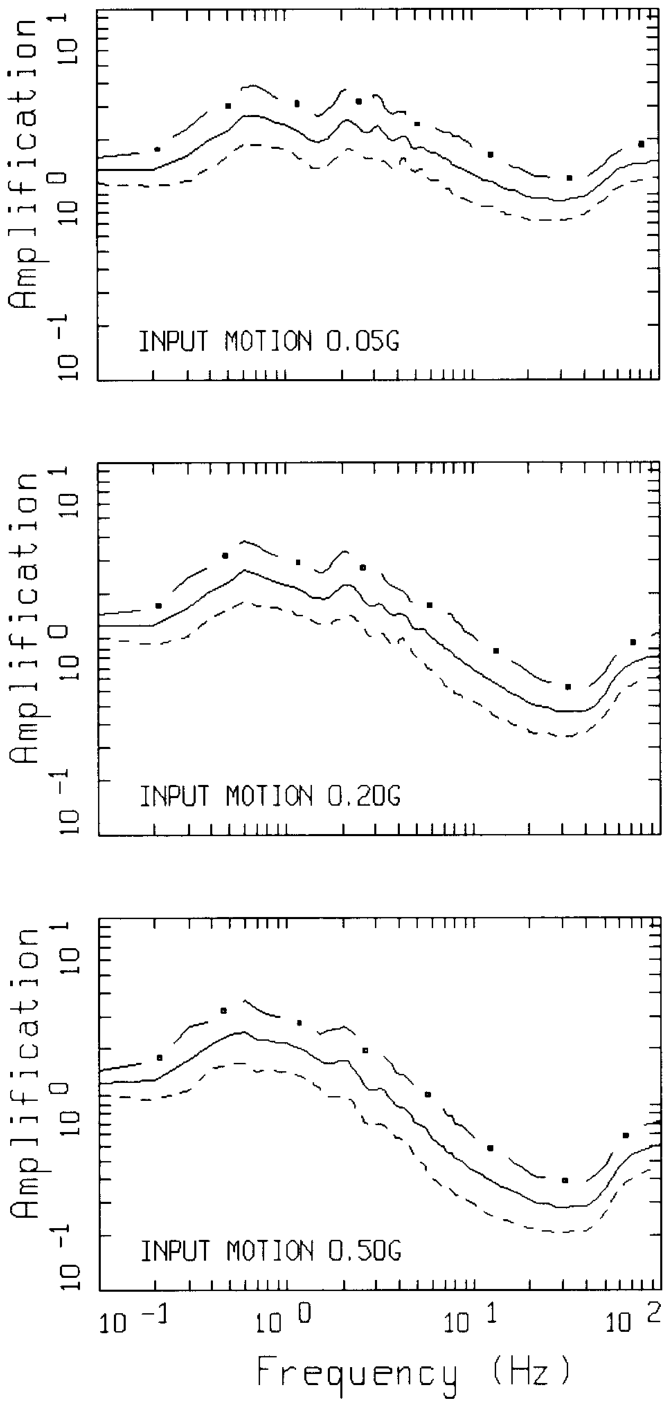

UPLANDS, CATEGORY 5, 500-1000 FT

EPRI CURVES

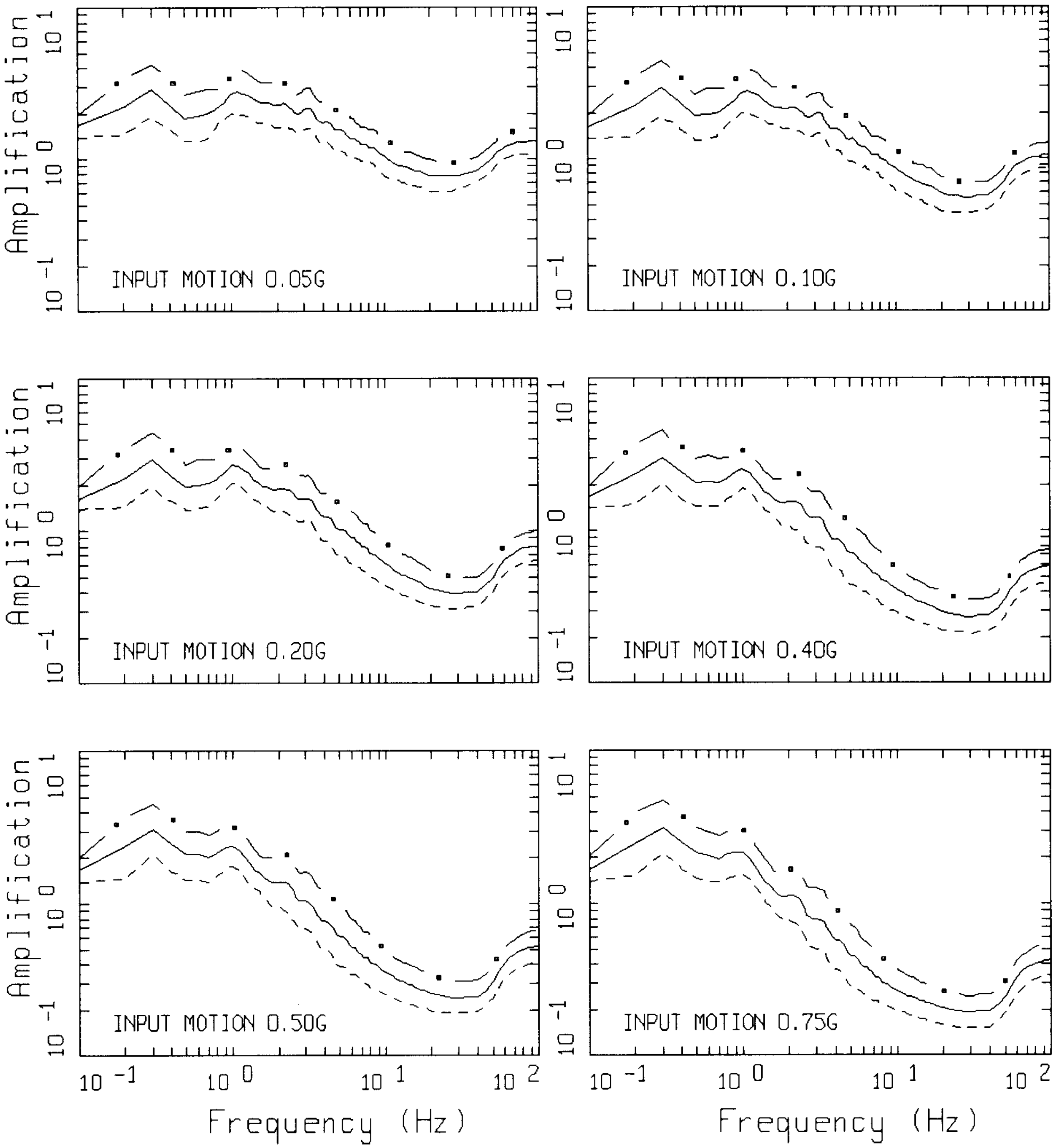

UPLANDS, CATEGORY 6, 1000-2000 FT

EPRI CURVES

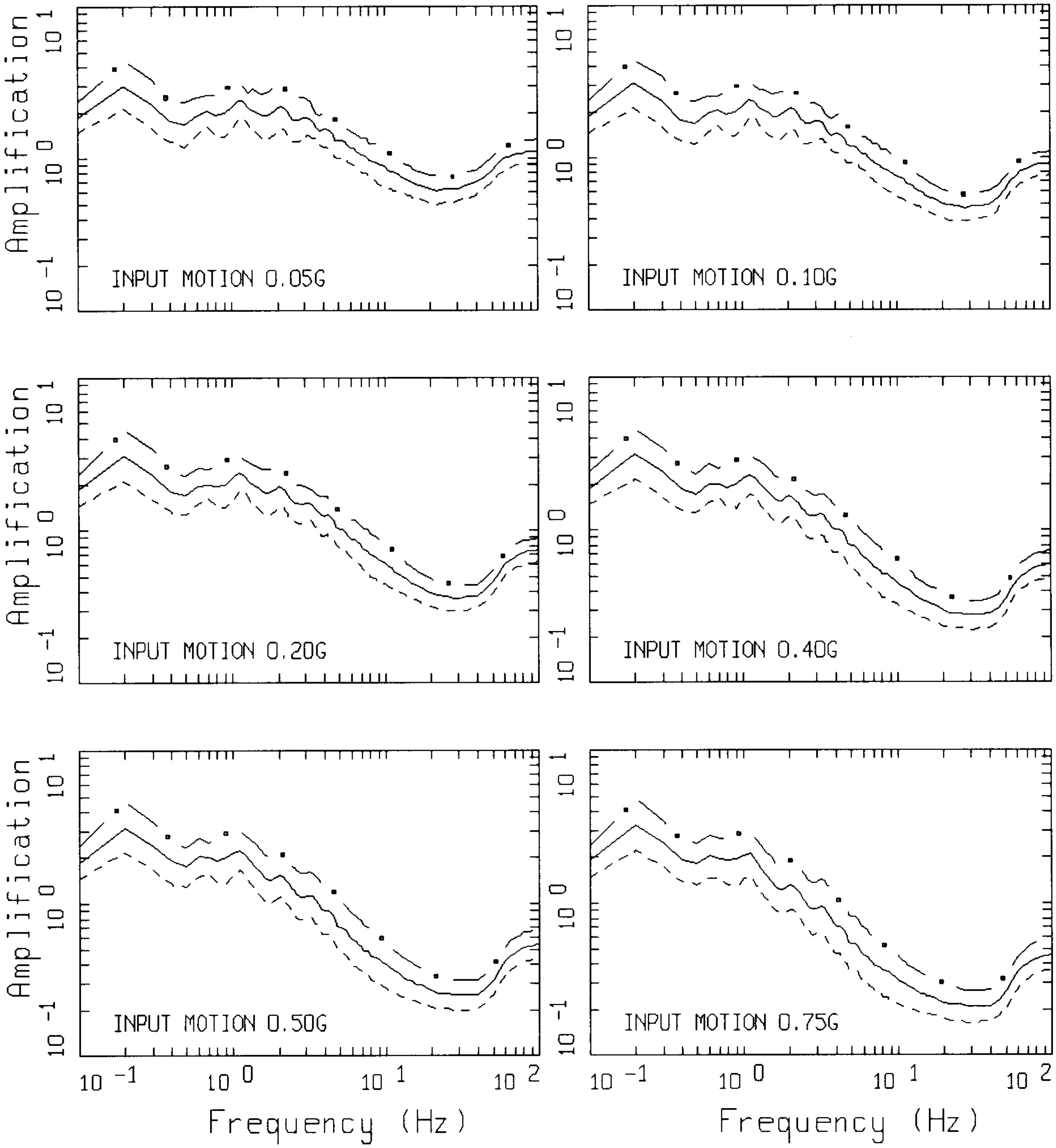

UPLANDS, CATEGORY 7, 2000-4000 FT

EPRI CURVES

Appendix C

AMPLIFICATION FACTORS FOR UPLANDS PROFILES WITH HIGH-VELOCITY LAYER

Amplification factors, median and ± 1σ 5% damped response spectra, for the Uplands high shallow velocity profiles (1, 2, 3) depth category 7. Peninsular Range and EPRI nonlinear dynamic material properties.

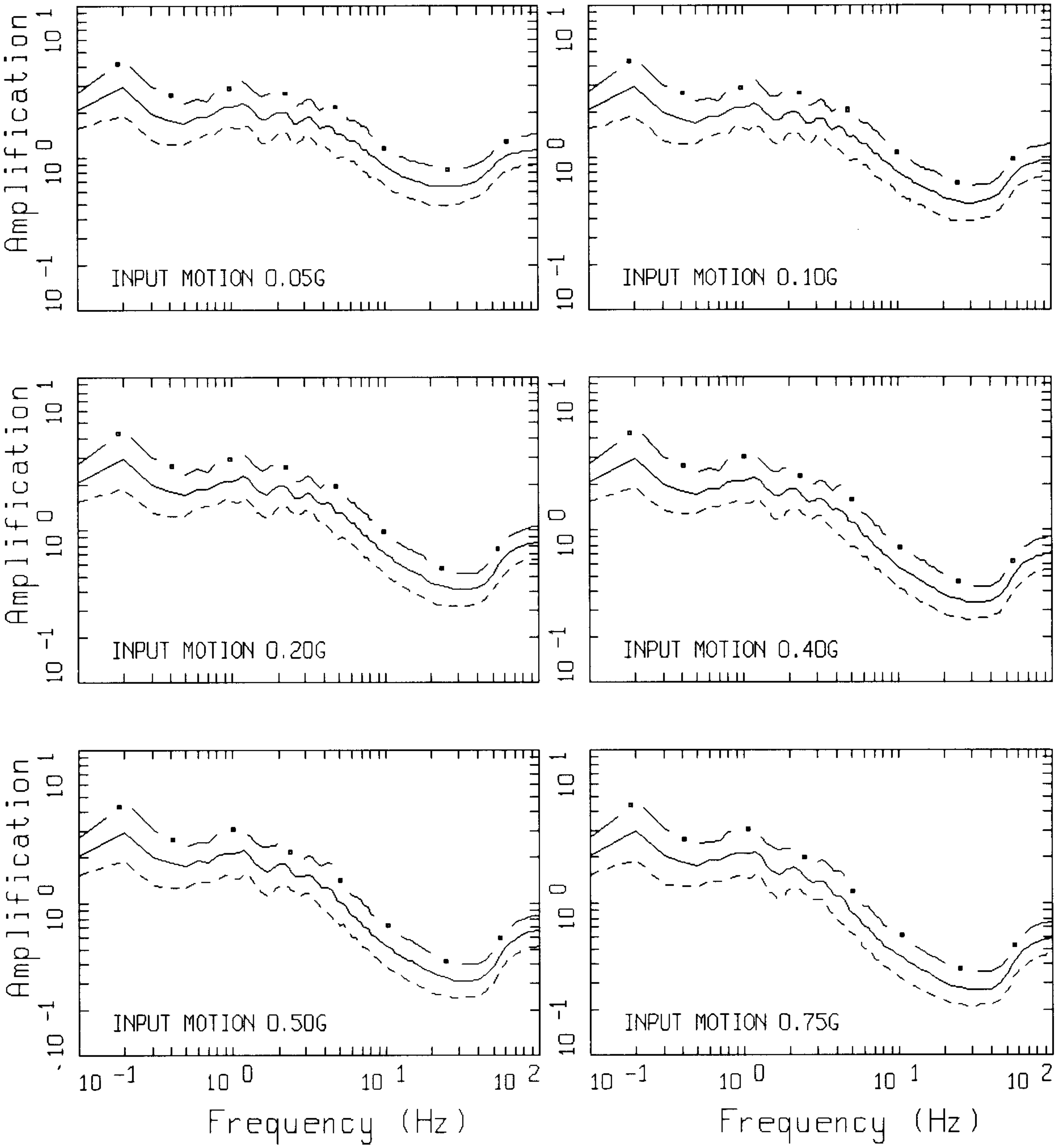

UPLANDS HIGH VELOCITY 1, CATEGORY 7, 2000-4000 FT
PENINSULAR RANGE CURVES

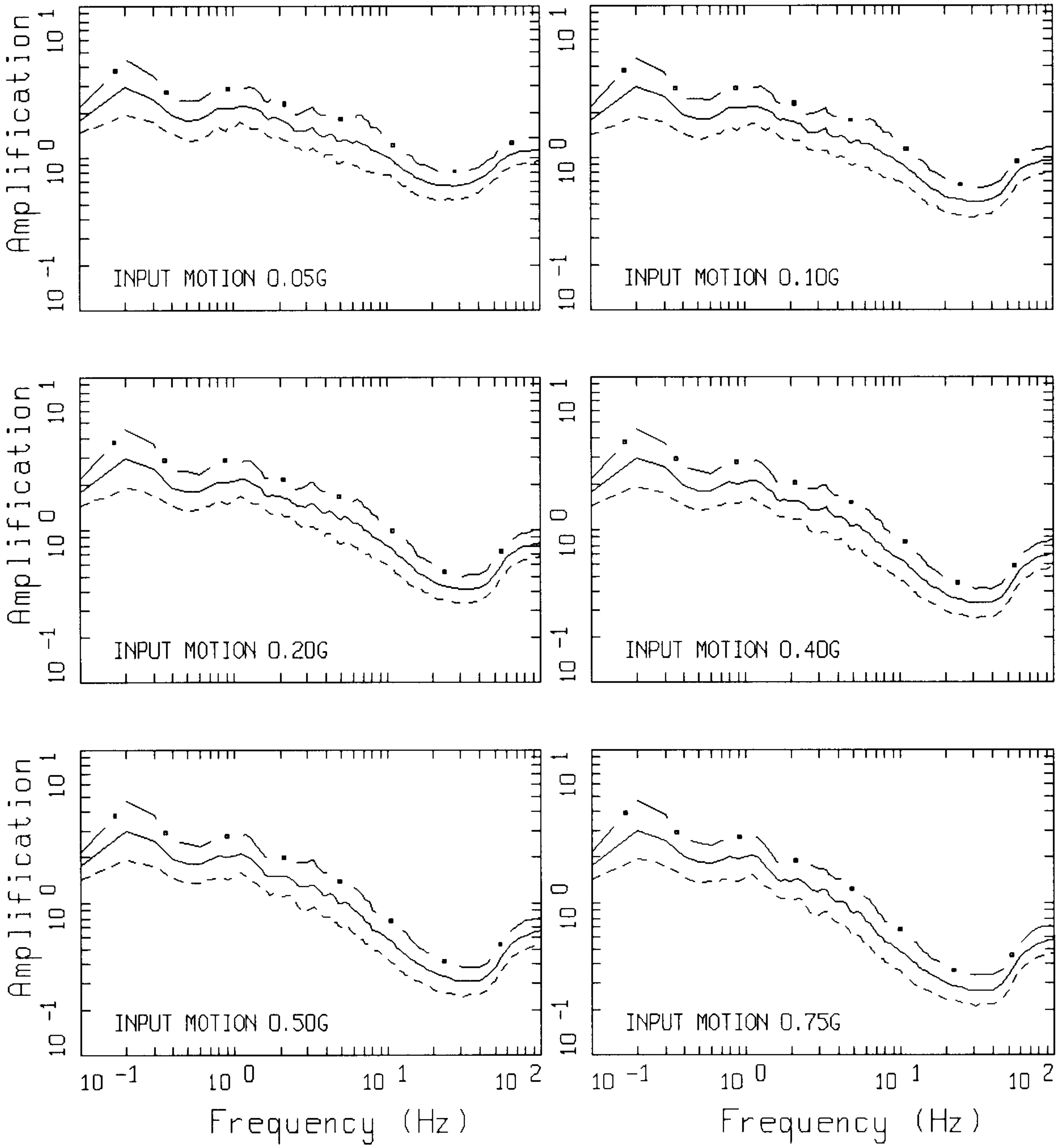

UPLANDS HIGH VELOCITY 2, CATEGORY 7, 2000-4000 FT
PENINSULAR RANGE CURVES

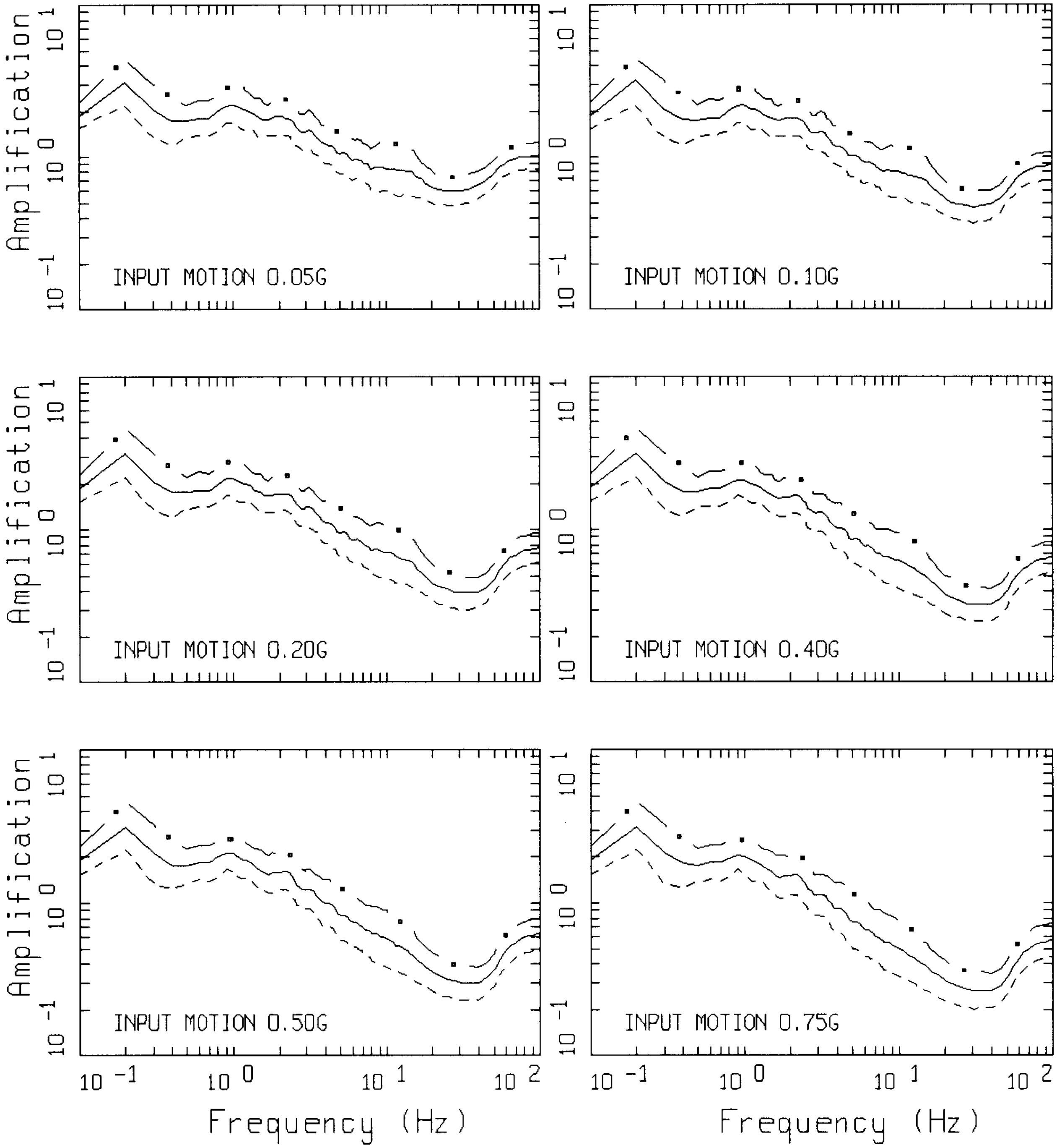

UPLANDS HIGH VELOCITY 3, CATEGORY 7, 2000-4000 FT
PENINSULAR RANGE CURVES

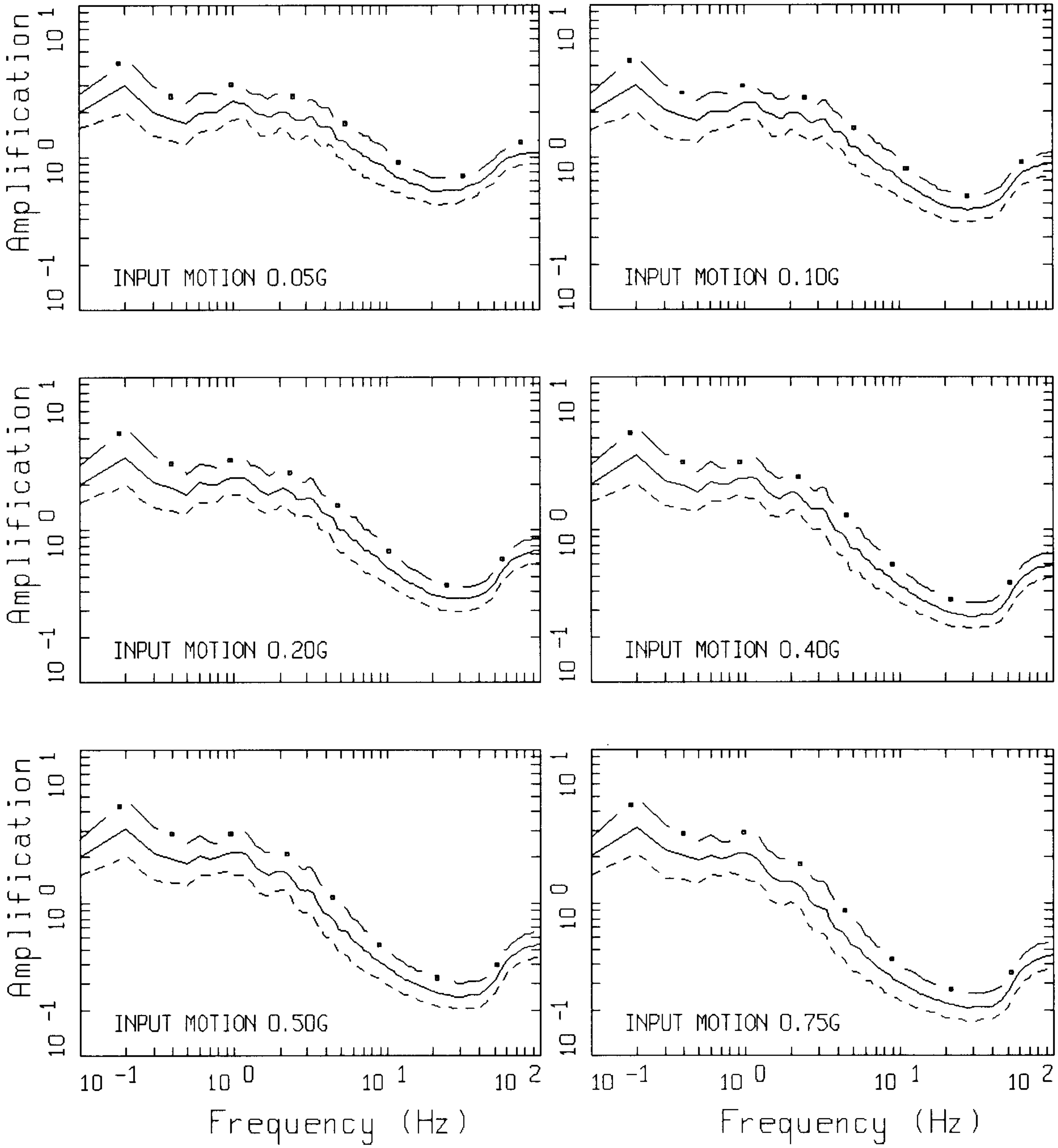

UPLANDS HIGH VELOCITY 1, CATEGORY 7, 2000-4000 FT
EPRI CURVES

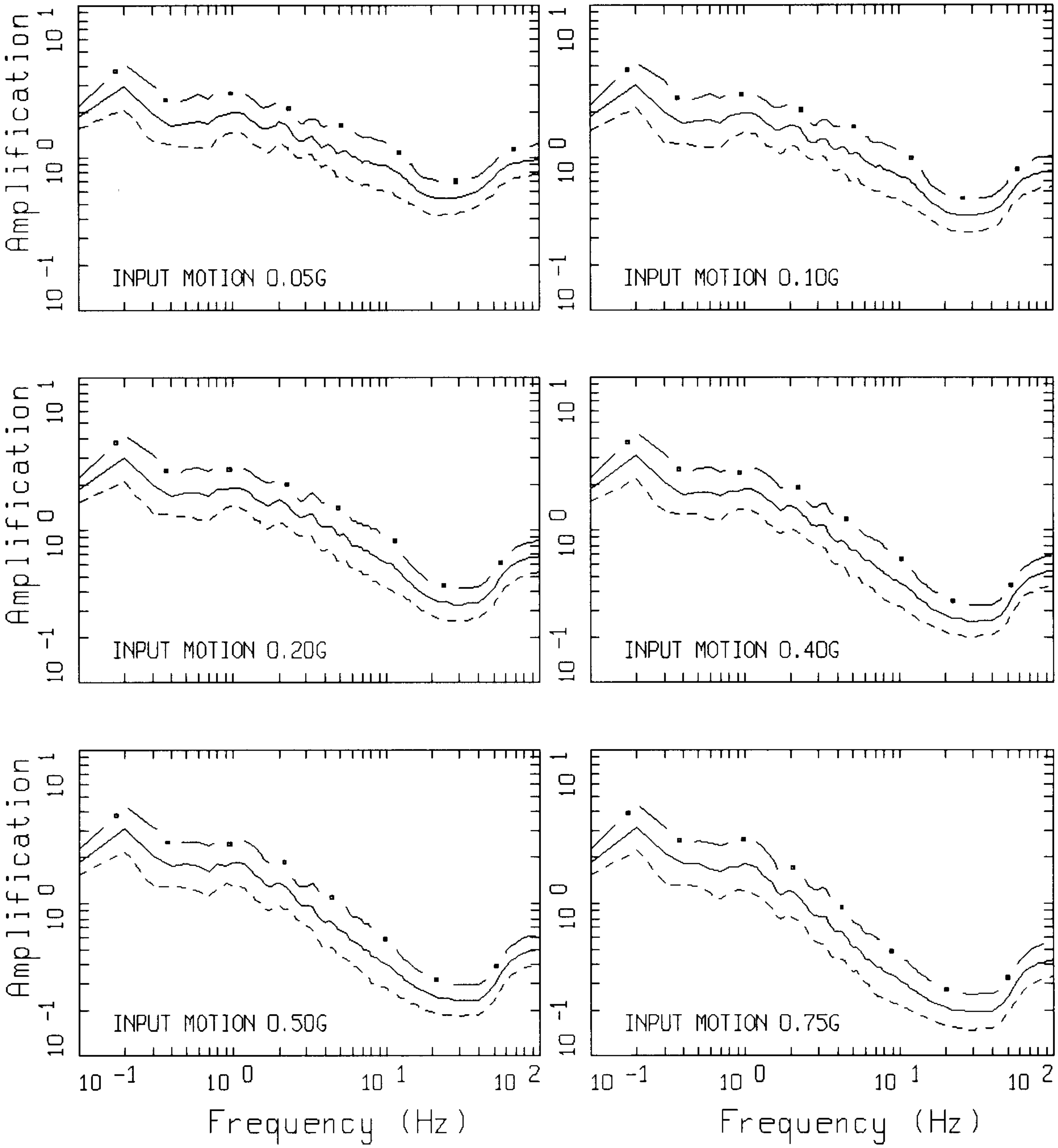

UPLANDS HIGH VELOCITY 2, CATEGORY 7, 2000-4000 FT
EPRI CURVES

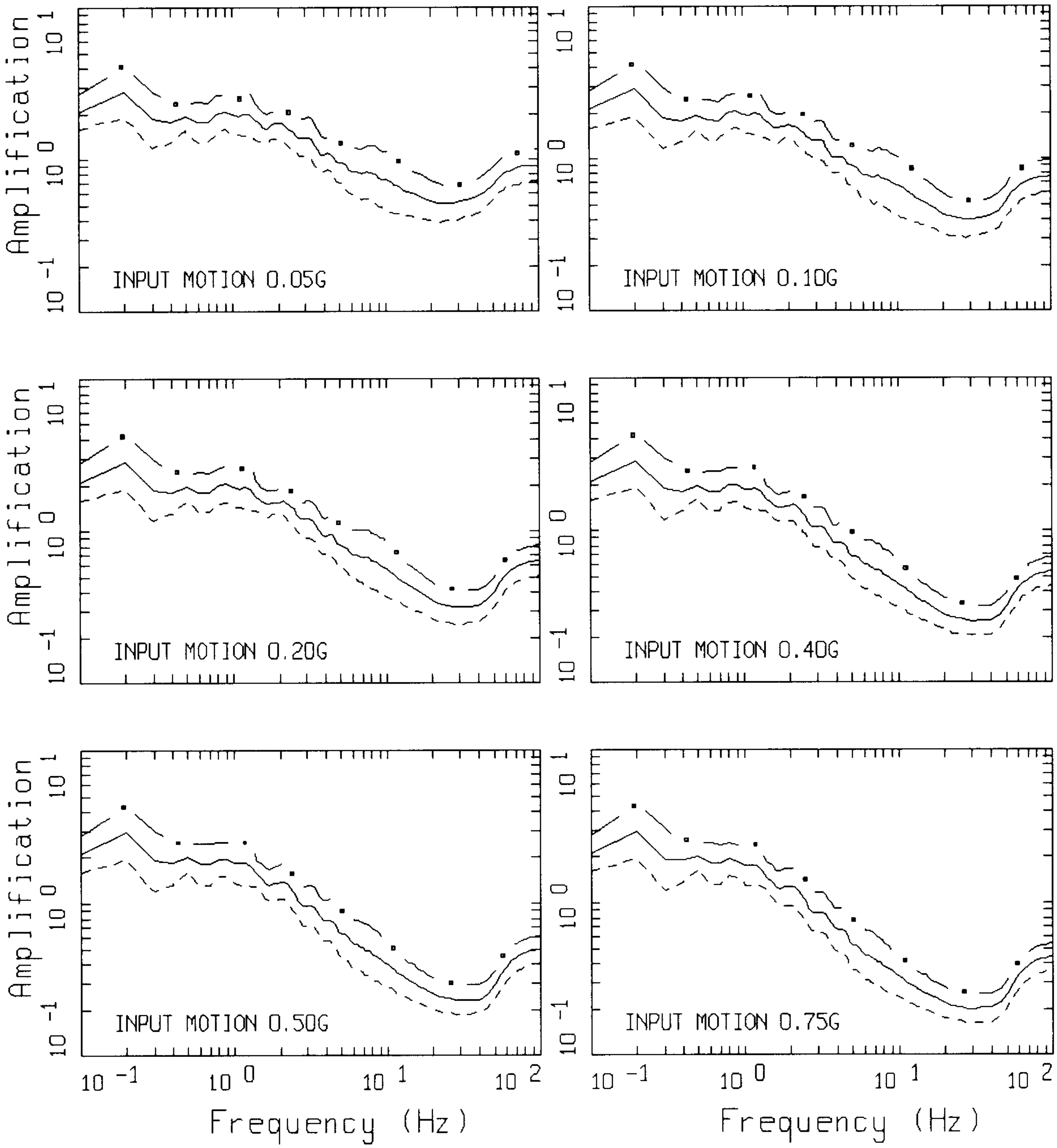

UPLANDS HIGH VELOCITY 3, CATEGORY 7, 2000-4000 FT
EPRI CURVES

Appendix D

AMPLIFICATION FACTORS FOR GLACIAL TILL PROFILE

Amplification factors, median and ± 1σ 5% damped response spectra, for the Glacial Till generic profile depth categories 1, 2, 3, 4, 5. EPRI nonlinear dynamic material properties.

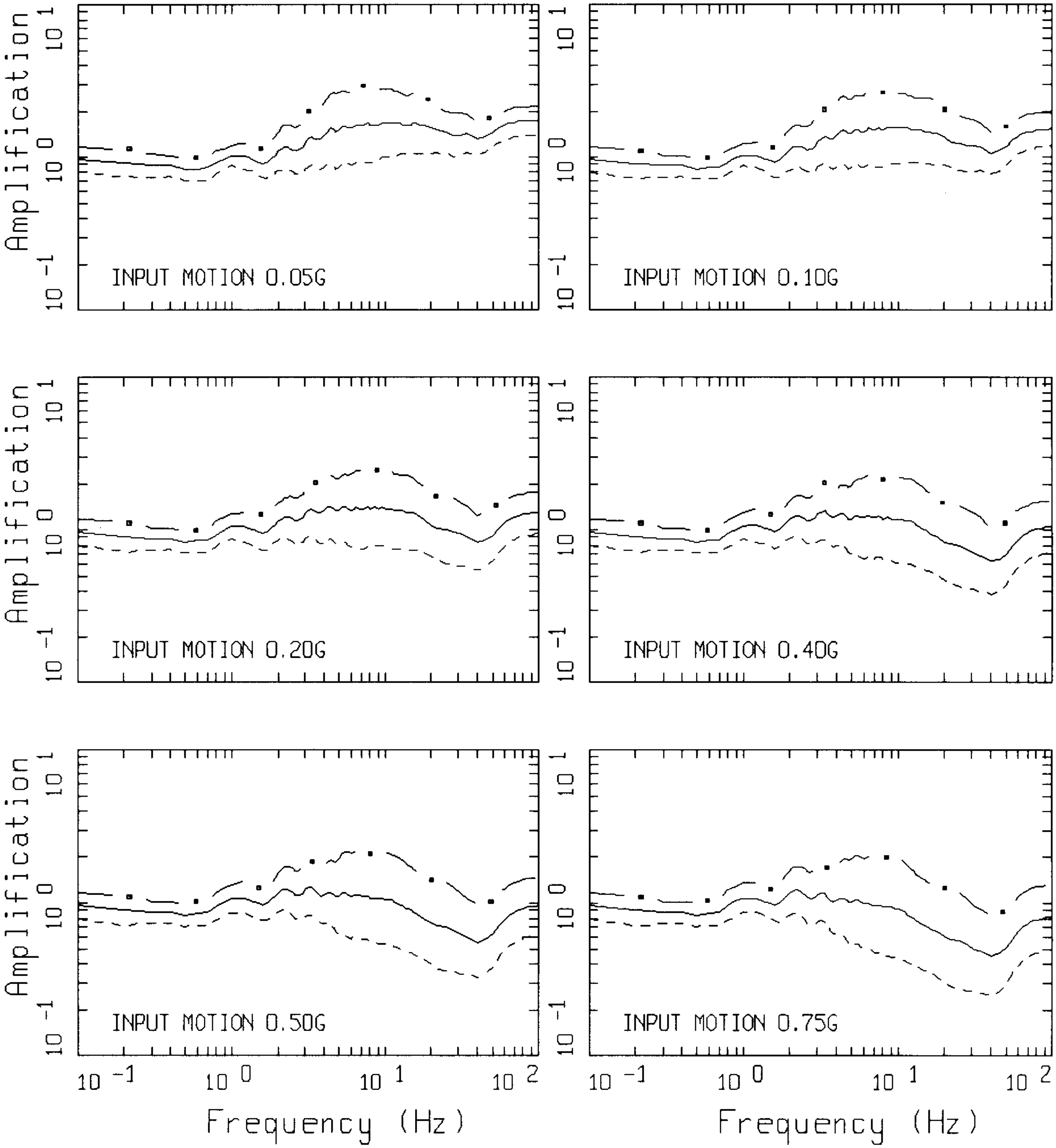

GLACIAL TILL, CATEGORY 1, 10-50 FT

EPRI CURVES

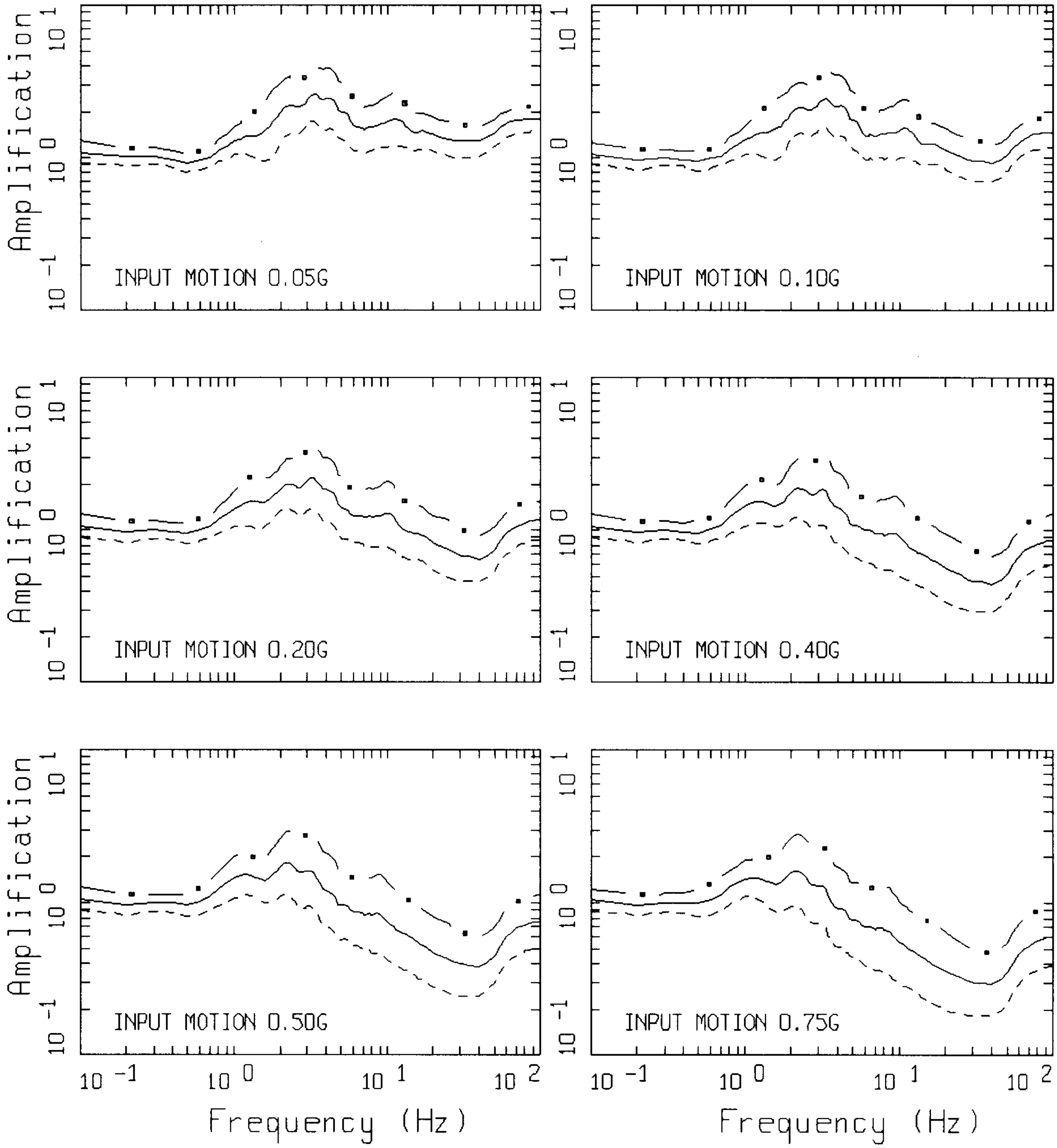

GLACIAL TILL, CATEGORY 2, 50-100 FT

EPRI CURVES

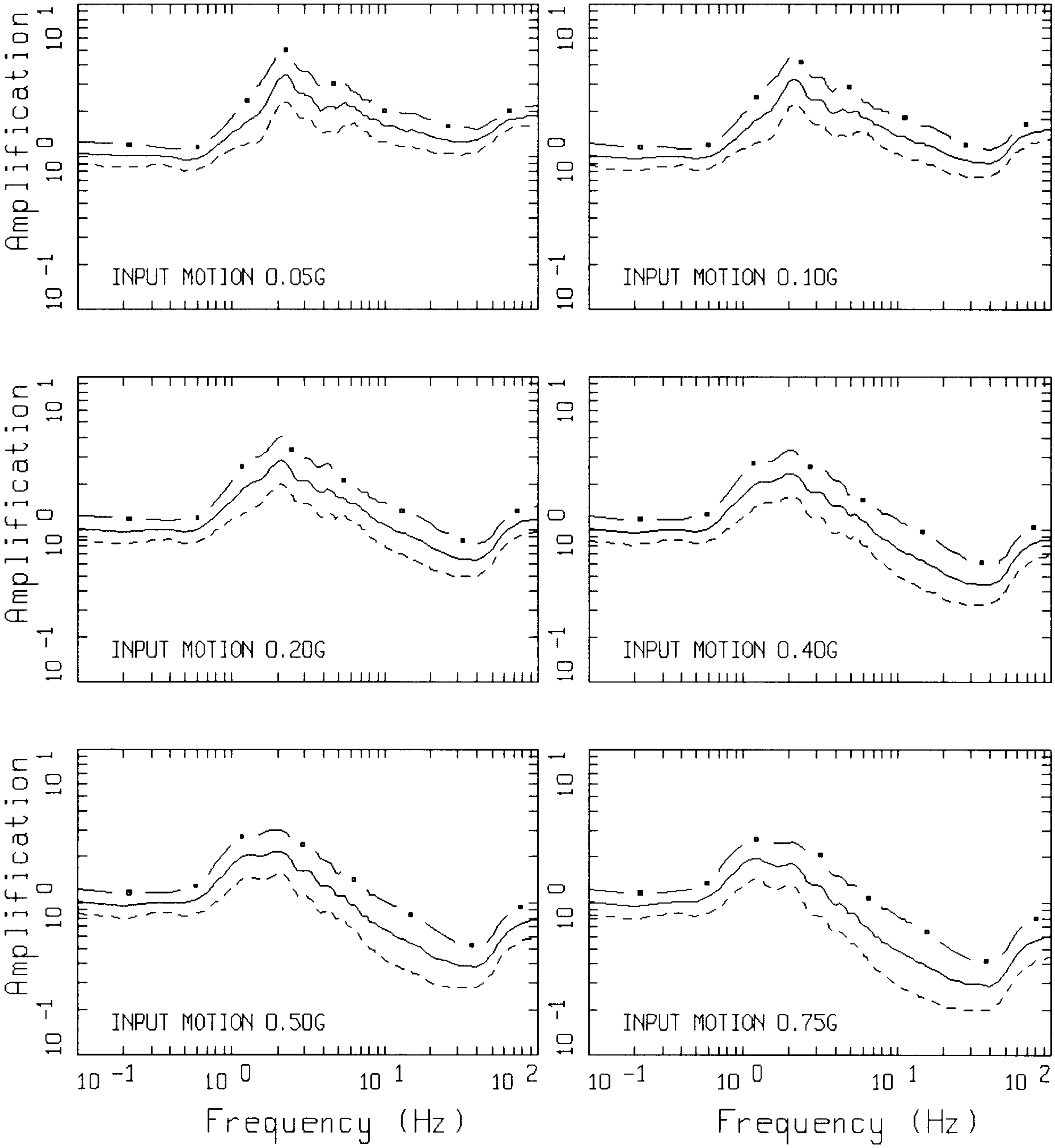

GLACIAL TILL, CATEGORY 3, 100-200 FT
EPRI CURVES

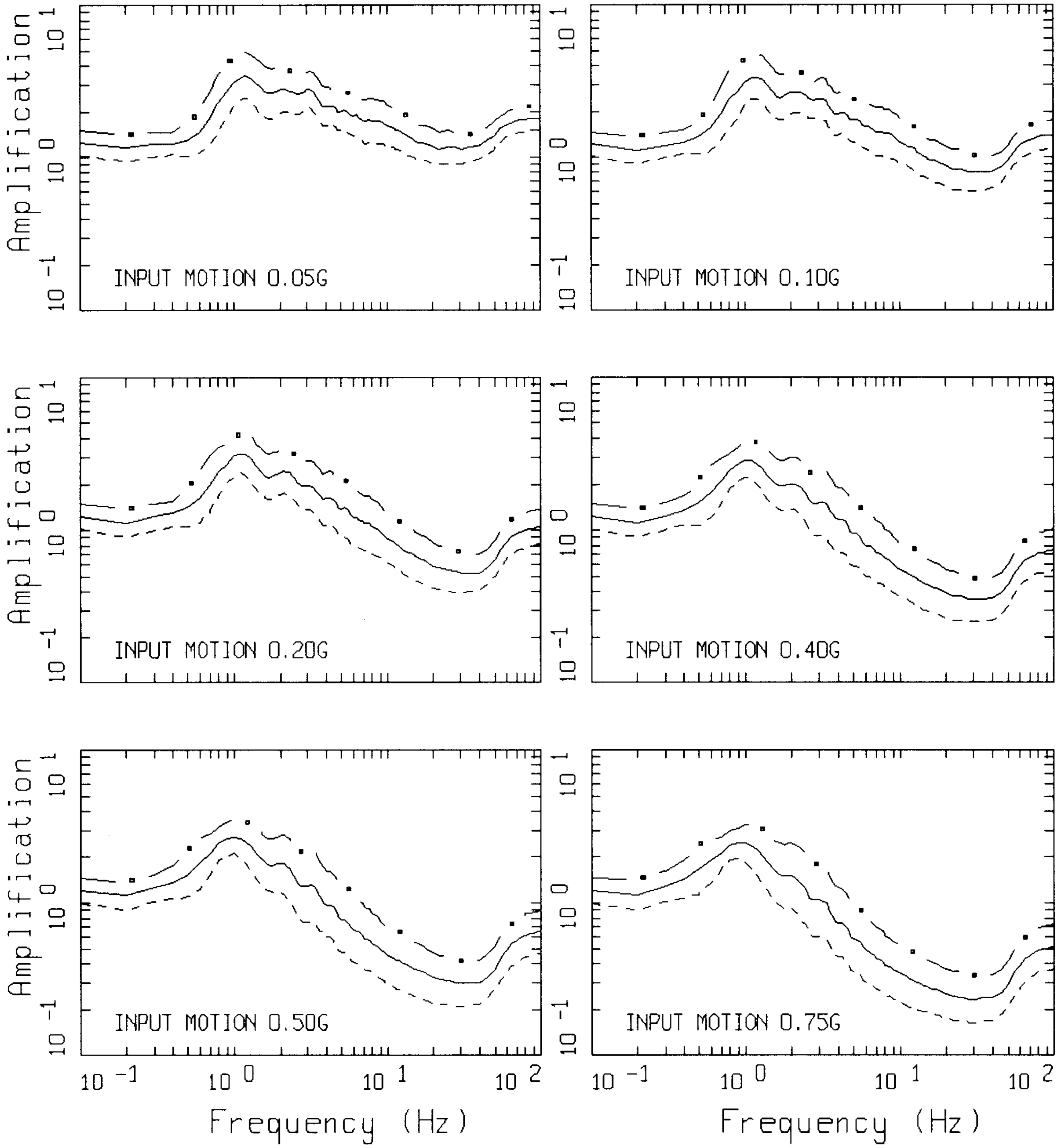

GLACIAL TILL, CATEGORY 4, 200-500 FT

EPRI CURVES

Appendix E

SEISMIC-HAZARD CALCULATIONS FOR TEMPORALLY CLUSTERED EVENTS IN THE NMSZ

In most seismic hazard calculations, the annual exceedence probability (considering all seismic sources) is approximated by the annual exceedence rate, which in turn is calculated using the equation:

$$\nu(A>a*)=\sum_i \nu_i \int\int G_{A|m,r}(a*)\ f_{M\ (i)}(m)\ f_{R\ (i)}(r|m)\ dm\ dr \qquad \text{(E-1)}$$

in which the summation is performed over all seismic sources *i* (see Risk Engineering, 1999 for the definition of other terms in the above equation).

Under the assumptions of independence typically made in seismic hazard analysis[1], and for the high (rare) ground motions, the annual rate of earthquakes with $A > a*$ is a very good approximation to the probability of exceeding amplitude $a*$ in one year.

In the situation considered in this study, however, Equation E-1 is not a good approximation to the exceedence probability. Because this study assumes temporal clustering of large earthquakes in the NMSZ, the rate of earthquakes with $A > a*$ is no longer a good approximation to the probability of exceeding amplitude $a*$, as will be shown below.

Consider the annual rate of earthquakes with $A > a*$, which can be expressed as

$$\nu(a^*)=1\times P[1]+2\times P[2]+3\times P[3]+\ \ldots \qquad \text{(E-2)}$$

where $P[i]$ is the probability of having i exceedences of amplitude $a*$ in one year. Consider also the annual exceedence probability can be expressed as

$$P[A>a^*\ \text{in}\ 1\ \text{yr.}]=P[1]+P[2]+P[3]+\ \ldots \qquad \text{(E-3)}$$

Under the assumption of independence, $P[2]$ and $P[3]$ are much smaller than $P[1]$, so that the quantities in equations E-2 and E-3 are nearly identical. On the other hand, if large earthquakes in the NMSZ occur in clusters with durations much shorter than the inter-arrival time of the clusters, then $P[2]$ and $P[3]$ are comparable to $P[1]$ for low and moderate values of $a*$, causing the exceedence rate in equation E-2 and the exceedence probability in equation E-3 to be significantly different.

---

[1]Namely, that earthquakes (most particularly, successive earthquakes) are independent in size, location, and occurrence time.

This study incorporates the assumption made in Section 2 and Appendix A of Risk Engineering (1999) that large earthquakes on any NMSZ segment are followed by large earthquakes in the other two segments (within a time interval much shorter than the time between these clustering episodes), by treating the three NMSZ segments as one special source. These three NMSZ segments are the Blytheville Arch (BA), the Reelfoot fault (RF), and East Prairie[2] (EP).

For this special source, the probability of exceeding amplitude *a** in one year due to earthquakes in this special seismic source is computed using the rules for the calculation of probabilities of unions of events, as follows:

$$\begin{aligned} P[A>a^* \text{ in 1 yr.}]_{NM} &= \nu_{NM} \quad P[A_{BA}>a^* \text{ or } A_{RF}>a^* \text{ or } A_{EP}>a^*] \\ &= \nu_{NM} \; \{P[A_{BA}>a^*]+P[A_{RF}>a^*]+P[A_{EP}>a^*] \\ &\qquad -P[A_{BA}>a^*]P[A_{RF}>a^*] \\ &\qquad -P[A_{RF}>a^*]P[A_{EP}>a^*] \\ &\qquad -P[A_{EP}>a^*]P[A_{BA}>a^*] \\ &\qquad +P[A_{BA}>a^*]P[A_{RF}>a^*]P[A_{EP}>a^*]\} \end{aligned} \tag{E-4}$$

where ν_{NM} is the annual rate of clustering episodes and $A_{BA}>a*$ represents the event of an exceedence of amplitude *a** given the occurrence of a large earthquake on the Blytheville arch (which is evaluated using the integral in Equation E-1). This formulation assumes that occurrences of large events in the NMSZ are tightly clustered in time (relative to the mean time between clusters). All other assumptions of independence are maintained. In particular, smaller events in the NMSZ segments (those associated with the exponential portion of the magnitude-recurrence model; see Section 2) are treated as independent. This modification to the standard formulation is appropriate (and necessary), given the assumption of clustering.

REFERENCES

Risk Engineering, Inc. (1999). *Rev. 3 to Updated Probabilistic Seismic Hazard Analysis for the Paducah Gaseous Diffusion Plant, Paducah, Kentucky--Final Report.* Prepared for Lockheed-Martin Utility Services, Available through NRC Public Documents Library, Accession Number 9905140175, docket no. 07007001.

[2]East Prairie itself will be divided into two seismic sources, namely East Prairie fault (EPF) and East Prairie extension (EPE). Large events in these two faults are treated as mutually exclusive. Therefore, their probabilities are additive.